New Developments in Vector, Matrix and Tensor Quantum Field Theories

Fedor Kalinovich Popov

A Dissertation
Presented to the Faculty
of Princeton University
in Candidacy for the Degree
of Doctor of Philosophy

Recommended for Acceptance
by the Department of
Physics

Adviser: Igor R. Klebanov

September 2021

Abstract

This thesis is devoted to studies of quantum field theories with dynamical fields in the vector, matrix or tensor representations of $O(N)$ symmetry groups. These models provide interesting classes of exactly solvable models that can be examined in detail and give insights into the properties of other, more complicated quantum field theories.

The introduction to the thesis reviews the general ideas about why such systems are interesting and exactly solvable. The different classes of Feynman diagrams which dominate the large N limits are exhibited. The introduction is partially based on work [1] with Igor R. Klebanov and Preethi Pallegar.

Chapter 2 is based on work [2] with Igor R. Klebanov, Preethi Pallegar, Gabriel Gaitan and Kiryl Pakrouski. It is dedicated to the study of quantum Majorana fermionic models. The refined energy bound is derived for these models. We study these models numerically, analytically and qualitavely. All of these results hint that the vector quantum mechanics undergoes second order phase transition and has a limiting temperature in the large N limit.

Chapter 3 is based on papers [3, 4] with Igor R. Klebanov, Simone Giombi, Grigory Tarnopolsky and Shiroman Prakash. It is dedicated to the search of a stable bosonic tensor and SYK-like theories in higher dimensions. We propose two models: prismatic and supersymmetric that have a positive potential and therefore these theories should be stable unlike the bosonic tensor models with quartic tetrahedral interactions.

Chapter 4 is based on papers [5, 6] with Igor R. Klebanov and Christian Jepsen. It studies the properties of RG flow and bifurcations that could arise in this case. We consider a theory of symmetric traceless matrices in $d = 3 - \epsilon$ dimensions and analytically continue the rank of these matrices to fractional values. At some values of N we managed to find a fixed point whose stability matrix has a pair of purely imaginary eigenvalues. From the theory of ordinary differential equations it is known that it corresponds to Hopf bifurcation and that at some values of N a stable limit cycle exists, that we also find numerically. Such an approach is

extended to the case of $O(N) \times O(M)$ group, where it is shown that a homoclinic RG flow exists, which starts and terminates at the same fixed point.

Acknowledgements

I am very grateful to my advisor Igor R. Klebanov for his constant guidance and patience throughout graduate school. His interesting problems, unconventional approach to them and physical intuition helped me to expand my view of quantum field theory. Igor's advice helped me to grow both as a physicist and as a person.

I am also thankful to Alexander M. Polyakov for conversations with him and his advanced classes on Quantum Field Theories. His vision on Theoretical Physics still invigorates me and gives me so many interesting ideas and problems that I hope I will be able to implement and solve in the future.

I would also be remiss if I did not thank Juan Maldacena for the great opportunity to work with him on the problem of creating and maintaining a wormhole solution. Thanks to him I learned a different and unique approach to theoretical physics.

I also want to thank Lyman A. Page for agreeing to be on this committee, being an excellent experimental project advisor and a kind landlord. I hope his experiment will find axions.

I am very grateful to other faculty of the Physics Department: Simone Giombi, for collaborating on the prismatic project, Silviu Pufu, for agreeing to be a second reader, Duncan Haldane, whom I helped to teach condensed matter class, and Kasey Wagner for being a wonderful lab manager. Also I want to thank our graduate administrator, Kate Brosowsky, for helping all graduate students throughout theirs years in Princeton.

I am indebted to my undergraduate adviser Akhmedov Emil Tofik ogly for introducing me to quantum field theory, continual support, his patience through Field Theory class and teaching the fundamental principle, that equations are the most important part of any science.

Also I would like to thank all my co-authors throughout my graduate years: Grigory Tarnopolsky, Shiroman Prakash, Ugo Moschella, Hadi Godazgar, Christian Jepsen, Kiryl Pakrousky, Alexei Milekhin and Preethi Pallegar. All of them have their unique approach to research in general, and I feel that each of these collaborations have given me separate parts of a jigsaw puzzle of theoretical physics.

Also I am very grateful to all people from Institute for Theoretical and Experimental Physics, who helped me at the first steps in Theoretical Physics: Valentin I. Zakharov, Alexei Yu. Morozov, Alexander S. Gorsky, Alexei Sleptsov, Phillip Burda, Dmitriy Vasiliev and Lena Suslova. Also I must thank Vadim N. Diesperov for being a good friend and mentor to me throughout my years in MIPT.

Of course, I would not be able to live all of these years in Princeton and in Dolgoprudny without my friends, that I also must thank: Danya Antonenko, Yakov Kononov, Volodya Kirilin, Andrey Sadofeyv, Kseniya Bulycheva, Kostya Matveev, Andrei Zeleneev, Igor Silin, Sasha Gavrilyuk, Pasha Avdeenko, Kolya Skryabin, Roma Turansky, Anna Voevodkina, Andrei Gladkih, Lina Ivanova, Nikita Sopenko, Sasha Avdoshkin, Vlad Kozii, Lev Krainov, Nina Krainova, Alina Khisameeva, Pavel Gusikhin, Tanya Artemova, Artem Rakov, Igor Poboyiko, Alina Tokmakova, Asya Aristova, Boris Runov, Valentin Slepukhin, Oleg Dubinkin, Grisha Starkov, Ivan Danilenko, Masha Danilenko, Sergey Ryabichko, Lena Demkina, Roma Kolevatov, Maksim Litskevich, Nikolay Sukhov, Artem Denisov, Misha Ivanov, Amina Kurbidaeva, Misha Mlodik, Lev Arzamasskiy, Valentin Skoutnev, Peter Czajka, James Loy, Nick Haubrich, Wayne Zhao, Samuel Higginbotham, Steven Li, Sarah Marie Bruno, Nana Shumiya, Joseph Van der List, Diana Sofia Valverde Mendez, James Teoh, Oak Nelson, Annie Levine, Joao Lucas Thereze Ferreira, David Buniyatyan, Charlie Murphy, Jiwon Choi, Lidia Tripiccione, Vivek Kumar, Tyler Cochran, Leander Thiele, Dumitru Calugaru, Akash Goel, Himanshu Khanchandani, Javier Roulet, Ro Kiman, Ho Tat Lam, Luca Illesiu, Damon Binder, Ziming Ji, Yiming Chen, Wenli Zhao. Thank you for sharing your views, common interests, wonderful conversations about physics and everything else, that made Princeton feel like home.

I am also very thankful to the students I helped mentor for the exceptional opportunity to help them with their first steps in science: Gabriel Gaitan, Liza Rozenberg and Matan Grinberg, who was also an excellent friend and a exceptional ghostwriter. I hope that all of them will pursue their dreams and become famous physicists in the future.

I am indebted to my high school teacher of physics, Polyanskiy Sergei Evgenyevich,

who in 2008 persuaded me to study physics and continue my education in MIPT in the department of general and applied physics.

Finally, I would like to express my graditutde and love to my family: my mom, Emelyanova Vera Falaleevna, my father, Popov Kalina Fedorovich, and my grandparents, Emelyanova Lyubov Ilinichna and Emelyanov Falalei Pavlovich. Thank you for your love and support throughout my PhD!

To my parents.

Contents

1 Introduction

In all branches of theoretical and experimental physics, people deal only with approximations to the real world. One of the main reasons for this is because we do not have full knowledge about the fundamental laws of physics. Thus, classical mechanics is an approximation to the quantum mechanics, and maybe quantum mechanics is an approximation to some other more fundamental theory. In some limits this fundamental theory reduces to quantum and classical mechanics. For instance, we use classical mechanics to describe the phenomena that occur at scales of everyday life, while quantum mechanics could be used to describe the physics of the hydrogen atom. Other approximations happen because we do not posses the complete information about the system in question. In a condensed matter experiment we do not have the detailed knowledge about microscopoc structure of a crystal — we do not know the exact distance between the 1000th and 1001st atom, what isotope the 2021st atom in a lattice is and etc. However, some of this information is not actually necessary for our purposes. Under the assumption that these minute details do not have a drastic effect on the larger-scale phenomena, we can neglect such exact knowledge.

One can think that we have listed all possible approximations that could arise in a physical problem and as soon as we remove them we could describe and solve any natural phenomenon. But there is another obstacle. Namely, the inability of humans to solve some problems. As Alexander Markovich Polyakov noted, "dogs are very smart, but they still can not solve simple linear equations". Maybe there are some limits for human mind [7]. Hence, if we pose a precise mathematical problem or a physical model with a given framework of fundamental laws perhaps we will still be unable to solve the problem. For example, we may not prove the Goldbach's Conjecture [8] or solve three body problem in classical gravity [9] .

The only problems that human mind could comprehend entirely are linear problems and a few non-linear models. And if we constrained ourselves only to these problems, which we can solve exactly, we would not be able to describe the natrual world around us. However, the real physics sometimes can be modeled as a small perturbation of an

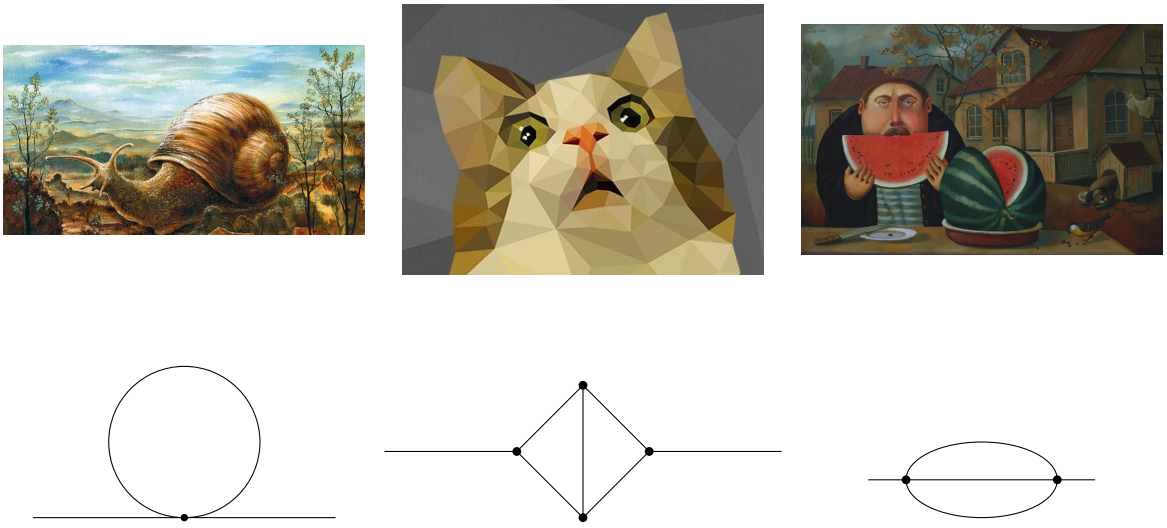

Figure 1.1: Three different large N limits and theirs "graphical" representations.

exactly solvable model. On this basis, a successful description, or at least qualitative understanding, can be built[1]. Therefore developing interesting and solvable models, or considering systems in some limits, where they can be solved, is one of the most fundamental endeavors of modern theoretical physics.

One of the earliest ideas of theoretical physics is, that models, in the limit of a large number of degrees of freedom, are much simpler than those containing a small number of degrees of freedom and can therefore be effectively solved. This happens because in the limit of a large number of degrees of freedoms, the common behavior of the system averages allowing us to disregard local fluctuations and other microscopic details. The embodiment of this principle is the famous central limit theorem, wherein we start from some unknown distribution and in the limit of large number we always end up with a Gaussian distribution. Another example of this idea can be found in the theory of second-order phase transitions. In this case, we assume that in the thermodynamic limit the system is described by some universal behavior and is not sensitive to the internal structure of the system. Therefore considering models with a large number of degrees of freedom, and successfully solving them could help us better understand how to solve problems of quantum field theory, as well as theoretical physics more broadly.

Usually people considered only two such systems with large numbers of degrees or

[1]Sometimes, we do not have even such a luxury, thus the fractional quantum hall effect already considers a complicated interaction without any approximations.

large N models, namely, vector and matrix large N models. Both of these models were quite important as tests for AdS/CFT correspondence and as key to understaning of low dimensional quantum gravity or string theory. Recently, people managed to generalize this approach to so called tensor models that give a quite different large N model, that is much simpler than the matrix one and more complicated than the vector large N limit. Therefore it gives some interesting new limits that could give some hints on the structure of the large N systems (see fig. 1.1). In this section we will briefly review the main results about systems with vector, matrix and tensor large N limits.

1.1 Vector Models

In 1952 Berlin and Kac introduced the generalized Ising model (see fig. 1.2), where the spin has N components and constrained to have length $\vec{S}_i \cdot \vec{S}_i = N$ [10, 11]. The Hamiltonian of this model is:

$$H = -\sum_{ij} J_{ij} \vec{S}_i \cdot \vec{S}_j, \tag{1.1}$$

at $N = 1$ the model reduces to a usual Ising model. This model posseses an exact solution at large N. This happens because the local fluctuations are suppressed in comparison to the collective behaviour. We will show it considering the model (1.1) in the continium limit at $d = 2$ [12, 13]. Namely, by rescaling $\vec{n}_i = \frac{\vec{S}_i}{\sqrt{N}}$ we get

$$\mathcal{L} = \frac{N}{2\lambda} \left(\partial_\mu \vec{n}\right)^2, \quad \vec{n}^2 = 1. \tag{1.2}$$

We introduce an auxilary field $\alpha(x)$ into the action, that imposes the condition $\vec{n}^2 = 1$

$$\mathcal{L} = \frac{N}{2\lambda} \left(\partial_\mu \vec{n}\right)^2 + \frac{iN}{2\lambda} \alpha \left(\vec{n}^2 - 1\right).$$

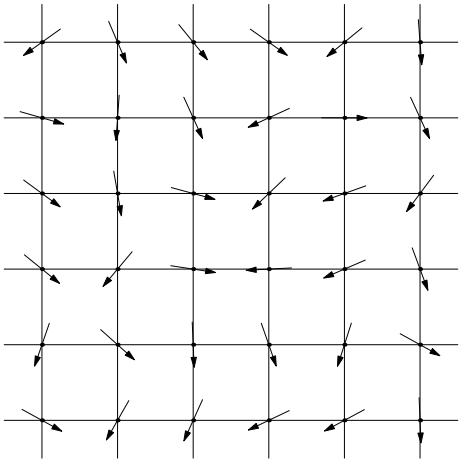

Figure 1.2: Generalized Ising model, where the each site has a N-component vector of length $\sqrt{N}$.

This action is quadratic in $\vec{n}$ and hence we can integrate out the field $\vec{n}$. The effective action reads as

$$S_{\text{eff}} = -\frac{N}{2}\left(\text{Tr}\log\left(-\partial_\mu^2 + i\alpha\right) + \frac{i}{\lambda}\int d^dx\,\alpha\right),$$

since the quantum averages are computed with the weight $e^{-S_{\text{eff}}}$, in the large N we can use saddle point approximation to evaluate the partition function for the action (1.1). Moreover, one can see that the number of degrees of freedom N plays the role of inverse of Plank constant $\frac{1}{\hbar}$ and therefore $\frac{1}{N}$ controls quantum corrections. Then only classical solution of the action contributes to the dynamics of the generalized Ising model. Thus varying the equation (1.1) we get the following equation for the field α:

$$G_\alpha^\Lambda(x,x) = \lambda, \quad \text{or} \quad \frac{1}{2\pi}\log\frac{\Lambda}{i\alpha} = \frac{1}{\lambda} \tag{1.3}$$

where $G_\alpha^\Lambda(x,x)$ is a regularized propagator of a free scalar field in 2 dimensions with mass $i\alpha(x)$, that could depend on the coordinates. For simplicity we assume that α is constant throughout space-time (one can strictly show it from the eq. (1.3)). Introducing cut-off Λ we get the value of α:

$$\alpha = i\Lambda\exp\left[-\frac{2\pi}{\lambda}\right]. \tag{1.4}$$

We can easily read off the dependence of λ on the cut-off Λ and get the beta-function for this model in the large N limit and we see in the large N limit the model (1.1) is described by a free massive scalar field. It happened again because we considered the limit of large numbers of degrees of freedom, that drastically simplified the analysis of the system. Therefore we could expect the same type of simplification for other large N vector theories. Namely, that the local fluctuation are suppressed while the collective behaviour is described by some classical model and $\frac{1}{N}$ corrections could be considered as quantum corrections.

While in the case of the $\vec{n}$ model it is quite hard to see this $\frac{1}{N}$ structure in terms of diagrams we can show it in the example of just 0-dimensional mechanics of a real vector. Namely, we want to study the following integral

$$Z = \int d\phi_i \exp\left[-\frac{1}{2}\phi_i^2 - \frac{\lambda}{24}\left(\phi_i^2\right)^2\right] \tag{1.5}$$

In the spirit of quantum field theory we will assume that λ is small and approximate the exponent by its Taylor series. It gives the following rules for drawing Feynman diagrams

$$\langle \phi_a \phi_b \rangle = \delta_{ab} = \text{————}, \quad \left(\phi_i^2\right)^2 \sim \text{ 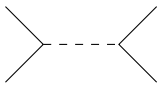 } \tag{1.6}$$

Each loop of field ϕ contributes a factor of N, and therefore to get large N limit we should maximize the number of loops at the given level of perturbation theory or in front of the coupling constant λ. To proceed further we need so-called Euler formula. This formula comes from computing Poincare-Hopf index of triangulation of Riemann surface of genus g by some graph. Namely, if a graph drawn on a Rieman surface of genus g then the number of vertices V, edges E and faces F satisfy the following linear relation

$$e = V - E + F = 2 - 2g. \tag{1.7}$$

Then let us consider some graph in this vector model that has V vertices or dashed lines. Let F_ϕ be the number of loops created by the field ϕ, each contributing a factor of

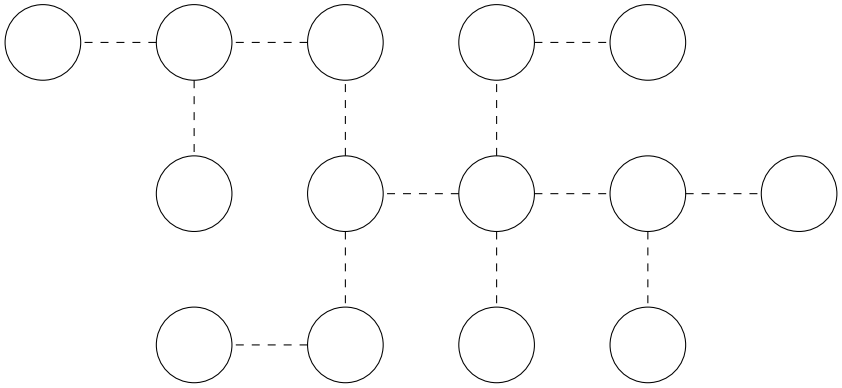

Figure 1.3: One of the leading diagrams that give dominant contribution to the partition function of the scalar vector model. The dashed lines correspond to the propagation of an auxilary field σ and the dashed lines to the real fields ϕ_i.

N to the amplitude. Then we can shrink each of the matter loop and get a graph that has F_ϕ vertices, V edges and F faces spanned by dashed lines. By Euler formula we get $F_\phi = 2 - 2g + V - F$ faces. Then the given graph will contribute as

$$A \sim \lambda^V N^{2-2g+V-F} = (\lambda N)^V N^{1-2g-(F-1)}, \tag{1.8}$$

if one introduces a rescaled coupling $\lambda_{tH} = \lambda N$ in the large N limit only planar diagrams with exactly one face $F = 1$ contribute.The last means that the graph should be tree. A tree graph can always be drawn on a plane. Hence $F = 1$ is a necessary and sufficient condition for the diagram domination. An example of such a diagram could be seen in the fig. 1.3, sometimes such a diagrams are called "snails" [14] or "cacti" [15].

The scaling (1.8) suggests that the partition function behaves as $\log Z \sim N f_0 + \ldots$. Let us get the f_0 from the summation over all possible tree diagrams. One can notice that tree diagrams are just a semiclassical approximation of some quantum model. Since in our case there could be vertices of any valence the action of such a model is

$$S_0 = -\frac{3}{\lambda_{tH}}\sigma^2 + \sum_{k=0}^{\infty} a_k \sigma^k, \tag{1.9}$$

where the normalization of the "kinetic term" comes from the fact the propagator of an auxillary field σ is induced by an interaction term of the original model. It is easy to see

that the coupling "constants" are $a_k = \frac{1}{k}$. The action reads as

$$S_0 = -\frac{3}{\lambda_{tH}}\sigma^2 + \log(1+\sigma), \tag{1.10}$$

It would be interesting to derive this action in the same fashion we derived an effective action for the $\vec{n}$-model. We again introduce an auxiliary variable σ, so that

$$Z(\lambda_{tH}) = \int_{-\infty}^{\infty} \prod_{j=1}^{N} d\phi_j \int d\sigma \exp\left(-\frac{3N}{2\lambda_{tH}}\sigma^2 - \frac{\phi^k\phi^k(1+i\sigma)}{2}\right) . \tag{1.11}$$

After performing the Gaussian integral over ϕ^j we find

$$Z(\lambda_{tH}) = \int d\sigma \exp\left(\frac{N}{2}\left[\frac{3}{\lambda_{tH}}\sigma^2 - \log(1+\sigma)\right]\right), \tag{1.12}$$

that coincides with the action we derived aboive. In large N the integral is dominated by the saddle point

$$\frac{6\sigma}{\lambda_{tH}} = \frac{1}{1+\sigma}\,. \tag{1.13}$$

The solution of this quadratic equation which matches onto the perturbation theory is

$$\sigma(\lambda_{tH}) = \frac{\sqrt{1+\frac{2\lambda_{tH}}{3}}-1}{2}\ , \tag{1.14}$$

and we find to all orders in λ_{tH},

$$f_0(\lambda_{tH}) = \sum_{k=1}^{\infty}(-\lambda_{tH})^k \frac{1}{4k(k+1)6^k}\binom{2k}{k}\,. \tag{1.15}$$

In this series the coefficients decrease, so it is convergent for sufficiently small $|\lambda_{tH}|$. This is one of the advantages of the large N limit – the functions that appear order by order in $1/N$ have perturbation series with a finite radius of convergence.

The next subleading contribution comes from the planar diagrams with $F = 2$ and $g = 0$. The subleading diagrams are shown in the fig. 2.2 and will be studied in the following sections.

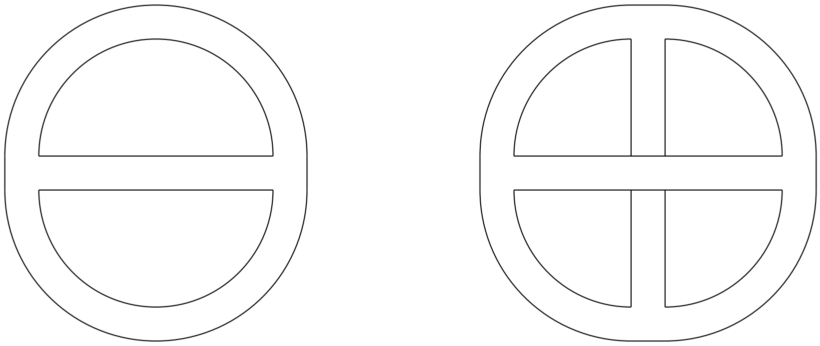

Figure 1.4: Examples of fat graphs in Yang-Mills theory. The graph on the left side could be drawn on a sphere, while the graph on the right could be drawn only a torus.

1.2 Matrix Models

The natural generalization of the previous model is to consider the dynamical matrices. This idea was originally proposed by ‘t-Hooft in 1973 [16] and comes from the study of the Yang-Mills theory. Namely, the dynamical degrees of freedom in this case are a d-dimensional vector of hermitian matricies of size $N \times N$. The propagator of this field is

$$\langle A_\mu^{ab} A_\nu^{cd} \rangle \sim g_{\mathrm{YM}}^2 \tag{1.16}$$

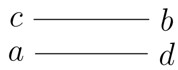

and the interaction terms are

$$\mathrm{tr}\, A_\mu^3 \sim \frac{1}{g_{\mathrm{YM}}^2} \qquad \mathrm{tr}\, A_\mu^4 \sim \frac{1}{g_{\mathrm{YM}}^2} \tag{1.17}$$

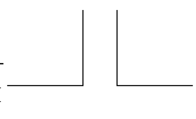

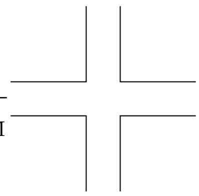

Graphically each Feynman diagram could be drawn as a fat graph (see fig. 1.4). It is easy to see that each of these fat graphs could be drawn only on a Riemann surface of a particular genus.

Again each face gives a factor of N. And if we have a graph with V vertices and E edges this graph comes with the following amplitude

$$A \sim g_{\mathrm{YM}}^{2(E-V)} N^F = N^{2-2g} \left(g_{\mathrm{YM}}^2 N\right)^{E-V} . \tag{1.18}$$

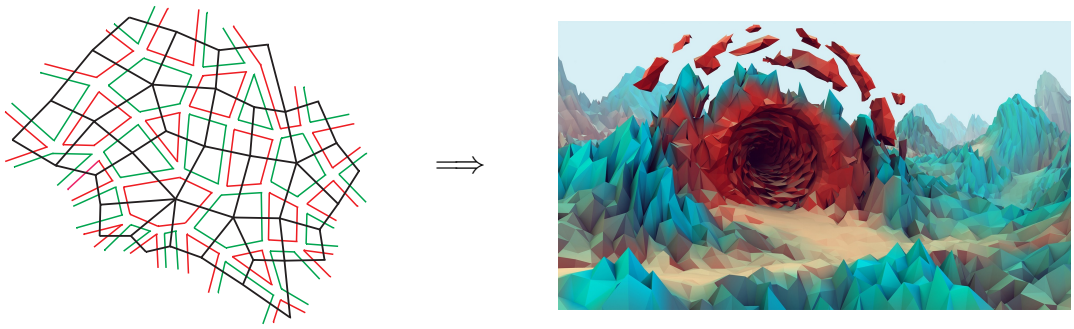

Figure 1.5: The triangulation of the plane generated by a 0-dimensional model (1.19)

Introducing $g^2_{\mathrm{YM}}N = g^2_{tH}$ the factor of N depends only on the genus of the surface and the dominant contribution is given by the planar diagrams while the other contributions are suppressed. It gives quite interesting picture — the $\frac{1}{N}$ corrections are given by the topological expansion in terms of Riemann surfaces. Thus $\frac{1}{N^2}$ corrections are given by the graphs that could be drawn on torus and etc. Each of the graphs would be a triangulation of such a surface and if we fine tune the coupling constant we would expect second order phase transition that make this triangulations smooth and give some 2d surface (see fig. 1.5). From this computation one can suggest that the actual dynamical degrees of freedom are strings (that sweep some smooth surface in 4 dimensional space-time) and after some suitable transformation or smart computation we can derive the action for these strings as it was shown in the case of vector models. But still we do not know how it should work. Thus, we still are not able to solve the Yang-Mills theory, even though we get a nice interpretation of the large N limit.

But as in the case of the vectors we can consider the zero dimensional model [17]. Namely,

$$Z(g) = \int dH_{ij} \exp\left(-\frac{1}{2}\operatorname{tr} H^2 - \frac{g}{24}\operatorname{tr} H^4\right), \quad H = H^\dagger, \tag{1.19}$$

this model has $U(N)$ invariance $H \to U^\dagger H U, U^\dagger U = 1$ would leave the action unchanged. Naively, we could have make a $U(N)$ transformation and make the action quite trivial $U_H^\dagger H U_H = \operatorname{diag}(\kappa_1, \ldots, \kappa_N)$. But the measure changes and adds some additional terms to the action. To take this into account we should compute the Fadeev-Popov determinant [18]. We pick the following gauge conditions

$$\forall a = \overline{1,N}\,, \quad [H, d_a] = 0, \quad (d_a)_{ij} = \delta_{ia}\delta_{ij}, \tag{1.20}$$

under a small gauge transformation $U \approx 1 - iA, A^\dagger = A$ the matrix H changes as $H \to H + i[A, H]$. Therefore we need to find the eigenvalues of the following equation

$$[d_a, [H, A]] = \lambda A, \quad (\delta_{ai} - \delta_{aj})\,(\kappa_i - \kappa_j)\,A_{ij} = \lambda A_{ij}. \tag{1.21}$$

The eigenvectors are $A_{ij} = A_{ji} = \delta_{ia}\delta_{jb}$ with eigenvalues $\kappa_a - \kappa_b$. The product of these eigenvalues gives a Fadeev-Popov determinant. So we come to the following action

$$Z(g) = \int \prod_{a=1}^{N} d\kappa_a \exp\left(2\sum_{a<b}\log|\kappa_a - \kappa_b| - \sum_a \left[\frac{1}{2}\kappa_a^2 + \frac{g}{24}\kappa_a^4\right]\right), \tag{1.22}$$

rescaling $\kappa_a \to \sqrt{N}x_a, g \to \frac{g_{tH}}{N}$ we get

$$Z(g_{tH}) = \int \prod_{a=1}^{N} dx_a \exp\left(2\sum_{a<b}\log|x_a - x_b| - N\sum_a \left[\frac{1}{2}x_a^2 + \frac{g_{tH}}{24}x_a^4\right]\right). \tag{1.23}$$

In the large N limit we should study a saddle point:

$$\frac{2}{N}\sum_{b\neq a}\frac{1}{x_a - x_b} = x_a + g_{tH}\frac{x_a^3}{6}, \tag{1.24}$$

if one introduces an eigenvalue destiny $\rho(x) = \frac{1}{N}\sum\limits_a \delta(x - x_a)$ we get

$$⨍\frac{\rho(y)dy}{x - y} = \frac{x}{2} + g_{tH}\frac{x^3}{12}. \tag{1.25}$$

To solve this equation we introduce an analytic function $\rho_A(z) = \int \frac{dy\rho(y)}{y-z}$. By construction this function is analytic everwhere except of the points where $\rho(x) \neq 0$ and at $z = \infty$ it should behave

$$\rho_A(z) \sim \frac{1}{z} + \ldots, \tag{1.26}$$

if the density is non-zero the analytic function $\rho(z)$ has a cut and the jump across it defines our function

$$\operatorname{Im}\rho_A(z) = \pi\rho(x), \tag{1.27}$$

and the equation (1.25) gives the real part of the function along the cut

$$\operatorname{Re}\rho_A(z) = \theta(\operatorname{Im}(\rho_A(z)))\left(\frac{z}{2} + g_{tH}\frac{z^3}{12}\right) \tag{1.28}$$

From this representation we can deduce the form of our analytic function and therefore solve the equation (1.25). First we notice that $\rho(x)$ is non-zero only on a finite interval. Indeed, otherwise the equation (1.28) would state that near the cut the analytic function $\rho_A(z = x) = \frac{x}{2} + g_{tH}\frac{x^3}{12} + i\pi\rho(x)$ that is unbound as $x \to \infty$ and it would mean that $\rho(z)$ violates (1.26). Therefore, we must conclude that there is some number $M > 0$, such that if $|x| > M$ then $\rho(x) = 0$.

We know that for a continuous function $\operatorname{supp}\rho(x) = \cup_{i\in I}[a_i, b_i]$, for physical reasons we assume that there is only one cut $[a, b]$. The function $\tilde{\rho}_A(z) = \rho_A(z) - \frac{z}{2} - g_{tH}\frac{z^3}{12} = \pm i\rho(x)$ is purely imaginary on the cut and equal to zero at $\tilde{\rho}_A(a) = \tilde{\rho}_A(b) = 0$. Hence the function $\delta(z) = \frac{\tilde{\rho}_A(z)}{\sqrt{(z-a)(b-z)}}$ does not have a cut and analytic in the whole complex plane. One can notice $|\tilde{\rho}_A(z)| \leq C|z|^2$ for big enough z the function $\tilde{\rho}(z)$ must be just a simple polynomial of degree 2 by Liouville theorem. Hence the analytic function must be of the following form

$$\rho_A(z) = \frac{z}{2} + g_{tH}\frac{z^3}{12} + \sqrt{(b-z)(z-a)}\left(dz^2 + ez + f\right), \tag{1.29}$$

and by comparing with large z expansion (1.26) we can find the unknown coefficients and finally get

$$\rho_A(z) = \frac{z}{2} + g_{tH}\frac{z^3}{12} + \sqrt{z^2 - a^2}\left(-g_{tH}\frac{z^2}{12} - \frac{1}{2} - a^2\frac{g_{tH}}{24}\right), \quad a = 2\sqrt{\frac{\sqrt{1+2g}-1}{g}}, \tag{1.30}$$

that predicts famous Wigner-Semicircle for eigenvalues distribution of a random matrix in the large N limit

$$\rho(x) = \sqrt{a^2 - x^2}\left(g_{tH}\frac{x^2}{12} + \frac{1}{2} + a^2\frac{g_{tH}}{24}\right) \tag{1.31}$$

1.3 Tensor Models

The natural generalization of the considered above models is a tensor model. We started with vector models — a model where the fundamental degrees of freedom with one index, then we generalized to the matrix one — models where the fundamental degrees of freedom having two index. The next logical step is to consider model with dergrees of freedom ψ_{abc} having three indicies [19, 14, 20, 21, 22, 23]. For example, we can consider the following model of Majorana fermions

$$S = \int dt \left[i\psi_{abc}\partial_t\psi_{abc} + V\left(\psi_{abc}\right)\right], \quad a = 1, \ldots, N_1, b = 1, \ldots, N_2, c = 1, \ldots, N_3, \tag{1.32}$$

naively the theory has $O(N)^3 = O(N_1) \times O(N_2) \times O(N_3)$ symmetry. But if there is no interaction term, the kinetic term actually does not feel the presence of three index structure in the field. We can introduce the multiindex $I = (abc)$ and see that a kinetic term has $O(N_1N_2N_3)$ symmetry. Therefore the actual symmetry of the system depends on the interaction term $V(\psi_{abc})$. If we restrict otherselves to quatric operators that are singlets under the action of $O(N)^3$ group (see fig. (1.6)) we get only 3 independent operators. The two "trivial" operators are

$$\mathcal{O}_{ds} = g_{ds}\left(\psi_{abc}\psi_{abc}\right)^2 = 0, \quad \mathcal{O}_p = g_p\psi_{abc}\psi_{abc'}\psi_{a'b'c}\psi_{a'b'c'}, \tag{1.33}$$

that we used that for grassman variables $\psi_{abc}^2 = 0$ but we can still consider such an operator if ψ_{abc} was a real valued non-grassmanian field. As one can see the first operator also respects the $O(N_1N_2N_3)$ symmetry while the second one respects the symmetry $O(N_1N_2) \times O(N_3)$. Therefore they would be described by the type of the models discussed above. Actually, one can show that these operators have vectorial large N limit.

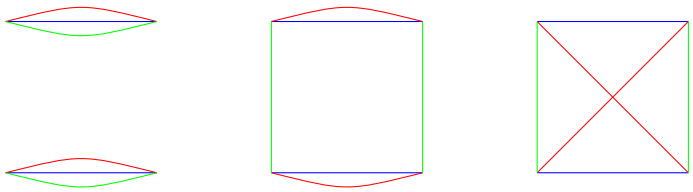

(a) (b) (c)

Figure 1.6: Diagrams of the double-trace operator (a), one of the pillow operators (b) and a tethrahedral opeartor (c).

To get a model that would have the $O(N)^3$ that is smaller than the above considered groups we should considered a little bit more complicated interaction

$$\mathcal{O}_t = g_t \phi_{abc} \phi_{ab'c'} \phi_{a'bc'} \phi_{a'b'c}, \tag{1.34}$$

one can see that each field in this interaction is connected by index contraction with other field. And the diagramatic expansion will be drastically different from the one considered in the case of vector and matrix models. Namely, one can show that the model is enhanced by so called melonic diagrams [23, 19]. The simple proof for the case of the interaction (1.34) could be found in [19].

Let us find the scaling of the coupling constants for these interactions in the large N limit. Thus let us consider the following interaction

$$H_t = \frac{g_t}{4} \psi_{a_1 b_1 c_1} \psi_{a_1 b_2 c_2} \psi_{a_2 b_1 c_2} \psi_{a_2 b_2 c_1} \ , \tag{1.35}$$

which is illustrated in fig. 1.6.

One can study this model perturbatively and find that indeed in the large N limit the melon diagrams dominates. The melonic diagrams are quite important for the study of Sachdev-Ye-Kitaev (SYK) model [24, 25]. The SYK model describes the interaction of Majorana fermion by a random quartic interaction. In contrast to the SYK model the tensor models do not contain disorder and therefore could be generalized to any dimension and field content. Also it allows the use of the usual tools of Quantum Field Theory such as ϵ-expansion. Hence, we will also consider the tensor analog of the SYK model, where

the Majorana fermions are tensors with interaction (1.34).

We can prove that only melonic diagrams dominate in the large N limit. Let us study the vacuum Feynman graphs of this theory (1.35) and take turns erasing the strands of a given color. We would get fat graphs similar to the one studied for the matrix models. To get maximal scaling, the remaining double-line diagrams are planar, since increasing their genus decreases the number of loops [22, 19]. If such a double-line diagram has n separate connected components, then the Euler theorem states that the number of index loops is given by

$$f_{rb} = 2n_{rb} + v_t, \quad \text{and} \quad f_{rg,bg} = 2n_{rg,bg} + v_t + v_p \ , \tag{1.36}$$

where v_t and v_p are the numbers of the tetrahedral and pillow vertices, respectively. Since the pillow vertex (1.6) becomes disconnected when the green strands are erased, we find that the number of separate components of the red-blue graph satisfies

$$n_{rb} \leq 1 + v_p \ . \tag{1.37}$$

On the other hand, the tetrahedral vertex stays connected when red or blue strands are erased, so that $n_{rg} = n_{bg} = 1$. These numbers are independent of v_t because the tetrahedral vertex stays connected when any color is erased

$$\begin{aligned} f_{rb} &= f_r + f_b \leq 2 + v_t + 2v_p \ , \\ f_{rg} &= f_r + f_g = 2 + v_t + v_p \ , \\ f_{bg} &= f_b + f_g = 2 + v_t + v_p \ . \end{aligned} \tag{1.38}$$

Adding these equations, we find that the *maximum* total number of closed loops is

$$f_r + f_b + f_g = 3 + \frac{3}{2} v_t + 2v_p \ . \tag{1.39}$$

This means that the maximum weight of a graph is $N^3 \lambda_t^{v_t} \lambda_p^{v_p}$. Here

$$\lambda_t = g_t N^{3/2} \ , \qquad \lambda_p = g_p N^2 \tag{1.40}$$

are the quantities which must be held fixed to achieve a smooth large N limit. These scalings apply to any rank-3 tensor theory with $O(N)^3$ symmetry and quartic interactions [22, 19, 26].[2]

The discussion above shows that the simplest melonic large N limit applies to the $g_p = 0$ model which has a purely tetrahedral interaction. The tetrahedron vertex stays connected when the strands of one color are erased and becomes a connected double-line vertex, which is found in the $O(N) \times O(N)$ symmetric matrix model with a single-trace interaction $g_t \, \mathrm{tr}(MM^T)^2$. In the $O(N)^3$ model, the tetrahedral vertex is the unique quartic vertex which is maximally single-trace.

There also some hints that these melonic limits also exist if one considers the fields ψ_{abc} to be some irreducible tensor representation of a group $O(N)$ [27]. Now one can wonder, what would happen if we consider models with much more complicated groups $O(N)^{q-1}$. Apparently, one can show that these models fall into one of these considered above groups.So let us now perform a similar analysis in the large N limit of $O(N)^{q-1}$ symmetric tensor models corresponding to higher even values of q. To achieve the simplest large N limit we will consider only the maximally single-trace interaction vertices [28], which stay connected whenever any $q-3$ colors or indices are erased. The unique such interaction vertex for $q = 6$ is shown in fig. 1.7. When colors i and j are left, the double-line vertex is of the kind found in a $O(N) \times O(N)$ symmetric matrix model with the single-trace interaction $g \, \mathrm{tr}(MM^T)^{q/2}$. Since this interaction is single-trace, the two-color graph may be drawn on a *connected* Riemann surface of genus g_{ij}, and we have the constraint

$$f_{ij} + v - e = 2 - 2g_{ij} \ , \tag{1.41}$$

[2]In the special case of quantum mechanics of Majorana fermions ψ_{abc}, the pillow operators are simply the quadratic Casimir invariants of the $O(N)$ groups. It is possible to show that their maximal values in the Hilbert space are of order N^5. This means that the energy shift for such states due to the pillow operator is $\sim g_p N^5 \sim \lambda_p N^3$. The fact that this scales as the number of degrees of freedom, N^3, is a confirmation that the scaling (1.40) is correct.

where e and v are the total numbers of the edges and the vertices. Since the graphs may be non-orientable, the possible values of the genera, g_{ij}, are $0, 1/2, 1, \ldots$. Using $e = qv/2$ and summing over all choices of remaining two colors we find

$$\sum_{i<j} f_{ij} = (q-1)(q-2) + (q-1)(q-2)^2 4v - 2\sum_{i<j} g_{ij} \ . \tag{1.42}$$

Since

$$\sum_{i<j} f_{ij} = (q-2)\sum_i f_i = (q-2) f_{\text{total}} \ , \tag{1.43}$$

we find

$$f_{\text{total}} = q - 1 + \frac{(q-1)(q-2)}{4} v - \frac{2}{q-2}\sum_{i<j} g_{ij} \ . \tag{1.44}$$

The maximum possible weight of a vacuum graph with v vertices, corresponding to all $g_{ij} = 0$, is

$$N^{q-1}\lambda^v \ , \tag{1.45}$$

and the large-N limit needs to be taken with

$$\lambda = g N^{(q-1)(q-2)/4} \tag{1.46}$$

held fixed.[3] We see that the large-N partition function of the $O(N)^{q-1}$ tensor model has the structure

$$\lim_{N\to\infty} N^{1-q} \ln Z = f(\lambda) \ . \tag{1.47}$$

Now we sketch a proof that the model with a maximally single-trace interaction vertex possesses the melonic dominance in the large N limit — for such an operator, forgetting any $q-3$ indices leads to a single-trace operator (a diagrammatic representation of this for $q = 6$ is shown in fig. 1.7). A more rigorous proof, which is however restricted to cases where $q-1$ is prime, was given in [28].

[3] This large-N scaling is the same as in the Gurau-Witten model [20, 23] for q flavors of rank $q-1$ tensors.

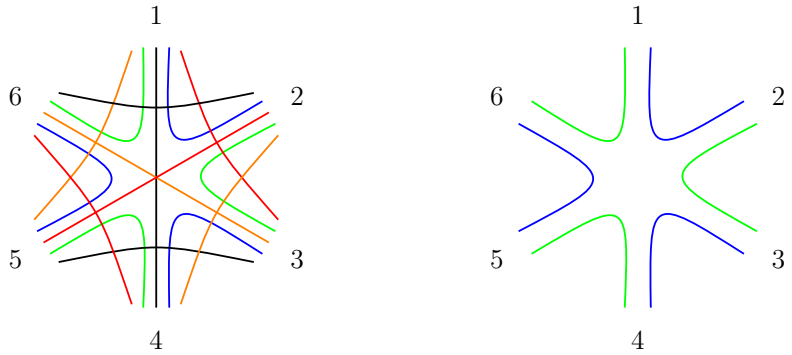

Figure 1.7: The vertex becomes single-trace if we keep any two colors.

As we have shown, the graphs giving the leading contribution in the large N limit have $g_{ij} = 0$, i.e., any choice of the double-line graph is planar. In this case we find

$$f_{\text{total}} = q - 1 + \frac{(q-1)(q-2)}{4} v \ . \tag{1.48}$$

Let us show that there is a loop passing through only 2 vertices and use the strategy analogous to that in the $q = 4$ case [19]. Let f_r denote the number of loops passing through r vertices. Since there are $\frac{q(q-1)}{2}$ strands meeting at every vertex, we find the sum rules

$$\sum f_r = f_{\text{total}} \ , \qquad \sum_r r f_r = \frac{q(q-1)}{2} v \ . \tag{1.49}$$

Combining these relations, we find

$$\sum_r \left(1 - r\frac{q-2}{2q}\right) f_r = q - 1 \ . \tag{1.50}$$

Assuming that there are no snail diagrams, so that $f_1 = 0$, we have[4]

$$\frac{2}{q} f_2 = q - 1 + \sum_{r>2} \left(r\frac{q-2}{2q} - 1\right) f_r \ . \tag{1.51}$$

For $q \geq 6$ the sum on the RHS of this equation is greater than zero. This implies that

[4]Indeed, for any snail diagram, some of the double-line subgraphs must be non-planar. For $q = 6$ this can be seen in fig. 1.7 by connecting a pair of fields and checking that some of the double-line propagators need to be twisted, thus causing non-planarity. For example, when connecting fields 1 and 3 the blue-green propagator clearly contains such a twist.

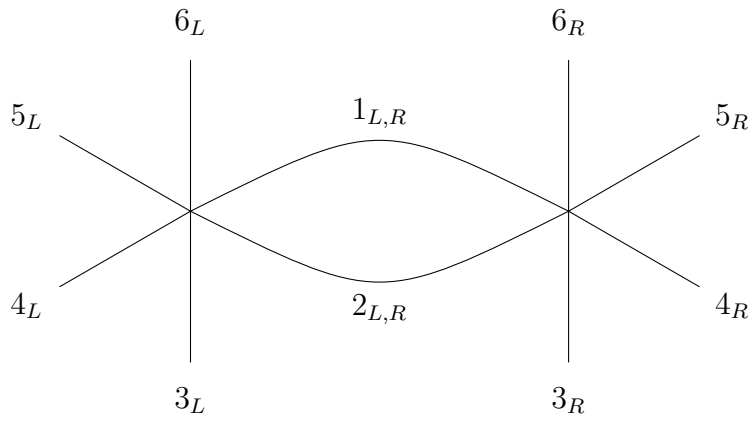

Figure 1.8: A basis pair of vertices that is connected by a pair of propagators.

there is a loop passing through exactly two vertices. We shall call them a *basis* pair of vertices. Without a loss of generality one can assume that these vertices can be drawn as in fig. 1.8. Also, for convenience we will number the fields in the vertices as in fig. 1.8. We can say that this loop, passing through two vertices, is a pair of bare propagators that connects the outputs with numbers 1_L with 1_R and 2_L with 2_R, see fig. 1.8. Now let us choose any other field in the left vertex, a_L, in the range from 3_L to q_L (for instance, we choose 3). Let us erase all colors except for $(1_L 3_L)$ and $(3_L 2_L)$. We can make a permutation of vertices such that the output will be between the first and second outputs (see fig. 1.9). However, the same does not hold for the right vertex; for example, between the 1_R and 2_R there could be another number of the field r_i, that must be non-zero.

Because the double-line graph constructed out of the colors $(1_L 3_L)$ and $(3_L 2_L)$ should be planar, the output 3_L on the left vertex can be connected **only** with these r_i outputs. It cannot be connected with the other fields, and these r_i fields in the right vertex could be connected **only** to this field 3_L on the left (for example, in fig. 1.9 the field 3_L can be connected only to the fields $3_R, 5_R, 4_R$ in order for the graph to be planar). From this we derive that for each field on the left we must assign a subset of the fields on the right. These subsets do not intersect with each other in order for the graph to be planar for any choice of the pairs of colors. From this we have

$$\sum_{a=3}^{q} r_a = q - 2 \ . \tag{1.52}$$

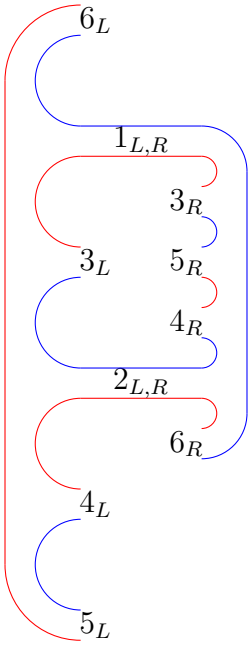

Figure 1.9: Because we consider a maximally single-trace operator, we can erase all except two colors and have a single-trace vertex. If they are connected to each other by two propagators, then the most general structure could be only the one shown in this figure. For the output 3_L in this case we assign the number $r_3 = 3$.

Since $r_a \geq 1$, this equation implies $r_a = 1$. Therefore, each output on the left is connected to the one on the right with a one-to-one correspondence. Thus, each ribbon graph, which is made by removing any set of $q-3$ colors, is planar. The graph has the structure depicted in fig. 1.10 for $q = 6$, where G_i are propagator insertions. We can connect the ends of these structures to get four other maximal vacuum diagrams and apply the same reasoning to them. From this one can see that the maximal graph must be melonic.

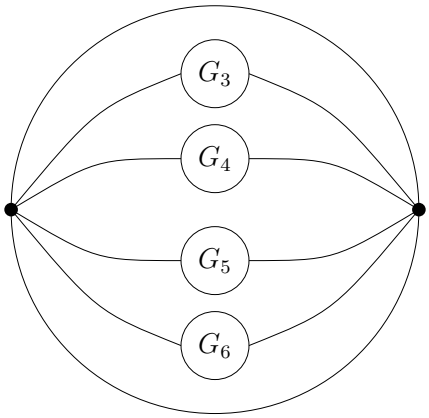

Figure 1.10: Any maximal graph for $q = 6$ must be of this form. G_i are arbitrary propagator insertions.

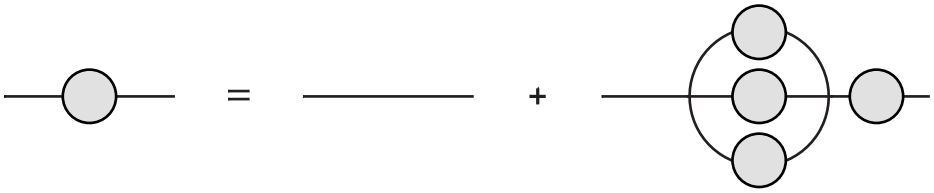

Figure 1.11: The graphic representation of Dyson-Schwinger equation for $q = 4$ melonic theory.

Thus, we have shown that, in order for a graph to have the maximal large-N scaling, it must be melonic. It is also not hard to see [28, 29] that, if we take two MST interaction vertices and connect each field from one vertex with the corresponding field in the other, we will find the maximal large-N scaling. This completes the argument that, for any MST interaction vertex, a graph has the maximal large-N scaling if and only if it is melonic.

Therefore, if have a MST interaction the system in the large N limit is dominated by the melonic diagrams. The proof provided above is purely combinatorial, therefore the same applies to any theories: in any dimension with any field content. As soon as the system provides a MST interaction in the large N limit we would get a melonic theory. Apparently, such melonic theories were firstly discussed in the context of the superfluidity [30], where it was shown that such theories are conformal even in the subleading orders in the perturbation theory. The problem in such a theories, that there some diagrams that give big corrections to the conformal solutions and therefore is no longer applicable. But one can check that in the tensor models this diagrams are suppressed in the large N limit and we have a nearly conformal field theory [19].

Here for simplicity we consider again a 0-dimensional model

$$Z(\lambda) = \int \frac{d\phi_{abc}}{\sqrt{2\pi}} \exp\left[-\frac{1}{2}\phi^2_{abc} + \frac{\lambda}{4N^{\frac{3}{2}}}\phi_{abc}\phi_{ab'c'}\phi_{a'bc'}\phi_{a'b'c}\right], \tag{1.53}$$

then we can use Dyson-Schwinger equation for this model. Namely, we notice that

$$0 = \frac{1}{Z(g_t)} \int \frac{d\phi_{abc}}{\sqrt{2\pi}} \frac{\partial}{\partial\phi_{a'b'c'}} \left(\phi_{a'b'c'} \exp\left[-\frac{1}{2}\phi^2_{abc} + \frac{\lambda}{4N^{\frac{3}{2}}}\phi_{abc}\phi_{ab'c'}\phi_{a'bc'}\phi_{a'b'c}\right]\right) =$$

$$= N^3 - N^3 G + 4\frac{\partial \log Z}{\partial \log \lambda} = 0 \tag{1.54}$$

The equation for G is easy to deduct from the diagramatic expansion of melonic theory (see fig. (1.11))

$$G(\lambda) = 1 + \lambda^2 G(\lambda)^3,$$
$$G(\lambda) = -\left(\frac{2}{3}\right)^{\frac{1}{3}} \frac{1}{\left(9\lambda^4 + \sqrt{81\lambda^8 - 23\lambda^6}\right)^{\frac{1}{3}}} - \frac{\left(9\lambda^4 + \sqrt{81\lambda^8 - 23\lambda^6}\right)^{\frac{1}{3}}}{2^{\frac{1}{3}} 3^{\frac{2}{3}} \lambda^2}, \tag{1.55}$$

substituting it in the relation for $Z(\lambda)$ we get

$$\frac{Z(\lambda)}{N^3} = \sum_{n=1}^{\infty} a_{2n} \lambda^{2n}, \quad a_{2n} = \frac{1}{8n(4n+1)} \binom{4n+1}{n} \tag{1.56}$$

Some of the results of this thesis were presented at the quantum field theory seminar in Columbia University, New York University California Institute of Technology and Moscow State University and at the conference "Quantum Gravity in Paris 2019".

2 Majorana Quantum Mechanics

Strongly interacting fermionic systems describe some of the most challenging and interesting problems in physics. For example, one of the big open questions in condensed matter physics is the microscopic description of the various phases observed in the high-temperature superconducting materials. Models relevant in this context [31, 32, 33] include the Hubbard [34, 35] and $t - J$ models [36]. The Hamiltonians of these models include the quadratic hopping terms for fermions on a lattice, as well as approximately local quartic interaction terms. The analysis of such models often begins with treating a quartic interaction term as a small perturbation. In the cases when such an expansion is not possible, for example, the fractional quantum Hall effect, one typically has to resort to numerical calculations. Fortunately, there are also fermionic systems which can be solved analytically in the strongly interacting regime, when the number of degrees of freedom is sent to infinity. Such large N systems include the Sachdev-Ye-Kitaev (SYK) models [37, 25, 38, 39, 24, 40] (see also the earlier work [41, 42]). The SYK models have been studied extensively in the recent years; for reviews and recent progress, see [43, 44, 45].

The simplest of them, the so-called Majorana SYK model [25, 40], has the Hamiltonian $H = J_{ijkl}\psi_i\psi_j\psi_k\psi_l$, which describes a large number $N_{\rm SYK}$ of Majorana fermions ψ_i (we assume summation over repeated indices throughout this work). They have random quartic couplings J_{ijkl} with appropriately chosen variance. A remarkable feature of this model is that, in the limit where $N_{\rm SYK} \to \infty$, it becomes nearly conformal at low energies. The low-lying spectrum exhibits gaps which are exponentially small in $N_{\rm SYK}$. In further work, models consisting of coupled pairs of Majorana SYK models [46, 47, 48], as well as the SYK chain models [49, 50], have produced a host of dynamical phenomena which include gapped phases and spontaneous symmetry breaking. In addition to the terms quartic in fermions, they can include quadratic terms which describe hopping between different SYK sites.

Another class of solvable large N fermionic models are those with degrees of freedom transforming as tensors under continuous symmetry groups [23, 19] (for reviews, see [14, 51]). A simple example [19] is the $O(N)^3$ symmetric quantum mechanics for N^3

Majorana fermions ψ_{abc}. In these tensor models the interaction is disorder-free, so the standard rules of quantum mechanics apply. Interestingly, the large N limit is similar to that in the SYK model because in both classes of models the perturbative expansion is dominated by the "melonic" Feynman diagrams, which can be summed [20, 52, 53, 54, 55, 56, 22, 57, 58, 28, 29, 3, 1, 59, 4]. Since the Hubbard and t-J models do not have any random couplings, the disorder-free tensor models may be viewed as their generalization, and it is interesting to investigate if they can incorporate some interesting physical effects in a solvable setting. One possibility is to interpret the three indices of the tensor ψ_{abc}, where $a, b, c = 1, \ldots, N$, as labeling the sites of a 3-dimensional cubic lattice [60]. Then the tensor models may perhaps be interpreted as non-local versions of the Hubbard model. [19] It is also natural to generalize the Majorana tensor model of [19] to the cases where the indices have different ranges: $a = 1, \ldots N_1$, $b = 1, \ldots N_2$, $c = 1, \ldots N_3$; then the model has $O(N_1) \times O(N_2) \times O(N_3)$ symmetry [61, 62] (see also [63, 28]). The traceless Hamiltonian of this model is [19, 62]

$$H = g\psi_{abc}\psi_{ab'c'}\psi_{a'bc'}\psi_{a'b'c} - \frac{g}{4}N_1N_2N_3\left(N_1 - N_2 + N_3\right) \ , \tag{2.1}$$

where $\{\psi_{abc}, \psi_{a'b'c'}\} = \delta_{aa'}\delta_{bb'}\delta_{cc'}$. If the ranks N_i are sent to infinity with fixed ratios, then the perturbation theory is dominated by the melonic graphs. However, it is also interesting to consider the cases where one or two of the N_i are not sent to infinity. Such models with $O(N) \times O(2)^2$ and $O(N)^2 \times O(2)$ symmetry were studied in [62] and were shown to be exactly solvable, with the integer energy spectrum in units of g. The $O(N) \times O(2)^2$ model has the familiar vector large N limit, where $gN = \lambda$ is held fixed. A closely related vector model, which we also study in this paper, has Majorana variables ψ_{aI}, $I = 1, \ldots, 4$, and symmetry enhanced to $O(N) \times SO(4)$:

$$H_{O(N)\times SO(4)} = \frac{g}{2}\epsilon_{IJKL}\psi_{aI}\psi_{aJ}\psi_{a'K}\psi_{a'L} \ . \tag{2.2}$$

The $O(N)^2 \times O(2)$ model, which may be viewed as a complex fermionic matrix model [62], has the 't Hooft large N limit where all the planar diagrams contribute (similar

fermionic matrix models were studied in [64, 65]).

In this paper we will carry out further analysis of the fermionic vector and matrix models. In particular, we study the large N densities of states ρ and analyze the resulting temperature dependence of the specific heat. In the matrix model case, the density of states is smooth and nearly Gaussian, which is a rather familiar behavior. In the large N vector models, we instead find a surprise: for a wide range of energies we find $\log \rho \approx -|E|/\lambda$ plus slowly varying terms. The approximately exponential growth of the density of states, discussed long ago in the context of hadronic physics and string theory [66, 67], leads to interesting behavior as the temperature approaches the Hagedorn temperature, $T_H = \lambda$. In the Majorana vector models we indeed find critical behavior as the temperature is tuned to λ, with a sharp peak in the specific heat. In the formal large N limit, the specific heat blows up as $(T_H - T)^{-2}$. This means that T_H is the limiting temperature, and it is impossible to heat the system above it. However, at any finite N, no matter how large, the specific heat does not blow up, so it is possible to reach arbitrarily large temperatures. Thus, our model provides a demonstration of how the finite N effects can smooth the Hagedorn transition.

In section 2.2, we study the $O(N) \times O(2)^2$ symmetric vector model. We find that the density of states exhibits exponential growth in a large range of energies, and match this with analytical results. In section 2.3 we study a related vector model, where the symmetry is enhanced to $O(N) \times SO(4)$. In this case, we obtain simple closed-form expressions for the large N density of states, free energy, and specific heat. In section 2.4, we consider the fermionic matrix model with $O(N)^2 \times O(2)$ symmetry and find that the spectrum now exhibits a nearly Gaussian distribution for sufficiently large N. In appendix A we study the structure of the Hilbert space of the above models, and derive the Cauchy identities from simple physical arguments.

2.1 Bound on the energy spectrum

In this section we present an energy bounds for the Hamiltonian (2.1). We note the following relation

$$H = \frac{g}{2}\sum_{abc}\left[\psi_{abc}, h_{abc}\right], \quad h_{abc} = \frac{1}{4}\partial_t\psi_{abc} = \psi_{ab'c'}\psi_{a'bc'}\psi_{a'b'c}, \tag{2.3}$$

then if we have an arbitary singlet density matrix ρ_s, that is invariant under the $O(N_1)\times O(N_2)\times O(N_3)$ rotations. One of the way to build it is to consider some representation $\mathcal{R}$ of the $O(N_1)\times O(N_2)\times O(N_3)$ in the Hilbert space $\mathcal{H}$ with a basis $|e_i\rangle, i = 1..\dim\mathcal{R}$. Then we can define the following density matrix

$$\rho_{\mathcal{R}} = \frac{1}{\dim\mathcal{R}}\sum_{i=1}^{\dim\mathcal{R}}|e_i\rangle\langle e_i|, \quad \operatorname{tr}\rho_R = 1, \quad \rho_{\mathcal{R}}^2 = \frac{1}{\dim\mathcal{R}}\rho_{\mathcal{R}}\,. \tag{2.4}$$

It is easy to see, that this density matrix is invariant under rotations $O^T\rho_{\mathcal{R}}O = \rho_{\mathcal{R}}$ for any $O\in O(N_1)\times O(N_2)\times O(N_3)$. We can calculate the expectation value of the energy for this density matrix as

$$E = \operatorname{tr}\left[\rho_s H\right] = \frac{g}{2}N_1N_2N_3\operatorname{tr}\left[\rho_s\left[\psi_{111}, h_{111}\right]\right], \tag{2.5}$$

where the sum over the repeated indexes does not depend on the indexes a, b, c. Therefore we can fix theirs value to be just some specific value and carry out the summation. Let us note that by symmetry argument we have $\operatorname{tr}\left[\rho_s\psi_{111}\right] = \operatorname{tr}\left[\rho_s h_{111}\right] = 0$. Then we can estimate the trace in the formula with the use of Heisenberg uncertantiy principle, we have

$$\operatorname{tr}\left[\rho_s\left[\psi_{111}, h_{111}\right]\right] \le 2\sqrt{\operatorname{tr}\left[\rho_s\psi_{111}^2\right]\operatorname{tr}\left[\rho_s h_{111}^\dagger h_{111}\right]} \tag{2.6}$$

$$\operatorname{tr}\left[\rho_s\psi_{111}^2\right]\operatorname{tr}\left[\rho_s h_{111}^\dagger h_{111}\right] = \frac{1}{2}\operatorname{tr}\left[\rho_s\psi_{ab1}\psi_{a1c}\psi_{1bc}\psi_{1b'c'}\psi_{a'1c'}\psi_{a'b'1}\right], \tag{2.7}$$

where we have used that $\psi^2_{111} = \frac{1}{2}$. Because the density matrix ρ is a singlet we can rotate indexes back to get

$$E^2 \leq \frac{g^2}{2N_1N_2N_3} \sum_{abc} \mathrm{tr}\left[\rho_s h^\dagger_{abc} h_{abc}\right] . \tag{2.8}$$

The square of the operator h_{abc} can be expressed as a sum of Casimir operators due to the virtue of the anticommutation relations. That gives us the bound on the energies of states in representation $\mathcal{R}$ [62]:

$$|E_{\mathcal{R}}| \leq \frac{g}{4} N_1N_2N_3 \Big(N_1N_2N_3 + N_1^2 + N_2^2 + N_3^2 - 4 - \frac{8}{N_1N_2N_3} \sum_{i=1}^{3} (N_i + 2)\, C_i^{\mathcal{R}} \Big)^{1/2} , \tag{2.9}$$

where $C_i^{\mathcal{R}}$ is the value of Casimir operator in the representation $\mathcal{R}$. For the singlet states this gives

$$|E| \leq \frac{g}{4} N_1N_2N_3 (N_1N_2N_3 + N_1^2 + N_2^2 + N_3^2 - 4)^{1/2} . \tag{2.10}$$

Since $C_i \geq 0$ this bound applies to all energies. Let us note that for $N_3 = 2$ the square root may be taken explicitly:

$$|E|_{N_3=2} \leq \frac{g}{2} N_1N_2(N_1 + N_2) . \tag{2.11}$$

For the case when $N_1 = N_2 = N_3 = N$ and $N > 2$ the bound is:

$$|E| \leq E_{bound} = \frac{g}{4} N^3 (N+2) \sqrt{N-1} \tag{2.12}$$

In the large N limit, $E_{bound} \to JN^3/4$, which is the expected behavior of the ground state energy; in the melonic limit it scales as N^3. This answer is off by 25 percent from the numerical result for the ground state energy in the SYK model [68]: $E_0 \approx -0.16 J N_{\mathrm{SYK}}$, that is believed should give the ground state energy of a tensor model. We can compare how this bound works for $O(4)^3$ model [69]. The refined bound [62] for this representation gives $|E_{(4,4,4)}| < 72\sqrt{5} \approx 160.997$, while the actual lowest state in this representation has $E \approx -140.743885$. That is in a good agreement.

2.2 The $O(N) \times O(2)^2$ model

Let us consider the Hamiltonian (2.1) in the case $N_1 = N$, $N_2 = N_3 = 2$, so that it has $O(N) \times O(2) \times O(2)$ symmetry. We may think of one of the $O(2)$ symmetries as corresponding to charge, and the other $O(2)$ as the third component of spin S_z. The first index of ψ_{abc}, which takes N values, can perhaps be interpreted as a generalized orbital quantum number.[5] It will be convenient to think of the last two indices as one composite index taking four values ($I \in \{(11), (12), (21), (22)\}$). Thus, we have Majorana fermions ψ_{aI} with anticommutation relations $\{\psi_{aI}, \psi_{bJ}\} = \delta_{ab}\delta_{IJ}$. Hence, the Hilbert space of this problem, according to the results of the appendix, has a simple decomposition in the irreducible representations of the $SO(N) \times SO(4)$ group

$$\mathcal{H} = \sum_{\mu \subset \mu_{\max} = ((2)^{N/2})} [\mu]_{O(N)} \otimes [(\mu_{\max}/\mu)^T]_{O(4)}, \tag{2.13}$$

where $[\mu]_G$ stands for a representation of the group G described by the Young Tableaux μ. In the Hilbert space of our model, the Young Tableaux of $SO(N)$ contains at most 2 columns and $N/2$ rows. In terms of fermions ψ_{aI}, the Hamiltonian (2.1) may be rewritten as

$$H = \frac{g}{2}\epsilon_{IJKL}\psi_{aI}\psi_{aJ}\psi_{a'K}\psi_{a'L} - 2g\left[(\psi_{ab1}\psi_{ab2})^2 - (\psi_{a1c}\psi_{a2c})^2\right] \ . \tag{2.14}$$

The last two terms are the charges of the two $O(2)$ groups, which break the $SO(4)$ symmetry of the first term containing the invariant tensor ϵ_{IJKL}. Each of the terms has a simple action on each of the terms of (2.13), since $O(2) \times O(2) \subset O(4)$ could be thought of as the Cartan subalgebra of $O(4)$, and we know how the Cartan subalgebra acts in the representations of $O(4)$. The normalized generators of the $SO(4)$ group have the form

$$J_{IJ} = \psi_{aI}\psi_{aJ}, \tag{2.15}$$

[5] We are grateful to Philipp Werner for this suggestion.

and can be used to split the lie algebra $\mathfrak{so}(4)$ into the direct sum of the two $\mathfrak{su}(2)$ algebras, which we have labeled by $+$ and $-$, as follows:

$$K_1^{\pm} = \frac{1}{2}J_{01} \pm \frac{1}{2}J_{23}, \quad K_2^{\pm} = \frac{1}{2}J_{02} \pm \frac{1}{2}J_{31}, \quad K_3^{\pm} = \frac{1}{2}J_{03} \pm \frac{1}{2}J_{12}. \tag{2.16}$$

It is easy to see that both sets K_i^+ and K_i^- comprise an $SU(2)$ algebra, and thus the representations of the two $SU(2)$ groups with spins $Q_+/2$ and $Q_-/2$, respectively, fully determine the representation of the $SO(4)$ group. One can derive the following algebraic relation:

$$\begin{aligned} \frac{g}{2}\epsilon_{IJKL}\psi_{aI}\psi_{aJ}\psi_{a'K}\psi_{a'L} = \frac{g}{2}\epsilon_{IJKL}J_{IJ}J_{KL} = \\ = 4g\sum_i \left[\left(K_i^+\right)^2 - \left(K_i^-\right)^2\right] = g\left[Q_+(Q_+ + 2) - Q_-(Q_- + 2)\right], \end{aligned} \tag{2.17}$$

where we have used that $\left(K_i^+\right)^2$ is the quadratic Casimir operator and we know its value in each of the representations of $SU(2)$. It is also interesting to notice that from (2.16) we have

$$\psi_{ab1}\psi_{ab2} = 2K_1^+, \quad \psi_{a1c}\psi_{a2c} = 2K_1^-. \tag{2.18}$$

This allows one to rewrite the Hamiltonian only in terms of the $SO(4)$ representations. If we have a representation with $SU(2)$ spins $(Q_+/2, Q_-/2)$, then all eigenvectors with definite $K_1^{\pm}$ are the eigenvalues of Hamiltonian with energies

$$\begin{aligned} E(Q_+, Q_-, q_+, q_-) = g\left[Q_+(Q_+ + 2) - Q_-(Q_- + 2) + 2q_-^2 - 2q_+^2\right], \\ K_1^{\pm}\left|Q_{\pm}, q_{\pm}\right\rangle = q_{\pm}\left|Q_{\pm}, q_{\pm}\right\rangle \ . \end{aligned} \tag{2.19}$$

The degeneracy of such a state is determined by the dimension of the corresponding $SO(N)$ representation. Because we know the structure of the Hilbert space (2.13), we can determine the complete structure of the spectrum. If we have a $SO(N)$ representation with a Young tableaux μ consisting of two columns of the length $\mu_1 \geq \mu_2 \geq 0$, the

corresponding representations of $SO(4)$ have $Q_+ = N - \mu_1 - \mu_2, Q_- = \mu_1 - \mu_2$, and the dimension of the representation of $SO(N)$ is [70]

$$\dim(Q_+, Q_-) = \frac{(Q_+ + 1)(Q_- + 1)N!(N+2)!}{\left(\frac{N-Q_+-Q_-}{2}\right)!\left(\frac{N+Q_+-Q_-+2}{2}\right)!\left(\frac{N-Q_++Q_-+2}{2}\right)!\left(\frac{N+Q_++Q_-+4}{2}\right)!}. \quad (2.20)$$

From this one can see that each set of pairs of non-negative integers (Q_+, Q_-) whose sum is constrained to take values $N, N-2, N-4, \ldots$ appears once. This formula allows us to study the density of states in the vicinity of the ground state and of $E = 0$.

The ground state ($E_0 = -gN(N+2)$) corresponds to the choice of $Q_+ = 0, Q_- = N$, thus $q_+ \equiv 0$ and the spectrum in its vicinity has the form,

$$E = 2gq_-^2 - gN(N+2), \quad \deg = \dim(N, 0) = 1, \quad -N \le q_- \le N. \quad (2.21)$$

The states immediately above the ground state are labeled by q_- and the gap between them is of the order $g \sim \frac{\lambda}{N}$. The next excited states correspond to the choice $Q_+ > 0$. The gap between such states and the ground state is of the order $\Delta E \sim gN \sim \lambda$ and is finite in the large N limit, but the dimension of the representation is of the order $\dim \sim N^{Q_+}$ and diverges in the large N limit. Immediately above the ground state ($\delta E \sim \lambda$, $Q_+ = 0$) the density of states may be approximated as

$$\Gamma(E) = \{\#\text{ of states: } E_{\text{st}} \le E + E_0\} = \left\{\#\text{ of } q_- : 2gq_-^2 - gN(N+2) \le E + E_0\right\} \approx \sqrt{\frac{E}{2g}},$$
$$\rho(E) = \frac{d\Gamma}{dE} \sim \sqrt{\frac{1}{8gE}}, \quad E \sim \frac{\lambda}{N}. \quad (2.22)$$

On the other hand, near $E = 0$, the logarithm of the density of states exhibits an unusual cusp-like behavior shown in figure 2.1. Another remarkable feature is its approximately linear behavior for a large range of energies.

For $|E|/\lambda$ of order 1, the dominant contributions come from the states with large charges $Q_\pm \sim \sqrt{N} \gg 1$. In this regime we can apply the Stirling approximation to the

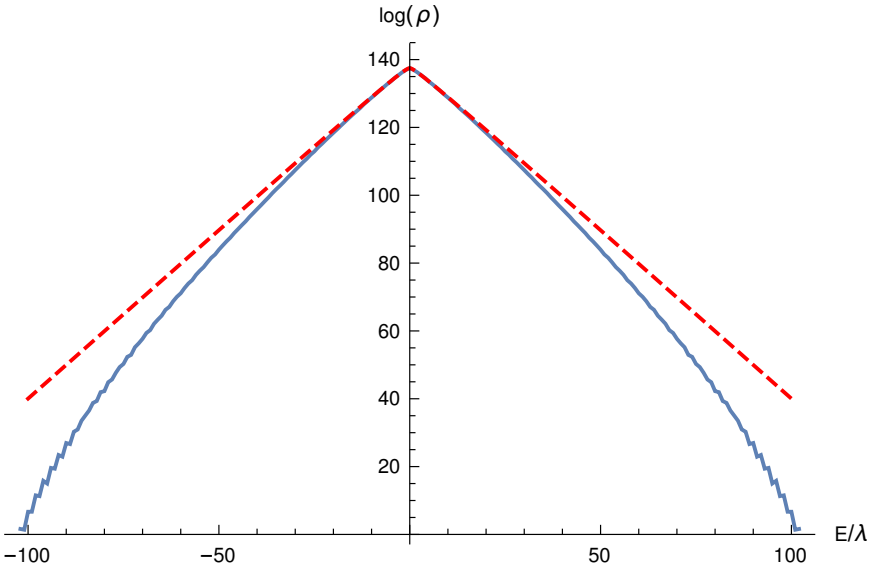

Figure 2.1: The logarithm of the density of states of the $O(N) \times O(2)^2$ vector model, shown for $N = 100$. For comparison, the large N result (2.25) is shown with a dashed line.

factorials in (2.20) to obtain

$$\dim(Q_+, Q_-) \approx 2^{2N} Q_+ Q_- \exp\left(-\frac{Q_+^2 + Q_-^2}{N}\right) . \tag{2.23}$$

To obtain the density of states in the large N limit, we introduce the variables $t_\pm = \frac{Q_\pm}{\sqrt{N}}$, $u_\pm = \frac{q_\pm}{\sqrt{N}}$, and $x = \frac{E}{\lambda}$. Then we have

$$\rho(x) \sim \int_0^\infty t_+ dt_+ \int_0^\infty t_- dt_- e^{-t_-^2 - t_+^2} \int_{-t_+}^{t_+} du_+ \int_{-t_-}^{t_-} du_- \delta\left(x + t_+^2 - t_-^2 + 2u_-^2 - 2u_+^2\right) . \tag{2.24}$$

This may be evaluated if we first perform the integrals over $T_\pm = t_\pm^2$:

$$\begin{aligned}
\rho(x) &\sim \int_{-\infty}^\infty du_+ \int_{-\infty}^\infty du_- \int_{u_+^2}^\infty dT_+ \int_{u_-^2}^\infty dT_- e^{-T_- - T_+} \delta\left(x + T_+ - T_- + 2u_-^2 - 2u_+^2\right) \sim \\
&\sim \int_0^\infty du\, e^{-2u^2 - |x|} \sqrt{|x| + u^2} + \int_{\sqrt{|x|}}^\infty du\, e^{|x| - 2u^2} \sqrt{u^2 - |x|} = \\
&= e^{-|x|} {}_1F_1\left(-\frac{1}{2}; 0; 2|x|\right) + \frac{e^{|x|}}{\sqrt{2}} \sqrt{|x|} G^{0,1}_{1,2}\left(\begin{matrix} 1 \\ -\frac{1}{2}, \frac{1}{2} \end{matrix} \middle| 2|x| \right) ,
\end{aligned} \tag{2.25}$$

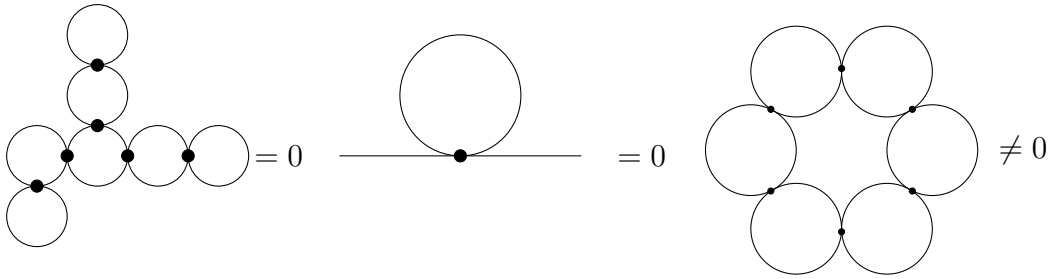

Figure 2.2: The cactus diagrams, which are of order N, vanish due to the Majorana nature of the variables. The "necklace" diagrams, are not equal to zero and give the leading contributions in the large N limit, which are of order N^0.

where the last term involves the Meijer G-function. The formula (2.25) is in good agreement with the numerical results (see figure 2.1). Expanding $\rho(x)$ near $x = 0$ we see that

$$\rho(x) \sim 1 + \frac{1}{4}\left(2\log\frac{|x|}{2} + 2\gamma - 1\right)x^2 \ , \tag{2.26}$$

which exhibits a singularity at $x = 0$: $\rho''(0)$ diverges, signaling a breakdown of the Gaussian approximation of the density of states. We also note that, for $x \gg 1$, $\rho(x) \sim |x|^{\frac{1}{2}} e^{-|x|}$.

We can present an argument for why the density of states is not Gaussian near the origin. The high temperature expansion of the free energy is:

$$\operatorname{tr} e^{-\beta H} = e^{-F}, \quad F = \sum_{n=1}^{\infty} (-1)^{n+1} \beta^n \operatorname{tr}_{\text{con}} [H^n] \ . \tag{2.27}$$

The quantity on the right-hand side of (2.27) may be computed with the use of Feynman diagrams. For vector models, the "cactus" or "snail" diagrams, shown in figure 2.2, typically dominate in the large N limit [14, 15]. However, in our problem they vanish due to the Majorana nature of the variables. Therefore, for any connected part, the trace begins with the subleading term

$$\frac{1}{N^n} \operatorname{tr}_{\text{con}} [H^n] = N^0 C_1 + N^{-1} C_2 + \dots \tag{2.28}$$

It is easy to see that C_1 comes from the necklace diagrams in figure 2.2, which give

$$C_1 = \sum_{k=1}^{\infty} \frac{(gN)^k}{k} \frac{(1+(-1)^k)}{2}, \tag{2.29}$$

where the factor of $\frac{1}{k}$ comes from the symmetries of the necklace diagrams. These necklace diagrams may be interpreted as trajectories of a particle propagating in one dimension. Introducing the 't-Hooft coupling $\lambda = gN$ and taking the large N limit while keeping λ finite, we calculate the free energy,

$$F = \sum_{k=1}^{\infty} \frac{(\beta\lambda)^k}{k} \frac{(1+(-1)^k)}{2} = -\frac{1}{2}\left(\log(1+\beta\lambda) + \log(1-\beta\lambda)\right) = -\frac{1}{2}\log\left[1-(\beta\lambda)^2\right]. \tag{2.30}$$

The inverse Laplace transformation with respect to β yields the density of states $\log \rho(E) \sim a - \frac{|E|}{\lambda}$. From this one can derive that the distribution must have a Laplace-like form, and this agrees with the numerical results.

Let us review the physical effects of the approximately exponential behavior of ρ. In the canonical ensemble, the partition function as a function of inverse temperature β is

$$Z = \int_0^{\infty} d\tilde{E}\rho(\tilde{E})e^{-\beta\tilde{E}}\ , \tag{2.31}$$

where we define $\tilde{E} = E - E_0$ to be the energy above the ground state. If $\rho(\tilde{E}) \sim e^{\tilde{E}/T_H}$, then Z diverges for $\beta < \beta_H$, where $\beta_H = 1/T_H$; this is the well-known Hagedorn behavior. For our vector model, the Hagedorn temperature is $T_H = \lambda$. However, the divergence is cut off by the fact that $\rho(\tilde{E})$ grows approimately exponentially only from some initial value $\tilde{E}_0$ up to some critical value $\tilde{E}_c$, as shown in figure 2.1. The contribution to Z from this region of energies is

$$Z_{\text{Hagedorn}} \sim \frac{e^{-(\beta-\beta_H)\tilde{E}_0} - e^{-(\beta-\beta_H)\tilde{E}_c}}{\beta-\beta_H}. \tag{2.32}$$

The presence of the denominator produces a logarithmic term in the free energy, but

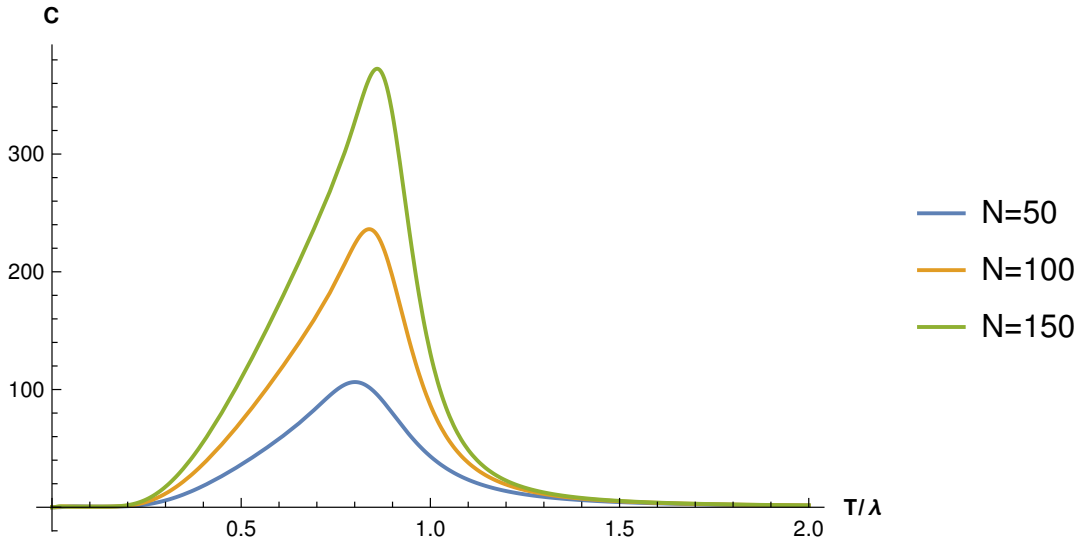

Figure 2.3: The plot of specific heat C for the $O(N) \times O(2)^2$ model, as a function of temperature T/λ, for $N = 50, 100, 150$. The specific heat has a pronounced peak which gets closer to $T/\lambda = 1$ as N grows.

it is cut off by the numerator before it diverges. It follows that the specific heat $C = -T\partial^2 F/\partial T^2$ may be approximated by

$$C = \frac{1}{\left(\frac{T}{T_H} - 1\right)^2} + \frac{\delta\tilde{E}^2}{4T^2 \sinh^2\left(\frac{\delta\tilde{E}}{2}\left[\frac{1}{T} - \frac{1}{T_H}\right]\right)}, \quad \delta\tilde{E} = \tilde{E}_c - \tilde{E}_0, \tag{2.33}$$

where $\delta\tilde{E}$ goes to infinity in the large N limit and the second term vanishes. Thus, for large enough N, there should be a clear peak in the specific heat. This simple analytic argument for the existence of a peak is supported by the numerical plots of specific heat shown in figure 2.3. For any finite N, the height of the peak in C is finite, so that it is possible to heat the system up to any temperature. However, in the formal large N limit, the specific heat blows up as $(T - T_H)^{-2}$ so the Hagedorn temperature is the limiting temperature. This shows that the finite N effects smooth out the Hagedorn transition.

2.3 The $O(N) \times SO(4)$ model

In this section we study the simpler vector model where we retain only the first term in the Hamiltonian (2.14). The symmetry is then enhanced to $O(N) \times SO(4)$ symmetry. Since $SO(4) \sim SU(2) \times SU(2)$, we can think of one of the $SU(2)$ groups as corresponding

to the spin of the fermions. From the previous section we know that the spectrum of the model may be expressed in terms of the two $SU(2)$ spins, $Q_\pm/2$, where $Q_\pm$ are non-negative integers whose sum is constrained to take values $N, N-2, N-4, \ldots$. The energies and their degeneracies are:

$$E(Q_+,Q_-) = g\left[Q_+(Q_++2) - Q_-(Q_-+2)\right] = g(Q_+-Q_-)(Q_++Q_-+2)\ ,$$
$$\deg(Q_+,Q_-) = \frac{(Q_++1)^2(Q_-+1)^2 N!(N+2)!}{\left(\frac{N-Q_+-Q_-}{2}\right)!\left(\frac{N+Q_+-Q_-+2}{2}\right)!\left(\frac{N-Q_++Q_-+2}{2}\right)!\left(\frac{N+Q_++Q_-+4}{2}\right)!}\ . \quad (2.34)$$

The ground state corresponds to $Q_+=0, Q_-=N$; it has energy $E_0=-\lambda(N+2)$ and degeneracy $N+1$. For the series of states $Q_+=m$, $Q_-=N-m$, where m are positive integers much smaller than N, we find the excitation energies $E_m - E_0 \approx 2m\lambda$. These states are equally spaced in the large N limit, and their degeneracies behave for large N as $\frac{N^{1+m}}{(m+1)!}$. Thus, the density of states $\rho(E)$ near the lower edge grows as $\sim N^{\frac{E-E_0}{2\lambda}}$. This edge behavior does not have a smooth large N limit; it is very different from the random matrix behavior $\sim\sqrt{E-E_0}$ which is observed in the SYK model.

Just like for the $O(N)\times O(2)^2$ model, we find that the large N limit of the $O(N)\times SO(4)$ model has a nearly linear behavior of the logarithm of density of states for a certain range of E/λ (see figure 2.4). Let us study this function more precisely near the middle of the distribution, following the procedure used in the previous section. We include the contributions of representations where $Q_\pm\sim\sqrt{N}$, and introduce variables $x_\pm = Q_\pm/\sqrt{N}$. The energy is then given by $E=\lambda\left(x_+^2-x_-^2\right)$. Using the Stirling approximation for the factorials in (2.34), we find that the density of states is

$$\rho(E) \sim \int_0^\infty dx_+ \int_0^\infty dx_- x_+^2 x_-^2 e^{-(x_+^2+x_-^2)}\delta\left(E-\lambda\left(x_+^2-x_-^2\right)\right)\ . \quad (2.35)$$

This integral can be evaluated in closed form:

$$\rho(E) = 2^{2N}\frac{|E|}{\pi\lambda^2}K_1\left(\frac{|E|}{\lambda}\right)\ , \quad (2.36)$$

where K_1 is the modified Bessel function, and the normalization is such that ρ integrates

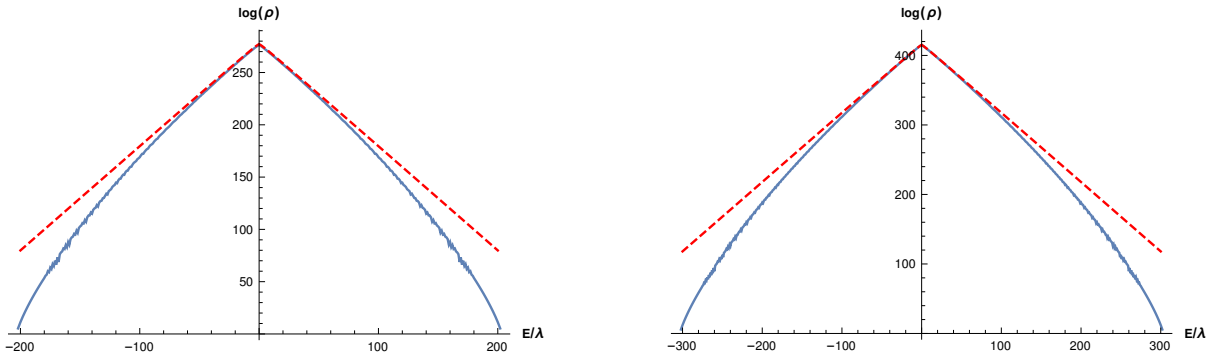

Figure 2.4: The logarithm of the density of states for the $O(200) \times SO(4)$ (on the left) and $O(300) \times SO(4)$ (on the right) models with Hamiltonian (2.2). For comparison, the large N result (2.36) is shown with a dashed line.

to the total number of states, 2^{2N}. Plotting (2.36), we see that in the range where $N^{-1}\langle |E|/\lambda \langle N$, it is close to the numerical results in figure 2.4. The expansion of (2.36) near the origin,

$$\rho = 2^{2N}\frac{1}{\pi\lambda}\left(1+\frac{1}{4}(2\log\frac{|x|}{2}+2\gamma-1)x^2+O(\log|x|x^4)\right)\,, \quad x=\frac{E}{\lambda}\,, \tag{2.37}$$

shows that $\rho''(0)$ diverges. The reasons for this unusual behavior in the large N limit were discussed in the previous section. We also note that $\rho \sim |x|^{1/2}e^{-|x|}$ for $|x| \gg 1$.

The approximation (2.36) can be used to get the large N limit of the free energy:

$$F(T) = -T\log Z(T) = \frac{3}{2}T\log\left(\frac{\lambda^2}{T^2}-1\right), \tag{2.38}$$

up to an additive term linear in T. The specific heat diverges at the Hagedorn temperature $T_H = \lambda$,

$$C(T) = -T\frac{\partial^2 F}{\partial T^2} = \frac{3\lambda^2\,(T^2+\lambda^2)}{(T^2-\lambda^2)^2}\,. \tag{2.39}$$

Note that this is of order N^0 for $T < T_H$, as usual for the Hagedorn transition. For a finite N, the divergence is cut off, but the peak is prominent; see figure 2.5.

We can write the Hamiltonian (2.2) in terms of complex fermions by introducing the following operators:

$$c_{a1} = \frac{1}{\sqrt{2}}\left(\psi_{a1}+i\psi_{a2}\right), \qquad \bar{c}_{a1} = \frac{1}{\sqrt{2}}\left(\psi_{a1}-i\psi_{a2}\right)\,,$$

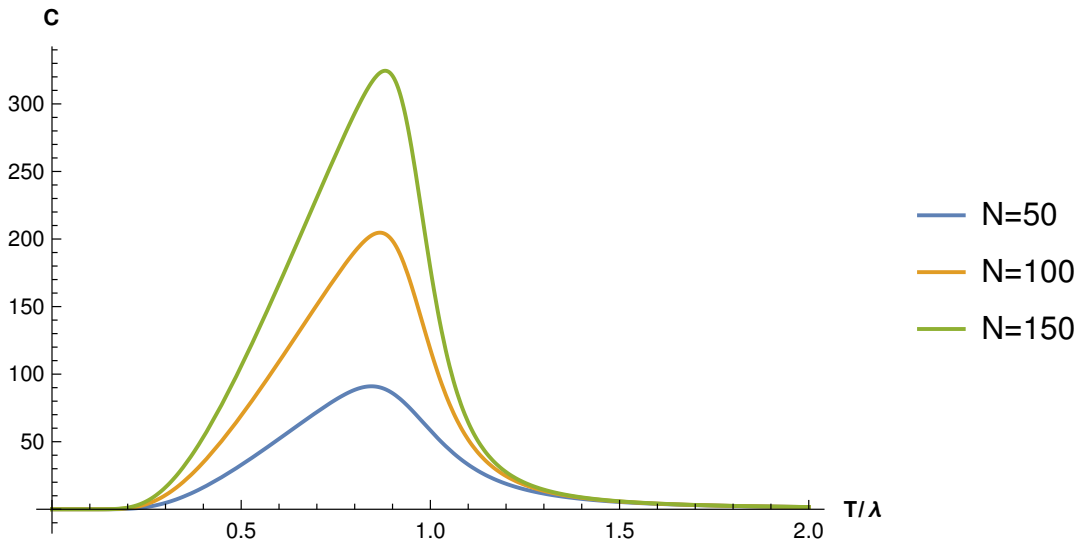

Figure 2.5: The plot of specific heat C for the $O(N) \times SO(4)$ model, as a function of temperature T/λ, for $N = 50, 100, 150$. The peak in specific heat gets closer to $T/\lambda = 1$ as N increases.

$$c_{a2} = \frac{1}{\sqrt{2}} \left(\psi_{a3} + i\psi_{a4}\right), \qquad \bar{c}_{a2} = \frac{1}{\sqrt{2}} \left(\psi_{a3} - i\psi_{a4}\right) \ . \tag{2.40}$$

We may think of $a = 1, \ldots N$ as a 1-dimensional lattice index, so that there are two complex fermions at each lattice site. The lattice Hamiltonian is then non-local:[6]

$$H_{O(N)\times SO(4)} = -\frac{gN}{2} - \frac{gN^2}{4} + g\bar{c}_{a1}\bar{c}_{a2}c_{b1}c_{b2} + g\left(\sum_a \vec{J}_a\right)^2 , \qquad \vec{J}_a = \bar{c}_{a\alpha}\vec{\sigma}_{\alpha\beta}c_{a\beta} \ . \tag{2.41}$$

It is then not surprising that this model exhibits a phase transition in the large N limit: it corresponds to the limit where the lattice becomes infinitely long.

For the Hilbert space of the model containing fermions ψ_{iJ}, the quadratic Casimirs of the $SO(N)$ and $SO(4)$ symmetry groups satisfy the constraint [62],

$$C_2^{SO(N)} + C_2^{SO(4)} = \frac{1}{2}N\left(N+2\right). \tag{2.42}$$

In later sections we will be interested in the $SO(N)$ invariant states, and (2.42) implies that these states must have $C_2^{SO(4)} = N\left(\frac{N}{2}+1\right)$. The corresponding representations of

[6]This Hamiltonian should be contrasted with the local fermionic $O(N)$ chains, where there are N fermions at each lattice site.

$SU(2) \times SU(2)$ have spins $j_+ = 0, j_- = N/2$ or $j_+ = N/2, j_- = 0$. The first set of $N+1$ states has the lowest energy, while the second set of $N+1$ states has the highest energy. In total there are $2N+2$ states which are $SO(N)$ invariant.

We may also work in terms of complex fermions c_{ai}, (2.40), which are naturally acted on by $SU(N) \times SU(2) \times U(1)$. The $SU(N)$ acts on the first index, $SU(2)$ on the second, and $U(1)$ by overall phase rotation. On the Hilbert space constructed this way, the quadratic Casimirs satisfy the constraint [62]

$$C_2^{SU(N)} + C_2^{SU(2)} = \frac{N+2}{4N}(N^2 - Q^2) \ , \tag{2.43}$$

where Q is the $U(1)$ charge. This implies that the $SU(N)$ invariant states with $Q = 0$ must be in the spin $N/2$ representation of $SU(2)$. Therefore, there are $N+1$ such states. There are also two $SU(N) \times SU(2)$ invariant states, which have $Q = \pm N$. Thus, the total number of $SU(N)$ invariant states is $N+3$.

We can generalize such a model to the case of $O(N) \times SO(2M)$ with the Hamiltonian

$$H = i^M \frac{g}{M!} \epsilon_{j_1 \dots j_{2M}} \psi_{a_1 j_1} \psi_{a_1 j_2} \dots \psi_{a_M j_{2M-1}} \psi_{a_M j_{2M}}. \tag{2.44}$$

This may be expressed via the higher Casimirs operators of the $SO(2M)$ group. For the case of $M = 1$ we would have a simple model $O(N) \times SO(2)$,

$$H = ig\epsilon_{ij}\psi_{ai}\psi_{aj} = 2ig\psi_{a1}\psi_{a2} = 2g\left(\bar{c}_a c_a - \frac{N}{2}\right), \quad c_a = \frac{\psi_{a1} + i\psi_{a2}}{\sqrt{2}}. \tag{2.45}$$

The spectrum consists of half-integers running from $E = -\frac{N}{2} + q$ and the degeneracy $\deg(E) = \frac{N!}{q!(N-q)!}$ corresponds to the representation of the fully antisymmetric tensors.

2.4 Fermionic matrix models

In this section we study the fermionic matrix models with $O(N_1) \times O(N_2) \times O(2)$ symmetry [62]. They contain $2N_1N_2$ Majorana fermions that are coupled by the Hamil-

tonian

$$H = g\psi_{abc}\psi_{ab'c'}\psi_{a'bc'}\psi_{a'b'c} - \frac{g}{2}N_1N_2\left(N_1 - N_2 + 2\right) \ . \tag{2.46}$$

The direct numerical diagonalization of this Hamiltonian is hampered by the exponential growth of the dimension of Hilbert space as $2^{N_1N_2}$. For $N_1 = N_2 = 6$ it is $\approx 7 \cdot 10^{10}$, while for $N_1 = N_2 = 8$ it is $\approx 2 \cdot 10^{18}$ states. For the former we were able to carry out Lanczos diagonalization giving the wave functions and energies of the lowest few states.

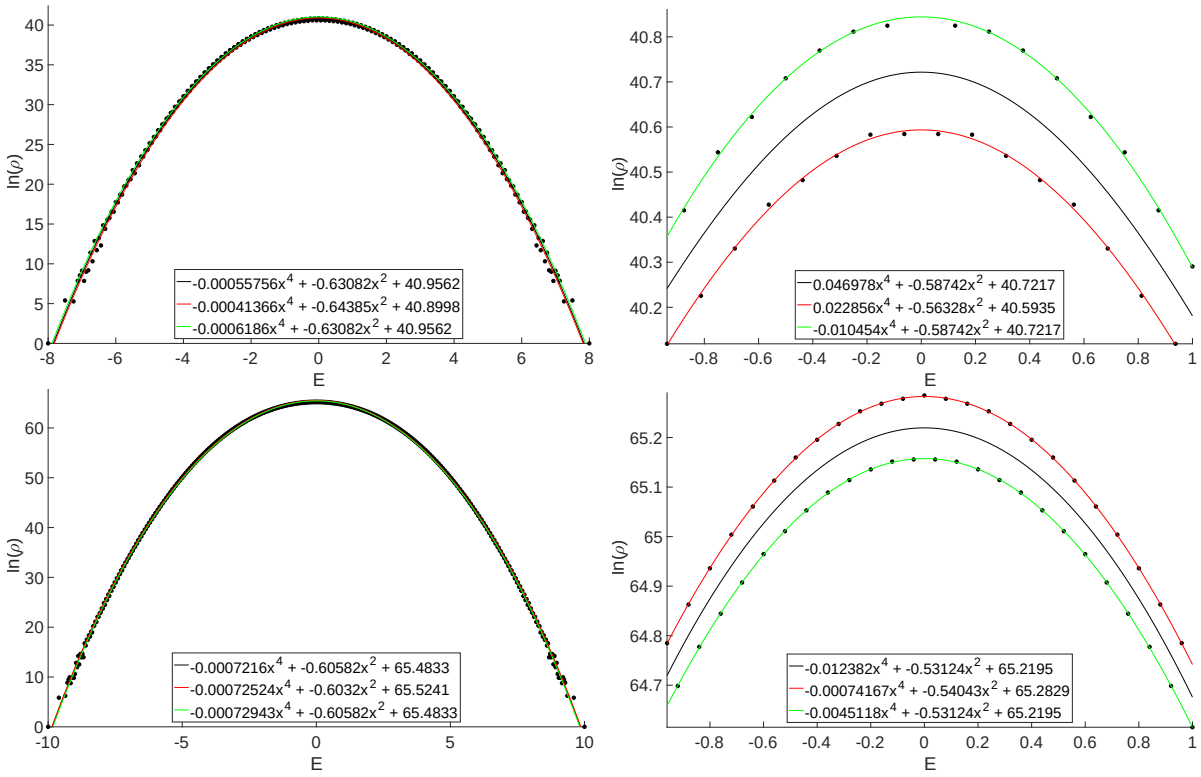

Figure 2.6: The spectrum for $N_1 = N_2 = 8$ and $N_1 = N_2 = 10$ on the top and the bottom row. One can see that the spectrum is Gaussian, but split into two branches. The fit is quite close to the theoretical predictions.

Fortunately, the Hamiltonian (2.46) may be expressed in terms of the $U(1)$ charge Q, the Casimir operators of the $SO(N_i)$ symmetry groups, as well as of the $SU(N_1)$ group which acts on the spectrum [62]:

$$H = -2g\left(4C_2^{SU(N_1)} - C_2^{SO(N_1)} + C_2^{SO(N_2)} + \frac{2}{N_1}Q^2 + (N_2 - N_1)Q - \frac{1}{4}N_1N_2(N_1 + N_2)\right) . \tag{2.47}$$

This analytical expression allows us to proceed to higher values of N_i. In general, all the

energy eigenvalues are integers in units of g, but finding their degeneracies requires some calculations via the group representation theory.

For $N_1 = N_2 = N$, we find that near $E \approx 0$ the density of states may be approximated by the Gaussian:

$$\log \rho(E) = N^2 \log 2 - \frac{1}{2}\left(\frac{E}{\lambda N}\right)^2 , \tag{2.48}$$

where $\lambda = gN$ is the 't-Hooft coupling, which is held fixed as $N \to \infty$. We find nice agreement, which is shown for $N_1 = N_2 = 8$ and $N_1 = N_2 = 10$ in figure 2.6 and for $N_1 = N_2 = 9$ in figure 2.7.

To demonstrate the validity of this approximation, let us compute

$$\langle E^n \rangle = \int dE\, \rho(E)\, E^n = \frac{\mathrm{tr}\,[H^n]}{\mathrm{tr}\,[1]} . \tag{2.49}$$

This may be computed via the path integral

$$\frac{\mathrm{tr}\,[H^n]}{\mathrm{tr}\,[1]} = \int \mathcal{D}\psi_{ab}\, H^n \, \exp\left(-\int_0^\beta d\tau\, \psi_{ab}(\tau)\, \partial_\tau \psi_{ab}(\tau)\right) . \tag{2.50}$$

Therefore we can use standard Feynman techniques with the propagator $\langle \psi_{ab}\psi_{a'b'}\rangle = \frac{1}{2}\delta_{aa'}\delta_{bb'}$ and H as an interaction vertex. Since H has the form of a single-trace operator in the large N limit, this product is dominated by the planar diagrams and moreover by the disconnected parts. From this point of view one can see that

$$\frac{\mathrm{tr}\,[H^{2n}]}{\mathrm{tr}\,[1]} = \frac{(2n)!}{2^n n!}\sigma_E^2, \quad \text{where} \quad \sigma_E^2 = \frac{\mathrm{tr}\,[H^2]}{\mathrm{tr}\,[1]} = \; H \; H. \tag{2.51}$$

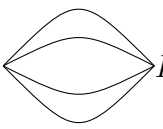

Then one can invert (2.49) and get that $\rho(E)$ is the Gaussian distribution

$$\rho(E) = \frac{1}{\sqrt{2\pi\sigma_E^2}} \exp\left(-\frac{E^2}{2\sigma_E^2}\right) . \tag{2.52}$$

The second moment, σ_E^2, is easy to compute using the diagrammatic technique: $\sigma_E^2 =$

$g^2\,(N^4 - N^3) \approx (\lambda N)^2$. To get the higher order corrections to the distribution function, we can continue calculating the energy moments, or we can instead simply compute the free energy and perform the inverse Laplace transformation to get the energy distribution. To be more precise, the free energy is defined as

$$F(\beta) = -\log \operatorname{tr} e^{-\beta H} = -\log \int dE\, \rho(E)\, e^{-\beta E}. \tag{2.53}$$

This gives us a formula to compute $F(\beta)$ as a sum of the connected diagrams with H as an interaction vertex

$$F(\beta) = \sum_{n=1}^{\infty} \beta^n \operatorname{tr} \left(H^n\right)_{\text{con}} = \beta^2 \operatorname{tr} \left(H^2\right)_{\text{con}} + \beta^4 \operatorname{tr} \left(H^n\right)_{\text{con}} + \dots \tag{2.54}$$

Continuing this function to imaginary temperatures $\beta \to i\beta$, we can use the inverse Fourier transform

$$\rho(E) = \int \frac{d\beta}{2\pi} e^{i\beta E} e^{-F(i\beta)} = \int \frac{d\beta}{2\pi} e^{i\beta E} e^{-\beta^2 \operatorname{tr}\left(H^2\right)_{\text{con}} - \beta^4 \operatorname{tr}\left(H^4\right)_{\text{con}} + \dots}. \tag{2.55}$$

This integral can be calculated with the use of general diagrammatic technique, where iE is the source for the energy, $\operatorname{tr}(H^2)_{\text{con}}$ is the propagator, and $\operatorname{tr}\left(H^4\right)_{\text{con}}$ and the higher correlators are the vertices. By using these procedures we can compute the connected contribution. It is easy to compute the leading contributions to the connected trace of H^4,

$$\left(\operatorname{tr} H^4\right)_{\text{con.}} = \left(\operatorname{tr} H^4\right) - 3\left(\operatorname{tr} H^2\right)^2_{\text{con.}} = 8g^4N^6\ . \tag{2.56}$$

After that we can restore

$$\log \rho(E) = N^2 \log 2 - \frac{1}{2}x^2 - \frac{1}{12N^2}x^4 + \dots, \quad E = gN^2 x\ . \tag{2.57}$$

Comparing this expression with the numerical data we find a nice agreement between these two formulas.

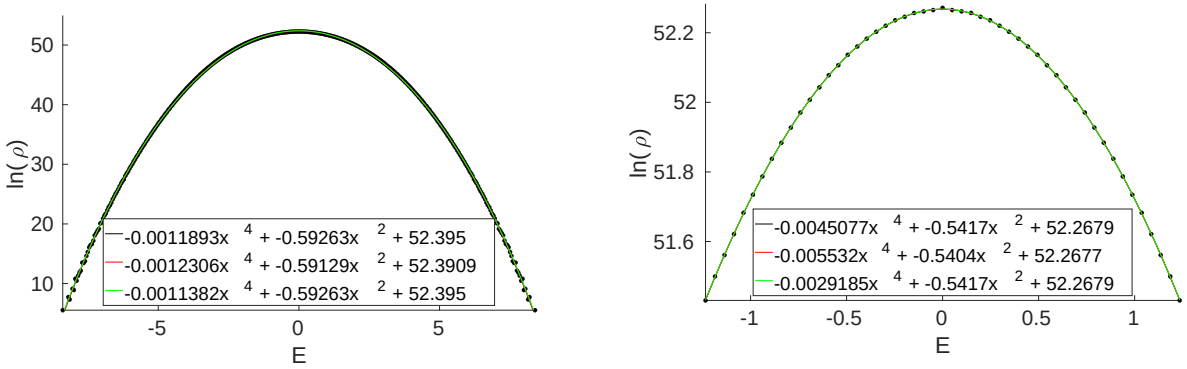

Figure 2.7: The spectrum for $N_1 = N_2 = 9$. As one can see it has the same features as for $N_1 = N_2 = 8$ and $N_1 = N_2 = 10$, but there is no separation between the even and the odd energy sectors. It could indicate that this difference has a purely group theoretic explanation.

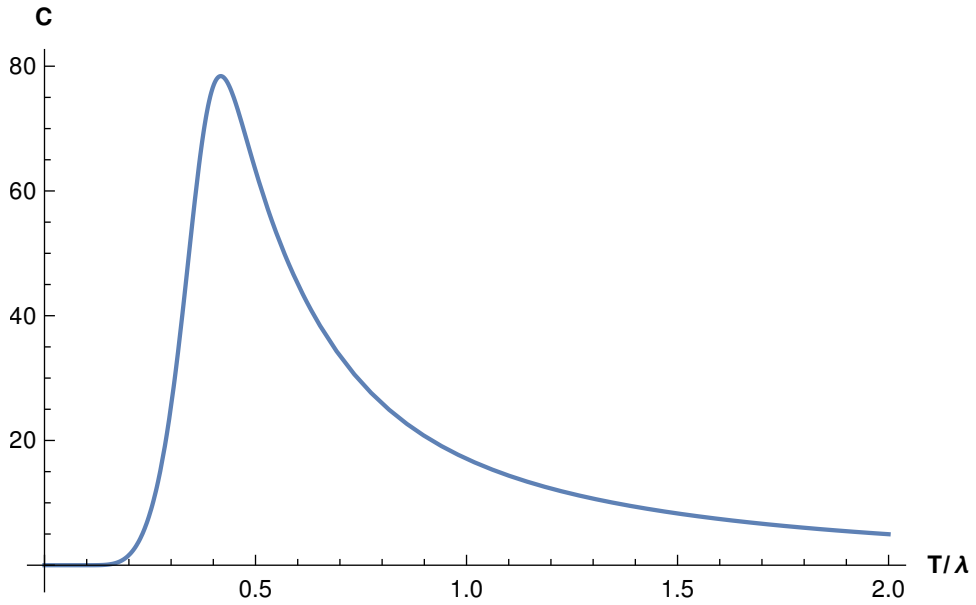

Figure 2.8: The specific heat as a function of temperature for the $O(N)^2 \times O(2)$ matrix model with $N = 10$. The low-temperature peak is due to the discreteness of the spectrum. At higher T, the specific heat falls off polynomially with the power $\alpha = \frac{d \log C}{d \log T} = -1.98$, close to that predicted by the analytic result (2.60).

Let us note the splitting between the even and the odd energies, which is seen in figure 2.6 but absent in figure 2.7. These two sets of energies are distinguished by the value of

$$P_C = (-1)^{\frac{1}{2}\left(C_{O_1}^2 - C_{O_2}^2\right)} . \tag{2.58}$$

The trace of this operator counts the difference between the number of these branches. The trace of this operator over the whole space can be computed via the representation theory and is equal to $\operatorname{tr} P_C = 2^{2N^2-N+1}$.

We can study the thermodynamic properties of the matrix model in a similar fashion as in the case of the vector models. The behavior of the system would be analogous to a system of the spins in an external magnetic field. The partition function is

$$Z(T) = \int_{-\infty}^{\infty} dE e^{-\frac{E}{T}} e^{-\frac{E^2}{2\lambda^2 N^2}} \sim e^{\frac{\lambda^2 N^2}{2T^2}}, \quad F = -T \log Z(T) = -\frac{\lambda^2 N^2}{2T}, \tag{2.59}$$

and the heat capacity C is

$$C = -T\frac{\partial^2 F}{\partial T^2} = \frac{\lambda^2 N^2}{T^2} . \tag{2.60}$$

This behavior is nicely captured by the numerical results shown in figure 2.8. Note that the peak near $T_{\text{peak}} \sim g \sim \frac{\lambda}{N}$ is due to the discreteness of the spectrum; it may be seen if we consider the contributions coming only from the ground state and the first excited state.

2.5 Decomposing the Hilbert Space

In this section we will review the structure of the Hilbert space of the $O(N_1) \times O(N_2) \times O(2)$ symmetric Majorana models. We will study the irreducible representation of this algebra, which is spanned by $2 \times N_1 \times N_2$ Majorana fermions ψ_{abc} subject to the anticommutation relations (2.46). To simplify the structure we introduce the Dirac

fermions by combining two Majorana fermions,

$$c_{ab} = \frac{1}{\sqrt{2}}\left(\psi_{ab1} + i\psi_{ab2}\right),\ \bar{c}_{ab} = \frac{1}{\sqrt{2}}\left(\psi_{ab1} - i\psi_{ab2}\right),$$
$$\{c_{ab}, \bar{c}_{a'b'}\} = \delta_{aa'}\delta_{bb'},\ \{c_{ab}, c_{a'b'}\} = \{\bar{c}_{ab}, \bar{c}_{a'b'}\} = 0. \tag{2.61}$$

These relations respect the larger symmetry group $U(N_1)_a \times U(N_2)_b$, and could be considered as symmetries of the Hilbert space, in contrast to the Hamiltonian (2.46) which does not respect these symmetries. We can now try to decompose the Hilbert space in terms of the representations of these unitary groups using the character theory [71]. We notice that the generator of the $U(N_1)_a$ and $U(N_2)_b$ groups could be rewritten in the following form

$$J_T^A = \frac{1}{2}T^A_{aa'}\left[\bar{c}_{ab}, c_{a'b}\right], \quad J_T^B = \frac{1}{2}T^B_{bb'}\left[\bar{c}_{ab}, c_{ab'}\right], \tag{2.62}$$

where $T^{A,B}_{aa'}$ are hermitian matrices and can be considered as elements of the $\mathfrak{u}(N_i)$ algebra. Then the operators $J_T^{A,B}$ are the corresponding representations of these elements of the $\mathfrak{u}(N_i)$ algebra. Hence, a general element of the $U_a(N_1) \times U_b(N_2)$ group, acting on the Hilbert space, is

$$g = e^{iT^A}, \quad \rho_\psi(g) = e^{\frac{i}{2}T^A_{aa'}[\bar{c}_{ab}, c_{a'b}]}. \tag{2.63}$$

Therefore we can compute the trace of this operator in the Hilbert space, and it is equal to the following:

$$\chi_{\mathcal{H}}(T^A, T^B) = \mathrm{tr}\left(e^{\frac{i}{2}T^A_{aa'}[\bar{c}_{ab}, c_{a'b}] + \frac{i}{2}T^B_{bb'}[\bar{c}_{ab}, c_{ab'}]}\right). \tag{2.64}$$

We can study this trace rigorously and expand this exponent to compute the trace order by order. Since the $T^{A,B}$ are hermitian matrices, we can diagonalize the matrix by some unitary transformation of the Hilbert space. Therefore, we can just consider the case

where the matrices $T^{A,B}$ are diagonal

$$T^A_{aa'} = x_a \delta_{aa'}, \quad T^B_{bb'} = y_b \delta_{bb'}. \tag{2.65}$$

This gives the following formula for the character

$$\chi_{\mathcal{H}}(x_a, y_b) = \mathrm{tr}\left(e^{\frac{i}{2}\sum_{a,b}(x_a+y_b)[\bar{c}_{ab}, c_{ab}]}\right). \tag{2.66}$$

Since each of the $N_1 N_2$ pairs $c_{ab}, \bar{c}_{ab}$ and $[\bar{c}_{ab}, c_{ab}]$ acts diagonally on the Hilbert space, the trace for each of the ab effectively decouples from the rest making the computation straightforward,

$$\chi_{\mathcal{H}}\left(x_a, y_b\right) = \prod_{a,b=1}^{N_1,N_2}\left(e^{-\frac{i}{2}(x_a+y_b)} + e^{\frac{i}{2}(x_a+y_b)}\right) = \prod_{a,b=1}^{N,M} 2\cos\left[\frac{x_a+y_b}{2}\right]. \tag{2.67}$$

One can see that this integral has the correct normalization, because if $x_a = y_b = 0$ we restore the dimension of the space and $\chi_{\mathcal{H}} = 2^{N_1 N_2}$ as it should be. We can decompose this product in terms of the Schur polynomials, which are the characters of the irreducible representations of $U(N_i)$. Fortunately, this problem is easily solved with the use of the dual Cauchy identity [72]

$$\prod_{a,b=1}^{N_1,N_2}\left(e^{-\frac{i}{2}(x_a+y_b)} + e^{\frac{i}{2}(x_a+y_b)}\right) = \sum_{\lambda \subset (N_1^{N_2})} s_\lambda\left(e^{ix_a}\right) s_{\lambda^T}\left(e^{iy_b}\right), \tag{2.68}$$

where the λ is the Young Tableaux and λ^T is the transpose. Therefore the Hilbert space has a very simple decomposition in terms of the $U(N_i)$ groups. To each Young tableaux $\lambda \subset (N_1^{N_2})$ with no more than N_1 columns and N_2 rows we assign only one $U_a(N_1)$ representation; this state is an irreducible representation for the second unitary group described by the transposed Young Tableaux λ^T: $\mathcal{H} = \sum_{\lambda \subset (N_1^{N_2})} [\lambda] \otimes \left[\lambda^T\right]$.

Our original problem came from the study of the Hamiltonians and the anticommutation relations respecting the $O(N_i)$ group, instead of the unitary group $U(N_i)$. Since $O(N_i) \subset U(N_i)$ we can simply decompose each of the representations $[\lambda]$ of the $U(N_i)$ into

irreducible representations of $O(N_i)$. This problem was successfully solved by Littlewood in 1947 [73] and he obtained the following result [74],

$$[\lambda]_{U(N_i)} = \sum_{\mu,\delta\prec\lambda,\delta\in\Delta_2} c^{\lambda}_{\delta,\mu}[\mu]_{O(N_i)}, \tag{2.69}$$

where $[\lambda]_{U(N_i)}$ and $[\mu]_{O(N_i)}$ are representations of the $U(N_i)$ and $O(N_i)$ groups described by Young Tableaux λ, and Δ_2 is the set of all Young Tableaux with an even number of rows, and $c^{\lambda}_{\delta,\mu}$ is a Littlewood-Richardson coefficient. While this rule gives a nice procedure for the decomposition of the Hilbert space in terms of the irreducible representations of $O(N_i)$, it complicates the analytical understanding of the structure of the Hilbert space.

It is interesting to notice that if, instead of complex fermions c_{ab}, we considered Majorana fermions ψ_{ab}, we can compute the partition function to get the following character,

$$\chi_{\mathcal{H}}(x_a, y_b) = \prod_{i=a,j=b}^{\frac{N_1}{2},\frac{N_2}{2}} \left(e^{ix_a} + e^{-ix_a} + e^{iy_b} + e^{-iy_b}\right). \tag{2.70}$$

We can deduce this structure heuristically. Note that, because of the Fermi-nature of each state λ of the $O(2n)$ representation, we must include the correspondence $\lambda \subset ((N_1/2)^{(N_2/2)})$. One can compute the dimension of all of these representations and find that it is equal to the full Hilbert space. This gives a new dual Cauchy identity for orthogonal Schur polynomials,

$$\sum_{\lambda\subset(n^m)} o_\lambda(x) o_{((N_1/2)^{(N_2/2)}/\lambda)'}(y) = \prod_{i,j} \left(x_i + x_i^{-1} + y_j + y_j^{-1}\right). \tag{2.71}$$

It is easy to show that this is true just from the definition of the orthogonal characters. First of all, we notice that the charater of $O(2n)$ in the even case has the following form [71, 75],

$$o_\lambda(x) = \frac{a_\lambda}{a_0} = \frac{\det\left(x_i^{\lambda_j+n-j} + x_i^{-(\lambda_j+n-j)}\right)}{\det\left(x_i^{n-j} + x_i^{-(n-j)}\right)}. \tag{2.72}$$

Then we notice that if we denote the length of rows in the diagram $((N_1/2)^{(N_2/2)}/\lambda)'$ as μ_i, the numbers μ_i+m-i, λ_j+n-j comprise a permutation $\sigma \in S_n$ of the numbers $I_n = \{0, 1, \ldots, n+m-1\}$. Therefore, we just need to sum up all over possible permutations of the set I_n. This gives us

$$\sum_{\lambda \subset (n^m)} o_\lambda(x) o_{((N_1/2)^{(N_2/2)}/\lambda)'}(y) = \frac{\sum_{\sigma \in S_n} a_{\sigma\lambda}(x) a_{\tilde{\lambda}}(y)}{a_0^2}, \tag{2.73}$$

where $\sigma(\lambda) = \sigma(\{0, \ldots, n-1\})$ $\sigma(\tilde{\lambda}) = \sigma(\{n, \ldots, n+m-1\})$. This could be rewritten using the Laplace rule for calculating determinants. We find that,

$$\begin{aligned} \sum_{\sigma \in S_n} a_{\sigma\lambda}(x) a_{\tilde{\lambda}}(y) &= \Delta\left(x_1 + x_1^{-1}, x_2 + x_2^{-1}, \ldots, -y_1 - y_1^{-1}, \ldots, -y_n - y_n^{-1}\right) = \\ &= a_0(x) a_0(y) \prod_{i=1,j=1}^{n,m} \left(x_i + x_i^{-1} + y_j + y_j^{-1}\right). \end{aligned} \tag{2.74}$$

The relation (2.71) directly follows. This concludes the proof of the structure of the $O(2n) \times O(2m)$ model. We can present a direct computation to show that this relation works for the $O(4) \times O(2)$ model. The content of the Hilbert space is

$$\mathcal{H} = \cdot \otimes \square\square + \square \otimes \square + \begin{array}{l}\square\\\square\end{array} \otimes \cdot \tag{2.75}$$

The characters of this representations are

$$\begin{aligned} &O(2): \chi_\cdot = 1, \quad \chi_{\square} = x_1 + x_1^{-1}, \quad \chi_{\square\square} = x_1^2 + x_1^{-2} \\ &O(4): \chi_\cdot = 1, \quad \chi_{\square} = y_1 + y_1^{-1} + y_2 + y_2^{-1}, \quad \chi_{\begin{array}{l}\square\\\square\end{array}} = 2 + y_1 y_2 + y_1 y_2^{-1} + y_1^{-1} y_2 + y_1^{-1} y_2^{-1}. \end{aligned} \tag{2.76}$$

Substituting these into the character of the Hilbert space we get

$$\chi_H = \left(x_1 + \frac{1}{x_1} + y_1 + \frac{1}{y_1}\right)\left(x_1 + \frac{1}{x_1} + y_2 + \frac{1}{y_2}\right). \tag{2.77}$$

As one can see, the representation of the one-dimensional fermions gives a very powerful tool for proving famous combinatorial equalities. It would be interesting to expand these ideas for other groups, say $Sp(N)$, and to generalize it for the case of MacDonald polynomials [72].

3 RG Flow and ϵ expansions

3.1 Prismatic Model

3.1.1 Introduction

In recent literature, there has been considerable interest in models where the degrees of freedom transform as tensors of rank 3 or higher. Such models with appropriately chosen interactions admit new kinds of large N limits, which are not of 't Hooft type and are dominated by the so-called melonic Feynman diagrams [20, 54, 22, 23, 19]. Much of the recent activity (for a review see [14]) has been on the quantum mechanical models of fermionic tensors [23, 19], which have large N limits similar to that in the Sachdev-Ye-Kitaev (SYK) model [37, 25, 39, 24, 76, 77, 40, 78].

It is also of interest to explore similar quantum theories of bosonic tensors [19, 26, 79]. In [19, 26] an $O(N)^3$ invariant theory of the scalar fields ϕ^{abc} was studied:

$$S_4 = \int d^d x \left(\frac{1}{2} (\partial_\mu \phi^{abc})^2 + \frac{g}{4!} O_{\text{tetra}} \right) ,$$
$$O_{\text{tetra}} = \phi^{a_1 b_1 c_1} \phi^{a_1 b_2 c_2} \phi^{a_2 b_1 c_2} \phi^{a_2 b_2 c_1} . \tag{3.1}$$

This QFT is super-renormalizable in $d < 4$ and is formally solvable using the Schwinger-Dyson equations in the large N limit where $gN^{3/2}$ is held fixed. However, this model has some instabilities. One problem is that the "tetrahedral" operator O_{tetra} is not positive definite. Even if we ignore this and consider the large N limit formally, we find that in $d < 4$ the $O(N)^3$ invariant operator $\phi^{abc}\phi^{abc}$ has a complex dimension of the form $\frac{d}{2} + i\alpha(d)$ [26].[7] From the dual AdS point of view, such a complex dimension corresponds to a scalar field whose m^2 is below the Breitenlohner-Freedman stability bound [84, 85]. The origin of the complex dimensions was elucidated using perturbation theory in $4-\epsilon$ dimensions: the fixed point was found to be at complex values of the couplings for the additional $O(N)^3$ invariant operators required by the renormalizability [26]. In [26] a $O(N)^5$ symmetric theory for tensor ϕ^{abcde} and sextic interactions was also considered. It was found that

[7] Such complex dimensions appear in various other large N theories; see, for example, [80, 81, 82, 83].

the dimension of operator $\phi^{abcde}\phi^{abcde}$ is real in the narrow range $d_{\text{crit}} < d < 3$, where $d_{\text{crit}} \approx 2.97$. However, the scalar potential of this theory is again unstable, so the theory may be defined only formally. In spite of these problems, some interesting formal results on melonic scalar theories of this type were found recently [86].

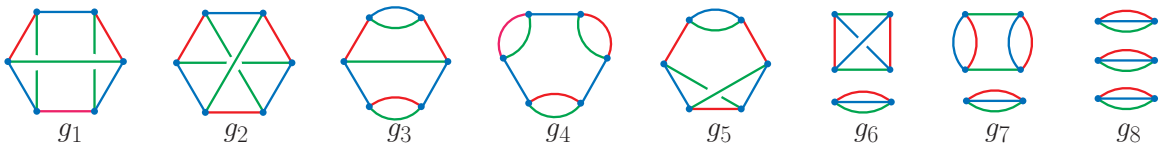

Figure 3.1: Diagrammatic representation of the eight possible $O(N)^3$ invariant sextic interaction terms.

In this paper, we continue the search for stable bosonic large N tensor models with multiple $O(N)$ symmetry groups. Specifically, we study the $O(N)^3$ symmetric theory of scalar fields ϕ^{abc} with a sixth-order interaction, whose Euclidean action is

$$S_6 = \int d^d x \left(\frac{1}{2}(\partial_\mu \phi^{abc})^2 + \frac{g_1}{6!}\phi^{a_1 b_1 c_1}\phi^{a_1 b_2 c_2}\phi^{a_2 b_1 c_2}\phi^{a_3 b_3 c_1}\phi^{a_3 b_2 c_3}\phi^{a_2 b_3 c_3} \right) . \tag{3.2}$$

This QFT is super-renormalizable in $d < 3$. When the fields ϕ^{abc} are represented by vertices and index contractions by edges, this interaction term looks like a prism (see figure 11 in [19]); it is the leftmost diagram in figure 3.1. Unlike with the tetrahedral quartic interaction (3.1), the action (3.2) is positive for $g_1 > 0$. In sections 3.1.2 and 3.1.3, we will show that there is a smooth large N limit where $g_1 N^3$ is held fixed and derive formulae for various operator dimensions in continuous d. We will call this large N limit the "prismatic" limit: the leading Feynman diagrams are not the same as the melonic diagrams, which appear in the $O(N)^5$ symmetric ϕ^6 QFT for a tensor ϕ^{abcde} [26]. However, as we discuss in section 3.1.2, the prismatic interaction may be reduced to a tetrahedral one, (3.3), by introducing an auxiliary tensor field χ^{abc}.

The theory (3.2) may be viewed as a tensor counterpart of the bosonic theory with random couplings, which was introduced in section 6.2 of [79]. Since both theories are dominated by the same class of diagrams in the large N limit, they have the same Schwinger-Dyson equations for the 2-point and 4-point functions. We will confirm the

conclusion of [79] that the $d = 2$ theory does not have a stable IR limit; this is due to the appearance of a complex scaling dimension. However, we find that in the ranges $2.81 < d < 3$ and $d < 1.68$, the large N prismatic theory does not have any complex dimensions for the bilinear operators. In section 3.1.5 we use renormalized perturbation theory to develop the $3 - \epsilon$ expansion of the prismatic QFT. We have to include all eight operators invariant under the $O(N)^3$ symmetry and the S_3 symmetry permuting the $O(N)$ groups; they are shown in figure 3.1 and written down in (3.76). For $N > N_{\text{crit}}$, where $N_{\text{crit}} \approx 53.65$, we find a prismatic RG fixed point where all eight coupling constants are real. At this fixed point, ϵ expansions of various operator dimensions agree in the large N limit with those obtained using the Schwinger-Dyson equations. Futhermore, the $3 - \epsilon$ expansion provides us with a method to calculate the $1/N$ corrections to operator dimensions, as shown in (3.65), (3.66). At $N = N_{\text{crit}}$ the prismatic fixed point merges with another fixed point, and for $N < N_{\text{crit}}$ both become complex.

In section 3.1.6 we discuss the $d = 1$ version of the model (3.2). Our large N solution gives a slightly negative scaling dimension, $\Delta_\phi \approx -0.09$, while the spectrum of bilinear operators is free of complex scaling dimensions.

3.1.2 Large N Limit

To study the large N limit of this theory, we will find it helpful to introduce an auxiliary field χ^{abc} so that[8]

$$S = \int d^d x \left(\frac{1}{2} (\partial_\mu \phi^{abc})^2 + \frac{g}{3!} \phi^{a_1 b_1 c_1} \phi^{a_1 b_2 c_2} \phi^{a_2 b_1 c_2} \chi^{a_2 b_2 c_1} - \frac{1}{2} \chi^{abc} \chi^{abc} \right) . \tag{3.3}$$

where $g \sim \sqrt{g}_1$. Integrating out χ^{abc} gives rise to the action (3.2). The advantage of keeping χ^{abc} explicitly is that the theory is then a theory with $O(N)^3$ symmetry dominated by the tetrahedral interactions, except it now involves two rank-3 fields; this shows that it has a smooth large N limit. Thus, a prismatic large N limit for the theory with one 3-tensor ϕ^{abc} may be viewed as a tetrahedral limit for two 3-tensors.

[8] If we added fermions to make the tensor model supersymmetric [19, 79, 87, 88] then χ^{abc} would be interpreted as the highest component of the superfield Φ^{abc}.

Let us define the following propagators:

$$\langle \phi(p)\phi(q)\rangle = (2\pi)^d \delta^d(p+q)G(p), \quad \langle \chi(p)\chi(q)\rangle = (2\pi)^d \delta^d(p+q)F(p). \tag{3.4}$$

In the free theory $G(p) = G_0(p) = \frac{1}{p^2}$, and $F(p) = F_0 = 1$. In the strong coupling limit the self-energies of the fields are given by the inverse propagators: $G(p)^{-1} = \Sigma_\phi$ and $F(p)^{-1} = \Sigma_\chi$. The Schwinger-Dyson equations for the exact two-point functions can be written as:

$$\begin{aligned} F(p) &= F_0 + g^2 N^3 F_0 \int \frac{d^d q d^d k}{(2\pi)^{2d}} G(p-q-k)G(q)G(k)F(p)\,, \\ G(p) &= G_0(p) + 3g^2 N^3 G_0(p) \int \frac{d^d q d^d k}{(2\pi)^{2d}} G(p-q-k)F(q)G(k)G(p)\,, \end{aligned} \tag{3.5}$$

and represented in figure 3.2.

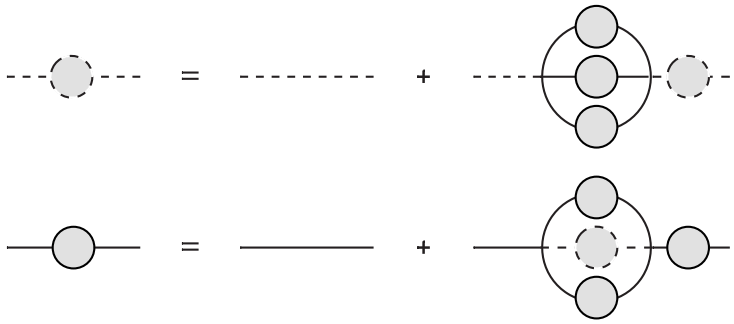

Figure 3.2: Diagramatic representation of the Schwinger-Dyson equations. Solid lines denote ϕ propagators, and dashed lines denote χ propagators.

Multiplying the first equation by F_0^{-1} on the left and $F(p)^{-1}$ on the right, and likewise for the second equation we obtain:

$$\begin{aligned} F(p)^{-1} &= F_0^{-1} - \lambda^2 \int \frac{d^d q d^d k}{(2\pi)^{2d}} G(p-q-k)G(q)G(k)\,, \\ G(p)^{-1} &= G_0(p)^{-1} - 3\lambda^2 \int \frac{d^d q d^d k}{(2\pi)^{2d}} G(p-q-k)F(q)G(k)\,, \end{aligned} \tag{3.6}$$

where $\lambda^2 = N^3 g^2 \sim N^3 g_1$. We have to take the large N limit keeping λ^2 fixed. In the IR

limit, let us assume

$$G(p) = \frac{A}{p^{2a}},\ F(p) = \frac{B}{p^{2b}}.$$

a is related to the scaling dimension of ϕ, Δ_ϕ via $a = d/2 - \Delta_\phi$.

For what range of a and b can we drop the free terms in the gap equations above? In the strong coupling limit we require $b < 0$ and $a < 1$. Since $b = -3a + d$, we have $d/3 < a < 1$. In terms of Δ_ϕ, we then find

$$3\Delta_\phi + \Delta_\chi = d\ , \qquad d/2 - 1 < \Delta_\phi < d/6. \tag{3.7}$$

Notice that, if we had the usual kinetic term for the χ field, the allowed range for Δ_ϕ would be larger. Therefore, our solution may also apply to a model with two dynamical scalar fields interacting via the particular interaction given above.

The gap equation is finally:

$$\begin{aligned} F(p)^{-1} &= -\lambda^2 \int \frac{d^d q d^d k}{(2\pi)^{2d}} G(p-q-k)G(q)G(k)\,, \\ G(p)^{-1} &= -3\lambda^2 \int \frac{d^d q d^d k}{(2\pi)^{2d}} G(p-q-k)F(q)G(k)\,. \end{aligned} \tag{3.8}$$

Dimensional analysis of the strong coupling fixed point actually does not fix a: we get $b = -3a + d$ from the first equation and $a = -2a - b + d$ from the second equation. Let us try to solve the above equations, in the hope that numerical factors arising from the Feynman integrals may determine a. The overall constant A is not determined from this procedure, but note that $[\lambda] = 3 - d$, and therefore $A \sim \lambda^{\frac{2(a-1)}{3-d}}$. This procedure is analogous to solving an eigenvalue equation, and perhaps it is not surprising that we have to do this, since a solution for a also determines the anomalous dimension of a composite operator ϕ^3. We then find

$$F(p) = \frac{-1}{A^3\lambda^2} \frac{(2\pi)^{2d}}{L_d(a,a)L_d(2a-d/2,a)} \frac{1}{p^{2b}}, \tag{3.9}$$

where

$$L_d(a,b) = \pi^{d/2}\frac{\Gamma(d/2-a)\Gamma(d/2-b)\Gamma(a+b-d/2)}{\Gamma(a)\Gamma(b)\Gamma(d-a-b)}. \tag{3.10}$$

The condition that must be satisfied by a is then:

$$3\frac{L_d(2a-d/2,d-3a)}{L_d(2a-d/2,a)} = 1\ . \tag{3.11}$$

In position space, the IR two-point functions take the form

$$G(x) = \frac{\Gamma(d/2-a)}{\pi^{d/2}2^{2a}\Gamma(a)}\frac{A}{(x^2)^{\Delta_\phi}}, \tag{3.12}$$

$$F(x) = \frac{\Gamma(d/2-b)}{\pi^{d/2}2^{2b}\Gamma(b)}\frac{(2\pi)^{2d}}{A^3\lambda^2 L_d(a,a)L_d(2a-d/2,a)}\frac{1}{(x^2)^{d-3\Delta_\phi}}. \tag{3.13}$$

In terms of Δ_ϕ, (3.11) may be written as

$$f(d,\Delta_\phi) \equiv \frac{1}{3}\frac{\Gamma(\frac{d}{2}-3\Delta_\phi)\Gamma(-\frac{d}{2}+3\Delta_\phi)\Gamma(\Delta_\phi)\Gamma(d-\Delta_\phi)}{\Gamma(\frac{d}{2}-\Delta_\phi)\Gamma(-\frac{d}{2}+\Delta_\phi)\Gamma(3\Delta_\phi)\Gamma(d-3\Delta_\phi)} = 1\,. \tag{3.14}$$

It can be verified numerically that that solutions to (3.14) within the allowed range (3.7) do exist in $d<3$. For example, for $d=2.9$ we have the solution shown in Figure 3.3:

$$\Delta_\phi \approx 0.456\ , \qquad \Delta_\chi \approx 1.531\ . \tag{3.15}$$

For $d=2.99$, we find $\Delta_\phi = 0.495$, and $d=2.999$, $\Delta_\phi = 0.4995$, consistent with the $3-\epsilon$ expansion (3.36). For $d=2$, (3.11) simplifies to

$$3(3\Delta_\phi - 1)^2 = (\Delta_\phi - 1)^2\ . \tag{3.16}$$

The solution $\Delta_\phi = \frac{1}{13}\left(4-\sqrt{3}\right)$ lies within the allowed range (3.7), while the one with the other branch of the square root is outside it.

For $d<2$ we find multiple solutions within the allowed range (3.7), as shown for $d=1$ in figure 3.4. One of the solutions gives $\Delta_\phi = 0$; this produces singularities in the large

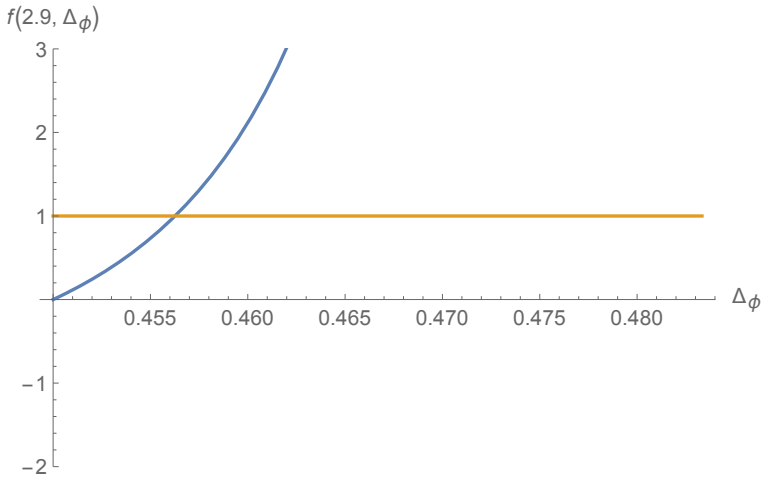

Figure 3.3: Solving (3.14) for $d = 2.9$.

N dimensions of scalar bilinears, and we will not use it. The other solution,

$$\Delta_\phi \approx -0.09055 \ , \qquad \Delta_\chi \approx 1.2717 \ , \tag{3.17}$$

appears to be acceptable. Although $\Delta_\phi > \frac{d-2}{2}$ it still violates the unitraity bound, since Δ_ϕ is negative. We note that there is also a positive solution $\Delta_\phi \approx 0.225$, which lies outside of the allowed range (although it would be allowed if the χ field was dynamical).

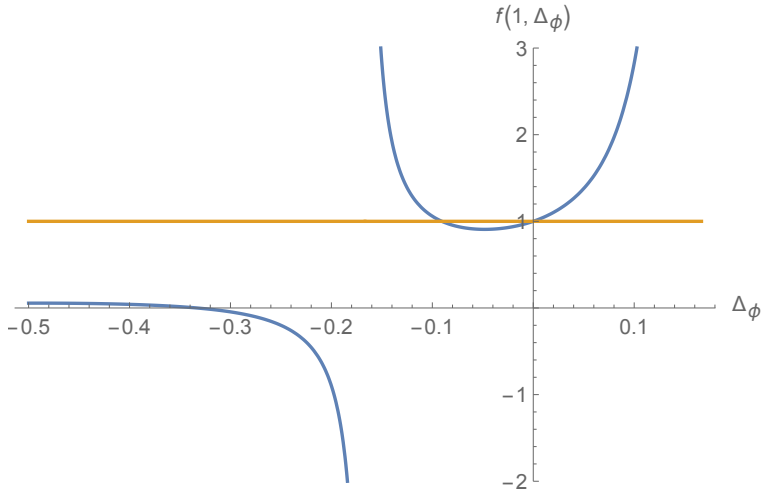

Figure 3.4: Solving (3.14) for $d = 1$.

There is an interesting transition in behavior which happens at $d = d_c$ where there is

a double root at $\Delta_\phi = 0$. The critical dimension d_c is the solution of

$$2 + d_c\pi \cot(d_c\pi/2) + d_c(\gamma + \psi(d_c)) = 0 \ . \tag{3.18}$$

Its numerical value is $d_c = 1.35287$. For d slightly above d_c one of the solutions for Δ_ϕ is zero, while the other is positive; we have to pick the positive one. However, for d slightly below d_c one of the solutions for Δ_ϕ is zero, while the other is negative. Special care may be needed for continuation to $d < d_c$; in particular, for studying the $d = 1$ case.

3.1.3 Bilinear Operators

There are three types of scalar bilinears one can consider, which are of the schematic form: $A = \phi(\xi \cdot \partial)^s(\partial^2)^n\phi$, $B = \phi(\xi \cdot \partial)^s(\partial^2)^n\chi$ and $C = \chi(\xi \cdot \partial)^s(\partial^2)^n\chi$, where ξ^μ is an auxiliary null vector introduced to encode the spin of the operators, $\xi \cdot \partial = \xi^\mu\partial_\mu$, and $\partial^2 = \partial^\mu\partial_\mu$. We note that there is mixing of operators of type A and C. It is easy to convince oneself that there is no mixing with the B operators by drawing a few diagrams.

Let us consider a bilinear of type B, of spin s and scaling dimension Δ, for which there is no mixing. The three-point functions take the form [89, 90]:

$$\begin{aligned} \langle \phi^{abc}(x_1)\chi^{abc}(x_2)B_s(x_3;\xi)\rangle = v^{(B)}(x_1,x_2,x_3) &= \frac{Q_3^s}{x_{31}^{\tau+\Delta_\phi-\Delta_\chi}x_{32}^{\tau+\Delta_\chi-\Delta_\phi}x_{12}^{\Delta_\phi+\Delta_\chi-\tau}} \\ \to v^{(B)}_{s,\tau}(x_1,x_2) &= (x_{12}\cdot\xi)^s x_{12}^{\tau-\Delta_\phi-\Delta_\chi} \ , \end{aligned} \tag{3.19}$$

where $\tau = \Delta - s$ is the twist of the bilinear, ξ is the null polarization vector, Q_3 is the conformally invariant tensor structure defined in [89, 90] and we took the limit $x_3 \to \infty$ in the second line. The eigenvalue equation, obtained using the integration kernel depicted schematically in figure 3.5, is

$$v_{s,\tau}(x_1,x_2) = 3\lambda^2 \int d^dy d^dz F(x_2,y)G(y,z)^2G(z,x_1)v_{s,\tau}(y,z) \tag{3.20}$$

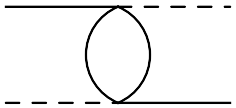

Figure 3.5: The integration kernel for type B bilinears.

When $s = 0$, we have:

$$|x_1 - x_2|^{-\Delta_\phi - \Delta_\chi + \Delta} = 3\tilde{A}^3\tilde{B}\lambda^2 \int d^d y d^d z \frac{1}{|x_2 - y|^{2\Delta_\chi}|y - z|^{5\Delta_\phi + \Delta_\chi - \Delta}|z - x_1|^{2\Delta_\phi}} \tag{3.21}$$

which translates into

$$\begin{aligned} g^{(B)}(d,\Delta) &\equiv -3\frac{\Gamma(3\Delta_\phi)\sin\left(\frac{1}{2}\pi(d-6\Delta_\phi)\right)\Gamma\left(\frac{d}{2}-\Delta_\phi\right)\Gamma\left(-\frac{d}{2}+3\Delta_\phi+1\right)\Gamma\left(\frac{\Delta}{2}-\Delta_\phi\right)\Gamma\left(\frac{1}{2}(d-\Delta-2\Delta_\phi)\right)}{\pi\Gamma(\Delta_\phi)\Gamma\left(\frac{\Delta}{2}+\Delta_\phi\right)\Gamma\left(\frac{d-\Delta}{2}+\Delta_\phi\right)} \\ &= 1\ . \end{aligned} \tag{3.22}$$

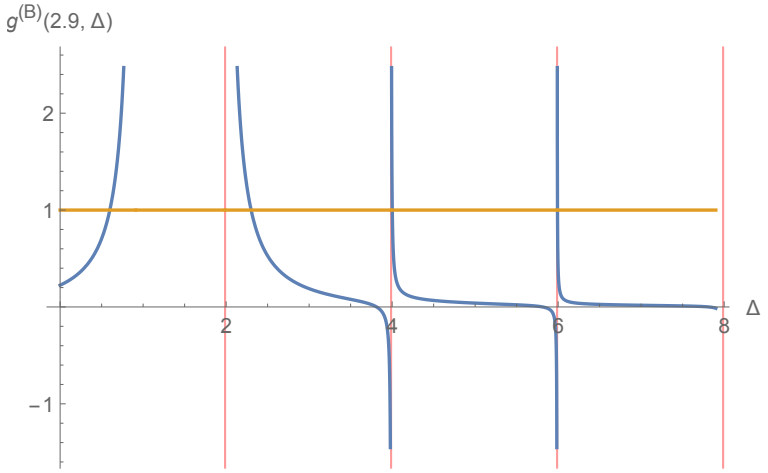

Figure 3.6: The spectrum of type B bilinears in $d = 2.9$. The red lines correspond to asympotes at $2n + \Delta_\phi + \Delta_\chi = 2n + 1.98747$.

We can solve equation (3.22) numerically to find the allowed scaling dimensions for type B operators in various dimensions. In $d = 2.9$ the type B scaling dimensions are

$$\Delta_B = 2.30120;\ 4.00173;\ 5.99214;\ 7.98983;\ 9.98891;\ \ldots, \tag{3.23}$$

as shown in figure 3.6. In the pure ϕ language, the first one can be identified with the

tetrahedral operator. The type B scaling approach the asymptotic formula

$$\Delta_B \to 2n + \Delta_\phi + \Delta_\chi = 2n + 1.98747 \ . \tag{3.24}$$

For example, for $n = 54$ we numerically find $\Delta = 109.98749$, which is very close to (3.24).

For spin $s > 0$ the eigenvalue equation is:

$$(x_{12} \cdot \xi)^s |x_1 - x_2|^{-\Delta_\phi - \Delta_\chi + \Delta} = 3\tilde{A}^3 \tilde{B} \lambda^2 \int d^d y d^d z \frac{((y-z)\cdot\xi)^s}{|x_2 - y|^{2\Delta_\chi} |y-z|^{5\Delta_\phi + \Delta_\chi - \Delta} |z - x_1|^{2\Delta_\phi}} \tag{3.25}$$

Note that the spectrum of type B bilinears does not contain the stress tensor, which is of type A/C.

Processing the equation we have the following condition for the allowed twists of higher spin bilinears:

$$\begin{aligned} &g^{(B)}(d,\tau,s) \equiv \\ &-3\frac{\Gamma(3\Delta_\phi)\sin\left(\frac{1}{2}\pi(d-6\Delta_\phi)\right)\Gamma\left(\frac{d}{2}-\Delta_\phi\right)\Gamma\left(-\frac{d}{2}+3\Delta_\phi+1\right)\Gamma\left(\frac{1}{2}(d-2\Delta_\phi-\tau)\right)\Gamma\left(s-\Delta_\phi+\frac{\tau}{2}\right)}{\pi\Gamma(\Delta_\phi)\Gamma\left(\frac{d}{2}+\Delta_\phi-\frac{\tau}{2}\right)\Gamma\left(s+\Delta_\phi+\frac{\tau}{2}\right)} \\ &= 1 \ . \end{aligned} \tag{3.26}$$

Using this equation one can find the allowed twists of spin-s type B bilinears. For example, the spectrum when $s = 2$ and $d = 2.9$ is found from figure 3.7 to be $\tau = 2.08,\ 3.99,\ 5.99,\ 7.99, \ldots$, which approach $\Delta_\chi + \Delta_\phi + 2n = 1.99 + 2n$ from above.

We find that the spectrum of type B bilinear appears to be real for all $d < 3$. However, there are ranges of d where the spectrum of type A/C operators do contain complex eigenvalues, as we discuss in the next section.

Let us now study the spectrum of bilinear operators of type A and C. As mentioned earlier, by drawing a few diagrams (see figure 3.8) one can see that these operators mix, in the sense that the two-point function $\langle A_s C_s \rangle \neq 0$. Let $\tau = \Delta - s$ be the twist of mixture of A and C operators, which we denote as $\tilde{A}_s$. From the three-point functions

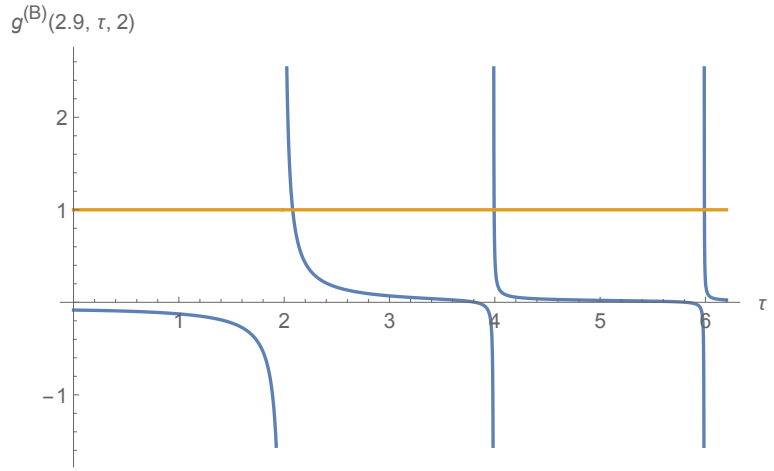

Figure 3.7: Solving equation (3.26) in $d = 2.9$ for the allowed twists of spin-2 type B bilinears.

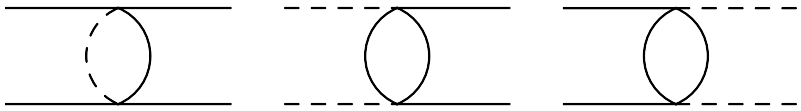

Figure 3.8: The integration kernels K_{AA}, K_{CA} and K_{AC} respectively for mixtures of type A and C bilinears.

$\langle \phi^{abc}(x_1)\phi^{abc}(x_2)\tilde{A}_s(x_3;\xi)\rangle$ and $\langle \chi^{abc}(x_1)\chi^{abc}(x_2)\tilde{A}_s(x_3;\xi)\rangle$, we define

$$v^{(A)}_{s,\tau}(x,y) = \frac{((x-y)\cdot\xi)^s}{(x-y)^{2\Delta_\phi-\tau}}, \quad v^{(C)}_{s,\tau}(x,y) = \frac{((x-y)\cdot\xi)^s}{(x-y)^{2\Delta_\chi-\tau}}. \tag{3.27}$$

We now define the following kernels, depicted schematically in figure 3.8:

$$K_{AA}[v^{(A)}] = 3\int d^dx d^dy G(x_1,x)G(x_2,y)G(x,y)F(x,y)v^{(A)}_{s,\tau}(x,y) \tag{3.28}$$

$$K_{CA}[v^{(A)}] = 3\int d^dx d^dy F(x_1,x)F(x_2,y)G(x,y)^2 v^{(A)}_{s,\tau}(x,y) \tag{3.29}$$

$$K_{AC}[v^{(C)}] = 3\int d^dx d^dy G(x_1,x)G(x_2,y)G(x,y)^2 v^{(C)}_{s,\tau}(x,y) \tag{3.30}$$

Note the factor of 3, which appears from a careful counting of the Wick contractions.

The integration kernel gives rise to the following matrix

$$\begin{pmatrix} 2K_{AA}[v^{(A)}]/v^{(A)} & K_{AC}[v^{(C)}]/v^{(A)} \\ K_{CA}[v^{(A)}]/v^{(C)} & 0 \end{pmatrix} \equiv \begin{pmatrix} 2K_1 & K_3 \\ K_2 & 0 \end{pmatrix}. \tag{3.31}$$

The condition for it to have eigenvalue 1, which determines the allowed values of τ, is

$$g^{(A)}(d,\tau,s) \equiv 2K_1 + K_3 K_2 = 1 \ . \tag{3.32}$$

Luckily, this condition is independent of the constant A, as one can see from the following expressions,

$$\begin{aligned}
K_1 &= \frac{3(d-6\Delta_\phi)\Gamma(3\Delta_\phi)\sin\left(\frac{1}{2}\pi(d-6\Delta_\phi)\right)\Gamma(d-3\Delta_\phi)\Gamma\left(\frac{d}{2}-\Delta_\phi\right)^2\Gamma\left(\Delta_\phi-\frac{\tau}{2}\right)\Gamma\left(-\frac{d}{2}+s+\Delta_\phi+\frac{\tau}{2}\right)}{2\pi\Gamma(\Delta_\phi)^2\Gamma\left(d-\Delta_\phi-\frac{\tau}{2}\right)\Gamma\left(\frac{1}{2}(d+2s-2\Delta_\phi+\tau)\right)} \ , \\
K_2 &= \frac{3\pi^d 2^{4(d-2\Delta_\phi)}\Gamma(3\Delta_\phi)^2\Gamma\left(\frac{d}{2}-\Delta_\phi\right)^4\Gamma\left(d-3\Delta_\phi-\frac{\tau}{2}\right)\Gamma\left(\frac{1}{2}(d+2s-6\Delta_\phi+\tau)\right)}{A^4\lambda^2\Gamma(\Delta_\phi)^4\Gamma\left(\frac{d}{2}-3\Delta_\phi\right)^2\Gamma\left(3\Delta_\phi-\frac{\tau}{2}\right)\Gamma\left(-\frac{d}{2}+s+3\Delta_\phi+\frac{\tau}{2}\right)} , \\
K_3 &= \frac{3A^4\pi^{-d}\lambda^2 2^{8\Delta_\phi-4d}\Gamma(\Delta_\phi)^2\Gamma\left(\Delta_\phi-\frac{\tau}{2}\right)\Gamma\left(-\frac{d}{2}+s+\Delta_\phi+\frac{\tau}{2}\right)}{\Gamma\left(\frac{d}{2}-\Delta_\phi\right)^2\Gamma\left(d-\Delta_\phi-\frac{\tau}{2}\right)\Gamma\left(\frac{1}{2}(d+2s-2\Delta_\phi+\tau)\right)} \ .
\end{aligned} \tag{3.33}$$

Thus, the equation we need to solve is:

$$\begin{aligned}
&\frac{\Gamma(\Delta_\phi)^2\Gamma\left(\frac{d}{2}-3\Delta_\phi\right)^2\Gamma\left(3\Delta_\phi-\frac{d}{2}\right)\Gamma\left(3\Delta_\phi-\frac{\tau}{2}\right)\Gamma\left(d-\Delta_\phi-\frac{\tau}{2}\right)}{3\Gamma(3\Delta_\phi)\Gamma\left(\frac{d}{2}-\Delta_\phi\right)^2\Gamma\left(\Delta_\phi-\frac{\tau}{2}\right)\Gamma\left(-\frac{d}{2}+s+\Delta_\phi+\frac{\tau}{2}\right)\Gamma\left(\frac{1}{2}(d+2s-2\Delta_\phi+\tau)\right)} \\
&\quad = 3\Gamma(3\Delta_\phi)\Gamma\left(3\Delta_\phi-\frac{d}{2}\right)\Gamma\left(d-3\Delta_\phi-\frac{\tau}{2}\right)\frac{\Gamma\left(\frac{1}{2}(d+2s-6\Delta_\phi+\tau)\right)}{\Gamma\left(-\frac{d}{2}+s+3\Delta_\phi+\frac{\tau}{2}\right)} - \\
&\qquad -2\Gamma\left(\frac{d}{2}-3\Delta_\phi\right)\Gamma(d-3\Delta_\phi)\Gamma\left(3\Delta_\phi-\frac{\tau}{2}\right) \ .
\end{aligned} \tag{3.34}$$

One can check that the stress-tensor, which has $s = 2$ and $\tau = d-2$, appears in this spectrum for any d.

The Schwinger-Dyson equations have a symmetry under $\Delta \to d - \Delta$. In a given CFT, only one of this pair of solutions corresponds to a primary operator dimension, while the other one is its "shadow." The $s = 0$ spectrum contains complex modes for $1.6799 < d < 2.8056$. In $d = 2.9$ the graphical solution for the scaling dimensions in the type A/C sector is shown in figure 3.9. The lowest few are

$$\Delta = 1.064,\ 1.836,\ 2.9,\ 3.114,\ 4.912,\ 5.063,\ 6.913,\ 7.063, \ldots \tag{3.35}$$

The eigenvalue at $\Delta = 2.9$ is exact, and in general $\Delta = d$ is an eigenvalue for any d. The

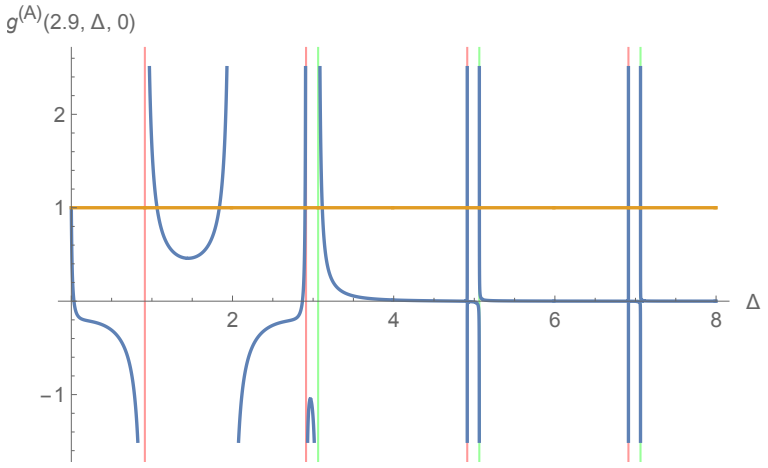

Figure 3.9: The spectrum of type A/C scalar bilinears in $d = 2.9$. The green lines correspond to the $2\Delta_\chi + 2n$ asymptotics and the red ones to $2\Delta_\phi + 2n$ asymptotics. We see that the solutions are real, and approach the expected values as $n \to \infty$.

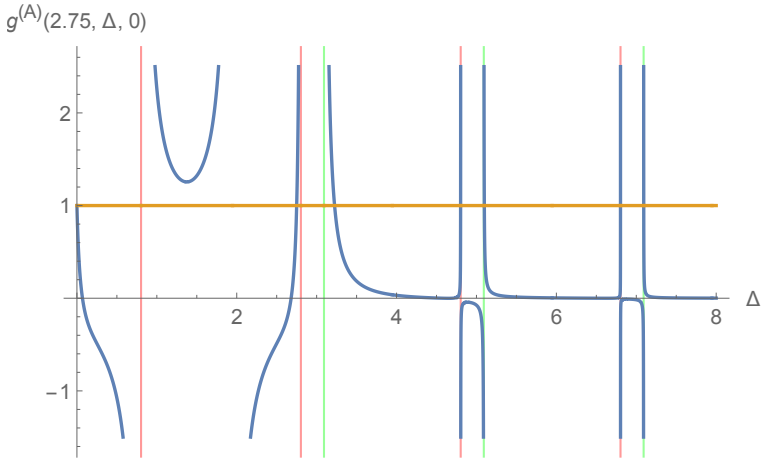

Figure 3.10: The spectrum of type A/C scalar bilinears in $d = 2.75$. The green lines correspond to the $2\Delta_\chi + 2n$ asymptotics and the red ones to $2\Delta_\phi + 2n$ asymptotics. We see that two real solutions are no longer present; they are now complex.

solution 1.836 corresponds to the shadow of 1.064. As d is further lowered, the part of the graph between 1 and 2 moves up so that the two solutions become closer. In $d = d_{\text{crit}}$, where $d_{\text{crit}} \approx 2.8056$, the two solutions merge into a single one at $d/2$ (for discussions of mergers of fixed points, see [91, 92, 93]). For $d < d_{\text{crit}}$, the solutions become complex $\frac{d}{2} \pm i\alpha(d)$ and the prismatic model becomes unstable. The plot for $d = 2.75$ is shown in figure 3.10.

For $d \leq 1.68$, the spectrum of bilinears is again real. The plot for $d = 1.68$, where $\Delta_\phi \approx 0.0867$, is shown in figure 3.11. At this critical value of d there are two solutions

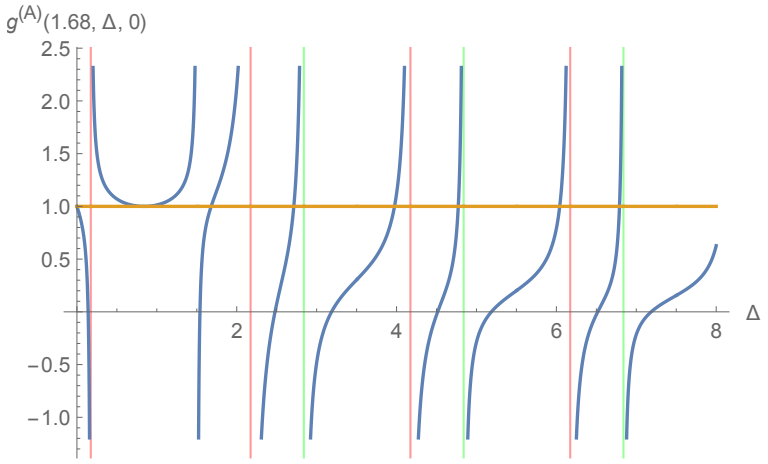

Figure 3.11: The spectrum of type A/C scalar bilinears in $d = 1.68$. The green vertical lines correspond to the $2\Delta_\chi + 2n$ asymptotics; the red ones to the $2\Delta_\phi + 2n$ asymptotics.

at $d/2$; one is the shadow of the other.

3.1.4 Large N results in $3-\epsilon$ dimensions

Let us solve the Schwinger-Dyson equations in $d = 3-\epsilon$. The results will be compared with renormalized perturbation theory in the following section. The scaling dimension of ϕ^{abc} is found to be

$$\Delta_\phi = \frac{1}{2} - \frac{\epsilon}{2} + \epsilon^2 - \frac{20\epsilon^3}{3} + \left(\frac{472}{9} + \frac{\pi^2}{3}\right)\epsilon^4 + \left(7\zeta(3) - \frac{12692}{27} - \frac{56\pi^2}{9}\right)\epsilon^5 + \mathcal{O}\left(\epsilon^6\right) \ . \quad (3.36)$$

This is within the allowed range (3.7) and is close to its upper boundary. The scaling dimension of χ^{abc} is

$$\Delta_\chi = d - 3\Delta_\phi = \frac{3}{2} + \frac{\epsilon}{2} - 3\epsilon^2 + 20\epsilon^3 - \left(\frac{472}{3} + \pi^2\right)\epsilon^4 - 3\left(7\zeta(3) - \frac{12692}{27} - \frac{56\pi^2}{9}\right)\epsilon^5 + \mathcal{O}\left(\epsilon^6\right) \ . \quad (3.37)$$

Let us consider the $s = 0$ type A/C bilinears. For the first eigenvalue we find,

$$\Delta_{\phi^2} = 1 - \epsilon + 32\epsilon^2 - \frac{976\epsilon^3}{3} + \left(\frac{30320}{9} + \frac{32\pi^2}{3}\right)\epsilon^4 + \mathcal{O}\left(\epsilon^5\right) \ . \quad (3.38)$$

It corresponds to the scaling dimension of operator $\phi^{abc}\phi^{abc}$, as we will show in the next

section. The next eigenvalue is the shadow dimension $d - \Delta_{\phi^2}$.

The next solution of the S-D equation is $\Delta = d = 3 - \epsilon$ for all d. While this seems to correspond to an exactly marginal operator, we believe that the corresponding operator is redundant: it is a linear combination of $\phi^{abc}\partial^2\phi^{abc}$ and $\chi^{abc}\chi^{abc}$. Similar redundant operators with $h = 1$ showed up in the Schwinger-Dyson analysis of multi-flavor models [77, 61]. They decouple in correlation functions [77] and were shown to vanish by the equations of motion [61]. The next eigenvalue is

$$\Delta_{\text{prism}} = 3 + \epsilon + 6\epsilon^2 - 84\epsilon^3 + \left(\frac{1532}{3} + 10\pi^2\right)\epsilon^4 + \left(18\zeta(3) - \frac{6392}{3} - \frac{452\pi^2}{3}\right)\epsilon^5 + \mathcal{O}\left(\epsilon^6\right) . \tag{3.39}$$

It should correspond to the sextic prism operator (3.2), which is related by the equations of motion to a linear combination of $\phi^{abc}\partial^2\phi^{abc}$ and $\chi^{abc}\chi^{abc}$.

The subsequent eigenvalues may be separated into two sets. One of them has the form, for integer $n \geq 0$,

$$\begin{aligned}\Delta_n^- =& 5 + 2n - \epsilon + 2\epsilon^2 - \frac{40\epsilon^3}{3} + \\ &+ \frac{\left(2\left(472 + 3\pi^2\right) n(2n+7)(n(2n+7)+11) + 180\pi^2 + 28212\right)\epsilon^4}{9(n+1)(n+2)(2n+3)(2n+5)} + \mathcal{O}\left(\epsilon^5\right) .\end{aligned} \tag{3.40}$$

For large n this approaches $4 + 2n + 2\Delta_\phi$, as expected for an operator of the form $\phi^{abc}(\partial^2)^{2+n}\phi^{abc}$. The other set of eigenvalues has the form, for integer $n \geq 0$,

$$\Delta_n^+ = 5 + 2n + \epsilon - 6\epsilon^2 + 4\left(\frac{9}{n+2} - \frac{18}{2n+3} - \frac{6}{2n+5} + \frac{3}{n+1} + 10\right)\epsilon^3 + \mathcal{O}\left(\epsilon^4\right) . \tag{3.41}$$

For large n this approaches $2 + 2n + 2\Delta_\chi$, as expected for an operator of the form $\chi^{abc}(\partial^2)^{1+n}\chi^{abc}$. These simple asymptotic forms suggest that for large n the mixing between operators $\phi^{abc}(\partial^2)^{2+n}\phi^{abc}$ and $\chi^{abc}(\partial^2)^{1+n}\chi^{abc}$ approaches zero.

We can also use (3.22) to derive the $3 - \epsilon$ expansions of the dimensions of type B operators,

$$O_{B,n} = \chi^{abc}(\partial_\mu\partial^\mu)^n\phi^{abc} + \dots , \tag{3.42}$$

where the additional terms are there to make them conformal primaries. For $n = 0$ we find

$$\Delta_{B,0} = 2 + 6\epsilon - 68\epsilon^2 + \frac{2848 + 24\pi^2}{3}\epsilon^3 + \mathcal{O}\left(\epsilon^4\right) \ . \tag{3.43}$$

This scaling dimension corresponds to the operator $\phi^{abc}\chi^{abc}$, which in the original ϕ language is the tetrahedron operator O_{tetra}. For the higher operators we get

$$\Delta_{B,1} = 4 + 4\epsilon^3 - 44\epsilon^4 + \mathcal{O}\left(\epsilon^5\right) \ , \tag{3.44}$$

$$\Delta_{B,2} = 6 - \frac{7}{5}\epsilon^2 + \frac{331}{30}\epsilon^3 - \left(\frac{199547}{2250} + \frac{7\pi^2}{15}\right)\epsilon^4 + \mathcal{O}\left(\epsilon^5\right) \ , \tag{3.45}$$

$$\Delta_{B,3} = 8 - \frac{12}{7}\epsilon^2 + \frac{9139}{735}\epsilon^3 - \left(\frac{7581556}{77175} + \frac{4\pi^2}{7}\right)\epsilon^4 + \mathcal{O}\left(\epsilon^5\right) \ , \text{ etc.} \tag{3.46}$$

Using the equations of motion, we can write $O_{B,1}$, up to a total derivative, as a sum of the three 8-particle operators shown in the leftmost column of figure 9 in [61]. In general, for $n > 0$,

$$\Delta_{B,n} = 2n + 2 - 2\left(1 - \frac{3}{n(2n+1)}\right)\epsilon^2 + \mathcal{O}\left(\epsilon^3\right) \ , \tag{3.47}$$

which agrees for large n with the expected asymptotic behavior

$$\Delta_{B,n} \to 2n + \Delta_\phi + \Delta_\chi = 2n + 2 - 2\epsilon^2 + \mathcal{O}\left(\epsilon^3\right) \ . \tag{3.48}$$

Let us also present the ϵ expansions for the higher spin bilinear operators which are mixtures of type A and C. The lowest eigenvalue of twist $\tau = \Delta - s$ for spin s is

$$\begin{aligned}\tau_0 =& 1 - \epsilon + \frac{8\left(s^2-4\right)\epsilon^2}{4s^2-1} \\ &+ \frac{4\epsilon^3\left(27\left(1-4s^2\right)H_{s-\frac{1}{2}} - 2s\left(80s^3 + s(54\log(4) - 508) + 45\right) - 244 + 27\log(4)\right)}{3\left(1-4s^2\right)^2} + \mathcal{O}\left(\epsilon^4\right)\end{aligned} \tag{3.49}$$

where H_n is the harmonic number and the last two terms (as well as all higher-order

terms) vanish when $s = 2$ as expected. In the large s limit, this becomes:

$$\tau_0 \to 1 - \epsilon + \epsilon^2 \left(2 - \frac{15}{2s^2} + \mathcal{O}(s^{-3})\right) + \mathcal{O}\left(\epsilon^4\right) . \tag{3.50}$$

Comparing with (3.65), we see that

$$\tau_0 = 2\Delta_\phi + O(\frac{1}{s^2}) \tag{3.51}$$

This is the expected large spin limit [94, 95, 96, 97] for an operator bilinear in ϕ, indicating that for large spin the mixing with χ bilinears is suppressed.

The next two twists are

$$\begin{aligned}\tau_1 =& 3 - \epsilon + \frac{8s(s+2)\epsilon^2}{4s(s+2)+3} \\ &+ \frac{4\epsilon^3}{3(4s(s+2)+3)^2}\Big(- 4(40s(s+4)+157)s^2 + 6(s+27) - 27\gamma(4s(s+2)+3) \\ &- 27(4s(s+2)+3)\log(4) - 27(4s(s+2)+3)\psi(s+\frac{3}{2})\Big) + \mathcal{O}\left(\epsilon^4\right) ,\end{aligned} \tag{3.52}$$

and

$$\begin{aligned}\tau_2 =& 3 + \epsilon + \left(\frac{36}{4s(s+2)+3} - 6\right)\epsilon^2 \\ &+ \frac{4\epsilon^3}{(4s(s+2)+3)^2}\Big(4s(2s(20s(s+4)+56+9\log 4) - 105 + 36\log 4) \\ &+ 18\gamma(4s(s+2)+3) + 18(4s(s+2)+3)\psi(s+\frac{3}{2}) - 297 + 54\log 4\Big) + \mathcal{O}\left(\epsilon^4\right) ,\end{aligned} \tag{3.53}$$

where $\psi(x)$ is the digamma function. In the large s limit, these take the form,

$$\begin{aligned}\tau_1 &\to 3 - \epsilon + \epsilon^2\left(2 - \frac{3}{2s^2} + O(s^{-3})\right) + O\left(\epsilon^3\right) \\ &= 2\Delta_\phi + 2 + O(\frac{1}{s^2}) ,\end{aligned} \tag{3.54}$$

and

$$\begin{aligned}\tau_2 &\to 3+\epsilon+\epsilon^2\left(-6+\frac{9}{s^2}+O(s^{-3})\right)+O\left(\epsilon^3\right)\\ &= 2\Delta_\chi+O(\frac{1}{s^2})\,,\end{aligned} \tag{3.55}$$

In general, for large spin we find the two towers of twists labelled by an integer n

$$\begin{aligned}\tau_n^A &= 2n+1-\epsilon+2\epsilon^2-\frac{40\epsilon^3}{3}+\mathcal{O}(\epsilon^4)=2\Delta_\phi+2n+\dots\\ \tau_n^C &= 2n+3+\epsilon-6\epsilon^2+\mathcal{O}(\epsilon^3)=2\Delta_\chi+2n+\dots\end{aligned} \tag{3.56}$$

again in agreement with the expected asymptotics and suppression of mixing at large spin.

We can similarly derive explicit results for spinning operators in the type B sector using (3.26). For the lowest two twists, we find

$$\begin{aligned}\tau_0 &= 2+\frac{6\epsilon}{2s+1}+\frac{2\epsilon^2\left(3(2s+1)^2\left(H_{s-\frac{1}{2}}+\log(4)\right)-8s^3-84s^2-72s-34\right)}{(2s+1)^3}+O(\epsilon^3)\\ &= \left(2-2\epsilon^2+O(\epsilon^3)\right)+O(\frac{1}{s})\,,\\ \tau_1 &= 4-\frac{4s\epsilon^2}{2s+3}+\frac{2\epsilon^3\left(9(2s+3)H_{s+\frac{1}{2}}+80s^2+12s(8+\log(8))+54\log(2)\right)}{3(2s+3)^2}+O(\epsilon^4)\\ &= \left(4-2\epsilon^2+\frac{40\epsilon^3}{3}+O(\epsilon^4)\right)+O(\frac{1}{s})\,,\end{aligned} \tag{3.57}$$

and higher twists may be analyzed similarly. One can see that these results are also in agreement with the expected large spin limit $\tau_n \to \Delta_\phi+\Delta_\chi+2n$ for fixed n.

3.1.5 Renormalized perturbation theory

In this section we use the renormalized perturbation theory to carry out the $3-\epsilon$ expansion for finite N. We will find a fixed point with real couplings, whose large N limit reproduces the results found using the $3-\epsilon$ expansion of the Schwinger-Dyson solution in the previous section. This is an excellent check of the Schwinger-Dyson approach to the prismatic theory.

To carry out the beta function calculation at finite N we need to include all the $O(N)^3$

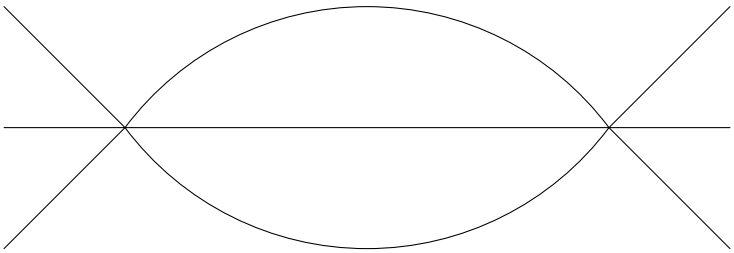

Figure 3.12: The two-loop contribution to the beta-function.

invariant sextic terms in the action (as usual in such calculations, we ignore the quartic and quadratic operators which are relevant in $d = 3$). The 11 such single-sum terms are shown diagrammatically in figure 5 of [61]. We will impose the additional constraint that the action is invariant under the permutation group S_3 which acts on the three $O(N)$ symmetry groups. This leaves us with 8 operators: 5 single-sum, 2 double-sum and 1 triple-sum. They are written down explicitly in (3.76) and shown schematically in figure 3.1. The first one and the most essential one for achieving the solvable large N limit is the "prism" term (3.2); it is positive definite and symmetric under the interchanges of the three $O(N)$ groups.

Our action is a special case of a general multi-field ϕ^6 tensor theory:

$$S = \int d^d x \left(\frac{1}{2} \partial_\mu \phi^{abc} \partial^\mu \phi^{abc} + \frac{1}{6!} g_{\kappa_1 \kappa_2 \kappa_3 \kappa_4 \kappa_5 \kappa_6} \phi^{\kappa_1} \phi^{\kappa_2} \phi^{\kappa_3} \phi^{\kappa_4} \phi^{\kappa_5} \phi^{\kappa_6} \right) . \tag{3.58}$$

The beta-functions and anomalous dimensions for such a general sextic coupling were calculated in [98, 99]; see also [100, 101] for earlier results on the $O(n)$ invariant sextic theory. The diagram topology contributing to the leading two-loop beta function is shown in figure 3.12.

In our case each index $\kappa_1, \kappa_2 \ldots, \kappa_6$ has three sub indices $\kappa_i = (a_i b_i c_i)$. The coupling $g_{\kappa_1 \kappa_2 \kappa_3 \kappa_4 \kappa_5 \kappa_6}$ contains 8 different types of interactions

$$g_{\kappa_1 \kappa_2 \kappa_3 \kappa_4 \kappa_5 \kappa_6} = g_1 T^{(1)}_{\kappa_1 \kappa_2 \kappa_3 \kappa_4 \kappa_5 \kappa_6} + g_2 T^{(2)}_{\kappa_1 \kappa_2 \kappa_3 \kappa_4 \kappa_5 \kappa_6} + \cdots + g_8 T^{(8)}_{\kappa_1 \kappa_2 \kappa_3 \kappa_4 \kappa_5 \kappa_6} , \tag{3.59}$$

which can be graphically represented as in figure 3.1. Each tensor structure $T^{(k)}_{\kappa_1 \kappa_2 \kappa_3 \kappa_4 \kappa_5 \kappa_6}$ consists of a sum of product of δ functions, which are symmetrized over the colors (abc)

and over the indices $\kappa_1, \ldots, \kappa_6$.

The two-loop beta functions and anomalous dimensions for general N are given in the Appendix. Let us use the large N scaling

$$
\begin{aligned}
g_1 &= 180 \cdot (8\pi)^2 \epsilon \frac{\tilde{g}_1}{N^3} \ , \qquad g_{2,4,6,7} = 180 \cdot (8\pi)^2 \epsilon \frac{\tilde{g}_{2,4,6,7}}{N^5} \ , \\
g_{3,5} &= 180 \cdot (8\pi)^2 \epsilon \frac{\tilde{g}_{3,5}}{N^4} \ , \qquad g_8 = 180 \cdot (8\pi)^2 \epsilon \frac{\tilde{g}_8}{N^7} \ ,
\end{aligned} \tag{3.60}
$$

which is chosen in such a way that all beta functions retain non-vanishing quadratic terms in the large N limit:

$$
\begin{aligned}
&\tilde{\beta}_1 = -2\tilde{g}_1 + 2\tilde{g}_1^2 \ , \quad \tilde{\beta}_2 = -2\tilde{g}_2 + 4\tilde{g}_1 \left(3\tilde{g}_1 + 2\tilde{g}_5\right) \ , \quad \tilde{\beta}_3 = -2\tilde{g}_3 + 12\tilde{g}_1^2 \ , \\
&\tilde{\beta}_4 = -2\tilde{g}_4 + \frac{2}{3}\left(2\left(3\tilde{g}_1 + \tilde{g}_3\right)^2 + \tilde{g}_5^2 + 12\tilde{g}_1\tilde{g}_5\right) \ , \quad \tilde{\beta}_5 = -2\tilde{g}_5 + 4\tilde{g}_1\left(6\tilde{g}_1 + \tilde{g}_5\right) \ , \\
&\tilde{\beta}_6 = -2\tilde{g}_6 + 4\tilde{g}_1\left(3\tilde{g}_1 + \tilde{g}_5 + 2\tilde{g}_6\right) , \quad \tilde{\beta}_7 = -2\tilde{g}_7 + 6\tilde{g}_1^2 \ , \\
&\tilde{\beta}_8 = -2\tilde{g}_8 + \frac{4}{3}\left(\tilde{g}_3^2 + 4\tilde{g}_7\tilde{g}_3 + \tilde{g}_5^2 + 6\tilde{g}_6^2 + 2\tilde{g}_7^2 + 6\tilde{g}_5\tilde{g}_6 + 3\tilde{g}_1\left(\tilde{g}_5 + 6\tilde{g}_6\right)\right) \ .
\end{aligned} \tag{3.61}
$$

The unique non-trivial fixed point of these scaled beta functions is at

$$
\begin{aligned}
&\tilde{g}_1^* = 1, \quad \tilde{g}_2^* = -42, \quad \tilde{g}_3^* = 6, \quad \tilde{g}_4^* = 54, \\
&\tilde{g}_5^* = -12, \quad \tilde{g}_6^* = 6, \quad \tilde{g}_7^* = 3, \quad \tilde{g}_8^* = 84.
\end{aligned} \tag{3.62}
$$

For this fixed point, the eigenvalues of the matrix $\frac{\partial \tilde{\beta}_i}{\partial \tilde{g}_j}$ are

$$
\lambda_i = 6,\ 2,\ 2,\ -2,\ -2,\ -2,\ -2,\ -2 \ . \tag{3.63}
$$

That there are unstable directions at the "prismatic" fixed point also follows from the solution of the Schwinger-Dyson equations.[9] Using (3.38) we see that the large N dimension of the triple-trace operator $(\phi^{abc}\phi^{abc})^3$ is $3(1-\epsilon) + \mathcal{O}(\epsilon^2)$, which means that it is relevant in $d = 3 - \epsilon$ and is one of the operators corresponding to eigenvalue -2. On the

[9] At finite N, using the beta functions given in the Appendix, we are able to find and study additional fixed points numerically. The analysis of behavior of the beta-functions shows that they are all saddle points and, therefore, neither stable in the IR nor in the UV.

other hand, the prism operator is irrelevant and corresponds to eigenvalue 2. Another irrelevant operator is $O_{\text{tetra}}\phi^{abc}\phi^{abc}$; from (3.43) it follows that its large N dimension is $3+5\epsilon+\mathcal{O}(\epsilon^2)$, so it corresponds to eigenvalue 6.

We have also calculated the $1/N$ corrections to the fixed point (3.62):

$$\begin{aligned}
\tilde{g}_1^* &= 1-\frac{6}{N}+\frac{18}{N^2}+\dots,\\
\tilde{g}_2^* &= -42+\frac{384}{N}+\frac{8592}{N^2}+\dots,\\
\tilde{g}_3^* &= 6+\frac{1848}{N^2}+\dots,\\
\tilde{g}_4^* &= 54-\frac{132}{N}+\frac{16392}{N^2}+\dots,\\
\tilde{g}_5^* &= -12+\frac{30}{N}+\frac{2340}{N^2}+\dots,\\
\tilde{g}_6^* &= 6+\frac{36}{N}-\frac{1320}{N^2}+\dots,\\
\tilde{g}_7^* &= 3+\frac{174}{N}+\frac{7080}{N^2}+\dots,\\
\tilde{g}_8^* &= 84+\frac{6732}{N}+\frac{309204}{N^2}+\dots
\end{aligned} \tag{3.64}$$

For the scaling dimension of ϕ, we find from (3.85):

$$\Delta_\phi=\frac{d-2}{2}+\gamma_\phi=\frac{1}{2}-\frac{\epsilon}{2}+\epsilon^2\left(1-\frac{12}{N}+\frac{75}{N^2}+\dots\right)+\mathcal{O}(\epsilon^3)\,. \tag{3.65}$$

In the large N limit, (3.65) is in agreement with the solution of the S-D equation (3.36). For the scaling dimension of $\phi^{abc}\phi^{abc}$, we find

$$\Delta_{\phi^2}=d-2+\gamma_{\phi^2}=1-\epsilon+32\epsilon^2\left(1-\frac{12}{N}+\frac{75}{N^2}+\dots\right)+\mathcal{O}(\epsilon^3)\,. \tag{3.66}$$

In the large N limit this is in agreement with (3.38). In general, calculating the $1/N$ corrections in tensor models seems to be quite difficult [102], but it is nice to see that in the prismatic QFT the $3-\epsilon$ expansion provides us with explicit results for the $1/N$ corrections to scaling dimensions of various operators.

The scaling dimension of the marginal prism operator is

$$\Delta_{\rm prism} = d + \frac{d\tilde{\beta}_1}{d\tilde{g}_1} = 3 - \epsilon - 2\epsilon + 4\epsilon\tilde{g}_1^* + \ldots = 3 + \epsilon + \mathcal{O}(\epsilon^2) \ , \tag{3.67}$$

which is in agreement with (3.39).

We have also performed two-loop calculations of the scaling dimensions of the tetrahedron and pillow operators; see the appendix for the anomalous dimension matrix. In the large N limit, we find

$$\begin{aligned} \Delta_{\rm tetra} &= 2(d-2) + \gamma_{\rm tetra} = 2 + 6\epsilon + \mathcal{O}(\epsilon^2) \ , \\ \Delta_{\rm pillow} &= 2(d-2) + \gamma_{\rm pillow} = 2 - 2\epsilon + \mathcal{O}(\epsilon^2) \ , \end{aligned} \tag{3.68}$$

which is in agreement with the S-D result (3.43). Thus, we see that the large N $3-\epsilon$ expansions from the Schwinger-Dyson approach have passed a number of 2-loop consistency checks.

We have also solved the equations for the fixed points of two-loop beta functions numerically for finite N. The results for the prismatic fixed point are shown in table 1. These results are in good agreement with the analytic $1/N$ expansions (3.64) for $N \geq 200$. At $N = N_{\rm crit}$, where $N_{\rm crit} \approx 53.65$, the prismatic fixed point in $3-\epsilon$ dimensions merges

N	$\tilde{g}_1^*$	$\tilde{g}_2^*$	$\tilde{g}_3^*$	$\tilde{g}_4^*$	$\tilde{g}_5^*$	$\tilde{g}_6^*$	$\tilde{g}_7^*$	$\tilde{g}_8^*$	γ_ϕ/ϵ^2
54	0.89	-33.06	7.87	83.69	-11.13	6.86	27.37	2047.16	0.80
100	0.94	-37.56	6.23	55.35	-11.53	6.28	5.98	212.08	0.89
200	0.97	-39.90	6.05	53.8	-11.80	6.15	4.09	127.90	0.94
400	0.99	-40.99	6.01	53.78	-11.91	6.08	3.48	103.03	0.97
2000	1.00	-41.81	6.00	53.94	-11.98	6.02	3.09	87.45	0.99
5000	1.00	-41.92	6.00	53.97	-11.99	6.01	3.04	85.36	0.998
10000	1.00	-41.96	6.00	53.99	-12.00	6.00	3.02	84.68	0.999
100000	1.00	-42.00	6.00	54.00	-12.00	6.00	3.00	84.07	1.00

Table 1: The numerical solutions for the coupling constants defined in (3.60)

with another fixed point;[10] they are located at

$$\tilde{g}_1^* = 0.89, \quad \tilde{g}_2^* = -32.90, \quad \tilde{g}_3^* = 8.24, \quad \tilde{g}_4^* = 92.01,$$
$$\tilde{g}_5^* = -11.15, \quad \tilde{g}_6^* = 7.00, \quad \tilde{g}_7^* = 35.33, \quad \tilde{g}_8^* = 3155.29\ . \tag{3.69}$$

For $N < N_{\text{crit}}$ both of them become complex. For example, for $N = 53.6$ the two complex fixed points are at

$$\tilde{g}_1^* = 0.89 - 0.0002i, \quad \tilde{g}_2^* = -32.89 + 0.04i, \quad \tilde{g}_3^* = 8.24 + 0.15i, \quad \tilde{g}_4^* = 91.98 + 3.51i,$$
$$\tilde{g}_5^* = -11.15 - 0.01i, \quad \tilde{g}_6^* = 7.00 + 0.06i, \quad \tilde{g}_7^* = 35.19 + 3.61i, \quad \tilde{g}_8^* = 3107.77 + 554.01i \tag{3.70}$$

and at the complex conjugate values.

3.1.6 Bosonic Quantum Mechanics

The action (3.2) for $d = 1$ describes the quantum mechanics of a particle moving in N^3 dimensions with a non-negative sextic potential which vanishes at the origin.[11] Such a problem should exhibit a discrete spectrum with positive energy levels, and it is conceivable that in the large N limit the gaps become exponentially small, leading to a nearly conformal behavior. For moderate values of N, this quantum mechanics problem may even be accessible to numerical studies.

Solving for the scaling dimensions of type A/C bilinears in $d = 1$, we find that the low-lying eigenvalues are

$$\Delta = 1,\ 1.57,\ 2,\ 3.29,\ 4.12,\ 5.36,\ 6.14,\ 7.38,\ 8.15,\ 9.39,\ 10.15,\ 11.40, \ldots \tag{3.71}$$

[10] This is similar, for example, to the situation in the $O(N)$ invariant cubic theory in $6 - \epsilon$ dimensions [103, 104], where $N_{\text{crit}} \approx 1038.266$. For general discussions of mergers of fixed points, see [91, 93].

[11] A very similar $d = 1$ model with a stable sextic potential was studied in [105, 106] using the formulation [63] where a rank-3 tensor is viewed as D matrices. It was argued [105, 106] that the sextic bosonic model does not have a good IR limit. We, however, don't find an obvious problem with the prismatic $d = 1$ model because the complex scaling dimensions are absent for the bilinear operators. We note that the negative scaling dimension (3.17), which we find for ϕ, is quite far from the 1/6 mentioned in [105, 106].

The plot for the eigenvalues is shown in figure 3.13.

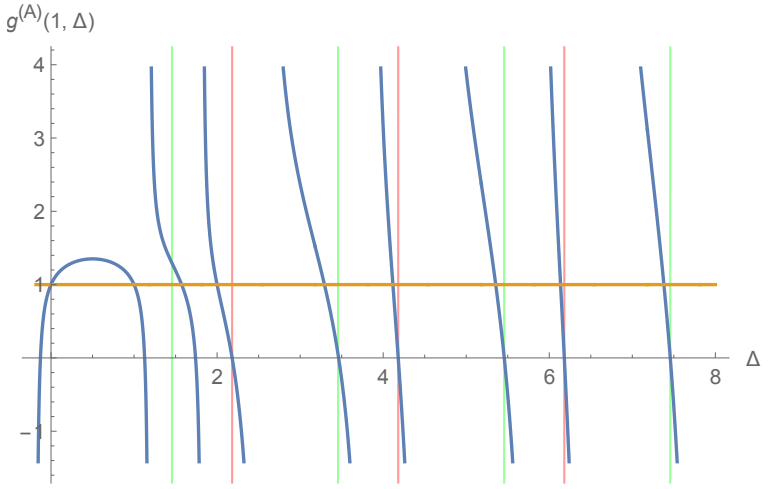

Figure 3.13: The spectrum of scalar type A/C bilinears in 1d. Red vertical lines are asymptotes corresponding to $-2\Delta_\phi + 2n$ and green vertical lines are asymptotes corresponding to $-2\Delta_\chi + 2n$.

The smallest positive eigenvalue, $\Delta = 1$, is the continuation of the solution $\Delta = d$ present for any d. As discussed in section (3.1.4), it may correspond to a redundant operator. The next scaling dimension, $\Delta = 1.57317$, may correspond to a mixture involving $\phi^{abc}\phi^{abc}$. The appearance of scaling dimension 2, which was also seen for the fermionic SYK and tensor models, means that the its dual[12] should involve dilaton gravity in AdS_2 [108, 109, 110, 111].

Let us also list the type B scaling dimensions, i.e. the ones corresponding to operators $\phi^{abc}\partial_t^{2n}\chi^{abc}$. Here we find real solutions $\Delta = 1.01,\ 2.96,\ 4.94,\ 6.93,\ \ldots$.

For large excitation numbers n, the type A/C scaling dimensions appear to (slowly) approach $-2\Delta_\phi + 2n$ and $-2\Delta_\chi + 2n$ rather than $2\Delta_\phi + 2n$ and $2\Delta_\chi + 2n$, as shown in figure 3.4. The type B scaling dimensions also appear to slowly approach $-\Delta_\phi - \Delta_\chi + 2n$ rather than $\Delta_\phi + \Delta_\chi + 2n$. This is likely due to the fact that Δ_ϕ is negative. Further work is needed to understand better the new features of the large N solution in the regime where $d < 1.35$ and $\Delta_\phi < 0$.

[12]Of course, as observed in [107, 61], there are important differences between the holographic duals of tensor models and SYK models.

3.1.7 Discussion

In this paper we presented exact results for the $O(N)^3$ invariant theory (3.2) in the prismatic large N limit where $g_1 N^3$ is held fixed. This approach may be generalized to an $O(N)^p$ invariant theory of a rank-p bosonic tensor $\phi^{a_1 \ldots a_p}$, with odd $p \geq 3$. It has a positive potential of order $2p$:

$$S_{2p} = \int d^d x \left(\frac{1}{2} (\partial_\mu \phi^{abc})^2 + \frac{g_1}{(2p)!} (\phi^p)^{a_1 \ldots a_p} (\phi^p)^{a_1 \ldots a_p} \right) . \tag{3.72}$$

To solve these models in the large N limit where $g_1 N^p$ is held fixed, we may rewrite the action with the help of an additional tensor field χ:

$$S = \int d^d x \left(\frac{1}{2} (\partial_\mu \phi^{abc})^2 + \frac{g}{p!} (\phi^p)^{a_1 \ldots a_p} \chi^{a_1 \ldots a_p} - \frac{1}{2} \chi^{a_1 \ldots a_p} \chi^{a_1 \ldots a_p} \right) . \tag{3.73}$$

For discussions of the structure of the interaction vertex with odd $p > 3$, see [19, 28, 29]. The models (3.72) are tensor counter-parts of the SYK-like models introduced in [79]; therefore, the Schwinger-Dyson equations derived there should be applicable to the tensor models. It would be interesting to study the large N solution of theories with $p > 3$ in more detail using methods analogous to the ones used for $p = 3$.

In this paper we analyzed the renormalization of the prismatic theory at the two-loop order, using the beta functions in [98, 99]. The general four-loop terms are also given there, and it would be interesting to study the effects they produce. It should be possible to extend the calculations to even higher loops by modifying the calculations in [101] to an arbitrary tensorial interaction, which we leave as a possible avenue for future work. In this context, it would also be interesting to study the possibility of fixed points with other large N scalings, perhaps dominated by the "wheel" interaction (g_2) of figure 3.1, in addition to the large N fixed point dominated by the prism interaction (g_1) studied in this paper.[13]

Another interesting extension of the $O(N)^3$ symmetric model (3.2) is to add a 2-component Majorana fermion ψ^{abc}, so that the fields can be assembled into a $d = 3$

[13] A $d = 0$ theory with wheel interactions was studied in [112].

$\mathcal{N}=1$ superfield

$$\Phi^{abc} = \phi^{abc} + \bar{\theta}\psi^{abc} + \bar{\theta}\theta\chi^{abc} \tag{3.74}$$

Then the prismatic scalar potential follows if we assume a tetrahedral superpotential for Φ^{abc} [19]. Large N treatments of supersymmetric tensor and SYK-like models with two supercharges have been given in [79, 88], and we expect the solution of the $\mathcal{N}=1$ super-tensor model in $d<3$ to work analogously. An advantage of the tensor QFT approach is that one can also develop the $3-\epsilon$ expansion using the standard renormalized perturbation theory. In the supersymmetric case, it is sufficient to introduce only three coupling constants:

$$\begin{aligned} W &= g_1 \Phi^{a_1 b_1 c_1}\Phi^{a_1 b_2 c_2}\Phi^{a_2 b_1 c_2}\Phi^{a_2 b_2 c_1} \\ &+ g_2\big(\Phi^{a_1 b_1 c_1}\Phi^{a_1 b_1 c_2}\Phi^{a_2 b_2 c_1}\Phi^{a_2 b_2 c_2} + \Phi^{a_1 b_1 c_1}\Phi^{a_2 b_1 c_1}\Phi^{a_1 b_2 c_2}\Phi^{a_2 b_2 c_2} + \Phi^{a_1 b_1 c_1}\Phi^{a_1 b_2 c_1}\Phi^{a_2 b_1 c_2}\Phi^{a_2 b_2 c_2}\big) \\ &+ g_3 \Phi^{a_1 b_1 c_1}\Phi^{a_1 b_1 c_1}\Phi^{a_2 b_2 c_2}\Phi^{a_2 b_2 c_2} \ , \end{aligned} \tag{3.75}$$

and it is possible to find explicit expressions for the beta functions and operator scaling dimensions [113]. Also, directly in $d=3$ it is possible to couple the $\mathcal{N}=1$ theory with the above superpotential to $O(N)_{k_1}\times O(N)_{k_2}\times O(N)_{k_3}$ supersymmetric Chern-Simons gauge theory with levels k_1, k_2, k_3, and derive the corresponding beta functions for couplings g_i [113].

3.1.8 The two-loop beta functions and anomalous dimensions

In this Appendix we state our explicit two-loop results for the $O(N)^3$ invariant theory with the 8 coupling constants and interaction terms

$$\begin{aligned} &\frac{g_1}{6!}\phi^{a_1 b_1 c_1}\phi^{a_1 b_2 c_2}\phi^{a_2 b_1 c_2}\phi^{a_3 b_3 c_1}\phi^{a_3 b_2 c_3}\phi^{a_2 b_3 c_3} + \frac{g_2}{6!}\phi^{a_1 b_1 c_1}\phi^{a_1 b_2 c_2}\phi^{a_2 b_2 c_3}\phi^{a_2 b_3 c_1}\phi^{a_3 b_3 c_2}\phi^{a_3 b_1 c_3} \\ &+ \frac{g_3}{3\cdot 6!}\big(\phi^{a_1 b_1 c_1}\phi^{a_2 b_1 c_1}\phi^{a_1 b_2 c_2}\phi^{a_2 b_2 c_3}\phi^{a_3 b_3 c_2}\phi^{a_3 b_3 c_3} + \phi^{a_1 b_1 c_1}\phi^{a_1 b_2 c_1}\phi^{a_2 b_1 c_2}\phi^{a_2 b_2 c_3}\phi^{a_3 b_3 c_2}\phi^{a_3 b_3 c_3} \\ &+ \phi^{a_1 b_1 c_1}\phi^{a_2 b_1 c_1}\phi^{a_1 b_2 c_2}\phi^{a_2 b_3 c_2}\phi^{a_3 b_2 c_3}\phi^{a_3 b_3 c_3}\big) \\ &+ \frac{g_4}{3\cdot 6!}\big(\phi^{a_1 b_1 c_1}\phi^{a_1 b_1 c_2}\phi^{a_2 b_2 c_2}\phi^{a_2 b_2 c_3}\phi^{a_3 b_3 c_3}\phi^{a_3 b_3 c_1} + \phi^{a_1 b_1 c_1}\phi^{a_2 b_1 c_1}\phi^{a_2 b_2 c_2}\phi^{a_3 b_2 c_2}\phi^{a_3 b_3 c_3}\phi^{a_1 b_3 c_3} \end{aligned}$$

$$+\phi^{a_1b_1c_1}\phi^{a_1b_2c_1}\phi^{a_2b_2c_2}\phi^{a_2b_3c_2}\phi^{a_3b_3c_3}\phi^{a_3b_1c_3}\Big)$$
$$+\frac{g_5}{3\cdot 6!}\Big(\phi^{a_1b_1c_1}\phi^{a_1b_2c_2}\phi^{a_2b_1c_2}\phi^{a_3b_2c_1}\phi^{a_2b_3c_3}\phi^{a_3b_3c_3}+\phi^{a_1b_1c_1}\phi^{a_2b_1c_2}\phi^{a_1b_2c_2}\phi^{a_1b_2c_3}\phi^{a_3b_2c_3}\phi^{a_3b_3c_3}$$
$$+\phi^{a_1b_1c_1}\phi^{a_2b_2c_1}\phi^{a_2b_1c_2}\phi^{a_1b_2c_3}\phi^{a_3b_3c_2}\phi^{a_3b_3c_3}\Big)$$
$$+\frac{g_6}{6!}\phi^{abc}\phi^{abc}\phi^{a_1b_1c_1}\phi^{a_1b_2c_2}\phi^{a_2b_1c_2}\phi^{a_2b_2c_1}$$
$$+\frac{g_7}{3\cdot 6!}\phi^{abc}\phi^{abc}(\phi^{a_1b_1c_1}\phi^{a_1b_1c_2}\phi^{a_2b_2c_1}\phi^{a_2b_2c_2}+\phi^{a_1b_1c_1}\phi^{a_2b_1c_1}\phi^{a_1b_2c_2}\phi^{a_2b_2c_2}+\phi^{a_1b_1c_1}\phi^{a_1b_2c_1}\phi^{a_2b_1c_2}\phi^{a_2b_2c_2})$$
$$+\frac{g_8}{6!}(\phi^{abc}\phi^{abc})^3\ . \tag{3.76}$$

We find

$$\begin{aligned}\beta_1 =& -2g_1\epsilon+\frac{1}{270(8\pi)^2}\Big((g_5^2+3(g_1^2+8g_6^2))N^3+3(3g_5^2+4(2g_1+3g_2+4g_6)g_5+6g_1(g_1+3g_2))N^2\\&+2(32g_5^2+(90g_1+72g_2+96g_6)g_5+6g_4(9g_2+4g_5)+9(5g_1^2+6g_2g_1+16g_6g_1+8g_7g_1+9g_2^2\\&+24g_2g_6))N+2g_3^2(N(N+6)+55)+2g_3(9N(g_1(N+8)+8g_2)+6g_4(N+6)\\&+2g_5(N+10)(2N+5)+2(60g_1+63g_2+96g_6+16g_7))+2(36g_4^2+36(5g_1+3g_2+2g_5)g_4\\&+80g_5^2+4g_5(45g_1+4(9g_2+6g_6+8g_7))+3(34g_1^2+12(7g_2+4g_6+2g_7+20g_8)g_1+27g_2^2\\&+128g_6^2+48g_2(g_6+2g_7))\Big)\end{aligned} \tag{3.77}$$

$$\begin{aligned}\beta_2 =& -2g_2\epsilon+\frac{1}{270(8\pi)^2}\Big(g_5(12g_1+g_5)N^2+2(13g_5^2+18(g_1+g_2)g_5+9g_1(g_1+2g_4+8g_6)+72g_2g_7)N\\&+2g_3^2(N(N+6)+19)+2g_3(3N(3g_2(N+4)+8g_1)+6g_4(N+2)+6g_5(N+6)+30g_1+36g_2\\&+32g_7)+2(36g_1^2+54g_2g_1+96g_7g_1+45g_2^2+12g_4^2+20g_5^2+12g_4(3g_1+9g_2+2g_5)\\&+12g_5(4g_1+3g_2+8g_6)+72g_2g_7+720g_2g_8)\Big)\end{aligned} \tag{3.78}$$

$$\begin{aligned}\beta_3 =& -2g_3\epsilon+\frac{1}{270(8\pi)^2}\Big(2(g_5^2+8g_7^2)N^3+3(6g_1^2+12g_5g_1+27g_2^2+5g_5^2)N^2+2(83g_5^2+2(66g_1\\&+63g_2+48g_6+64g_7)g_5+9(2g_1+3g_2)(4g_1+3g_2)+96(g_1+3g_2)g_7)N+g_3^2(N(N(2N+31)\end{aligned}$$

$$
\begin{aligned}
&+ 244) + 388) + 18g_4^2(N(N+16)+12) + 12g_4(3g_1(N+1)(N+14) + g_5(5N(N+6)+72)\\
&+ (N+2)(9g_2(N+3)+8g_7N) + 96g_6 + 64g_7) + 4g_3(3g_4(N(N(N+6)+28)+102)\\
&+ N(g_5(11N+74) + 6(g_1+3g_2+4g_7)N + 66g_1 + 72g_2 + 60g_6 + 84g_7) + 194g_5\\
&+ 3(71g_1 + 81g_2 + 32g_6 + 76g_7 + 120g_8)) + 4(92g_5^2 + 2(93g_1 + 90g_2 + 72g_6 + 80g_7)g_5\\
&+ 128g_7^2 + 9(7g_1^2 + 15g_2g_1 + 9g_2^2 + 24(g_1+g_2)g_6) + 144(g_1+g_2)g_7)\Big) \qquad (3.79)
\end{aligned}
$$

$$
\begin{aligned}
\beta_4 =& -2g_4\epsilon + \frac{1}{270(8\pi)^2}\Big((g_5^2+8g_7^2)N^3 + 4g_5(3g_1+g_5)N^2 + 6(3g_1^2+9g_5^2+8(g_1+3g_2)g_7\\
&+ 2g_5(5g_1+9g_2+4(g_6+3g_7)))N + 2g_3^2(N(N(N+7)+34)+113) + 9g_4^2(N(N+2)^2+52)\\
&+ 4g_3(9g_2(N+2)^2 + 3g_1(N+1)(N+13) + N(g_4(6N+75) + g_5(6N+31) + 8g_7(N+4))\\
&+ 16(3g_4+5g_5+6g_6+5g_7)) + 12g_4(3g_1(N+12) + 2g_5(N(N+6)+13) + 8N(g_7(N+2)+3g_6)\\
&+ 48g_2 + 44g_7 + 120g_8) + 2(54g_1^2 + 162g_2g_1 + 96g_7g_1 + 81g_2^2 + 58g_5^2 + 128g_7^2\\
&+ 4g_5(27g_1 + 27g_2 + 24g_6 + 32g_7))\Big) \qquad (3.80)
\end{aligned}
$$

$$
\begin{aligned}
\beta_5 =& -2g_5\epsilon + \frac{2}{270(8\pi)^2}\Big((3(g_1g_5+8g_6g_7)N^3 + 2(9g_1^2 + 9(3g_2+g_5)g_1 + g_5(27g_2+6g_5+16g_7))N^2\\
&+ (99g_1^2 + 6(45g_2+35g_5+36g_6+40g_7)g_1 + 81g_2^2 + 216g_2(g_5+g_6)\\
&+ 4g_5(21g_5+42g_6+38g_7))N + g_3^2(N(5N+52)+161) + 36g_4^2(N+3)\\
&+ 3g_4(12g_1(N(N+5)+12) + g_5(N(N(N+6)+52)+132) + 6(N+2)(4g_6N+9g_2)\\
&+ 96g_6 + 64g_7) + 2g_3(6g_1(N(3N+16)+37) + 9g_2(10N+23) + N(g_4(6N+39)\\
&+ g_5(N(N+13)+97) + 24g_6(N+4)) + 6(23g_4+33g_5+32g_6+24g_7)) + 270g_1^2\\
&+ 243g_2^2 + 212g_5^2 + 432g_1g_2 + 444g_1g_5 + 504g_2g_5 + 432g_1g_6 + 432g_2g_6\\
&+ 384g_5g_6 + 384g_1g_7 + 288g_2g_7 + 328g_5g_7 + 768g_6g_7 + 720g_5g_8)\Big) \qquad (3.81)
\end{aligned}
$$

$$\beta_6 = -2g_6\epsilon + \frac{2}{270(8\pi)^2}\Big(2(g_5g_7 + 3g_6(g_1 + 12g_8))N^3 + (6(9g_2g_6 + 4(g_1 + 2g_6)g_7)$$
$$+ g_5(3g_1 + 12g_6 + 10g_7 + 72g_8))N^2 + (7g_5^2 + 2(3g_1 + 9g_2 + 12g_6 + 32g_7 + 72g_8)g_5$$
$$+ 3(3g_1 + 12(2g_6 + g_7 + 12g_8)g_1 + 48g_6^2 + 8(3g_2 + 5g_6)g_7))N + g_3^2(4N + 6)$$
$$+ 3g_4(12g_1N + g_5(N(N + 6) + 10) + 4g_7(N + 2) + 18g_2 + 60g_6) + 2g_3(6g_1(N + 4)$$
$$+ g_5(N(N + 6) + 19) + 3g_6(N(N + 10) + 4) + 2g_7N(N + 5) + 9g_2 + 21g_4 + 18(g_7 + 4g_8))$$
$$+ 13g_5^2 + 48g_7^2 + 36g_1g_2 + 30g_1g_5 + 18g_2g_5 + 48g_1g_6 + 72g_2g_6 + 108g_5g_6 + 120g_1g_7$$
$$+ 36g_2g_7 + 92g_5g_7 + 120g_6g_7 + 432g_2g_8 + 144g_5g_8 + 1296g_6g_8\Big) \tag{3.82}$$

$$\beta_7 = -2g_7\epsilon + \frac{1}{270(8\pi)^2}\Big(4(3g_5g_6 + g_7(2g_3 + 3g_4 + 36g_8))N^3 + (10g_3^2 + 24(g_4 + 3g_6$$
$$+ 2(g_7 + 6g_8))g_3 + 7g_5^2 + 3(9g_4^2 + 8(3g_6 + 2(g_7 + 9g_8))g_4 + 8(5g_7^2 + (g_1 + 3g_2 + 2g_5)g_7$$
$$+ (3g_1 + g_5)g_6)))N^2 + (9g_1^2 + 54g_5g_1 + 72g_6g_1 + 216g_7g_1 + 48g_3^2 + 63g_4^2 + 22g_5^2 + 216g_6^2$$
$$+ 216g_7^2 + 216g_2g_6 + 216g_5g_6 + 144g_2g_7 + 160g_5g_7 + 576g_6g_7 + 144(3g_1 + 9g_2 + 5g_5)g_8$$
$$+ 6g_4(6g_1 + 18g_2 + 21g_5 + 36g_6 + 52g_7 + 72g_8) + 4g_3(3g_1 + 9g_2 + 36g_4 + 19g_5 + 42g_6$$
$$+ 90g_7 + 144g_8))N + 2(27g_1^2 + 3(9g_2 + 23g_3 + 30g_4 + 12g_5 + 48g_6 + 40g_7 + 144g_8)g_1$$
$$+ 9g_2(7g_3 + 6(g_5 + 2g_6 + 4g_7)) + 2(31g_3^2 + (81g_4 + 50g_5 + 114g_6 + 112g_7 + 216g_8)g_3$$
$$+ 54g_4^2 + 21g_5^2 + 108g_6^2 + 96g_7^2 + 66g_5g_6 + 106g_5g_7 + 144g_6g_7 + 72(2g_5 + 9g_7)g_8$$
$$+ 3g_4(17g_5 + 36g_6 + 66g_7 + 72g_8)))\Big) \tag{3.83}$$

$$\beta_8 = -2g_8\epsilon + \frac{1}{270(8\pi)^2}\Big(2(g_5(2(3g_6(N^2 + N + 3) + 7g_7(N + 1) + 36g_8) + 3g_1) + 2(3g_6^2N^3$$
$$+ g_7^2N^3 + 18g_8^2(3N^3 + 22) + 3g_7^2N^2 + 12g_6g_7N^2 + 72g_8(g_7(N^2 + N + 1) + 3g_6N) + 9g_6^2N$$
$$+ 21g_7^2N + 12g_6g_7N + g_1(9g_6N + 6g_7) + 6g_6^2 + 23g_7^2 + 9g_2g_6 + 48g_6g_7) + g_5^2(N + 1)$$

$$+ 3g_4(2(6g_6N + g_7(N(N+3)+5) + 36g_8) + 3g_5)) + g_3^2(2N+9) + 4g_3(3g_4N + 3g_6(2N+5)$$
$$+ 2g_7(N(N+3)+7) + 36g_8N + 2g_5) + 9g_2^2 + 39g_4^2\Big) \tag{3.84}$$

and

$$\gamma_\phi = \frac{1}{12\cdot 90^2(8\pi)^4}\Big((3g_1^2 + 9g_2^2 + g_3^2 + 3g_4^2 + g_5^2 + 12g_6^2 + 4g_7^2 + 72g_8^2)N^6 + (6g_3^2 + 2(3g_1 + 9g_2$$
$$+ 6(g_4+g_5) + 8g_7)g_3 + 9g_4^2 + 5g_5^2 + 12g_7^2 + 54g_1g_2 + 24g_1g_5 + 24g_5g_6 + 48g_6g_7$$
$$+ 12g_4(g_5+2g_7) + 144g_7g_8)N^5 + (81g_1^2 + 12(9g_3 + 6g_4 + 5g_5 + 12g_6 + 2g_7)g_1 + 81g_2^2$$
$$+ 39g_3^2 + 27g_4^2 + 51g_5^2 + 36g_6^2 + 84g_7^2 + 108g_3g_4 + 76g_3g_5 + 72g_4g_5 + 96g_3g_6 + 144g_4g_6$$
$$+ 48g_5g_6 + 80g_3g_7 + 96g_4g_7 + 88g_5g_7 + 48g_6g_7 + 36g_2(2g_3 + g_4 + 4g_5 + 2g_7)$$
$$+ 144(g_3 + g_4 + 3g_6 + g_7)g_8)N^4 + (102g_1^2 + 6(75g_2 + 47g_3 + 54g_4 + 64g_5 + 24g_6$$
$$+ 68g_7 + 24g_8)g_1 + 54g_2^2 + 160g_3^2 + 171g_4^2 + 143g_5^2 + 120g_6^2 + 148g_7^2 + 432g_8^2 + 288g_3g_4$$
$$+ 344g_3g_5 + 336g_4g_5 + 336g_3g_6 + 288g_4g_6 + 360g_5g_6 + 336g_3g_7 + 336g_4g_7 + 296g_5g_7$$
$$+ 336g_6g_7 + 144(2g_3 + 3(g_4+g_5) + g_7)g_8 + 18g_2(19g_3 + 24g_4 + 14g_5 + 32g_6 + 12g_7 + 24g_8))N^3$$
$$+ 2(189g_1^2 + 6(45g_2 + 58g_3 + 66g_4 + 49g_5 + 72g_6 + 54g_7 + 108g_8)g_1 + 216g_2^2 + 177g_3^2$$
$$+ 189g_4^2 + 176g_5^2 + 216g_6^2 + 120g_7^2 + 318g_3g_4 + 330g_3g_5 + 336g_4g_5 + 360g_3g_6 + 288g_4g_6$$
$$+ 312g_5g_6 + 328g_3g_7 + 312g_4g_7 + 372g_5g_7 + 336g_6g_7 + 72(4g_3 + 4g_4 + 5g_5 + 4g_7)g_8$$
$$+ 18g_2(17g_3 + 19g_4 + 20g_5 + 12g_6 + 26g_7 + 12g_8))N^2 + 4(81g_1^2 + 3(63g_2 + 63g_3$$
$$+ 51g_4 + 64g_5 + 60g_6 + 70g_7 + 36g_8)g_1 + 81g_2^2 + 87g_3^2 + 72g_4^2 + 90g_5^2 + 72g_6^2 + 96g_7^2$$
$$+ 207g_3g_4 + 185g_3g_5 + 189g_4g_5 + 156g_3g_6 + 216g_4g_6 + 204g_5g_6 + 184g_3g_7 + 174g_4g_7$$
$$+ 182g_5g_7 + 168g_6g_7 + 36(6g_3 + 3g_4 + 5g_5 + 12g_6 + 4g_7)g_8 + 9g_2(23g_3 + 18g_4 + 19g_5$$
$$+ 24g_6 + 18g_7 + 36g_8))N + 4(48g_1^2 + (90g_2 + 78g_3 + 90g_4 + 84g_5 + 72g_6 + 60g_7 + 72g_8)g_1$$
$$+ 45g_2^2 + 43g_3^2 + 51g_4^2 + 42g_5^2 + 48g_6^2 + 52g_7^2 + 144g_8^2 + 72g_3g_4 + 82g_3g_5 + 78g_4g_5 + 96g_3g_6$$
$$+ 72g_4g_6 + 72g_5g_6 + 84g_3g_7 + 96g_4g_7 + 76g_5g_7 + 96g_6g_7 + 18g_2(4g_3 + 5g_4 + 5g_5 + 4(g_6+g_7))$$
$$+ 72(g_3 + 2g_4 + g_5 + 2g_7)g_8)\Big) \tag{3.85}$$

At the two-loop level we also find the relation $\gamma_{\phi^2} = 32\gamma_\phi$.

We can study the anomalous dimensions for quartic operators

$$O_1 = O_{\text{tetra}} = \phi^{a_1 b_1 c_1}\phi^{a_1 b_2 c_2}\phi^{a_2 b_1 c_2}\phi^{a_2 b_2 c_1},$$
$$O_2 = O_{\text{pillow}} = \frac{1}{3}\left(\phi_{a_1 b_1 c_1}\phi_{a_2 b_1 c_1}\phi_{a_1 b_2 c_2}\phi_{a_2 b_2 c_2} + \phi_{a_1 b_1 c_1}\phi_{a_1 b_2 c_1}\phi_{a_2 b_1 c_2}\phi_{a_2 b_2 c_2} + \phi_{a_1 b_1 c_1}\phi_{a_1 b_1 c_2}\phi_{a_2 b_2 c_1}\phi_{a_2 b_2 c_2}\right)$$
$$O_3 = O_{\text{d.t.}} = \phi^{a_1 b_1 c_1}\phi^{a_1 b_1 c_1}\phi^{a_2 b_2 c_2}\phi^{a_2 b_2 c_2}. \tag{3.86}$$

The matrix of anomalous dimensions for quartic operators can be written in the following way

$$\gamma_O^{11} = \frac{1}{720\pi^2}\left(2(6g_1 + 2g_3 + 3g_4 + 5g_5 + 2g_7 + 12g_8) + g_1(N^3 + 12N + 8) + 4(g_5 + 3g_6 + g_7)N + \right.$$
$$\left. + 9g_2N^2 + 2g_5N^2 + g_3\left(6N + N^2\right)\right),$$
$$\gamma_O^{12} = \frac{1}{2160\pi^2}\left(2(9g_2 + 9g_3 + 6g_4 + 11g_5 + 12g_6 + 8g_7) + 6g_1(6 + 3N + 2N^2) + 36g_2N + 6g_4N + \right.$$
$$\left. + 12g_6(2N + N^2) + 2g_3(5N + N^2) + g_5(24N + 5N^2 + N^3)\right)$$
$$\gamma_O^{13} = \frac{1}{180\pi^2}\left(6g_2 + 2g_3 + 6g_1N + g_6(8 + N^3) + g_5(2 + 2N + N^2)\right)$$
$$\gamma_O^{21} = \frac{1}{720\pi^2}\left(2(12g_1 + 9g_2 + 11g_3 + 12g_4 + 9g_5 + 12g_6 + 8g_7) + g_5N^3 + \right.$$
$$\left. + 2(3g_1 + 9g_2 + 7g_3 + 9g_4 + 9g_5 + 6g_6 + 10g_7)N + 2(3(g_1 + g_3 + g_4) + g_5)N^2\right)$$
$$\gamma_O^{22} = \frac{1}{2160\pi^2}\left(64g_3 + 66g_4 + 62g_5 + 48g_6 + 60g_7 + 72g_8 + 6g_1(N + 1)(N + 8) + 18g_2(4 + 2N + N^2) + \right.$$
$$\left. + 3g_4(18N + 4N^2 + N^3) + 2g_3(27N + 6N^2 + N^3) + 4(6g_6N + 4g_7(2N + N^2) + g_5(10N + 3N^2))\right)$$
$$\gamma_O^{23} = \frac{1}{180\pi^2}\left(6g_3 + 6g_4 + 4g_5 + 8g_7 + 3g_1(N + 2) + 9g_2N + 5g_5N + g_7N^3 + 3g_4(N^2 + N) + \right.$$
$$\left. + 2g_3(2N + N^2)\right)$$
$$\gamma_O^{31} = \frac{1}{720\pi^2}\left(3g_2 + 3g_5 + 4g_6 + 8g_7 + 3g_1N + g_3(5 + 2N) + 6g_4N + g_5(N^2 + N) + \right.$$
$$\left. + 4(g_7N + 9g_8N + g_7N^2) + 2g_6(3N + N^3)\right)$$
$$\gamma_O^{32} = \frac{1}{2160\pi^2}\left(6g_1 + 7g_5 + 24g_6 + 22g_7 + 36g_8 + 2g_3(5 + 3N + N^2) + 3g_4(5 + 3N + N^2) + 7g_5N + \right.$$
$$\left. + 12g_6(N + N^2) + 36g_8(N + N^2) + 2g_7(13N + 3N^2 + N^3)\right) \tag{3.87}$$

The results for the quartic operator dimensions in the prismatic large N limit are listed in (3.68).

A consistent truncation of the system of eight coupling constants is to keep only g_8 non-vanishing, since the triple-trace term is the only one which has $O(N^3)$ symmetry. Then we find

$$\beta_8 = -2g_8\epsilon + \frac{1}{15(8\pi)^2} g_8^2(3N^3+22) \ , \qquad \gamma_\phi = \frac{1}{1350(8\pi)^4} g_8^2(N^3+2)(N^3+4) \ , \quad (3.88)$$

in agreement with [101, 99]. Thus, there is a fixed point with

$$g_8^* = \frac{30(8\pi)^2\epsilon}{3N^3+22} \ , \qquad g_i^* = 0, \quad i = 1, \ldots, 7 \ . \quad (3.89)$$

At this fixed point,

$$\partial\beta_8/\partial g_8 = -2\epsilon + \frac{2}{15(8\pi)^2} g_8^*(3N^3+22) = 2\epsilon + \mathcal{O}(\epsilon^2) \ , \quad (3.90)$$

so the triple-trace operator is irrelevant. However, the other 7 operators appear to be relevant for sufficiently large N. For example,

$$\frac{\partial\beta_1}{\partial g_1} = -2\epsilon + \frac{2g_8^*}{9(8\pi)^2} = \epsilon\left(-2 + \frac{20}{3(3N^3+22)}\right) + \mathcal{O}(\epsilon^2) \ . \quad (3.91)$$

So, this fixed point has 7 unstable directions. Examination of 4-loop and higher corrections [101, 99] shows that the $3-\epsilon$ expansions of operator dimensions at this fixed point do not generally have a finite large N limit starting with order ϵ^3. This is in contrast with the prismatic fixed point where all the g_i^* are non-vanishing and scale as (3.60); as a result, the large N limit is smooth.

3.2 Supersymmetric Model

3.2.1 Introduction

In recent literature, there has been strong interest in theories whose dynamical fields are tensors of rank 3 or higher (for reviews, see [21, 114, 14]). Such theories possess a number of interesting features. For example, only the melonic diagrams dominate in

the large N limit, in contrast to the vector models, where only snail diagrams dominate [14], and the matrix models, where all the planar diagrams survive in the large N limit. This fact makes the tensor models similar to the famous Sachdev-Ye-Kitaev (SYK) model [37, 25, 24]. The SYK model contains a disordered coupling constant, making it hard to use standard tools of quantum field theory. The SYK model is believed to describe quantum properties of the extremal charged black holes [109, 110, 111] and therefore may help to serve as a toy model for understanding the AdS/CFT correspondence [115, 116, 117]. It is already used for understanding the properties of the traversable wormholes [118, 119, 46, 48]. While the tensor models [21] exhibit the same properties at the large N limit, they do not have disorder therefore giving us hope that they can be understood at finite N via standard techniques of quantum field theories. These techniques have already brought many interesting results [120, 121, 52, 23, 19, 83, 106, 122, 123, 124, 125]. [126] We shall consider a supersymmetric analogue of such theories, which has been recently considered as a generalization of SYK model [127, 79, 87] or as a quantum mechanical supersymmetric tensor model [88, 128, 129, 130]. Here we will present a similar model in continuous dimension d. We consider a minimal $\mathcal{N}=1$ supersymmetric model, where we have some number of scalar superfields $\Phi_{abc}(x,\theta)$, and indices a,b,c run from 1 to N. These fields are coupled via a "tetrahedral" superpotential[14]

$$S=\int d^dx\, d^2\theta\, \left[\frac{1}{2}\left(D_\alpha\Phi_{abc}\right)^2+g\Phi_{abc}\Phi_{ab'c'}\Phi_{a'bc'}\Phi_{ab'c'}\right]. \tag{3.92}$$

This theory, which is renormalizable in $d<3$, possesses $O(N)\times O(N)\times O(N)$ symmetry rather than $O(N^3)$ (the superpotential breaks such a symmetry, while the free theory, of course, posses the $O(N^3)$ symmetry). This model has been proposed in the paper [19] as a generalization of the scalar melonic theory. It was proved that the non-supersymmetric analogue of this theory has a so-called melonic dominance in the limit when $N\to\infty, g\to 0$ but $gN^{\frac{3}{2}}$ is kept fixed [22]. The proof of this peculiar fact relies on the combinatorial properties of the potential, and therefore is applicable in any di-

[14]Here we will refer to the appendix 3.2.6 and the paper [131] for the notations and the other helpful formulas that will be used through the paper.

mensions and in various theories, provided that the combinatorial properties are left the same. In the case of the supersymmetric theories, the Feynman diagrams, written down in terms of the components, look quite complicated and, at first glance, do not possesses a melonic limit as in the case of scalar model or the SYK model. However, one can develop a supersymmetric version of the usual Feynman diagrams technique and work explicitly with the superfields Φ_{abc} and see that the combinatorial and topological properties are the same as in the case of the scalar tensor models. Therefore, the proof of the dominance of melonic diagrams [23, 132, 19, 22, 133] is applicable in this case and the theory (3.92) also possesses a melonic dominance in the large N limit. We generalize the theory (3.92) where the tethrahydral term is replaced by q-valent maximally single-trace operator to study models with different numbers of the internal propagators in each melon [28, 132].

The properties of such theories in the IR limit can be investigated by solving the Dyson-Schwinger (DS) equations, which are drastically simplified if the theory is melonic. Namely, the dominance of the melonic diagrams in the large N limit can be understood as a suppression of the corrections to the vertex operators in the system of DS equations. The solution of the DS equation in the IR yields a conformal propagator, suggesting that the theory in the IR flows to the fixed point, which is described by some conformal field theory. The existence of the stress-energy tensor with the correct dimension, and the spectra of the operators confirm this hypothesis. Therefore, one can wonder whether it is possible to describe such a transition from the UV scale (where we have a bare conformal propagator determined by commutation relations) to the IR region by means of RG flow and ϵ expansion. Several attempts have been made towards this idea. For example, the melonic scalar theory in 4 dimensions [26] has been considered at the second order of the perturbation theory. For this theory, a melonic fixed point of RG flow was found, even though the corresponding couplings are complex. The complex couplings indicate that the theory is unstable. For example, the dimensions of some operators have imaginary part. One of the reasons of instability could be that the potential is unbounded from below, leading to the decay of the vacuum state. The theory (3.92), being supersymmetric, lacks such a disadvantage.

It is quite interesting that if one drops the fermionic part of the action (3.92) and integrates out the auxiliary field, the theory still possesses the melonic dominance in the large N limit. Such a "prismatic" theory was considered in the paper [3]. The solution of this theory was found in the large N limit and the RG properties were investigated at two loops. As opposed to the standard melonic theory [26], the fixed point is real and first order of ϵ expansion recovers the exact solution in the large N limit.

In this paper we solve the model (3.92) in the large N limit, assuming that the supersymmetry is not broken and that in the IR region the theory is described by the conformal propagator. The solution is found for general dimension d and general q-valent MST potential [28, 132]. The dimension of the operators at given d and spin s can be found as a solution of the corresponding transcendental equation. It is shown that at any dimension d, there is always a stress-energy operator of dimension d and a supercurrent operator of dimension $d - \frac{1}{2}$, which indicates that the theory is indeed described by a conformal field theory. While the model (3.92) exists only in the fractional dimensions between one and three dimensions, the counterpart SYK model with $q = 3$ can work at the integer dimension $d = 3$ and describe a good conformal field theory with the melonic dominance in the large N limit. After that we derive a perturbation theory in $3 - \epsilon$ dimensions of the theory (3.92) to find a fixed point that could describe the IR solution of the large N limit of the model (3.92). We find that the ϵ expansion is consistent with the exact large N solution up to the first order in ϵ. The two-loop analysis also suggests that the found melonic fixed point is IR stable.

The structure of the paper is as follows: in section two, we discuss the properties of the theory (3.92) in the large N limit. The dimensions of the operators are found and the DS equation is solved in the superspace formalism. In section three, we consider $q = 3$ supersymmetric SYK model and study the stability of such a theory. In section four, we study the RG properties of the quartic super theories in 3 dimensions and compare to the exact solutions in the large N limit. In section five, we discuss the possibility of introducing higher order supersymmetry and speculate about the consequences of gauging the supersymmetric tensor models. The appendix provides supplemental materials

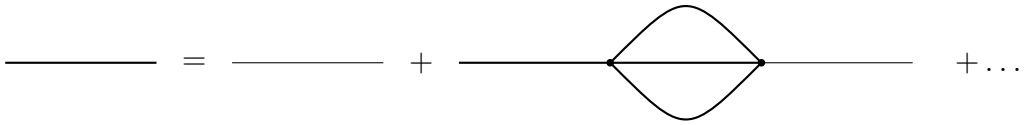

Figure 3.14: A supersymmetric version of the Dyson-Schwinger equation for melonic theories in the large N limit.

including the notations and useful formulas that are used throughout the paper.

3.2.2 Solution of the Large N Theory

In this section, we will try to find the solution of DS equations for the theory (3.92) in the large N limit. As mentioned in the introduction, the theory possesses a melonic dominance in the large N limit. This means that only specific diagrams survive in the large N limit, namely the ones generated recursively by the Dyson-Schwinger (DS) equation (schematically depicted in the fig.(3.14)). The resulting equation for scalar or fermion field theories was investigated analytically and numerically for many different theories [24, 19, 30]. For example, the DS equation can be solved in the IR limit and the solution possesses a conformal symmetry in that limit. In the case of the supersymmetric theories, one of the important differences is that one can demand the solution to respect supersymmetry. In order to do it manifestly the DS equation should be formulated in terms of the superfields. Of course, one can do this calculation in terms of the components as in the paper [88] and check that these two approaches give the same answers. To make the discussion more general we consider the case where there are $q-1$ internal propagators in the melon diagrams and suitable MST operator is considered [132]. The DS equation in the supersymmetric case reads as

$$G(p;\theta,\theta') = G_0(p;\theta,\theta') + \tag{3.93}$$
$$+\frac{1}{16}\lambda^2 \int d^2\theta_1\, d^2\theta_2\, G_0(p;\theta,\theta_1) \int \prod_{i=1}^{q-1} \frac{d^d k_i}{(2\pi)^d} G(k_i;\theta_1,\theta_2)(2\pi)^d \delta^d \left(p - \sum_{i=1}^{q-1} k_i\right) G(p;\theta_2,\theta'),$$

where $G_0(p;\theta,\theta')$ is a bare superpropagator (3.164), $G(p;\theta,\theta')$ is an exact superpropagator and $g = \lambda N^{\frac{3}{2}}$ is a 't Hooft coupling. Analogously to the scalar case, we consider a

conformal propagator as an ansatz for the solution. But if we also demand to preserve supersymmetry and $O(N) \times O(N) \times O(N)$ symmetry, that yields only one form of the solution

$$\langle \Phi_{abc}(p,\theta)\Phi_{a'b'c'}(-p,\theta')\rangle = \delta_{aa'}\delta_{bb'}\delta_{cc'}G(p;\theta,\theta'), \quad G(p;\theta,\theta') = A\frac{D^2\delta(\theta-\theta')}{p^{2\Delta}}, \quad (3.94)$$

where $\Delta < \Delta_0 = 1$ for the solution to be valid in the IR limit [109] (namely, we can neglect by bare propagator in comparison to the exact one $G_0^{-1}\langle G^{-1}, p \to 0\ \rangle$. Substituting the ansatz in the DS equation (3.93) we get

$$A\frac{D^2\delta(\theta-\theta')}{p^{2\Delta}} = \frac{D^2\delta(\theta-\theta')}{p^2} + \quad (3.95)$$
$$+A^q\lambda^2\int d^2\theta_1\, d^2\theta_2\, \frac{D^2\delta(\theta-\theta_1)}{p^2}\prod_{i=1}^{q-1}\int\frac{d^dk_i}{(2\pi)^d}(2\pi)^d\delta^d\left(p-\sum_{i=1}^{q-1}k_i\right)\frac{D^2\delta(\theta_1-\theta_2)}{k_i^{2\Delta}}\frac{D^2\delta(\theta_2-\theta')}{p^{2\Delta}}.$$

As soon as $\Delta < 1$ we can neglect the LHS of the equation by the RHS in the limit $p \to 0$. After that one can integrate out Grassman variables using identities for the superderivative to get

$$\lambda^2 A^q\prod_{i=1}^{q-1}\int\frac{d^dk_i}{(2\pi)^d}\frac{1}{k_i^{2\Delta}}(2\pi)^d\delta^d\left(p-\sum_{i=1}^{q-1}k_i\right)\frac{1}{p^{2\Delta-2}} = -1. \quad (3.96)$$

This equation gives the dimension of the superfield to be $\Delta = \frac{d(q-2)+2}{2q}$ and

$$A^q = \frac{(4\pi)^{\frac{d(q-2)}{2}}}{\lambda^2}\frac{\Gamma^{q-1}\left(\frac{d}{2}-\frac{d-1}{q}\right)\Gamma\left(d-1-\frac{d-1}{q}\right)}{\Gamma^{q-1}\left(\frac{d-1}{q}\right)\Gamma\left(\frac{d-1}{q}-\frac{d}{2}+1\right)}. \quad (3.97)$$

The solution suggests that we cannot work directly in $d_{\text{crit}}(q) = \frac{2q-2}{q-2}$ dimensions because the bare propagator is not suppressed in the IR limit and change the solution. For example, for the case of tetrahydral potential $q = 4$, $d_{\text{crit}} = 3$, therefore the tensorial melonic theory is not conformal in 3 dimensions. Nevertheless, we can still study the theory slightly below 3 dimensions and compare it with the ϵ expansion.

If one chooses the case of $q = 3$, the critical dimension is $d_{\text{crit}} = 4$ and such a melonic

theory should describe a conformal field theory in 3 dimensions. In the next section we will review this model in more details.

We calculated the propagator (3.94) in the momentum representation. One can carry out the calculation in the coordinate space. With the use of the relation

$$\int \frac{d^dk}{(2\pi)^d} e^{ikx} D^2\delta(\theta-\theta') = \int \frac{d^dk}{(2\pi)^d} e^{ikx}\left(1 - ik^\mu \bar\theta'\gamma_\mu\theta + k^2\bar\theta'\theta'\bar\theta\theta\right) = e^{\bar\theta'\gamma^\mu\theta\frac{\partial}{\partial x^\mu}}, \quad (3.98)$$

the propagator in the coordinate representation is

$$G(x,\theta,\theta') = \frac{B}{|x_\mu - \bar\theta'\gamma_\mu\theta|^{\frac{2(d-1)}{q}}}, \quad B^q = \frac{1}{4\pi^d\lambda^2}\frac{\Gamma\left(\frac{d-1}{q}\right)\Gamma\left(d-1-\frac{d-1}{q}\right)}{\Gamma\left(\frac{d}{2}-\frac{d-1}{q}\right)\Gamma\left(\frac{d-1}{q}-\frac{d}{2}+1\right)}. \quad (3.99)$$

Another way to see that the dimension of the superfield is $\frac{d-1}{q}$ is to rewrite the action in terms of the components and impose the conditions $\Delta_\psi = \Delta_\phi + \frac{1}{2}$, then the action contains a term

$$W(\Phi) = \Phi^q \Rightarrow W(\phi) = \phi^{q-2}\psi^2 \Rightarrow [W] = d \Rightarrow (q-2)\Delta_\phi + 2\Delta_\psi = d, \quad \Delta_\phi = \frac{d-1}{q}. \quad (3.100)$$

The solution (3.94) suggests that in the IR limit, the theory is described by some conformal field theory (CFT). One of the interesting questions that one may ask is, what is the spectrum of the bipartite conformal operators in this theory? The supersymmetric theory (3.92) has different types of the bipartite operators, as the prismatic one [3]. We should consider these families separetly. The most simple ones have the following structure [79]

$$V_{FF} = \Phi(x,\theta)\Box^h\Phi(x,\theta), \quad V_{BB} = \Phi(x,\theta)\Box^h D^2\Phi(x,\theta). \quad (3.101)$$

These operator should be considered as a collection of operators with different spins and dimensions, that transforms through each other when the supersymmetry transformations are applied. For instance, these operators could be rewritten in the terms of components

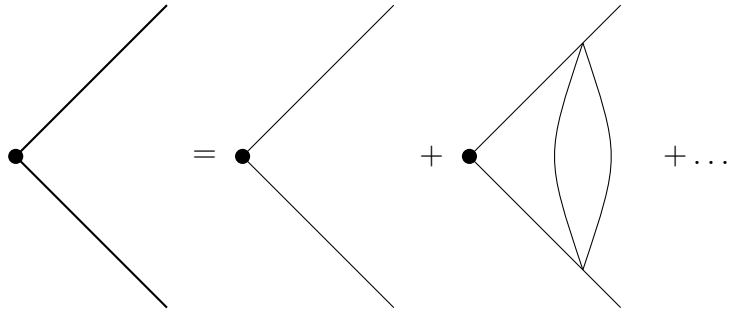

Figure 3.15: The corrections to the bipartite conformal operator can be summed with the use of the Bethe-Salpeter equation. The diagrams should be considered to be in the superspace.

(3.157) as

$$V_{FF}(x,\theta) = \phi(x)\Box^h\phi(x) + \phi(x)\Box^h\psi^\alpha(x)\theta_\alpha + \theta^2\left(\phi(x)\Box^h F(x) + \Box^h\phi(x)F(x) + \bar\psi(x)\Box^h\psi(x)\right),$$
$$V_{BB}(x,\theta) = \bar\psi\Box^h\psi + \left(F\Box^h\psi_\alpha + \Box^h F\psi_\alpha + (\gamma^\mu\psi)_\alpha\partial_\mu\Box^h\phi + (\gamma^\mu\Box^h\psi)_\alpha\partial_\mu\Box^h\phi\right)\theta^\alpha +$$
$$+\theta^2\left(\partial_\mu\phi\Box^h\partial_\mu\phi + i\bar\psi\gamma^\mu\Box^h\partial_\mu\psi + F\Box^h F\right). \qquad (3.102)$$

A similar set of the operators was considered in the paper [79] in 2 dimensions and [88] in 1 dimension. Later we shall compare the results of these papers with the continuous solution for arbitrary d. We can try to put more D^2 in (3.101) to get more familes, but with the use of the identity $(D^2)^2 = \Box$, one can descend these operators to the BB or FF series. That's why we can consider only these two families to get the whole spectrum of bipartite operators with the lowest component having spin $s = 0$.

As usual, the corrections to the bilinear operators in the large N limit are given by the ladder diagrams (but again, in comparison to [109, 19], these diagrams should be considered to be in superspace). We assume the following ansatz in momentum space for the three-point correlation function for these families,

$$G_{FF}(k,\theta,\theta') = \langle V_{FF}\Phi(-k,\theta)\Phi(k,\theta')\rangle = \frac{\delta(\theta-\theta')}{k^{\Delta_V+2\Delta}},$$
$$G_{BB}(k,\theta,\theta') = \langle V_{BB}\Phi(-k,\theta)\Phi(k,\theta')\rangle = \frac{D^2\delta(\theta-\theta')}{k^{\Delta_V+2\Delta}}, \qquad (3.103)$$

where we have set the operators V_{BB}, V_{FF} to be at infinity and made a Fourier transformation with respect to the spatial coordinates, and Δ_V is the corresponding dimensions

of the operator. The derivation of the equations for the dimensions Δ_V is just a straightforward generalization of the analogous calculation for the scalar model [19] or the SYK model [24]. Here we will show the derivation of such equation for the BB operators.

The addition of one step of the ladder can be considered as the action of the *kernel* operator,

$$\hat{K} = K(p,k;\theta,\theta',\theta_1,\theta_2) =$$
$$= (q-1)\prod_{i=1}^{q-2}\int \frac{d^d q_i}{(2\pi)^d}\frac{D^2\delta(\theta_1-\theta_2)}{q_i^{2\Delta}}\frac{D^2\delta(\theta-\theta_1)}{p^{2\Delta}}\frac{D^2\delta(\theta_2-\theta')}{p^{2\Delta}}(2\pi)^d\delta^d\left(\sum q_i-(p-k)\right). \tag{3.104}$$

We act on the (3.101) by one step of the ladder,

$$(\hat{K}G_{BB})(p,\theta,\theta') = \int d^2\theta_1 d^2\theta_2 \int \frac{d^d k}{(2\pi)^d} K(p,k;\theta,\theta',\theta_1,\theta_2)G_{BB}(k,\theta_1,\theta_2). \tag{3.105}$$

The Grassman variables can be integrated out with the use of identities from the section 3.2.6. After that we are left with a simple integral

$$(\hat{K}G_{BB})(p,\theta,\theta') =$$
$$= (q-1)A^q\lambda^2 D^2\delta(\theta-\theta')\int \frac{d^d k}{(2\pi)^d}\prod_{i=1}^{q-2}\frac{d^d q_i}{(2\pi)^d}\frac{1}{q_i^{2\Delta}}\frac{1}{k^{\Delta_V+2\Delta}p^{2\Delta-2}}(2\pi)^d\delta^d\left(\sum q_i-(p-k)\right) =$$
$$= g_B\left(\Delta_V\right)G_{BB}(p,\theta,\theta'), \tag{3.106}$$

where

$$g_B(\Delta_V) = -(q-1)\frac{\Gamma\left(\frac{2+d(q-2)}{2q}\right)\Gamma\left(\frac{(q-1)(d-1)}{4}\right)\Gamma\left(\frac{d}{4}-\frac{1}{q}-\frac{\Delta_V}{2}\right)\Gamma\left(1-\frac{d}{2}-\frac{1}{q}+\frac{d}{q}+\frac{\Delta_V}{2}\right)}{\Gamma\left(1-\frac{d}{2}+\frac{d-1}{q}\right)\Gamma\left(\frac{d-1}{q}\right)\Gamma\left(\frac{(q-1)(d-1)}{q}-\frac{\Delta_V}{2}\right)\Gamma\left(\frac{d}{2}+\frac{1}{q}-\frac{d}{q}+\frac{\Delta_V}{2}\right)}. \tag{3.107}$$

In order for the operator to be primary, the equation $g_B(\Delta_V) = 1$ must hold. An

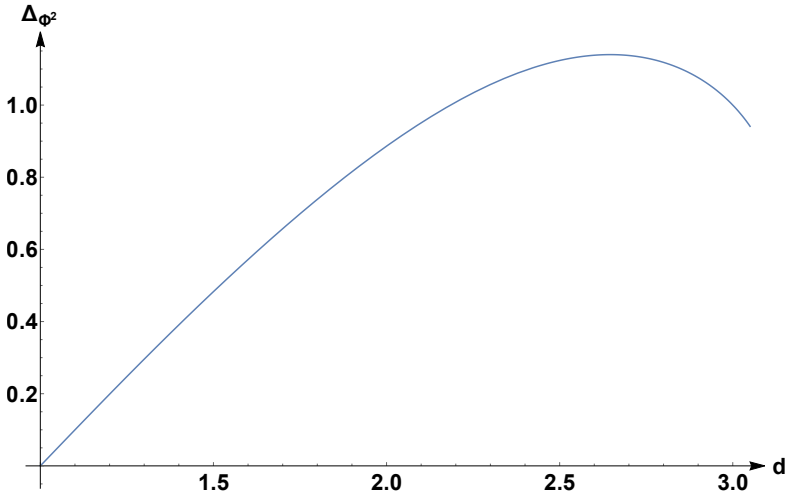

Figure 3.16: The dimension of the operator Φ^2 as a function of the dimension. As $d \to 1$ the dimension goes to zero.

analogous equation can be written for the V_{FF} operator, but one can see that

$$g_F(\Delta_V) = g_B\left(\Delta_V - 1\right), \tag{3.108}$$

This suggests that we might build a bigger multiplet and enhance the supersymmetry to be $\mathcal{N} = 2$ (later we shall see that this does not actually happen, because there is no additional fermionic counterparts to finish supermultiplet).

From now on we shall consider the case only $q = 4$ to get $3 - \epsilon$ expansion unless the other is specified. Thus, we can get the ϵ expansion in the large N limit of the Φ^2 operator

$$\Delta_{\Phi^2} = 1 + \epsilon + 3\epsilon^2 - \frac{\pi^2 + 24}{4}\epsilon^3 + \mathcal{O}(\epsilon^4). \tag{3.109}$$

The plot of the Δ_{Φ^2} as a function of the dimension is depicted in the figure 3.16. Analogously we get the dimension of $\Phi D^2 \Phi$ operator

$$\Delta_{\Phi D^2 \Phi} = 2 + \epsilon + 3\epsilon^2 - \frac{\pi^2 + 24}{4}\epsilon^3 + \mathcal{O}(\epsilon^4). \tag{3.110}$$

We can discuss dimensions of non-singlet operators of the form $\Phi_{abc}\Phi_{a'bc}$. The equation

for the dimension of this operator can be rewritten as

$$g_B(\Delta_{aa'}) = q - 1, \tag{3.111}$$

where a factor $q-1$ appears from the combinatorics [61], and $\Delta_{aa'}$ is the dimension of the operator. The ϵ expansion near three dimensions for $q = 4$ has the following form

$$\Delta_{aa'} = 1 - \frac{1}{2}\epsilon^2 + \frac{\pi^2}{24}\epsilon^3 + \mathcal{O}(\epsilon^4). \tag{3.112}$$

Later, we shall show that the solution coincides with the ϵ expansion in the second level of perturbation theory.

From this, the next step would be to study the spectrum of the higher-spin operators. A generalization for the higher spin operators is

$$V^s_{FF} = \Phi(x,\theta)\Box\partial_{\mu_1}\dots\partial_{\mu_s}\Phi(x,\theta), \quad V^s_{BB} = \Phi(x,\theta)\Box\partial_{\mu_1}\dots\partial_{\mu_s}D^2\Phi(x,\theta), \tag{3.113}$$

with the corresponding modifications for the ansatz. For example, for higher spin spectrum of the BB operators the ansatz is

$$G^s_{\mu_1\dots\mu_s,BB}(k,\theta,\theta') = \langle V^s_{\mu_1\mu_2\dots\mu_s,BB}\Phi(-k,\theta)\Phi(k,\theta')\rangle = \frac{D^2\delta(\theta-\theta')k_{\mu_1}\dots k_{\mu_s}}{k^{\Delta_V+\frac{d+1}{2}+s}}. \tag{3.114}$$

In this case we consider an arbitrarily chosen null-vector ξ^μ and consider the convolution of the ansatz (3.114) with the vector ξ. After that one can integrate out the Grassman variables and carry out the integration over the real pace with the use of a relation [26]:

$$\int d^dx \frac{(\xi\cdot x)^s}{x^{2\alpha}(x-y)^{2\beta}} = \pi^{\frac{d}{2}}\frac{\Gamma\left(\frac{d}{2}-\alpha+s\right)\Gamma\left(\frac{d}{2}-\beta\right)\Gamma\left(\alpha+\beta-\frac{d}{2}\right)}{\Gamma(\alpha)\Gamma(\beta)\Gamma(d+s-\alpha-\beta)}\frac{(\xi\cdot y)^s}{y^{2\alpha+2\beta-d}}. \tag{3.115}$$

Eventually, the equation for the dimension at given spin s reads as

$$g_B(d,\Delta_V,s) = \tag{3.116}$$

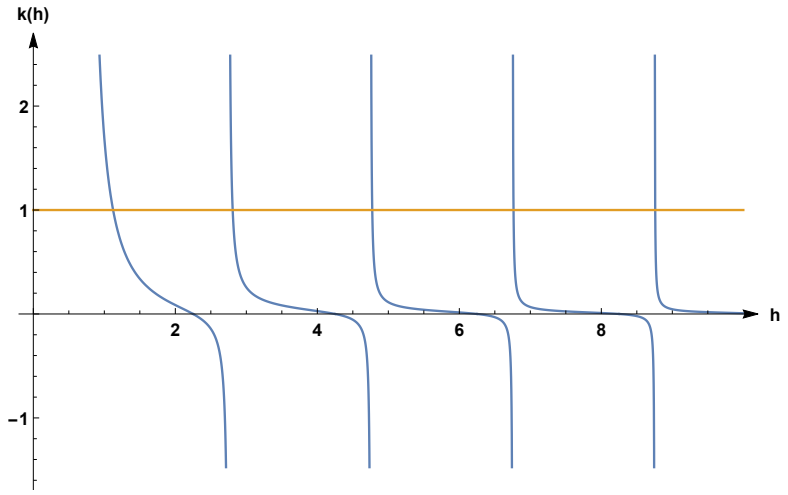

Figure 3.17: The dimension of the operator Φ^2 can be found graphically. The plot of $k(h)$ is drawn for the case of $d = 2.5$

$$= -(q-1)\frac{\Gamma\left(\frac{2+d(q-2)}{2q}\right)\Gamma\left(\frac{(q-1)(d-1)}{4}\right)\Gamma\left(\frac{d}{4}-\frac{1}{q}-\frac{\Delta_V-s}{2}\right)\Gamma\left(1-\frac{d}{2}-\frac{1}{q}+\frac{d}{q}+\frac{\Delta_V+s}{2}\right)}{\Gamma\left(1-\frac{d}{2}+\frac{d-1}{q}\right)\Gamma\left(\frac{d-1}{q}\right)\Gamma\left(\frac{(q-1)(d-1)}{q}-\frac{\Delta_V-s}{2}\right)\Gamma\left(\frac{d}{2}+\frac{1}{q}-\frac{d}{q}+\frac{\Delta_V+s}{2}\right)} = 1,$$

One would expect that there is a solution at any d and $s = 2$ with $\Delta = d$, because of the existence of the stress-energy tensor. However one cannot find this solution. The reason is quite simple. First of all, there is no stress-energy tensor in the field decomposition of the BB and FF operators. Second, the stress-energy tensor has a superpartner $\mathcal{S}^{\alpha}_{\mu}$ (corresponding to supertranslations) that has spin $\frac{3}{2}$, and therefore to find it we should consider a whole different family of operators, with lowest component being a Rarita-Schwinger field . Namely, let us consider a Fermi conformal primary operator

$$V_{BF,\mu_1\ldots\mu_{2n+1}}(x,\theta) = \partial^{2n+1}_{\mu_i}\Phi(x,\theta)D_{\alpha}\Phi(x,\theta), \tag{3.117}$$

where the odd number of the space-time derivatives should be inserted to get a primary operator. Indeed, if we consider a zero number of the derivatives

$$V_{BF} = \Phi_{abc}D_{\alpha}\Phi_{abc} = \frac{1}{2}D_{\alpha}\left(\Phi^2_{abc}\right), \tag{3.118}$$

it is just a descendant of the FF operator. To get a supercurrent multiplet we have to project the operators (3.117) on the specific component. The ansatz for the three-point

function has the following form

$$\langle V_{BF}\Phi(k,\theta)\Phi(-k,\theta')\rangle = \frac{D_\alpha\delta(\theta-\theta')}{k^{\Delta_V+2\Delta}}. \tag{3.119}$$

The derivation of the equation for the spectrum of the dimensions is straightforward

$$g_{BF}(d,\Delta_V,s) = -g_B\left(d,\Delta_V-\frac{1}{2},s-\frac{1}{2}\right) = 1, \tag{3.120}$$

where the spin should be chosen to be of the form $s = 2n - \frac{1}{2}$. Now we can try to find the stress-energy momentum and its partner. And indeed at any d, q and $s = \frac{3}{2}$ there is an operator with dimension $\Delta = d - \frac{1}{2}$ that corresponds to the usual stress-energy supermultiplet.

At this point one can wonder whether the current $J_{aa'}$, responsible for the $O(N)$'s transformations, is a primary operator. The supersymmetric multiplet containing the current should be also a Fermi supermultiplet with spin $s = 1/2$ (this operator is not a singlet operator and therefore (3.117) is not applicable). The current should satisfy the equation [61]

$$g^{aa'}_{BF}(d,\Delta_V,s) = \frac{1}{3}g_{BF}(d,\Delta_V,s) = 1, \tag{3.121}$$

at any d and q there is always a solution $\Delta_V = d-3/2$. One can see that the dimension of square of this operator is given by the direct sum of the dimensions $\Delta_{J\tilde{J}} = 2\Delta_V = 2d-3$. This operator becomes relevant when $\Delta_{J\tilde{J}} = 2d-3 \leq d-1$, where minus 1 comes from the accounting the dimension of the superspace. From this one can see the operator becomes marginal in $d = 2$ and relevant as $d < 2$. This extra marginal operator in $d = 2$ may destabilize the CFT. The only exception is the case $N = 1$, where the theory does not have any continuous symmetry and has superpotential Φ^4. In $d = 2$ this theory flows to the $m = 4$ superconformal minimal model, which has central charge $c = 1$. [15]

The relation (3.116) can be thought as a generalization of the equation for the kernel at

[15] I would like to thank I.R.Klebanov for pointing out these facts.

2 dimensions derived by Murugan et al. [79]. In this case they introduced two dimensions, $h = \frac{\Delta+s}{2}$ and $\tilde{h} = \frac{\Delta-s}{2}$, and one can check that

$$k(h,\tilde{h}) = g_B(d=2, h+\tilde{h}, h-\tilde{h}) = -(q-1)\frac{\Gamma^2(1-1/q)\Gamma(1/q-\tilde{h})\Gamma(1/q+h)}{\Gamma^2(1/q)\Gamma(1-1/q-\tilde{h})\Gamma(h+1-1/q)}, \tag{3.122}$$

which coincides with the equation (7.17) in [79].

The relation (3.120) also shows that if there is a scalar bilinear multiplet with dimension h, there is no BF operator with higher spin and the dimension $\Delta = \Delta + \frac{1}{2}$. This shows that we cannot complete the $\mathcal{N} = 2$ supermultiplet and the enhancement does not happen. It is interesting that there is an argument in $d = 1$ stating that it actually must happen. Basically, it comes from the fact that group of diffeormorphims of supertransformations in 1-dimension comprises the $\mathcal{N} = 2$ superalgebra [79].

Finally we discuss the dimension of the quartic operators, because there is a fundamental relation between their dimensions and the eigenvalues of the matrix $\frac{\partial\beta_i}{\partial g_j}$. We can find the dimensions of some quartic operators in the large N limit. For example, in the matrix models the anomalous dimension of a double trace operator is just the sum of the anomalous dimensions of the corresponding single trace operators. By the same analysis, we get that the anomalous dimension of the double trace operator is

$$\Delta_{\Phi^4} = 2\Delta_{\Phi^2} = 2 + 2\epsilon + \mathcal{O}(\epsilon^2). \tag{3.123}$$

Analogous analysis gives that

$$\Delta_{\text{Pillow}} = 2\Delta_{aa'} = 2 + \mathcal{O}(\epsilon^2). \tag{3.124}$$

Finally, the dimension of the tetrahedral operator can be determined as the dimension of the operator $\Phi_{abc}D^2\Phi_{abc}$ (namely, it follows from the equations of motion) and it gives us

$$\Delta_{\text{Tetra}} = 2 + \epsilon + \mathcal{O}(\epsilon^2). \tag{3.125}$$

One can try to study the behaviour of the model (3.92) near 1 dimension. The case of $d = 1$ supersymmetric tensor models was considered recently (see [88]). It was found that the supersymmetry is broken in the IR region. The easiest way to see this is to assume a conformal ansatz and plug it in the DS equation (3.93). The solution suggests $\Delta = 0$ in one dimensions, but constant or logarithm function do not satisfy the DS equation. The conformal solution found in [88] shows, that the dimensions of the superfield components are not related to each other by usual supersymmetric relations. It might be the case that for the system in 1 dimensions the conformal solution does not describe the true vacuum state, while the true vacuum respect supersymmetry and the propagators exponentially decays at large distances. It might be shown by studying the stability of the conformal solution in a way described in [48] for two coupled SYK models.

Also, if one consider a limit $d \to 1$ in the equations derived in the previous sections, the propagator does not have a smooth limit in 1 dimension and the kernel is equal to the constant $\lim_{d\to 1} g_B(d, h, s) = -1$. The last fact confirms that in 1 dimension the conformal IR solution does not respect the supersymmetry. But, in the vicinity of dimension 1, everything works fine. Thus, one can study the $1 + \epsilon$ expansion. We shall consider the case of tensor models and set $q = 4$. For example, the dimension of the Φ^2 operator is

$$\Delta_{\Phi^2} = \epsilon - \frac{\pi^2}{48}\epsilon^3 + \frac{3\zeta(3)}{16}\epsilon^4 + \mathcal{O}(\epsilon^5), \quad \Delta_{\Phi D^2 \Phi} = 1 + \epsilon - \frac{\pi^2}{48}\epsilon^3 + \frac{3\zeta(3)}{16}\epsilon^4 + \mathcal{O}(\epsilon^5). \tag{3.126}$$

And the dimension of the colored operators $\Phi_{abc}\Phi_{a'bc}$ is

$$\Delta_{aa'} = \frac{3}{4}\epsilon - \frac{3\pi^2}{256}\epsilon^3 + \frac{9\zeta(3)}{128}\epsilon^4 + \mathcal{O}(\epsilon^5) \tag{3.127}$$

It would be interesting to derive this results by considering a one dimensional supersymmetric melonic quantum mechanics and lift the solution to $1+\epsilon$ dimenion. Or just derive these results starting with the conformal solution found in one dimension [88] and show that in higher dimensions the supersymmetry is immediately restored.

3.2.3 Supersymmetric SYK model with $q = 3$ in $d = 3$

In the previous section we mostly work with the tensor models in non-integer dimensions. The main problem that did not allow us to work directly in 3 dimensions was that the critical dimension for such a interaction is $d_{\text{cr}} = \frac{2q-2}{q-2} = 3$, meaning that directly at 3 dimensions the conformal IR solution does not work. Nevertheless, if one considers $q = 3$ case the critical dimension becomes $d_{\text{cr}} = 4$ and therefore should work perfectly in 3 dimensions. Unfortunately, we do not know any $q = 3$ tensor model and in order to somehow study this melonic model we shall consider a SYK like model with disorder, which is a special case of the models [79].

Thus, we shall try to study the following model

$$S = \int d^d x\, d^2\theta \left[\frac{1}{2}\left(D\Phi_i\right)^2 + C_{ijk}\Phi_i\Phi_j\Phi_k\right], \quad \langle C_{ijk}^2\rangle = \frac{J^2}{3N^2}, i, j, k = 1, \ldots, N, \quad (3.128)$$

where we consider a quenched disorder for the coupling C_{ijk}. One might worry, that such a theory violates the causality, because the field C_{ijk} is assumed to have the same value across the space-time and therefore the excitation of such a field changes the value of it everywhere, thus violating causality. But the procedure of quenching requires firstly to fix the value of C_{ijk} that makes the theory casual and after that average over this field. It means that we can not excite the field C_{ijk} and violate casuality.

This model is similar to the tensor one considered in the previous section, because again only melonic diagrams survive in the large N limit, but with two iternal propagators in each melon. Therefore the formulas derived in the previous section are applicable in this case and with the replacement of $\lambda \to J$ and setting $q = 3$ we can recover the large N solution of this model. For example, the propagator in this case is

$$G(x, \theta, \theta') = \frac{B}{\left|x_\mu - \bar{\theta}'\gamma_\mu\theta\right|^{\frac{4}{3}}}, \quad B^3 = \frac{1}{12\sqrt{3}\pi^3 J^2}, \quad (3.129)$$

and the dimension of the field Φ_i is $\Delta = \frac{2}{3}$. Again the spectrum of the operators could be separated into three sectors, described in the previous section. The equation for the

BB operators is determined by the equation

$$g_{BB}^{3,3}(h,s) = -\frac{2^{\frac{4}{3}}\sqrt{\pi}\Gamma\left(\frac{2}{3}-\frac{h}{2}+\frac{s}{2}\right)\Gamma\left(\frac{1}{6}+\frac{h}{2}+\frac{s}{2}\right)}{3\Gamma\left(\frac{1}{6}\right)\Gamma\left(\frac{4}{3}-\frac{h}{2}+\frac{s}{2}\right)\Gamma\left(\frac{5}{6}+\frac{h}{2}+\frac{s}{2}\right)}, \tag{3.130}$$

where s is the spin and should be chosen even. One can try to find the spectra of low lying states (3.18)

$[\Phi^2]_{\theta=0}\, s=0$	$h = 1.69944, 3.42951, 5.38013, 7.36259, 9.354, \ldots$
$[D_\alpha(\Phi^2)]_{\theta=0}\, s=1/2$	$h = 2.19944, 3.92951, 5.88013, 7.86259, 9.854, \ldots$
$[\Phi\partial_{\mu_1}\partial_{\mu_2}\Phi]_{\theta=0}\, s=2$	$h = 3.51911, 5.39016, 7.3654, 9.35514, 11.3496, \ldots$
$[D_\alpha(\Phi\partial_{\mu_1}\partial_{\mu_2}\Phi)]_{\theta=0}\, s=5/2$	$h = 4.01911, 5.89016, 7.8654, 9.85514, 11.8496, \ldots$

It is easy to see that the spectrum has the following asymptotic behavior at large spins

$$h \approx \frac{4}{3} + 2n + s + \mathcal{O}\left(1/n, 1/s\right), n \to \infty, s \to \infty.$$

On a principal line $h = \frac{d}{2} + i\alpha$ the kernel is complex, it is connected to the fact that there is no well-defined metric in the space of two-point functions [79]. Therefore there is no problems with the complex modes, that could possibly destroy the conformal solution in the IR [48]. Thus $q = 3$ supersymmetric SYK model is stable at least in the BB channel. Also one can check there are no additional solutions to the equation $g_{BB}^{3,3}(h,s) = 1$ in the complex plane except the ones on the real line. The spectrum of the FF operators coincides with the spectrum of the BB operators but shifted with $h \to h+1$, therefore we don't have to worry about the instabilities of the theory in this sector.

Analogous calculations could be conducted for the BF series

$$g_{BF}^{3,3}(h,s) = -g_{BB}^{3,3}\left(h-\frac{1}{2}, s-\frac{1}{2}\right), \tag{3.131}$$

where the spin s should be in the form $s = 2n - \frac{1}{2}$. One can notice that there is a solution $g_{BF}^{3,3}(5/2, 3/2) = 1$ corresponding to the existence of the supercurrent and energy momentum tensor (the energy momentum is not seen directly because it belongs to the supermultiplet of the supercurrent, but if one studies the theory in terms of the

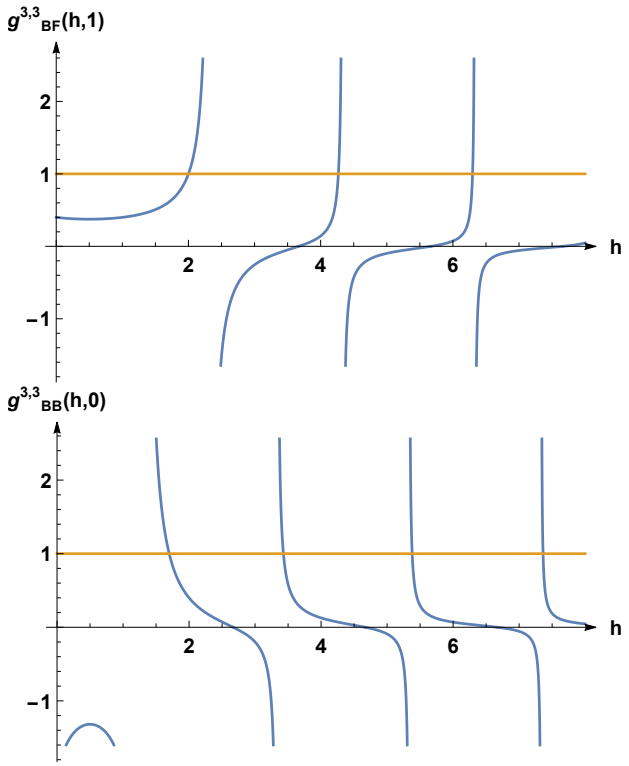

Figure 3.18: Plots for $g^{3,3}_{BF}(h,1)$ and $g^{3,3}_{BB}(h,0)$ that can help to understand the structure of the spectrum of the the theory (3.128)

components, he or she will of course find the energy momentum tensor). There is a list of some low lying operators in the FF sector (3.18)

$[\partial_\mu \Phi D_\alpha \Phi]_{\theta=0}$	$s=\frac{3}{2}: h=2.5, 4.76759, 6.79738, 8.80934, 10.8157, \ldots$
$[D_\beta (\partial_\mu \Phi D_\alpha \Phi)]_{\theta=0}$	$s=2: h=3, 5.26759, 7.29738, 9.30934, 11.3157, \ldots$
$[\partial_{\mu_1}\partial_{\mu_2}\partial_{\mu_3} \Phi D_\alpha \Phi]_{\theta=0}$	$s=\frac{7}{2}: h=4.15398, 6.28752, 8.30627, 10.3143, 12.3189, \ldots$
$[\partial_{\mu_1}\partial_{\mu_2}\partial_{\mu_3} D_\beta (\Phi D_\alpha \Phi)]_{\theta=0}$	$s=4: h=4.65398, 6.78752, 8.80627, 10.8143, 12.8189, \ldots$

The spectrum has the following form asymptotic behavior

$$h \approx \frac{5}{6} + 2n + s + \mathcal{O}\left(1/n, 1/s\right), n \to \infty.$$

The kernel is again complex on the principal line, but if one chooses $s=\frac{1}{2}$ there would be an additional solution of the equation $g^{3,3}_{BF}=1$ at $h=1+0.496i$, but as soon as it is not on the principal line and s is not permissible we do not have to worry about this complex mode and expect that it could break the conformal solution. Thus this $q=3$ supersymmetric SYK model could provide us with a conformal field theory that

is melonic and stable at integer dimensions. It would be interesting to study the $4-\epsilon$ expansion for this model, where it will be close to its critical dimension.

3.2.4 $3-\epsilon$ expansion

In this section, we continue the investigation of the supersymmetric tensor model (3.92) from the point of view of the ϵ expansion. The calculation is similar to the ones performed in the papers [26, 3, 134]. We include all possible $O(N)^3$ symmetric marginal interactions that respect the supersymmetry. Thus the superpotential has the following form

$$W(\Phi) = g_1 \Phi_{abc}\Phi_{ab'c'}\Phi_{a'bc'}\Phi_{a'b'c}+$$
$$+\frac{g_2}{3}\left(\Phi_{abc}\Phi_{a'bc}\Phi_{ab'c'}\Phi_{a'b'c'}+\Phi_{abc}\Phi_{ab'c}\Phi_{a'bc'}\Phi_{a'b'c}+\Phi_{abc}\Phi_{abc'}\Phi_{a'b'c}\Phi_{a'b'c'}\right)+g_3\left(\Phi^2_{abc}\right)^2, \tag{3.132}$$

where we imposed a symmetry under the exchange of the colors. In comparison to the "prismatic" theory [3], which has 8 coupling constants, the supersymmetric theory has only 3; this is a significant simplification.

Let us first consider the general renormalizable $d=3$ theory of $\mathcal{N}=1$ superfields Φ^i, $i=1,\dots n$:

$$S[\Phi_i] = \int d^3x d^2\theta \left[\frac{1}{2}(D\Phi_i)^2 + \frac{Y_{ijkl}}{4!}\Phi_i\Phi_j\Phi_k\Phi_l\right], \tag{3.133}$$

where Y_{ijkl} is a real symmetric tensor. Adapting the results from [135, 136], we find that the two-loop corrections to the gamma and beta functions are

$$\gamma^{(2)}_{ab} = \frac{1}{3(8\pi)^2}Y_{ajkl}Y_{bjkl},$$
$$\beta^{(2)}_{abcd} = \frac{1}{3(8\pi)^2}Y_{ijkl}\left(Y_{jkla}Y_{bcdi}+Y_{jklb}Y_{cdai}+Y_{jklc}Y_{acdi}+Y_{jkld}Y_{abci}\right)+$$
$$+\frac{2}{(8\pi)^2}\left(Y_{anom}Y_{bfom}Y_{nfcd}+Y_{anom}Y_{cfom}Y_{nfbd}+Y_{anom}Y_{dfom}Y_{nfbc}+\right.$$
$$\left.+Y_{bnom}Y_{cfom}Y_{nfad}+Y_{bnom}Y_{dfom}Y_{nfac}+Y_{cnom}Y_{dfom}Y_{nfab}\right). \tag{3.134}$$

These two-loop results are closely related to those in a non-supersymmetric theory with Yukawa coupling $\frac{1}{4}Y_{ijkl}\psi^i\psi^j\phi^k\phi^l$ (see [136]), except the supersymmetry requires Y_{ijkl} to be fully symmetric.

Substituting Y_{ijkl} corresponding to the superpotential (3.132), we find from (3.134):

$$\begin{aligned}
\gamma^{\Phi}_{abc,a'b'c'} &= \delta_{aa'}\delta_{bb'}\delta_{cc'}\gamma^{\Phi} \\
\gamma^{\Phi} &= \frac{1}{6\pi^2}\left[12g_2g_1(1+N+N^2)+6g_3^2(2+N^3)+3g_1^2(2+3N+N^3)+\right. \\
&\left.+g_2^2(5+9N+3N^2+N^3)+36g_3g_1N+12g_3g_2(1+N+N^2)\right]
\end{aligned} \tag{3.135}$$

and

$$\begin{aligned}
\beta_1 &= -\epsilon g_1+\frac{2}{9\pi^2}\left(6g_1\left(12g_3^2\left(N^3+11\right)+g_2^2(N^3+6N^2+30N+29)+12g_3g_2(2N^2+5N+5)\right)+\right. \\
&\left.+9g_1^3\left(N^3+12N+8\right)+18g_1^2\left(g_2(4N^2+7N+16)+24g_3N\right)+2g_2^2\left(g_2(2N^2+13N+24)+72g_3\right)\right), \\
\beta_2 &= -\epsilon g_2+\frac{2}{9\pi^2}\left(g_2\left(72g_3^2\left(N^3+11\right)+g_2^2(7N^3+36N^2+162N+194)+36g_3g_2((5N^2+9N+16)\right)+\right. \\
&+54g_1^3\left(N^2+N+4\right)+18g_1^2\left(g_2(N^3+3N^2+27N+26)+18g_3(N+2)\right)+ \\
&\left.+18g_2g_1\left(g_2(7N^2+21N+32)+48g_3(N+1)\right)\right), \\
\beta_3 &= -\epsilon g_3+\frac{2}{9\pi^2}\left(108g_3^3\left(N^3+4\right)+252g_2g_3^2\left(N^2+N+1\right)+7g_2^3(N^2+3N+5)+\right. \\
&\left.+18g_1^2\left(2g_3\left(N^3+3N+2\right)+g_2\left(N^2+N+4\right)\right)+27g_1^3N++12g_2^2g_3(N^3+3N^2+15N+14)+\right. \\
&\left.36g_1\left(2g_2^2(N+1)+2g_3g_2(2N^2+2N+5)+21g_3^2N\right)\right)
\end{aligned} \tag{3.136}$$

If one sets $g_1 = g_2 = 0$, the symmetry gets enhanced to $O(N^3)$ and corresponds to the $O(n)$ vector model, which was considered in [135].[16] For the supersymmetric $O(n)$ model with superpotential $g(\Phi^i\Phi^i)^2$,

$$\beta_g = -\epsilon g+\frac{24(n+4)}{\pi^2}g^3+O(g^5)\ , \tag{3.137}$$

in agreement with [135].

[16]Please note that they considered $SU(n)$ case that corresponds to $N^3 = 2n$ and their definition of γ^{Φ} includes a factor of two.

If we choose $N = 1$, the couplings g_1, g_2, g_3 becomes degenerate because they describe the same operator. Therefore, the beta-functions should be added to get the right expression. And indeed, if we choose $N = 1$ and sum up the couplings we get

$$\beta_1 + \beta_2 + \beta_3 = \mu \frac{d(g_1 + g_2 + g_3)}{d\mu} = -\epsilon(g_1 + g_2 + g_3) + \frac{120}{\pi^2}(g_1 + g_2 + g_3)^3, \qquad (3.138)$$

which is the correct beta function for the theory with superpotential $(g_1+g_2+g_3)\Phi^4$ for a single chiral superfield Φ. This special case of our theory is conformal in the entire range $2 \leq d < 3$. Indeed, in $d = 2$ the $\mathcal{N} = 1$ supersymmetric theory with superpotential Φ^m for one superfield Φ flows to the superconformal minimal model with central charge

$$c = \frac{3}{2}\left(1 - \frac{8}{m(m+2)}\right) . \qquad (3.139)$$

Therefore, the $N = 1$ case of the supertensor model gives the $m = 4$, $c = 1$ superminimal model in $d = 2$. For $N > 2$ the $O(N)^3$ supertensor model is expected to be conformal in $2 < d < 3$, but not in $d = 2$.

Let us consider the large N limit where we scale the coupling constants in the following way:

$$g_1 = \frac{\pi}{2}\frac{\sqrt{2\epsilon}\lambda_1}{N^{\frac{3}{2}}}, \quad g_2 = \frac{\pi}{2}\frac{\sqrt{2\epsilon}\lambda_2}{N^{\frac{5}{2}}}, \quad g_3 = \frac{\pi}{2}\frac{\sqrt{2\epsilon}\lambda_3}{N^{\frac{7}{2}}}. \qquad (3.140)$$

The scaling is taken to be the same as in the paper [26]. Applying this scaling to the formula (3.2.4), we get

$$\gamma_\Phi = \epsilon\frac{\lambda_1^2}{4}, \qquad \beta_1 = -\lambda_1 + \lambda_1^3, \qquad (3.141)$$
$$\beta_2 = -\lambda_2 + 2\lambda_2\lambda_1^2 + 6\lambda_1^3, \qquad \beta_3 = -\lambda_3 + 2(2\lambda_3 + \lambda_2)\lambda_1^2 + 3\lambda_1^3 .$$

From this one can find the fixed point in the large N limit. Namely,

$$\lambda_1^\infty = \pm 1, \quad \lambda_2^\infty = \mp 6, \quad \lambda_3^\infty = \pm 3, \quad \Delta_\Phi = \frac{d-2}{2} + \gamma_\Phi = \frac{1}{2} - \frac{\epsilon}{4}. \qquad (3.142)$$

N	$\frac{\lambda_1}{\lambda_1^\infty}$	$\frac{\lambda_2}{\lambda_2^\infty}$	$\frac{\lambda_3}{\lambda_3^\infty}$
100000	1.000	1.000	1.000
10000	1.000	1.001	1.002
1000	1.000	0.995	0.995
100	1.001	0.953	0.950
10	1.033	0.691	0.670
5	1.068	0.546	0.527
2	1.049	0.350	0.322
1	1.093	0.273	0.139

Table 2: The approach of the finite N fixed points in $3-\epsilon$ dimensions to the large N limit. We note that the fixed point exists for all values of N.

We may try to compute the $1/N$ corrections to these results to get

$$\lambda_1 = 1 + \mathcal{O}\left(\frac{1}{N^2}\right), \quad \lambda_2 = -6 + \frac{20}{N} + \mathcal{O}\left(\frac{1}{N^2}\right),$$
$$\lambda_3 = 3 - \frac{16}{N} + \mathcal{O}\left(\frac{1}{N^2}\right), \quad \gamma^\Phi = \frac{1}{2} - \frac{\epsilon}{4} + \mathcal{O}\left(\frac{1}{N^2}\right). \tag{3.143}$$

The anomalous dimension of the matter field operator Φ coincides with the exact dimension of the field by solving the DS equation found above. This might indicate that the higher-loop corrections to the RG equations (3.2.4) are suppressed in the large N limit. It would be interesting to study these suppressions in N for a general superpotential (3.132) from a combinatorial diagrammatic point of view and compare the results with the investigation of the finite N solutions of the equations (3.2.4).

If one considers the large N fixed point (3.142) of the RG flow governed by the equations (3.2.4) and tries to descend to finite N, one can find that the solution always exists (see the table (2)) and quite close to the found fixed point (3.142) (of course with the appropriate chosen scaling), in comparison to the "prismatic" model, where the melonic fixed point exists only at $N > 54$ [3].

We can study the dimension of various operators in the fixed point (3.142). One of these operators is Φ^2_{abc}, which belongs to the BB spectrum. We can find that the anomalous dimension of this operator is

$$\Delta_{\Phi^2} = \Delta^0_{\Phi^2} + 2\gamma_\Phi + \gamma_{\Phi^2} = 1 + \epsilon + \mathcal{O}(\epsilon^2), \tag{3.144}$$

where we have used the relation $\gamma_{\Phi^2} = 6\gamma_\Phi$, which is true only at the second level of perturbation theory. The answer coincides with the exact solution found earlier (3.109).

As one can see, the fixed point (3.142) is IR stable, which means that the dimensions of the operators is bigger than the dimension of the space-time. Indeed, the linearized equations of RG flow near the fixed point (3.142) have the following eigenvalues

$$\left(\frac{\partial\beta_i}{\partial\lambda_j}\right) = \begin{pmatrix} -1+3\lambda_1^2 & 0 & 0 \\ 4\lambda_2\lambda_1 + 18\lambda_1^2 & -1+2\lambda_1^2 & 0 \\ 4(2\lambda_3+\lambda_2)\lambda_1 + 9\lambda_1^2 & 2\lambda_1^2 & -1+4\lambda_1^2 \end{pmatrix}, \quad \Lambda = [2,1,3]\,, \tag{3.145}$$

but as it is known the eigenvalues of this matrix gives the dimensions of quartic operators

$$\Delta_i = d - \epsilon + \Lambda_i. \tag{3.146}$$

Thus we get

$$\Delta_{\Phi^4} = 2 - \epsilon + 3\epsilon = 2 + 2\epsilon + \mathcal{O}(\epsilon^2), \quad \Delta_{\text{pillow}} = 2 - \epsilon + \epsilon = 2 + \mathcal{O}(\epsilon^2),$$
$$\Delta_{\text{tetra}} = 2 - \epsilon + 2\epsilon = 2 + \epsilon + \mathcal{O}(\epsilon^2). \tag{3.147}$$

This is in the agreement with the large N solution. As one can see, $\Lambda_i > 0$, indicating that the fixed point is IR stable. The agreement found between the exact large N solution and perturbative ϵ expansion indicates that there is a nice flow from the UV scale to the IR one where the bare, free propagator flows to the one found by direct solving the DS equations (3.93). The study of the higher loop corrections might help to understand this relation better.

3.2.5 $\mathcal{N} = 2$ supersymmetry and gauging

One can try to consider $\mathcal{N} = 2$ supersymmetry and study the properties of such a model. Here we are not going to present the solution of the corresponding DS equation , but we will just calculate the beta-functions and find the fixed point of the resulting equations. The SYK model with $\mathcal{N} = 2$ supersymmetry at 2 dimensions was considered

in the paper [87].

The theory is built analogously to the $\mathcal{N}=1$ case. It can be obtained by dimensional reduction from $\mathcal{N}=1$ supersymmetry in 4 dimensions. In this case, we have a set of chiral superfields Ψ_{abc} with the action

$$S=\int d^3x\, d^2\theta\, d^2\bar{\theta}\,\bar{\Psi}_{abc}\Psi_{abc}+\int d^3x\, d^2\theta\, W(\Psi_{abc}),\quad \bar{D}_\alpha\Psi_{abc}=0, \tag{3.148}$$

where the superpotential is taken to be the same as in the case of $\mathcal{N}=1$ supersymmetry. The beta-function for a general quartic superpotential was considered in the paper [137]. The beta-function receives corrections only from the field renormalizations, meaning that it has the following form

$$\begin{aligned}\beta_{1,2,3}&=\left(-\epsilon+4\gamma^\Phi\right)g_{1,2,3}\\ \gamma^\Phi&=\frac{1}{6\pi^2}\left(12g_2g_1\left(1+N+N^2\right)+6g_3^2(2+N^3)+3g_1^2(2+3N+N^3)+\right.\\ &\left.+g_2^2(5+9N+3N^2+N^3)+36g_3g_1N+12g_3g_2(1+N+N^2)\right).\end{aligned} \tag{3.149}$$

The fixed point is determined by demanding that the anomalous dimension of the field must be $\Delta_\Phi=\Delta_\Phi^0+\gamma^\Phi=\frac{d-1}{4}$, as we got for a general melonic theory in arbitrary dimensions. Apparently, for $\mathcal{N}=2$ models this fact comes not from the melonic dominance, but from the consideration of the supersymmetric algebra that fixes the dimensions to be proportional to the R charge of the corresponding operator. This condition defines a whole manifold in the space of marginal couplings. Applying the scaling (3.140), in the large N limit we get the equation

$$\gamma(\lambda_1,\lambda_2,\lambda_3)=\frac{\lambda_1^2}{4}=\frac{1}{4},\quad \lambda_1=1. \tag{3.150}$$

It is quite interesting that this equation does not fix λ_2,λ_3 in the large N limit. One can study the stability of these fixed points at arbitrary $\lambda_{2,3}$. The RG flow near the fixed

point could be linearized to get the stability matrix

$$\left(\frac{\partial\beta_i}{\partial g_j}\right) = \begin{pmatrix} 2 & 0 & 0 \\ 2\lambda_2 & 0 & 0 \\ 2\lambda_2 & 0 & 0 \end{pmatrix}, \quad \Lambda = [2,0,0]\,. \tag{3.151}$$

The given solution is marginally stable, because of the existence of two marginal operators. These two zero directions correspond to the previously discussed existence of a whole manifold of IR fixed points.

From this consideration, it would be interesting to study the large N limit of the considered $\mathcal{N}=2$ theory and corresponding DS equations. This model must have the same combinatorial properties as the $\mathcal{N}=1$ and scalar tensor model, but some cancellation happens that drastically simplifies the theory.

One can try to examine a gauged version of $\mathcal{N}=2$ theory. The gauging of the tensor models is one of the important aspects that makes them different from the SYK model. In the latter, due to the presence of the disorder in the system, the theory can possess only the global $O(N)$ symmetry and can not be gauged, while in the tensor models there are no such obstructions and one can add gauge field and couple to the tensor models at any dimensions.

Gauging should be important for understanding the actual AdS/CFT correspondence. In 1 dimension, the gauging singles out from the spectrum all non-singlet states from the Hilbert states. There have been many attempts to understand of the structure of the tensorial quantum mechanics of Majorana fermions from numerical and analytical calculations [62, 69, 138, 139]. These gave some interesting results, such as the structure of the spectrum of the matrix quantum mechanics and the importance of the discrete symmetries for explaining huge degenaracies of the spectra. Still, the general impact of gauging of the tensorial theory is not clear and demands a new approach. Here, we will give some comments of the combinatorial character and study how the gauging of $\mathcal{N}=2$ theory, studied in the previous section, changes.

In 3 dimensions one can gauge a theory by adding a Chern-Simons term instead of

the usual Yang-Mills term

$$S = \int d^3x d^2\theta \left[-k \left(D_\alpha \Gamma^a_\beta \right)^2 + \left| \left(D_\alpha \delta^a_b + g \Gamma^a_{b\,\alpha} \right) T^a \Phi_{abc} \right|^2 + W(\Phi_{abc}) \right], \tag{3.152}$$

where $W(\Phi_{abc})$ is the same as in the (3.132), T^a are the generators of the group $O(N) \times O(N) \times O(N)$, and Γ^α are vector superfields that have a gauge potential $A^a_{b\mu}$ as one of the components. If one rewrites the kinetic term for the gauge field in terms of usual components, he will get a usual Chern-Simons theory. Since the theory is gauge invariant, we can choose an axial gauge to simplifty the action [17] $A^a_{b3} = 0$, which eliminates the non-linear term from the theory and the Fadeev-Popov ghosts decouple from the theory. Therefore the A^a_{b1}, A^a_{b2} can be integrated out to get an effective potential. For example, such a term appears in the action

$$W_{\text{eff}} \sim \frac{1}{k} \int \frac{d^3q}{(2\pi)^3} \frac{(\Phi_{abc} D_\alpha \Phi_{ab'c'})(q)(\Phi_{a'bc} D_\alpha \Phi_{a'b'c'})(-q)}{q_\perp} + \text{perm.}, \tag{3.153}$$

which can be considered as a non-local pillow operator with the wrong scaling, because the level of CS action usually scales as $k = \lambda N$. Therefore some diagrams would have large N factor and diverge in the large N limit. To fix it we should consider the unusual scaling for the CS level $k = \lambda N^2$.

One can check that only specific Feynman propagators containing the non-local vertex (3.153) contribute in the large N limit [134]. Namely only snail diagrams contribute in the large N limit and usually are equal to zero by dimensional regularization for massless fields. Therefore, one can suggest that the gauge field in the large N limit does not get any large corrections and does not change the dynamics of the theory. This argument being purely combinatorial should be applied for any theory coupled to the CS action.

We can confirm this argument by direct calculation of the dimensions of the fields in the ϵ expansion for the $\mathcal{N} = 2$ supertensor model at two-loops and see whether the dimensions of the fields gets modified. The beta-functions for a general $\mathcal{N} = 2$ theory coupled to a CS action was considered in the paper [137] and have the following form at

[17] I would like to thank S.Prakash for the suggested argument.

finite N

$$\beta_{1,2,3} = \left(-\epsilon + 4\gamma^{\Phi}\right) g_{1,2,3}, \quad \gamma^{\Phi} = \gamma^{\Phi}_{k=0} - \frac{3N(N-1)}{64\pi^2 k^2}. \tag{3.154}$$

As $k \sim N^2, N \to \infty$ the corrections to the gamma-functions vanish in the large N limit. Thus, the gauging in three dimensions indeed does not bring any new corrections to the theory. It would be interesting to study such a behavior in different dimensions. For example, if in 1 dimension the gauging does not change structure of the solutions, one may conclude that the main physical degrees of freedom are singlets and there is a gap between the non-singlet and singlet sectors. Also it would be interesting to confirm this observation by a direct computation for the prismatic theories and for Yang-Mills theories.

3.2.6 Supersymmetry in 3 dimensions

In this section we will introduce the notations and useful identities for the $\mathcal{N} = 1$ supersymmetric theories in 3 dimensions. We will mostly follow the lectures [131]. The Lorentz group in 3 dimensions is $SL(2, \mathbb{R})$; that is a group of all unimodular real matrices of dimension 2. The gamma matrices can be chosen to be real

$$\gamma^0 = \begin{pmatrix} 0 & -1 \\ 1 & 0 \end{pmatrix}, \quad \gamma^1 = \begin{pmatrix} 0 & 1 \\ 1 & 0 \end{pmatrix}, \quad \gamma^2 = \begin{pmatrix} 1 & 0 \\ 0 & -1 \end{pmatrix}, \quad \{\gamma^\mu, \gamma^\nu\} = 2\eta^{\mu\nu}. \tag{3.155}$$

There is no γ^5 matrix, so we can't split the spinor representation into small Weyl ones. Because of this, the smallest spinor representation is 2 dimensional and real. It is endowed with a scalar product defined as

$$\bar{\xi}\eta = \xi^\alpha \eta_\alpha = i\xi^\alpha \gamma^0_{\alpha\beta}\eta^\beta, \quad \theta^2 = \frac{1}{2}\bar{\theta}\theta. \tag{3.156}$$

Because of these facts, the $\mathcal{N} = 1$ superspace, in addition to the usual space-time coordinates, will include two real Grassman variables $\theta^\pm$. The fields on the superspace can be decomposed in terms of fields in the usual Minkowski space. For instance, a scalar

superfield (that is our major interest) has the following decomposition

$$\Phi(x,\theta^\alpha) = \phi(x) + \bar{\theta}\psi(x) + \theta^2 F(x). \tag{3.157}$$

As usual, the algebra supersymmetry in superspace can be realized via the derivatives that act on the superfields (3.157) and mix different components

$$Q_\alpha = \partial_\alpha + i\gamma^\mu_{\alpha\beta}\theta^\beta\partial_\mu, \quad \{Q_\alpha, Q_\beta\} = 2i\gamma^\mu_{\alpha\beta}\partial_\mu \tag{3.158}$$

where ∂_μ stands for differentiation with respect to the usual space-time variables, and ∂_α for the anticommuting ones. One can define a superderivative that anticommutes with supersymmetry generators, and therefore preserves the supersymmetry

$$D_\alpha = \partial_\alpha - i\gamma^\mu_{\alpha\beta}\theta^\beta\partial_\mu, \quad \{D_\alpha, Q_\beta\} = 0. \tag{3.159}$$

Out of these ingredients, namely (3.157),(3.159), we can build an explicit version of a supersymmetric Lagrangian. For example, we can consider the following Lagrangian

$$S = \int d^3x d^2\theta \left[-\frac{1}{2}\left(D_\alpha\Phi\right)^2 + W(\Phi) \right], \tag{3.160}$$

where the integral over Grassman variables is defined in the usual way with the normalization $\int d^2\theta\bar{\theta}\theta = 1$. Writing out the explicit form of (3.160) we get

$$S = \int d^3x \left[\frac{1}{2}(\partial_\mu\phi)^2 + i\psi^\alpha\gamma^\mu_{\alpha\beta}\partial_\mu\psi^\beta + F^2 + W'(\phi)F + W''(\phi)\psi^2 \right]. \tag{3.161}$$

The field F does not have a kinetic term, and therefore is not dynamical and can be integrated out (that we will not do). For a further investigation we have to develop the technique of super Feynman graphs. We start with considering the partition function of the theory (3.160)

$$Z[J] = \int [d\Phi] \exp\left[\int d^3x d^2\theta \left(\frac{1}{2}\left(D_\alpha\Phi\right)^2 + W(\Phi) + J\Phi \right) \right] =$$

$$= \exp\left(W\left(\frac{\delta}{\delta J}\right)\right)\int [d\Phi]\exp\left[\int d^3x d^2\theta\left(\frac{1}{2}\Phi D^2\Phi + J\Phi\right)\right]. \tag{3.162}$$

The last integral is gaussian and therefore can be evaluated and is equal to

$$Z[J] = \exp\left(W\left(\frac{\delta}{\delta J}\right)\right)\exp\left(-\int d^3x d^2\theta\left[\frac{1}{2}J\frac{1}{D^2}J\right]\right). \tag{3.163}$$

From this one can recover the usual Feynman diagrammatic technique, where the vertex is taken from the superpotential $W(\Phi)$ rather than the integrated version, and the propagator is defined as

$$\langle\Phi(x_1,\theta_1)\Phi(x_2,\theta_2)\rangle = \frac{1}{D^2}\delta^2(\theta_1-\theta_2) = \frac{D^2}{\Box}\delta^2(\theta_1-\theta_2), \tag{3.164}$$

which can be calculated by double differentiation of the partition function (3.162), and the operator $\Box$ is the usual laplacian.

4 Bifurcations and RG Limit Cycles

The Renormalization Group (RG) is among the deepest ideas in modern theoretical physics. There is a variety of possible RG behaviors, and limit cycles are among the most exotic and mysterious. Their possibility was mentioned in the classic review [140] in the context of connections between RG and dynamical systems (for a recent discussion of these connections, see [141]). However, there has been relatively little research on RG limit cycles. They have appeared in quantum mechanical systems [142, 143, 144, 145], in particular, in a description of the Efimov bound states [146] (for a review, see [147]). The status of RG limit cycles in QFT is less clear. They have been searched for in unitary 4-dimensional QFT [148], but turned out to be impossible [149, 150], essentially due to the constraints imposed by the a-theorem [151, 152, 153].[18]

In this paper we report some progress on RG limit cycles in the context of perturbative QFT. We demonstrate their existence in a simple $O(N)$ symmetric model of scalar fields with sextic interactions in $3-\epsilon$ dimensions. As expected, the limit cycles appear when the theory is continued to a range of parameters where it is non-unitary. The scalar fields form a symmetric traceless $N\times N$ matrix, and imposition of the $O(N)$ symmetry restricts the number of sextic operators to 4. When we consider an analytic continuation of this model to non-integer real values of N (a mathematical framework for such a continuation was presented in [156]), we find a surprise. In the range $4.465 < N < 4.534$, as well as in three other small ranges of N, there are special RG fixed points which we call "spooky." These fixed points are located at real values of the sextic couplings g^i, but only two of the eigenvalues of the Jacobian matrix $\partial\beta_i/\partial g_j$ are real; the other two are complex conjugates of each other. This means that a pair of nearly marginal operators at the spooky fixed points have complex scaling dimensions.[19] At the critical value $N_{\rm crit}\approx 4.475$, the two complex eigenvalues of the Jacobian become purely imaginary. As a result, for

[18] See, however, [154, 155], where it is argued that QFTs may exhibit multi-valued c or a-functions that do not rule out limit cycles.

[19] These special complex dimensions appear in addition to the complex dimensions of certain evanescent operators that are typically present in ϵ expansions [157]. The latter dimensions have large real parts and are easily distinguished from our nearly marginal operators. Some of the operators with complex dimensions we observe resemble evanescent operators in that they interpolate to vanishing operators at integer values of N; this is discussed in section 4.3.

N slightly bigger than $N_{\rm crit}$, where the real part of the complex eigenvalues becomes negative, there are RG flows which lead to limit cycles. In the theory of dynamical systems this phenomenon is called a Hopf (or Poincarè-Andronov-Hopf) bifurcation [158]. The possibility of RG limit cycles appearing via a Hopf bifurcation was generally raised in [141], but no specific examples were provided. As we demonstrate in section 4.3, the symmetric traceless $O(N)$ model in $3-\epsilon$ dimensions provides a simple perturbative example of this phenomenon.

We show that there is no conflict between the limit cycles we have found and the F-theorem [159, 160, 161, 162, 163, 164, 136, 165]. This is because the analytic continuation to non-integer values of N below 5 violates the unitarity of the symmetric traceless $O(N)$ model, so that the F-function is not monotonic. We feel that the simple perturbative realization of limit cycles we have found is interesting, and we hope that there are analogous phenomena in other models and dimensions.

Our paper also sheds new light on the large N behavior of the matrix models in $3-\epsilon$ dimensions. Among the fascinating features of various large N limits (for a recent brief overview, see [14]) are the "large N equivalences," which relate models that are certainly different at finite N. An incomplete list of the conjectured large N equivalences includes [166, 167, 168, 169, 170, 171, 172, 173]. Some of them appear to be valid, even non-perturbatively, while others are known to break down dynamically. For example, in the non-supersymmetric orbifolds of the $\mathcal{N}=4$ supersymmetric Yang-Mills theory [174, 167, 168, 169, 170], there are perturbative instabilities in the large N limit due to the beta functions for certain double-trace couplings having no real zeros [175, 80, 176, 81].

In section 4.2 we study the RG flows of three scalar theories in $3-\epsilon$ dimensions with sextic interactions: the parent $O(N)^2$ symmetric model of $N\times N$ matrices ϕ^{ab}, and its two daughter theories which have $O(N)$ symmetry. For each model, we list all sextic operators marginal in three dimensions, compute the associated beta functions up to 4 loops, and determine the fixed points. One of our motivations for this study is to investigate the large N orbifold equivalence and its violation in the simple context of purely scalar theories. We observe evidence of large N equivalence between the parent

$O(N)^2$ theory and the daughter $O(N)$ theory of antisymmetric matrices: both theories have 3 invariant operators, and the large N beta functions are identical. However, the large N equivalence of the parent theory with the daughter $O(N)$ theory of symmetric traceless matrices is violated by appearance of an additional invariant operator in the latter. The large N fixed points in this theory occur at a complex value of the coefficient of this operator. As a result, instead of the conventional CFT in the parent theory, we find a "complex CFT" [93, 177] (see also [91]) in the daughter theory. As discussed above, analytical continuation of this model to small non-integer N leads to the appearance of the spooky fixed points and limit cycles.

4.1 The Beta Function Master Formula

In a general sextic scalar theory with potential

$$V(\phi) = \frac{\lambda_{iklmnp}}{6!}\phi_i\phi_k\phi_l\phi_m\phi_n\phi_p \tag{4.1}$$

the beta function receives a two-loop contribution from the Feynman diagram

In [136, 165, 99] one can find explicit formulas for the corresponding two-loop beta function in $d = 3 - \epsilon$ dimensions. Equation (6.1) of the latter reference reads

$$\beta_V(\phi) = -2\epsilon\, V(\phi) + \frac{1}{3(8\pi)^2} V_{ijk}(\phi)V_{ijk}(\phi)\,, \tag{4.2}$$

where $V_{i\ldots j}(\phi) \equiv \frac{\partial}{\partial\phi^i}\ldots\frac{\partial}{\partial\phi^j}V(\phi)$. By taking the indices to stand for doublets of sub-indices, this formula can be used to compute the beta functions of matrix tensor models. In order to apply the formula to models of symmetric or anti-symmetric matrices, however, we need to slightly modify it. Letting i and j stand for dublets of indices, we define the

object C^{ij} via the momentum space propagator:

$$\left\langle \widetilde{\phi}^i(k)\widetilde{\phi}^j(-k)\right\rangle_0 = \frac{C^{ij}}{k^2}\,. \tag{4.3}$$

With this definition in hand, equation (4.2) straightforwardly generalizes to

$$\beta_V(\phi) = -2\epsilon\, V(\phi) + \frac{C^{ii'}C^{jj'}C^{kk'}}{3(8\pi)^2} V_{ijk}(\phi)V_{i'j'k'}(\phi)\,. \tag{4.4}$$

At four-loops the following four kind of Feynman diagrams contribute to the beta function:

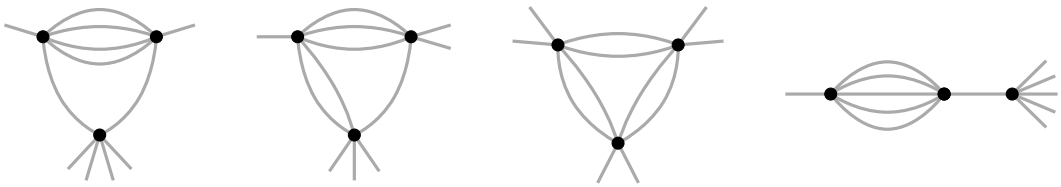

The resulting four-loop beta function can be read off from equation (6.2) of [99]:

$$\beta_V^{(4)} = \frac{1}{(8\pi)^4}\left(\frac{1}{6}V_{ij}V_{iklmn}V_{jklmn} - \frac{4}{3}V_{ijk}V_{ilmn}V_{jklmn} - \frac{\pi^2}{12}V_{ijkl}V_{klmn} + \right) + \phi_i\gamma^\phi_{ij}V_j\,, \tag{4.5}$$

where the anomalous dimension γ^ϕ_{ij} is given by

$$\gamma^\phi_{ij} = \frac{1}{90(8\pi)^4}\lambda_{iklmnp}\lambda_{jklmnp}\,. \tag{4.6}$$

The above two equations also admit of straightforward generalizations by contracting indices through the C^{ij} matrix.

Before proceeding to matrix models, we can review the beta function obtained by the above formulas in the case of a sextic $O(M)$ vector model described by the action

$$S = \int d^{3-\epsilon}x \left(\frac{1}{2}\left(\partial_\mu\phi^j\right)^2 + \frac{g}{6!}\left(\phi^i\phi^i\right)^3\right), \tag{4.7}$$

where the field ϕ^i is a M-component vector. The four-loop beta function of this vector

model is given by [101, 99]

$$\beta_g = -2\epsilon g + \frac{192(3M+22)}{6!(8\pi)^2} g^2 \tag{4.8}$$
$$-\frac{1}{(6!)^2(8\pi)^4}\Big(9216(53M^2+858M+3304)+1152\pi^2(M^3+34M^2+620M+2720)\Big)g^3\,.$$

This equation provides a means of checking the beta functions of the matrix models, which reduce to the vector model when all couplings are set to zero except for the coupling, denoted g_3 below, associated to the triple trace operator.

4.2 Sextic Matrix Models

We now turn to matrix models in $d = 3-\epsilon$ dimensions. The parent theory we consider has the Lagrangian given by

$$S = \int d^{3-\epsilon}x \left[\frac{1}{2}\left(\partial_\mu \phi^{ab}\right)^2 + \frac{1}{6!}\Big(g_1 O_1(x) + g_2 O_2(x) + g_3 O_3(x)\ ,\Big)\right] \tag{4.9}$$

where the dynamical degrees of freedom are scalar matrices ϕ^{ab} which transform under the action of a global $O(N)\times O(N)$ symmetry. The three operators in the potential are

$$\begin{aligned} O_1 =& \phi^{a_1b_1}\phi^{a_2b_1}\phi^{a_2b_2}\phi^{a_3b_2}\phi^{a_3b_3}\phi^{a_1b_3} = \mathrm{tr}\left[\phi\phi^T\right]^3 \\ O_2 =& \phi^{ab}\phi^{ab}\phi^{a_1b_1}\phi^{a_2b_1}\phi^{a_2b_2}\phi^{a_1b_2} = \mathrm{tr}\left[\phi\phi^T\right]\mathrm{tr}\left[\phi\phi^T\right]^2 \\ O_3 =& (\phi^{ab}\phi^{ab})^3 = \left(\mathrm{tr}\left[\phi\phi^T\right]\right)^3. \end{aligned} \tag{4.10}$$

They make up all sextic operators that are invariant under the global symmetry. Later we will also study projections of the parent theory that have only a global $O(N)$ symmetry that rotates first and second indices at the same time. In such models it becomes possible to construct singlets via contractions between first and second indices, and therefore there is an additional sextic scalar:

$$O_4 = \left(\phi^{a_1a_2}\phi^{a_2a_3}\phi^{a_3a_1}\right)^2 = \left(\mathrm{tr}\left[\phi^3\right]\right)^2\,. \tag{4.11}$$

O_1 O_2 O_3 O_4

Figure 4.1: The sextic operators in matrix models. The double trace operator O_4 exists only in the theory of symmetric matrices.

The sextic operators are depicted diagrammatically in fig. 4.1. We could also introduce an operator containing tr $[\phi]$, but since the orbifolds we will study are models of symmetric traceless and anti-symmetric matrices, the trace is identically zero. In the anti-symmetric model, the operator O_4 vanishes, but it is non-vanishing in the symmetric orbifold, and so in this case we will introduce this additional marginal operator to the Lagrangian and take the potential to be given by

$$V(x) = \frac{1}{6!}\Big(g_1 O_1(x) + g_2 O_2(x) + g_3 O_3(x) + g_4 O_4(x)\Big)\,. \tag{4.12}$$

To study the large N behavior of these matrix models, we introduce rescaled coupling constants λ_1, λ_2, λ_3, λ_4. To simplify expressions, it will be convenient to also rescale the coupling constants by a numerical prefactor. We therefore define the rescaled couplings by

$$g_1 = 6!(8\pi)^2\frac{\lambda_1}{N^2} \qquad g_2 = 6!(8\pi)^2\frac{\lambda_2}{N^3} \qquad g_3 = 6!(8\pi)^2\frac{\lambda_3}{N^4} \qquad g_4 = 6!(8\pi)^2\frac{\lambda_4}{N^3}\,. \tag{4.13}$$

To justify these powers of N, let us perform a scaling $\phi^{ab} \to \sqrt{N}\phi^{ab}$. Then the coefficient of each q-trace term in the action scales as N^{2-q}. This is the standard scaling in the 't Hooft limit, which insures that each term in the action is of order N^2.

4.2.1 The $O(N)^2$ parent theory

For the matrix model parent theory, the momentum space propagator is given by

$$\left\langle \widetilde{\phi}^{ab}(k)\widetilde{\phi}^{a'b'}(-k)\right\rangle_0 = \frac{\delta^{aa'}\delta^{bb'}}{k^2}\,. \tag{4.14}$$

Computing the four-loop beta functions and taking the large N limit with scalings (4.13), we find that, up to $\mathcal{O}(\frac{1}{N})$ corrections,

$$\begin{aligned}
\beta_{\lambda_1} =& -2\lambda_1\epsilon + 72\lambda_1^2 - 288(17+\pi^2)\lambda_1^3 \\
\beta_{\lambda_2} =& -2\lambda_2\epsilon + 432\lambda_1^2 + 96\lambda_1\lambda_2 - 864(90+7\pi^2)\lambda_1^3 - 864(10+\pi^2)\lambda_1^2\lambda_2 \\
\beta_{\lambda_3} =& -2\lambda_3\epsilon + 168\lambda_1^2 + 192\lambda_1\lambda_2 + 32\lambda_2^2 - 432(210+23\pi^2)\lambda_1^3 - 1152(39+4\pi^2)\lambda_1^2\lambda_2 \\
&+ 4608\lambda_1^2\lambda_3 - 768(6+\pi^2)\lambda_1\lambda_2^2 - \frac{128}{3}\pi^2\lambda_2^3
\end{aligned} \tag{4.15}$$

These beta functions have two non-trivial fixed points, which are both real. But one of these fixed points, which comes from balancing the 2-loop and 4-loop contributions, is not perturbatively reliable in an ϵ expansion around $\epsilon = 0$ because all the couplings at this fixed points contain terms of order $\mathcal{O}(\epsilon^0)$. The other fixed point is given by

$$\lambda_1 = \frac{\epsilon}{36} + \frac{17+\pi^2}{324}\epsilon^2, \quad \lambda_2 = -\frac{\epsilon}{2} - \frac{22+7\pi^2}{36}\epsilon^2, \quad \lambda_3 = \frac{295}{108}\epsilon + \frac{4714+6301\pi^2}{1944}\epsilon^2 . \tag{4.16}$$

At this fixed point the matrix $\frac{\partial\beta_{\lambda_i}}{\partial\lambda_j}$ has eigenvalues

$$\left\{-2\epsilon + \frac{32}{9}\epsilon^2, \frac{2\epsilon}{3} - \frac{44+10\pi^2}{27}\epsilon^2, 2\epsilon - \frac{34+2\pi^2}{9}\epsilon^2\right\}. \tag{4.17}$$

Each eigenvalue m_i corresponds to a nearly marginal operator with scaling dimension

$$\Delta_i = d + m_i = 3 - \epsilon + m_i \ . \tag{4.18}$$

Thus, negative eigenvalues correspond to slightly relevant operators, which cause an instability of the fixed point. The only unstable direction, corresponding to eigenvalue $-2\epsilon + \frac{32}{9}\epsilon^2$, is

$$\left(\frac{245}{3} + \frac{4225\pi^2 - 4188}{36}\epsilon\right)\lambda_1 + \left(10 + \frac{67\pi^2 - 28}{6}\right)\lambda_2 + \lambda_3. \tag{4.19}$$

The above comments relate to the $O(N)^2$ matrix model at $N = \infty$. We can also study the model at finite N. One interesting quantity is $N_{\min}$, the smallest value of N at which the fixed-point that interpolates to the large N solution (4.16) appears as a solution to the beta functions. This fixed point emerges along with another fixed point, and right at $N_{\min}$ these solutions to the beta functions are identical, so that the matrix $\left(\frac{\partial \beta_i}{\partial g_j}\right)$ is degenerate. So we arrive at the following system of equations

$$\beta_i(\lambda_i, N) = 0, \qquad \det\left(\frac{\partial \beta_i}{\partial \lambda_j}\right)(\lambda_i, N) = 0. \tag{4.20}$$

This system of equations can easily be solved numerically to zeroth order in ϵ, and with a zeroth order solution in hand the first order solution can be obtained by linearizing the system of equations. We find that $N_{\min} = 23.2541 - 577.350\epsilon$, which nicely fits the results of a numerical study where we compute $N_{\min}$ at different values of ϵ:

ϵ	0	0.001	0.002	0.003	0.004	0.005
$N_{\min}$	23.255	22.682	22.124	21.576	21.039	20.511

These values result in a numerical fit $N_{\min}(\epsilon) = 23.255 - 553.7\epsilon$, which coincides with the result stated above.

If we take N to be finite and $\epsilon \langle \frac{1}{N^2}$, we can provide some more details about the number and stability of fixed points for different values of N. For $N > 23.2541 - 577.350\epsilon$ there are three non-trivial, real, perturbatively accesible fixed points, which in the large N limit , to leading order in ϵ, scale with N as

$$\begin{gathered} g_1 = g_2 = 0, \qquad g_3 = \frac{6!(8\pi)^2}{288}\frac{\epsilon}{N^2}, \\ g_1 = \frac{6!(8\pi)^2}{36}\frac{\epsilon}{N^2}, \qquad g_2 = -\frac{10}{36}\cdot 6!(8\pi)^2\frac{\epsilon}{N^3}, \qquad g_3 = \frac{6!(8\pi)^2}{288}\frac{\epsilon}{N^2}, \\ g_1 = \frac{6!(8\pi)^2}{36}\frac{\epsilon}{N^2}, \qquad g_2 = -\frac{1}{2}\cdot 6!(8\pi)^2\frac{\epsilon}{N^3}, \qquad g_3 = \frac{295}{108}\cdot 6!(8\pi)^2\frac{\epsilon}{N^4}. \end{gathered} \tag{4.21}$$

The first of these three fixed points is identical to the vector model fixed point; that is to say, the symmetry is enhanced from $O(N)^2$ to $O(N^2)$. This fixed point extends to all

N in the small ϵ regime we are considering:

$$g_1 = g_2 = 0, \qquad g_3 = \frac{6!(8\pi)^2}{96(22+3N^2)}\epsilon. \tag{4.22}$$

The third fixed point in (4.21) extends to the regime where $N^2 > \frac{1}{\epsilon}$ and becomes the large N solution discussed above. This fixed point merges with the second fixed point in (4.21) at a critical point situated at $N(\epsilon) = 23.2541 - 577.350\epsilon$ And so at intermediate values of N, only the vector model fixed point exists. But as we keep decreasing N we encounter another critical point at $N(\epsilon) = 5.01072 + 14.4537\epsilon$, from which two new solutions to the vanishing beta functions emerge. As N further decreases past the value $N(\epsilon) = 2.75605 - 0.0161858\epsilon$, another pair of fixed points appear, but then at $N(\epsilon) = 2.72717 - 0.757475\epsilon$ two of the fixed points merge and become complex. Then at $N(\epsilon) = 2.33265 - 0.316279\epsilon$ two new fixed points appear, but these disappear again at $N(\epsilon) = 0.827007 + 8.10374\epsilon$, so that for N below this value there are a total of three real non-trivial fixed points.

4.2.2 The $O(N)$ model of antisymmetric matrices

For the theory of antisymmetric matrices $\phi^T = -\phi$ the momentum space propagator is given by

$$\left\langle \widetilde{\phi}^{ab}(k)\widetilde{\phi}^{a'b'}(-k)\right\rangle_0 = \frac{1}{2k^2}\left(\delta^{aa'}\delta^{bb'} - \delta^{ab'}\delta^{ba'}\right). \tag{4.23}$$

Performing the large N expansion using the scalings (4.13) we get the large N beta functions

$$\begin{aligned}
\beta_{\lambda_1} =& -2\lambda_1\epsilon + 18\lambda_1^2 - 18(17+\pi^2)\lambda_1^3 \\
\beta_{\lambda_2} =& -2\lambda_2\epsilon + 108\lambda_1^2 + 24\lambda_1\lambda_2 - 54(90+7\pi^2)\lambda_1^3 - 54(10+\pi^2)\lambda_1^2\lambda_2 \\
\beta_{\lambda_3} =& -2\lambda_3\epsilon + 42\lambda_1^2 + 48\lambda_1\lambda_2 + 8\lambda_2^2 - 27(210+23\pi^2)\lambda_1^3 - 72(39+4\pi^2)\lambda_1^2\lambda_2 \\
&+ 288\lambda_1^2\lambda_3 - 48(6+\pi^2)\lambda_1\lambda_2^2 - \frac{8}{3}\pi^2\lambda_2^3 .
\end{aligned} \tag{4.24}$$

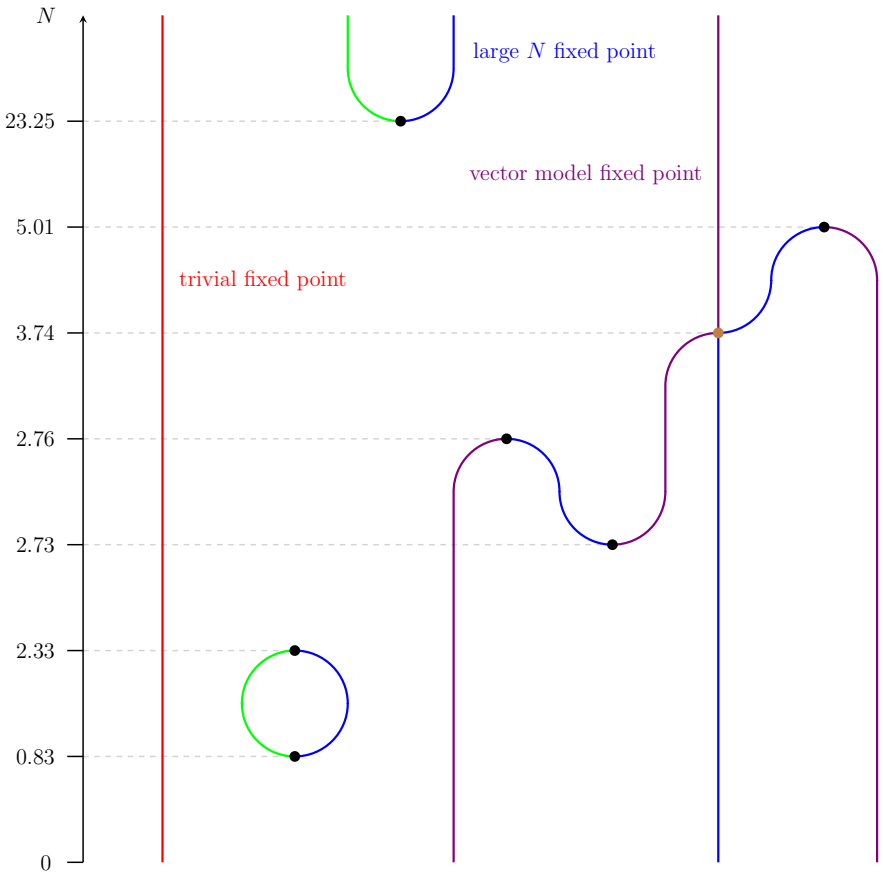

N	g_1/ϵ	g_2/ϵ	g_3/ϵ
$23.2541 - 577.350\epsilon$	$20.3055 + 1085.34\epsilon$	$-10.2467 - 671.121\epsilon$	$2.64544 + 226.967\epsilon$
$5.01072 + 14.4537\epsilon$	$18.4283 + 56.2132\epsilon$	$37.3192 + 141.611\epsilon$	$22.5095 + 65.4233\epsilon$
$\sqrt{14} + \mathcal{O}(\epsilon)$	$\mathcal{O}(\epsilon^2)$	undetermined $\mathcal{O}(\epsilon)$	$15\pi^2/2 + \mathcal{O}(\epsilon)$
$2.75605 - 0.0161858\epsilon$	$477.273 + 5099.17\epsilon$	$-829.732 - 8328.37\epsilon$	$382.831 + 3255.35\epsilon$
$2.72717 - 0.757475\epsilon$	$210.819 + 1081.1\epsilon$	$-428.594 - 2397.37\epsilon$	$270.026 + 1676.65\epsilon$
$2.33265 - 0.316279\epsilon$	$755.558 + 5809.01\epsilon$	$-1059.23 - 8206.69\epsilon$	$438.184 + 3265.96\epsilon$
$0.827007 + 8.10374\epsilon$	$237.478 + 3365.73\epsilon$	$-261.049 - 4508.85\epsilon$	$220.926 + 2109.71\epsilon$

Figure 4.2: The real perturbative fixed points of the $O(N)^2$ matrix model parent theory, the intersection point (marked in brown), and the critical points at which they merge and disappear (marked in **black**) as a function of N for small ϵ. Fixed points that are IR-unstable in all three directions are drawn in red, those unstable in two directions are drawn in violet, those unstable in one direction are drawn in blue, and those that are stable in all three directions are drawn in green. The four-loop corrections to the third point on the list, where two fixed lines intersect, are undetermined for any $\mathcal{O}(\epsilon^2)$ value of λ_2.

These beta-functions are equivalent to (4.15) up to a redefinition of the rescaled couplings by a factor of four, which is compatible with this daughter theory being equivalent in the large N limit to the parent theory studied in the previous section.

We can also study the behaviour of this model for finite N and $\epsilon\langle 1$. For $N > 35.3546 - 673.428\,\epsilon$ there are three (real, perturbatively accesible) fixed points, which in the large N limit (keeping $\epsilon\langle\frac{1}{N^2}$) to leading order in ϵ scale with N as

$$\begin{aligned} g_1 = g_2 = 0, \qquad & g_3 = \frac{6!(8\pi)^2}{144}\frac{\epsilon}{N^2}, \\ g_1 = \frac{6!(8\pi)^2}{9}\frac{\epsilon}{N^2}, \qquad & g_2 = -\frac{10}{9}\cdot 6!(8\pi)^2\frac{\epsilon}{N^3}, \qquad g_3 = \frac{6!(8\pi)^2}{144}\frac{\epsilon}{N^2}, \\ g_1 = \frac{6!(8\pi)^2}{9}\frac{\epsilon}{N^2}, \qquad & g_2 = -2\cdot 6!(8\pi)^2\frac{\epsilon}{N^3}, \qquad g_3 = \frac{295}{27}\cdot 6!(8\pi)^2\frac{\epsilon}{N^4}. \end{aligned} \tag{4.25}$$

The first of these three fixed points is the vector model fixed point, and it is present more generally in the small ϵ regime we are considering:

$$g_1 = g_2 = 0, \qquad g_3 = \frac{6!(8\pi)^2}{48(44 - 3N + 3N^2)}\epsilon. \tag{4.26}$$

The third fixed point in (4.25) extends to the regime where $N^2 > \frac{1}{\epsilon}$ and becomes the large N solution discussed above. This fixed point merges with the second fixed point in (4.25) at a critical point situated at $N(\epsilon) = 35.3546 - 673.428\,\epsilon$ And so at intermediate values of N, only the vector model fixed point exists. But as we keep decreasing N we encounter another critical point at $N(\epsilon) = 6.02669 + 7.37013\epsilon$, from which two new solutions to the vanishing beta functions emerge. As N further decreases past the value $N(\epsilon) = 5.70601 + 0.540694\epsilon$, another pair of fixed points appear, and past $N(\epsilon) = 5.075310 - 0.0278896\epsilon$ yet another pair of fixed point appear (in this range of N, all seven non-trivial solutions to the vanishing beta functions are real). But already below $N(\epsilon) = 5.03275 - 0.586724\epsilon$, two of the fixed points become complex, and below $N(\epsilon) = 3.08122 + 8.26176\epsilon$ two more fixed points become complex, so that for N below this value there are a total of three real non-trivial fixed points.

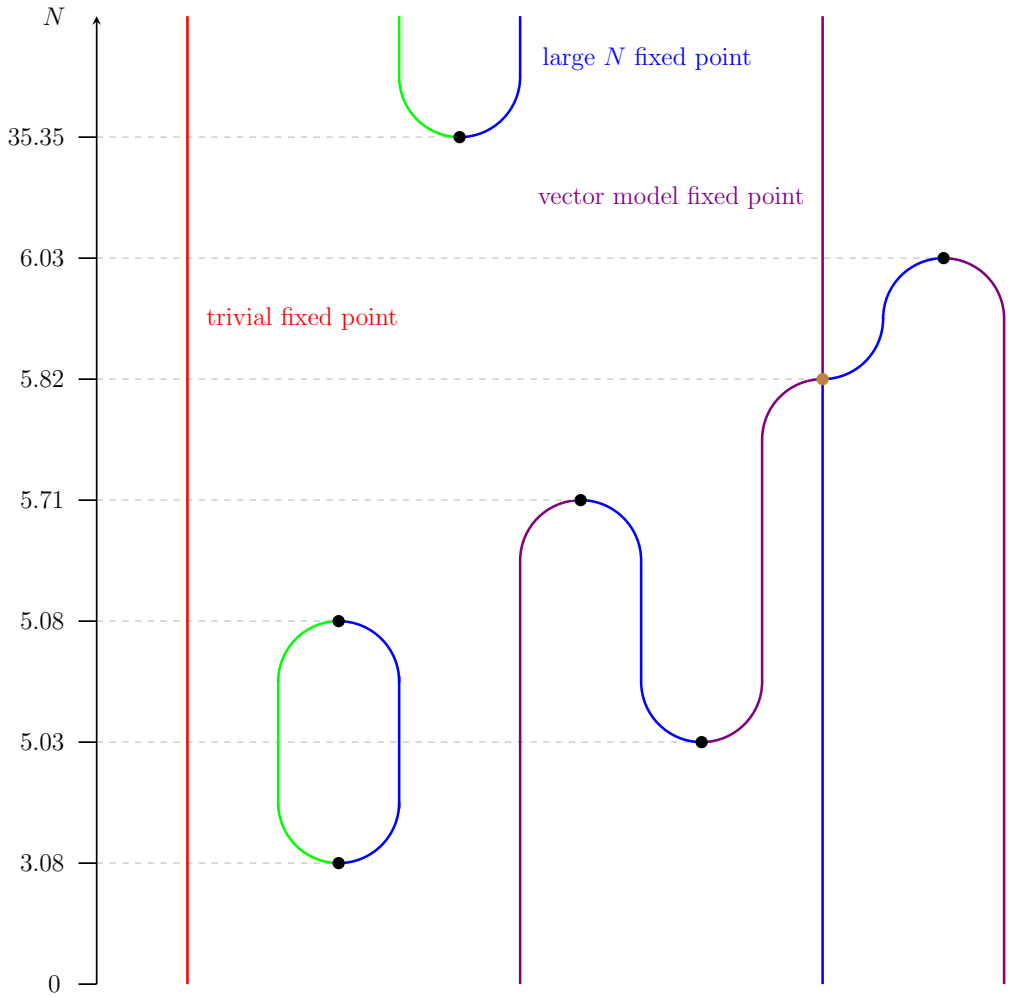

N	λ_1/ϵ	λ_2/ϵ	λ_3/ϵ
$35.3546 - 673.428\epsilon$	$49.5253 + 2344.67\epsilon$	$-14.7886 - 819.812\epsilon$	$2.27483 + 172.497\epsilon$
$6.02669 + 7.37013\epsilon$	$13.2186 + 135.952\epsilon$	$46.5606 + 358.588\epsilon$	$52.3442 + 184.725\epsilon$
$(1+\sqrt{113})/2 + \mathcal{O}(\epsilon)$	$\mathcal{O}(\epsilon^2)$	undetermined $\mathcal{O}(\epsilon)$	$15\pi^2/2 + \mathcal{O}(\epsilon)$
$5.70601 + 0.540694\epsilon$	$1835.96 + 12199.7\epsilon$	$-1514.42 - 9969.85\epsilon$	$315.529 + 1975.47\epsilon$
$5.07531 - 0.0278896\epsilon$	$1742.93 + 14681.9\epsilon$	$-1228.95 - 10464.7\epsilon$	$275.926 + 2170.35\epsilon$
$5.03275 - 0.586724\epsilon$	$350.124 + 3001.15\epsilon$	$-404.283 - 3356.64\epsilon$	$180.867 + 1310.49\epsilon$
$3.08122 + 8.26176\epsilon$	$666.939 + 7903.77\epsilon$	$-373.592 - 5369.46\epsilon$	$170.179 + 1403.34\epsilon$

Figure 4.3: The real perturbative fixed points of the antisymmetric matrix model, their intersection point (marked in brown), and the critical points at which they merge and disappear (marked in **black**) as a function of N for small ϵ. Fixed points that are IR-unstable in all three directions are drawn in red, those unstable in two directions are drawn in violet, those unstable in one direction are drawn in blue, and those that are stable in all three directions are drawn in green.

4.2.3 Symmetric traceless matrices and violation of large N equivalence

There is a projection of the parent theory of general real matrices ϕ^{ab} which restricts them to symmetric matrices $\phi = \phi^T$. In order to have an irreducible representation of $O(N)$ we should also require them to be traceless $\mathrm{tr}\,\phi = 0$. Then the propagator is given by

$$\left\langle \widetilde{\phi}^{ab}(k)\widetilde{\phi}^{a'b'}(-k)\right\rangle_0 = \frac{1}{2k^2}\Big(\delta^{aa'}\delta^{bb'} + \delta^{ab'}\delta^{ba'} - \frac{2}{N}\delta^{ab}\delta^{a'b'}\Big)\,. \tag{4.27}$$

The operators $O_{1,2,3,4}$ are actually independent for $N > 5$, while for $N = 2, 3, 4, 5$ there are linear relations between them:

- $N = 2 : O_4 = 0, \quad O_3 = 2O_2 = 4O_1,$
- $N = 3 : O_3 = 2O_2, \quad 2O_4 = 3O_3 + 6O_1,$
- $N = 4, 5 : 18O_2 + 8O_4 = 24O_1 + 3O_3.$

We will see that the existence of these relations for small integer values of N has interesting implications for the analytic continuation of the theory from $N > 5$ to $N < 5$.

Let us first discuss the large N theory. For the rescaled couplings λ_1, λ_2, and λ_3, the large N beta functions are the same as (4.24) for the anti-symmetric model. But now there is an additional coupling constant, whose large N beta function is given by

$$\beta_{\lambda_4} = -2\epsilon\lambda_4 + 72\lambda_1^2 + 36\lambda_1\lambda_4 + 6\lambda_4^2 - 738\lambda_1^2\lambda_4 - 18(180 + 11\pi^2)\lambda_1^3\,. \tag{4.28}$$

Consequently, the RG flow now has five non-trivial fixed points, two of which are real fixed points but with coupling constants containing $\mathcal{O}(\epsilon^0)$ terms. Another pair of fixed points is given by

$$\lambda_1 = \frac{\epsilon}{9} + \frac{17+\pi^2}{81}\epsilon^2, \quad \lambda_2 = -2\epsilon - \frac{22+7\pi^2}{9}\epsilon^2, \quad \lambda_3 = \frac{295}{27}\epsilon + \frac{4714+6301\pi^2}{486}\epsilon^2,$$
$$\lambda_4 = \frac{-3 \pm i\sqrt{39}}{18}\epsilon + \frac{273 - 78\pi^2 \pm i\sqrt{39}(67+12\pi^2)}{2106}\epsilon^2\,. \tag{4.29}$$

The first three coupling constants assume the same value as for the anti-symmetric model, a rescaled version of (4.16) of the parent theory, but the additional coupling constant assumes a complex value, thus breaking large N equiavalence and suggesting that the fixed point is unstable and described by a complex CFT [93, 177].

We find that the eigenvalues of $\frac{\partial\beta_{\lambda_i}}{\partial\lambda_j}$ at this complex fixed point are

$$\Big\{-2\epsilon+\frac{32}{9}\epsilon^2,\, \mp 2i\sqrt{\frac{13}{3}}\epsilon\pm 2i\frac{67+12\pi^2}{9\sqrt{39}}\epsilon^2,\, \frac{2}{3}\epsilon-2\frac{22+5\pi^2}{27}\epsilon^2,\, 2\epsilon-2\frac{17+\pi^2}{9}\epsilon^2\Big\} \quad (4.30)$$

where the imaginary eigenvalue is associated to a complex linear combination of λ_1 and λ_4. Thus, there is actually a pair of complex large N fixed points: at one of them there is an operator of complex dimension $d+iA = 3-\epsilon+iA$, while at the other it has dimension $d-iA$,[20] where $A = 2\sqrt{\frac{13}{3}}\epsilon - 2\frac{67+12\pi^2}{9\sqrt{39}}\epsilon^2$. Thus, this pair of complex fixed points satisfy the criteria to be identified as complex CFTs [93, 177]. In our large N theory, the scaling dimensions $d\pm iA$ correspond to the double-trace operator O_4, so that the single-trace operator $\mathrm{tr}\,\phi^3$ should have scaling dimension $\frac{1}{2}(d\pm iA)$. Indeed, we find that its two-loop anomalous dimension is, for large N,

$$\gamma_{\mathrm{tr}\,\phi^3} = 6\,(3\lambda_1+\lambda_2) = \epsilon \pm i\sqrt{\frac{13}{3}}\epsilon\ . \quad (4.31)$$

Therefore,

$$\Delta_{\mathrm{tr}\,\phi^3} = 3\left(\frac{d}{2}-1\right)+\gamma_{\mathrm{tr}\,\phi^3} = \frac{3-\epsilon}{2}\pm i\sqrt{\frac{13}{3}}\epsilon = \frac{d\pm iA}{2}\ . \quad (4.32)$$

Scaling dimensions of this form are ubiquitous in large N complex CFTs [81, 91, 26, 3]. In the dual AdS description they correspond to fields violating the Breitenlohner-Freedman stability bound.

Let us also note that the symmetric orbifold has a fixed point where only the twisted sector coupling is non-vanishing:

$$\lambda_{1,2,3} = 0, \quad \lambda_4 = \frac{\epsilon}{3}\,. \quad (4.33)$$

[20] As N is reduced, the two complex conjugate fixed points persist down to arbitrarily small N. For finite N, however, the complex scaling dimensions are no longer of the form $d\pm iA$: the real part deviates from d, which is consistent with the behavior of general complex CFTs [93, 177].

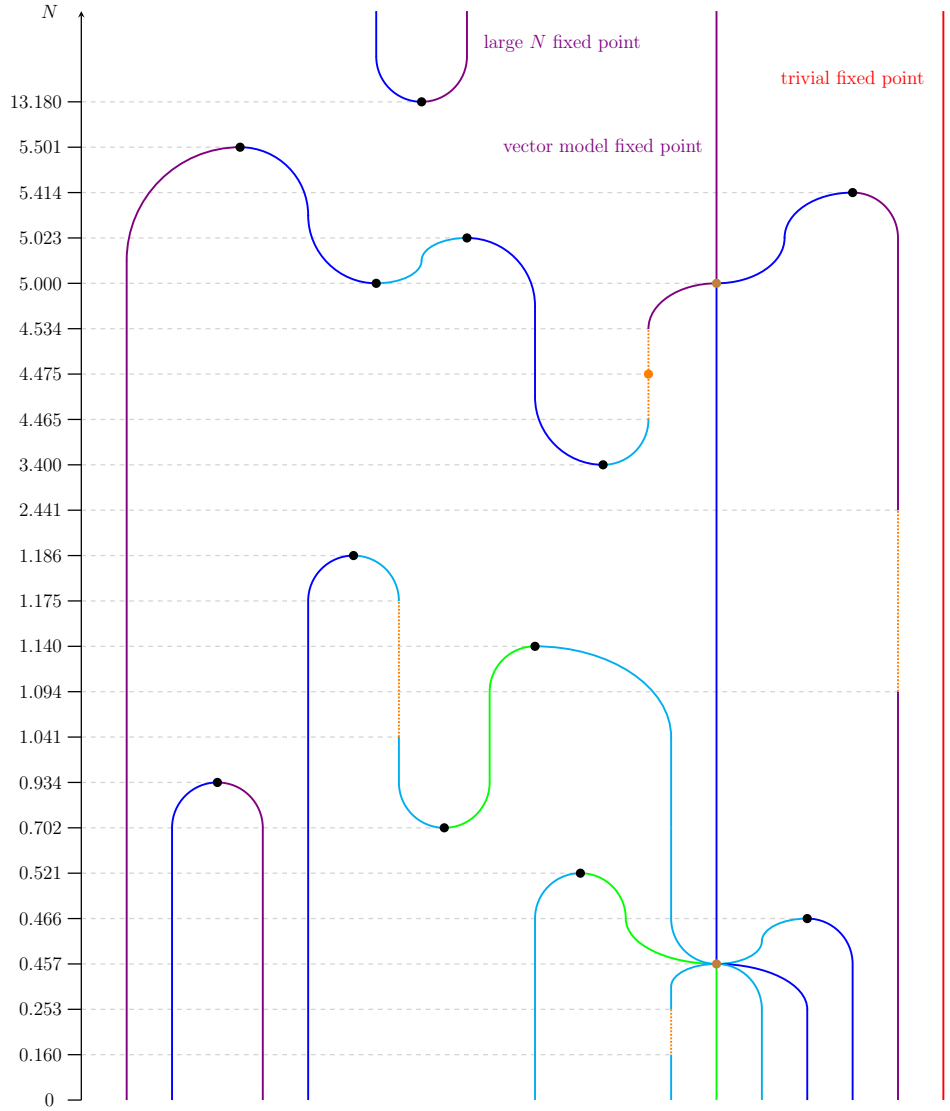

N	g_1/ϵ	g_2/ϵ	g_3/ϵ	g_4/ϵ
$13.1802 - 57.5808\epsilon$	$37.9805 + 498.738\epsilon$	$13.7692 + 157.614\epsilon$	$0.774624 + 9.43200\epsilon$	$21.5178 + 155.312\epsilon$
$5.50104 - 0.966432\epsilon$	$1424.22 + 11076.8\epsilon$	$-1176.03 - 9116.73\epsilon$	$247.515 + 1873.61\epsilon$	$-454.872 - 3511.98\epsilon$
$5.41410 + 13.7204\epsilon$	$24.4748 + 360.178\epsilon$	$57.2276 + 450.992\epsilon$	$39.8006 - 29.6552\epsilon$	$-2.62055 - 19.2614\epsilon$
$5.02251 + 0.314146\epsilon$	$1132.14 + 13268.0\epsilon$	$-775.767 - 9368.16\epsilon$	$185.009 + 1864.18\epsilon$	$-372.446 - 4364.10\epsilon$
$5 + \mathcal{O}(\epsilon)$	$\mathcal{O}(\epsilon^2)$	undetermined $\mathcal{O}(\epsilon)$	$15\pi^2/2 + \mathcal{O}(\epsilon)$	$\mathcal{O}(\epsilon^2)$
5	$868.525 + 8195.57\epsilon$	$-651.394 - 6497.79\epsilon$	$182.588 + 1618.14\epsilon$	$-289.508 - 2731.86\epsilon$
$3.39974 + 5.04412\epsilon$	$308.575 + 3818.19\epsilon$	$-149.500 - 2394.44\epsilon$	$113.071 + 818.926\epsilon$	$-100.935 - 1242.36\epsilon$
$1.18613 - 1.96911\epsilon$	$113.631 + 136.626\epsilon$	$-445.062 - 3310.43\epsilon$	$475.932 + 3758.3\epsilon$	$573.101 + 3747.7\epsilon$
$1.139999 - 0.0564804\epsilon$	$7.14941 + 103.455\epsilon$	$-121.617 - 1749.67\epsilon$	$281.382 + 2487.82\epsilon$	$113.505 + 1635.81\epsilon$
$0.934072 - 0.0890231\epsilon$	$0.0911386 + 344.846\epsilon$	$-2777.40 - 9338.97\epsilon$	$1172.45 + 4559.95\epsilon$	$2333.04 + 8376.93\epsilon$
$0.701527 + 10.3604\epsilon$	$12.8934 + 848.994\epsilon$	$-57.8652 - 4059.74\epsilon$	$279.112 + 3827.54\epsilon$	$67.4704 + 4336.08\epsilon$
$0.521281 - 14.4794\epsilon$	$3.96346 - 441.552\epsilon$	$-16.5232 + 1957.63\epsilon$	$257.847 + 606.789\epsilon$	$22.3424 - 2270.44\epsilon$
$0.465602 - 6.81219\epsilon$	$1.79072 - 162.063\epsilon$	$24.3958 - 1503.26\epsilon$	$228.454 + 2430.09\epsilon$	$-15.2518 + 919.203\epsilon$
$(\sqrt{33} - 3)/6 + \mathcal{O}(\epsilon)$	undetermined $\mathcal{O}(\epsilon)$	undetermined $\mathcal{O}(\epsilon)$	$24\pi^2 + \mathcal{O}(\epsilon)$	$\mathcal{O}(\epsilon)$

Figure 4.4: The perturbative real fixed points of the symmetric matrix model, the intersection points (marked in brown), and the critical points at which they merge and disappear (marked in **black**) as a function of N for small ϵ. Fixed points that are IR-unstable in all four directions are drawn in red, those unstable in three directions are drawn in violet, those unstable in two direction are drawn in blue, those unstable in one direction are drawn in cyan, and those that are stable in all four directions are drawn in green. The orange dotted lines denote the segments of "spooky" fixed points, where two eigenvalues of $\frac{\partial \beta_i}{\partial g_j}$ are complex, and at the orange vertex those eigenvalues are purely imaginary.

It could be connected to the fact that in the large N limit of the parent theory the O_4 could not contribute to the beta functions of the other operators and therefore we can safely set $\lambda_{1,2,3} = 0$ without setting $\lambda_4 \neq 0$.

We can also study the behaviour of this model for finite N and $\epsilon \langle 1$. For $N > 13.1802 - 57.5808\,\epsilon$ there are three (real, perturbatively accesible) fixed points, which in the large N limit (keeping $\epsilon \langle \frac{1}{N^2}$) to leading order in ϵ scale with N as

$$\begin{aligned} &0 = g_1 = g_2 = g_4 \qquad g_3 = \frac{6!(8\pi)^2}{144N^2}\epsilon \\ &g_1 = 144\frac{6!(8\pi)^2}{N^6}\epsilon \quad g_2 = 66\frac{6!(8\pi)^2}{N^5}\epsilon \quad g_3 = \frac{6!(8\pi)^2}{144N^2}\epsilon \quad g_4 = \frac{6!(8\pi)^2}{3N^3}\epsilon \\ &g_1 = -144\frac{6!(8\pi)^2}{N^6}\epsilon \quad g_2 = 18\frac{6!(8\pi)^2}{N^5}\epsilon \quad g_3 = -18\frac{6!(8\pi)^2}{N^6}\epsilon \quad g_4 = \frac{6!(8\pi)^2}{3N^3}\epsilon \end{aligned} \tag{4.34}$$

The first of these three fixed points is the vector model fixed point, which is present generally N in the small ϵ regime:

$$0 = g_1 = g_2 = g_4 \qquad g_3 = \frac{6!(8\pi)^2}{48(38 + 3N + 3N^2)}\epsilon \tag{4.35}$$

The third fixed point in (4.34) connects to the large N solution discussed above. This fixed point merges with the second fixed point in (4.34) at a critical point situated at $N(\epsilon) = 13.1802 - 57.5808\,\epsilon$ And so at intermediate values of N, only the vector model fixed point exists. But as we keep decreasing N we encounter another critical point at $N(\epsilon) = 5.41410 + 13.7204\,\epsilon$ whence two new fixed points emerge.

4.3 Spooky Fixed Points and Limit Cycles

As indicated in figure 4.4, in the $O(N)$ symmetric traceless model there exist four segments of real, but spooky fixed points as a function of N.[21] For these fixed points the Jacobian matrix $\left(\frac{\partial \beta_i}{\partial g_j}\right)$ has, in addition to one negative and one positive eigenvalue, a pair of complex conjugate eigenvalues. Therefore, there are two complex scaling dimensions (4.18) at these spooky fixed points, so that they correspond to non-unitary CFTs. The

[21] If we allow negative N, there is a fifth segment of spooky fixed points at $N \in (-3.148, -3.183)$.

eigenvectors corresponding to the complex eigenvalues have zero norm (a derivation of this fact is given later in this section). Let us note that, in the $O(N)^2$ model and $O(N)$ model with antisymmetric matrix there are no real fixed points with complex eigenvalues. The symmetric traceless model provides a simple setting where they occur. In this section we take a close look at the spooky fixed points and show that they lead to a Hopf bifurcation and RG limit cycles.

Of the four segments of spooky fixed points with positive N, three, namely those that fall within the ranges given by $N \in (1.094, 2.441)$, $N \in (1.041, 1.175)$, and $N \in (0.160, 0.253)$, share the property that the complex eigenvalues never become purely imaginary. The number of stable and unstable directions therefore remain the same within these intervals. Something special happens, however, at the integer value $N = 2$ that lies within the first interval. Here the two operators with complex dimensions are given by linear combinations of operators O_i that vanish by virtue of the linear relations between these operators at $N = 2$.[22] As a result, for $N = 2$ there are no nearly marginal operators with complex dimensions, as expected.

The fourth segment of spooky fixed points stands out in that it includes a fixed point with imaginary eigenvalues. This fourth segment lies in the range $N \in (N_{\text{lower}}, N_{\text{upper}})$, where, at four-loop level,

$$N_{\text{upper}} \approx 4.5339959143 + 1.54247\epsilon \ , \qquad N_{\text{lower}} \approx 4.4654144982 + 0.693698\epsilon \ . \tag{4.36}$$

As N approaches N_{upper} from above, $\left(\frac{\partial \beta_i}{\partial g_j}\right)$ has one positive and three negative eigenvalues, and two of the negative eigenvalues converge on the same value. As N dips below N_{upper}, the two erstwhile identical eigenvalues become complex and form a pair of complex conjugate values. As we continue to decrease N, the complex conjugate eigenvalues traverse mirrored trajectories in the complex plane until they meet at the same positive value for N equal to N_{lower}. These trajectories are depicted in figure 4.5. For a critical value $N = N_{\text{crit}}$ with $N_{\text{lower}} < N < N_{\text{upper}}$, the trajectories intersect the imaginary axis

[22] This is similar to what happens to evanescent operators when they are continued to an integer dimension.

such that the two eigenvalues are purely imaginary. At the two-loop order we find that

$$N_{\text{crit}} \approx 4.47507431683 \ , \tag{4.37}$$

and the fixed point is located at

$$\begin{aligned} g_1^* &= 158.684\epsilon, \quad g_2^* = -211.383\epsilon, \\ g_3^* &= 138.686\epsilon, \quad g_4^* = -49.4564\epsilon \ . \end{aligned} \tag{4.38}$$

The Jacobian matrix evaluated at this fixed point is

$$\left(\frac{\partial \beta_i}{\partial g_j}\right) = \begin{pmatrix} -1.65273 & -1.58311 & 1.33984 & -1.19641 \\ 1.0242 & 0.358518 & -3.24194 & 1.21102 \\ 0.128059 & 0.749009 & 2.9199 & -0.210872 \\ -0.0618889 & 0.428409 & -0.417582 & -1.20064 \end{pmatrix} \epsilon \tag{4.39}$$

with eigenvalues $\{2, -1.57495, -0.153965i, 0.153965i\}\,\epsilon$. These quantities are subject to further perturbative corrections in powers of ϵ; for example, after including the four-loop corrections $N_{\text{crit}} \approx 4.47507431683 + 3.12476\epsilon$. The existence of a special spooky fixed point with imaginary eigenvalues is robust under loop corrections that are suppressed by a small expansion parameter, since small perturbations of the trajectories still result in curves that intersect the imaginary axis. In light of the negative value of g_4^*, one may worry that the potential is unbounded from below at the spooky fixed points. It is not clear how to resolve this question for non-integer N, but at the fixed-points at $N = 4$ and $N = 5$ that this spooky fixed point interpolates between, one can explicitly check that the potential is bounded from below.

The appearance of complex eigenvalues changes the behavior of the RG flow around the spooky fixed point. Since the fixed point has one negative eigenvalue for all $N \in (N_{\text{lower}}, N_{\text{upper}})$, there is an unstable direction in the space of coupling constants that renders the fixed point IR-unstable. But we can ask the following question: How do the coupling constants flow in the two-dimensional manifold that is invariant under the RG

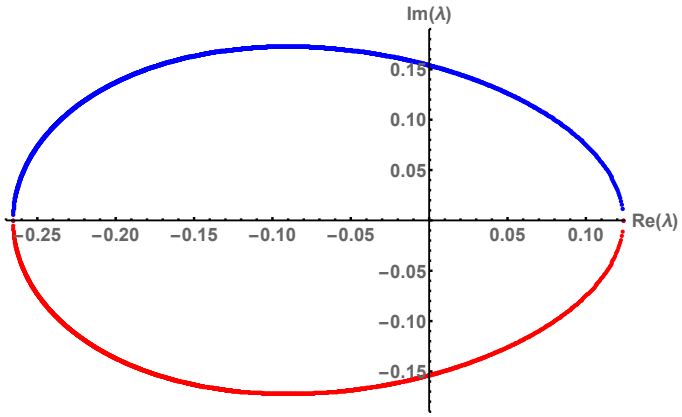

Figure 4.5: The trajectories of the complex eigenvalues of the Jacobian matrix $\left(\frac{\partial \beta_i}{\partial g_j}\right)$ as N is varied from N_{lower} to N_{upper}.

flow and that is tangent to the plane spanned by the eigenvectors of the Jacobian matrix with complex eigenvalues?

If the real parts of these eigenvalues are non-zero, the spooky fixed point is a *focus* and the flow around it is described by spirals steadily moving inwards or outwards from the fixed point. For $N > N_{\text{crit}}$, the real parts are negative and the fixed point is IR-unstable, while for $N < N_{\text{crit}}$ the real parts are positive and the fixed point is stable. By the Hartman-Grobman theorem [178, 179], one can locally change coordinates (redefine the coupling constants) such that the beta-functions near the fixed points are linear. Furthermore, one can get rid of the imaginary part of the eigenvalues in this subspace by a suitable field redefinition[23]. An analogous statement was given in [149].

When $N = N_{\text{crit}}$, the real parts of the complex eigenvalues are equal to zero. In this case the equilibrium point is a *center*, the Hartman-Grobman theorem is not applicable, and the behavior near the fixed point is controlled by the higher non-linear terms in the autonomous equations. If we consider N as a parameter of the the RG flow, $N = N_{\text{crit}}$ corresponds to a bifurcation point, as first introduced by Poincarè. A standard method of analyzing bifurcations is to reduce the full system to a set of lower dimensional systems by use of the center manifold theorem [180]. Denoting by λ the eigenvalues of the Jabobian matrix at a given fixed point, this theorem guarantees the existence of invariant manifolds

[23]For instance, in two dimensions with $z = x + iy$, the equation $\dot{z} = (-\alpha + i\omega)z$ can via a change of variable $z \to ze^{i\frac{\omega}{\alpha}\log|z|}$ be reduced to $\dot{z} = -\alpha z$.

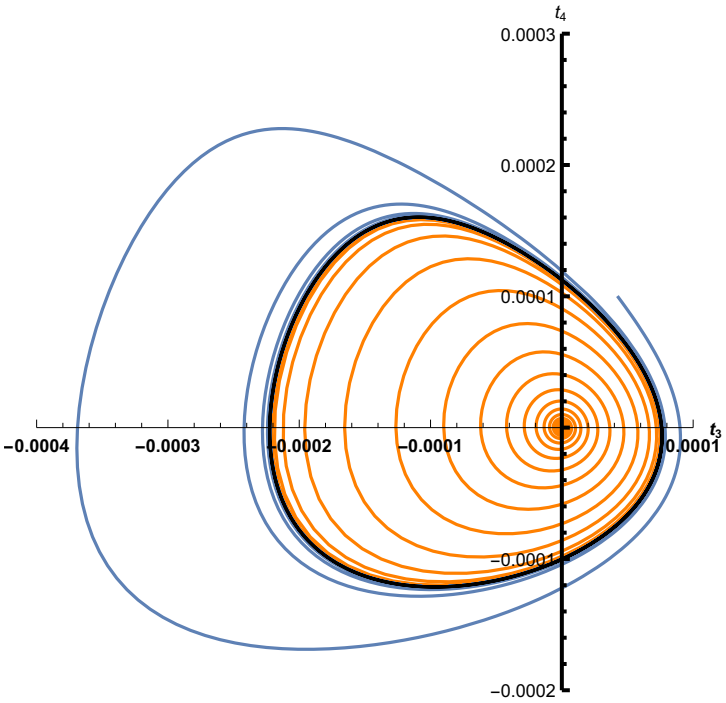

Figure 4.6: The RG flow in the invariant manifold tangent to the plane spanned by the eigenvectors with complex eigenvalues in the space of coupling constants for $N = 4.476$. In the IR, the blue curve whirls inwards towards a limit cycle marked in **black**, while the orange curve whirls outwards towards the limit cycle. The coordinates t_3 and t_4 are given by linear combinations of the couplings g_1, g_2, g_3, and g_4 and are defined in appendix 4.4. The RG flow on the invariant manifold admits of a description in an infinite expansion in powers of t_3 and t_4. This plot is drawn retaining terms up to cubic order.

tangent to the eigenspaces with $\mathrm{Re}\,\lambda > 0$, $\mathrm{Re}\,\lambda < 0$, and $\mathrm{Re}\,\lambda = 0$ respectively. The latter manifold is known as the center manifold, and in general it need neither be unique nor smooth. But when, as in our case, the center at g^* is part of a line of fixed points in the space (g, N) that vary smoothly with a parameter N, and the complex eigenvalues satisfy

$$\kappa = \frac{d}{dN}\mathrm{Re}[\lambda(N_{\mathrm{crit}})] \neq 0\,, \tag{4.40}$$

then there exists a unique 3-dimensional center manifold in $(\vec{g}, N)$ passing through (g^*, N_{crit}). On planes of constant N in this manifold, there exist coordinates (x, y) such that the third order Taylor expansion can be written in the form

$$\begin{aligned}
\frac{dx}{dt} &= \Big(\kappa N + a(x^2+y^2)\Big)x - \Big(\omega + cN + b(x^2+y^2)\Big)y\,,\\
\frac{dy}{dt} &= \Big(\omega + cN + b(x^2+y^2)\Big)x + \Big(\kappa N + a(x^2+y^2)\Big)y\,,
\end{aligned} \tag{4.41}$$

where $t = \ln\mu$. The constant a in these equations is known as the Hopf constant. By a theorem due to Hopf [158], there exists an IR-attractive limit cycle in the center manifold if $a > 0$, while if $a < 0$ there exists an IR-repulsive limit cycle. In appendix 4.4, we present an explicit calculation of a for the critical point in the symmetric matrix model, and we find that a is positive. Hence, we conclude that on analytically continuing in N, the RG flow of this QFT contains a periodic orbit in the space of coupling constants, an orbit that is unstable but which in the center manifold constitutes an attractive limit cycle. This conclusion holds true at all orders in perturbation theory, since the criteria of Hopf's theorem, being topological in nature, are not invalidated by small perturbative corrections.

Now that we have demonstrated the existence of limit cycles, we should ask about their consistency with the known RG monotonicity theorems. In particularly, in 3 dimensions the F-theorem has been conjectured and established [159, 160, 162]. Furthermore, in perturbative 3-dimensional QFT, one can make a stronger statement that the RG flow is

a gradient flow, i.e.

$$G_{ij}\beta^j = \frac{\partial F}{\partial g^i} \ , \tag{4.42}$$

where F and the metric G_{ij} are functions of the coupling constants which can be calculated perturbatively [161, 163, 164, 136, 165].[24] At leading order, G_{ij} may be read off from the two-point functions of the nearly marginal operators [163, 164]:

$$\langle O_i(x) O_j(y)\rangle = \frac{G_{ij}}{|x-y|^6} \ . \tag{4.43}$$

The F-function satisfies the RG equation

$$\mu\frac{\partial}{\partial\mu}F = \frac{\partial}{\partial t}F = \beta^i\beta^j G_{ij} \ . \tag{4.44}$$

This shows that, if the metric is positive definite, then F descreases monotonically as the theory flows towards the IR. These perturbative statements continue to be applicable in $3-\epsilon$ dimensions.

At leading order, the metric G_{ij} is exhibited in appendix B. Its determinant is given by

$$\frac{(N-5)(N-4)(N-3)^2(N-2)^3N^2(N+1)^3(N+3)(N+4)^3(N+6)^2(N+8)(N+10)}{2654208} \ . \tag{4.45}$$

This shows that the metric has three zero eigenvalues for $N=2$, two zero eigenvalues for $N=3$, and one zero eigenvalue for $N=4$ and 5. This is due to the linear relations between operators O_i at these integer values of N. For example, for $N=2$ there is only one independent operator. In the range $4<N<5$, $\det G_{ij}<0$, the metric has one negative and three positive eigenvalues. This is what explains the possibility of RG limit cycles in the range $N_{\text{lower}}<N<N_{\text{upper}}$. For $N>5$, G_{ij} is positive definite, and for $N<-10$, G_{ij} is negative definite. This is consistent with our observing spooky fixed points only outside of these regimes.[25]

[24] In [136, 165] the terminology a-function was used, but we prefer to call it F-function instead, since a typically refers to a Weyl anomaly coefficient in $d=4$.

[25] We have also found the metric for the parent $O(N)^2$ theory. In this case it is positive definite for

In general, the norms of vectors computed with this metric are not positive definite for $N < 5$. In particular, we can show that the eigenvectors corresponding to complex eigenvalues of the Jacobian matrix evaluated at real fixed points have zero norm. Indeed, let us assume that we have a complex eigenvalue $m \in \mathbb{C}$ with eigenvector u^i

$$\frac{\partial \beta^i}{\partial g^j} u^j = m u^i \ . \tag{4.46}$$

Now let us differentiate the relation (4.42) with respect to g^K:

$$\partial_K G_{IJ} \beta^J + G_{IJ} \partial_K \beta^J = \partial_I \partial_K F \ . \tag{4.47}$$

At a spooky fixed point we have $\beta^J(g) = 0$ for real couplings g. Contracting the relation (4.47) with u^K and $\bar{u}^I$ at a spooky fixed point we get

$$\bar{u}^I G_{IJ} \partial_K \beta^J u^K = u^K \bar{u}^I \partial_I \partial_K F \ . \tag{4.48}$$

Using (4.46) we arrive at the following relations

$$m \bar{u}^I u^J G_{IJ} = \bar{u}^I u^J \partial_I \partial_J F \ . \tag{4.49}$$

Since G_{IJ} and $\partial_I \partial_J F$ are real symmetric matrices, the norm $u^2 = G_{IJ} u^I \bar{u}^J$ and $f = \bar{u}^I u^J \partial_I \partial_J F$ are real numbers. If they are not equal to zero, then we must have $m \in \mathbb{R}$, which contradicts our assumption. Therefore, the norm $u^2 = 0$.

Another consequence of the negative eigenvalues of G_{ij} is that dF/dt can have either sign, as follows from (4.44). In fig. (4.7) we plot $F(t)$ for the limit cycle of fig. 4.6, showing that it oscillates. This can also be shown analytically for a small limit cycle surrounding a fixed point. We may expand around it to find

$$\beta^i(t) = a(t) v^i + \bar{a}(t) \bar{v}^i \ , \tag{4.50}$$

all N except $N \in \{-4, -2, 1, 2\}$, where there are zero eigenvalues. We further found the metric for the anti-symmetric matrix model. In certain intervals within the range $N \in (-4, 5)$ it has both positive and negative eigenvalues, but numerical searches reveal no spooky fixed points in these intervals.

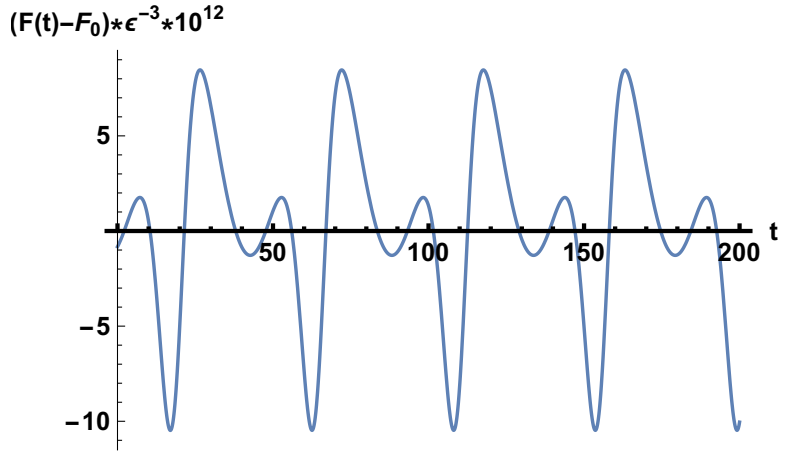

Figure 4.7: The plot of $10^{12}(F(t) - F_0)/\epsilon^3$, where F_0 is the value at the spooky fixed point, for the cyclic solution found in section 4.3 for $N = 4.476$.

where v^i and $\bar{v}^i$ are the eigenvectors corresponding to the complex eigenvalues of the Jacobian matrix at the spooky fixed point. While $G_{ij}v^i\bar{v}^j$ vanishes, $G_{ij}v^iv^j \neq 0$. Therefore, (4.44) implies that $dF/dt \neq 0$ for a small limit cycle.

4.4 Calculating the Hopf constant

In this appendix we compute the Hopf constant a at two loops. Introducing rescaled couplings $g_i = 720(8\pi)^2\epsilon\, \mathcal{g}_i$, the beta functions at the critical value $N = N_{\text{crit}} = 4.475$ in units of ϵ become

$$\beta_{\mathcal{g}_1} = -2\mathcal{g}_1 + \left(2339.99\mathcal{g}_1 + 4273.55\mathcal{g}_2 + 3840.\mathcal{g}_3 + 4325.08\mathcal{g}_4\right)\mathcal{g}_1 + 2768.04\mathcal{g}_2^2 + 2592.\mathcal{g}_4^2 + 4608.\mathcal{g}_2\mathcal{g}_4$$

$$\beta_{\mathcal{g}_2} = -2\mathcal{g}_2 + \left(509.966\mathcal{g}_1 + 2962.93\mathcal{g}_2 + 6748.16\mathcal{g}_3 + 113.519\mathcal{g}_4\right)\mathcal{g}_1 + \left(3456.\mathcal{g}_3 + 360.299\mathcal{g}_4\right)\mathcal{g}_4 + \left(2308.94\mathcal{g}_2 + 11232.3\mathcal{g}_3 - 421.438\mathcal{g}_4\right)\mathcal{g}_2$$

$$\beta_{\mathcal{g}_3} = -2\mathcal{g}_3 + \left(42\mathcal{g}_1 + 221.912\mathcal{g}_2 + 576.\mathcal{g}_3 - 241.337\mathcal{g}_4\right)\mathcal{g}_1 + 10704.4\mathcal{g}_3^2 - 209.942\mathcal{g}_4^2 - 772.278\mathcal{g}_3\mathcal{g}_4 + \left(629.906\mathcal{g}_2 + 4074.01\mathcal{g}_3 - 135.923\mathcal{g}_4\right)\mathcal{g}_2$$

$$\beta_{\mathcal{g}_4} = -2\mathcal{g}_4 + \left(226.417\mathcal{g}_1 + 73.3524\mathcal{g}_2 + 1708.55\mathcal{g}_4\right)\mathcal{g}_1 - 618.547\mathcal{g}_2^2 + \left(1583.3\mathcal{g}_2 + 3840.\mathcal{g}_3 + 1066.11\mathcal{g}_4\right)\mathcal{g}_4$$

These beta functions have a fixed point at

$$\mathcal{g}^*(N_{\text{crit}}) = 10^{-4}\cdot(3.48916, -4.64792, 3.04945, -1.08745)\,. \tag{4.51}$$

Letting $V = (v_1, v_2, v_3, \overline{v}_3)$ be the matrix of eigenvectors v_i of the stability matrix $\left(\frac{\partial \beta_{g_i}}{\partial g_j}\right)$ evaluated at this fixed point,

$$V^{-1}\left(\frac{\partial \beta_{g_i}}{\partial g_j}\right) V = \mathrm{diag}\left(2, -1.57495, -0.153965i, 0.153965i\right). \tag{4.52}$$

One can check that these eigenvalues change on varying N. In particular, the real parts of the complex eigenvalues change linearly with N for N close to N_{crit}. Changing to variables $t_1 = v_1 \cdot g$, $t_2 = v_2 \cdot g$, $t_3 = \Re[v_3 \cdot g]$, $t_4 = \Im[v_3 \cdot g]$, we get the equations

$$\begin{aligned}
\beta_{t_1} &= 2t_1 - 3006.27t_1^2 - 635.361t_2^2 - 4.22379t_3^2 + 4.22379t_4^2 + 7.65924t_3t_4 \\
\beta_{t_2} &= -1.57495t_2 + \left(-638.903t_1 + 1471.36t_2 - 96.8862t_3 + 72.0709t_4\right)t_2 + \\
&\quad +1.0131t_3^2 - 0.34628t_4^2 - 1.37241t_3t_4 \\
\beta_{t_3} &= -0.153965t_4 + \left(231.430t_4 - 3006.27t_3\right)t_1 + \left(-31746.2t_2 + 1284.37t_3 - 347.122t_4\right)t_2 \\
&\quad -49.5972t_3^2 + 492.731t_4^2 + 178.686t_3t_4 \\
\beta_{t_4} &= 0.153965t_3 + \left(-231.43t_3 - 3006.27t_4\right)t_1 + \left(638.003t_2 + 730.144t_4 - 82.7131t_3\right)t_2 \\
&\quad +8.73689t_3^2 + 823.772t_4^2 + 153.731t_3t_4\,.
\end{aligned} \tag{4.53}$$

We wish to study the RG flow in the manifold that is tangent to the center eigenspace. We cannot simply set t_1 and t_2 to zero, since this plane is not invariant under the RG flow: the t_3^2, t_4^2, and t_3t_3 terms in β_{t_1} and β_{t_2} generate a flow in t_1 and t_2. But by introducing new variables with t_1 and t_2 suitably shifted,

$$u_1 = t_1 - 1.77501t_3^2 + 4.3762t_4t_3 + 1.77501t_4^2, \tag{4.54}$$

$$u_2 = t_2 - 0.709414t_3^2 + 0.676770t_4t_3 + 0.286027t_4^2\,, \tag{4.55}$$

the t_3^2, t_4^2, and t_3t_3 terms in β_{u_1} and β_{u_2} cancel out. While β_{u_1} and β_{u_2} do couple to t_3 and t_4 at third order, one can introduce new variables yet again and shift u_1 and u_2 by cubic terms in t_3 and t_4 to remove this third order coupling. This procedure may be iterated indefinitely to obtain a coordinate expansion of the center manifold to arbitrary

order, in accordance with the center manifold theorem. We will content ourselves with the cubic approximation of the center manifold, which consists of the surface $u_1 = u_2 = 0$, since this approximation suffices to determine the Hopf constant. Eliminating t_1 and t_2 in favour of u_1 and u_2 in the equations for β_{t_3} and β_{t_4}, setting u_1 and u_2 to zero, and discarding unreliable quartic terms gives

$$\begin{aligned}
\beta_{t_3} &= -49.5972 t_3^2 + 178.686 t_4 t_3 + 492.731 t_4^2 - 0.153965 t_4 \\
&-4425.01 \left(1. t_3^3 - 2.81386 t_4 t_3^2 - 0.947101 t_4^2 t_3 + 0.0703961 t_4^3\right) \\
\beta_{t_4} &= 8.73689 t_3^2 + 153.731 t_4 t_3 + 0.153965 t_3 + 823.772 t_4^2 \\
&-469.468 \left(1. t_3^3 + 7.98654 t_4 t_3^2 - 27.8962 t_4^2 t_3 - 10.9216 t_4^3\right) .
\end{aligned} \tag{4.56}$$

From these equations the Hopf constant can be directly obtained by the use of equation (3.4.11) in [180] or by the equivalent formula in [181]. We find that

$$a \approx 6204790 \tag{4.57}$$

so that Hopf's theorem guarantees the existence of a periodic orbit that is IR-attractive in the center manifold, implying that if we fine-tune the couplings in the vicinity of N_{crit}, there is a cyclic solution to the beta functions that comes back precisely to itself.

4.5 Other bifurcations

Since the classic review by Kogut and Wilson [140] on the ϵ expansion and renormalization group (RG) flow, the general properties of RG flows have been the subject of active research. In the cases usually considered, once a theory starts flowing, it ends up at a fixed point where it is described by some conformal field theory (CFT). From a general point of view, the equations describing instances of RG flow form systems of autonomous differential equations, and the properties of such systems and the kinds of flows they admit are well understood [180, 182, 141, 183]. In particular, dynamical systems can exhibit flows more peculiar than that between distinct fixed points, and Kogut and Wilson speculated in 1974 on the possibility of limit cycles as well as ergodic and turbulent behaviour in RG flow. Since then, however, a number of monotonicity theorems have been proven that severely restrict the RG flow of unitary quantum field theories (QFTs). The first such theorem was Zamolodchikov's c-theorem [184], which in two dimensions establishes a function that interpolates between central charges at CFTs and decreases monotonically along RG flow. Analogous theorems were proven in four dimensions (a-theorem) [153, 150] and three dimensions (F-theorem) [161, 160, 162]. The monotonicity implied by these theorems excludes the possibility of limit cycles, except for a loophole pointed out in [185, 155]: multi-valued c functions. This loophole had in fact been previously realized in certain deformed Wess-Zumino-Witten models [186, 187, 188], although these models required coupling constants to pass between infinity and minus infinity in order to realize cyclic RG flow. There are also examples of cyclics RG flow in quantum mechanics [189, 142, 147, 144, 190, 191].

Recently, ref. [5] put forward a QFT of interacting symmetric traceless matrices transforming under the action of the $O(N)$ group, while allowing N to assume non-integer values. $O(N)$ models for non-integer N, an idea widely used in polymer physics [192], had been previously given a formal definition in [156], which demonstrated the non-unitarity of these models. Hence, the c, a, F-theorems are no longer valid and do not constrain the RG flow, and consequently ref. [5] was able to show that the model studied therein possesses a closed limit cycle for N slightly above 4.475. The main tool used to

make this discovery was Hopf's theorem [158], which guarantees the existence of a limit cycle in the vicinity of the codimension-one bifurcation known as the Andronov-Hopf bifurcation.

Turning to dynamical systems parameterized by two real numbers, codimension-two bifurcations can be used to prove the occurrence of yet other kinds of flow. Specifically, R.Bogdanov [193] and F.Takens [194] have established powerful theorems by which, from properties of autonomous differential equations known only to second order in the dynamical variables, one can deduce the existence of homoclinic orbits, ie. flow curves that connect a fixed point to itself. In addition to mild genericity conditions, the conditions that must be satisfied in order for the theorems to apply can be checked merely by studying the stability of fixed points, despite the fact that homoclinic orbits signal global bifurcations [180] since they arise when a limit cycles collides with a saddle point.

An interesting fact about homoclinic orbits is that they can be used to diagnose chaos. In applications of the theory of dynamical systems to physics, chaotic behavior [195] occurs in many instances, such as in turbulence [196, 197], meteorology [198] and even in scattering amplitudes in string theory [199]. Usually, chaotic behaviour is proven via numerical investigations of concrete systems. One of the few analytical tools that can hint at the emergence of chaos is a theorem due to Shilnikov [200] that, for systems possessing homoclinic orbits, stipulates conditions by which to show they are chaotic. Therefore, one important step towards uncovering chaotic RG flow is to establish the existence of homoclinic RG flow.

Brief previous mention of homoclinic RG flow can be found in [201, 202], which study non-linear sigma models and QCD_4 in the Veneziano limit. These references, however, mention the phenomenon solely for the purpose of pointing out its impossibility in those contexts.

In this short letter, we study a QFT with global $O(N) \times O(M)$ symmetry. Examining the RG flow of the theory as a function of M and N, we determine the regime where the flow is non-monotonic. In this regime, we are able to establish the locations of a number of Bogdanov-Takens bifurcations, by which we are able to conclude that the theory exhibits

homoclinic RG flow. In other words, the model contains fixed point with the peculiar property that a deformation by a *relevant* operator induces a flow that leads back to the original point: an RG flow where the IR and UV theories are one and the same. Homoclinic RG flow can be thought of as interpolating between the familiar type of RG flow (where a system flows from one fixed point to another) and the more exotic RG limit cycles (like limit cycles, homoclinic orbits are closed). In unitary QFTs, homoclinic RG flows are still forbidden by c, a, F-theorems, but a fixed point situated in a homoclinic orbit could possibly be described by a standard CFT, in contrast to fixed points that give rise to limit cycles by undergoing a Hopf bifurcation, and which require operators with complex scaling dimensions.

4.6 The model

The approach we consider in this short letter could be used in any two-parameteric family of theories. But we present just the very first example, where such phenomenon emerges. Thus, we consider an $\mathcal{N} = 1$ supersymmetric model of interacting scalar superfields Φ^i_{ab} that are invariant under the action of an $O(N) \times O(M)$ group in $d = 3 - \epsilon$ dimensions. The superfields are traceless-symmetric matrices with respect to the action of an $O(N)$ group and vectors under the action of an $O(M)$ group. There are four singlet marginal operators

$$\begin{aligned} O_1 &= \mathrm{tr}\left[\Phi^i\Phi^i\Phi^j\Phi^j\right], \quad O_2 = \mathrm{tr}\left[\Phi^i\Phi^j\Phi^i\Phi^j\right], \\ O_3 &= \mathrm{tr}\left[\Phi^i\Phi^i\right]^2, \quad O_4 = \mathrm{tr}\left[\Phi^i\Phi^j\right]\mathrm{tr}\left[\Phi^i\Phi^j\right], \end{aligned} \tag{4.58}$$

and so the full action is

$$S = \int d^dx d^2\theta \left[\mathrm{tr}\,\Phi^i D^2_\alpha \Phi^i + \sum_i g_i O_i\right]. \tag{4.59}$$

The RG flow of this model is gradient, meaning that there exists a function F of the couplings and a four-by-four matrix G_{ij} such that the beta functions of the theory satisfy

the equation

$$\beta_i = \mu \frac{dg_i}{d\mu} = G_{ij} \frac{\partial F}{\partial g_j} \,. \tag{4.60}$$

If G_{ij} is positive or negative definite, this equation implies that F changes monotonically with the RG flow, so that cyclic and homoclinic flow lines are impossible. By explicit computation to leading order in perturbation theory, we find that the metric has determinant

$$\begin{aligned} \det G = \frac{1}{4}(M-1)^2(M+2)^2 \times \\ \times (N-3)(N-2)^2(N+1)^2(N+4)^2(N+6) \,. \end{aligned} \tag{4.61}$$

We list the beta functions and the components of the metric in appendix C. The zeroes in $\det G$ occur because of linear relations among the four operator of the theory at special values of M and N, and their presence indicates that eigenvalues change sign as N and M are varied. Indeed one can check that the metric is sign-indefinite if $M \in (-2, 1)$ or $N \in (-6, 3)$, so that unusual RG flows are possible in this regime, and operators may develop complex scaling dimensions at real fixed points, which, in the terminology of [5], are then termed "spooky" (see fig. (4.8)). At integer values of N and M, such operators are identically zero owing to the linear relations between the operators. The situation is closely analogous to the occurrence of evanescent operators at non-integer spacetime dimensions [203, 204, 205, 206, 207, 157].

In the following, we will allow M and N to assume general real values. This means we are dealing with a two-parameter autonomous system of ordinary differential equations. Such systems can exhibit a rich variety of flows as compared with one-parameter systems. The possible codimension-two bifurcations can be classed into five types [182, 180] – Bautin, Bogdanov-Takens, cusp, double-Hopf, and zero-Hopf – which signal different kinds of flow not present in generic one-parameter systems. As we shall now see, some of these possibilities are realized by the QFT (4.59).

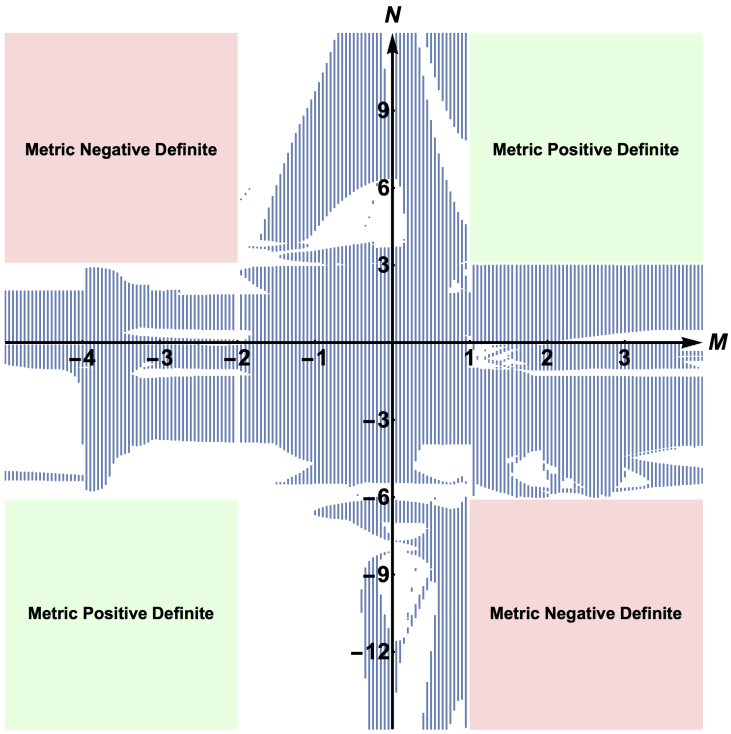

Figure 4.8: The values of M and N for which spooky fixed points appear. The appearance of vertical lines is due to finite numeric resolution.

4.7 Bogdanov-Takens Bifurcation

A Bogdanov-Takens bifurcation occurs generically when, at a fixed point, two eigenvalues of the stability matrix $\left(\frac{\partial\beta_i}{\partial g_j}\right)$ tend to zero as two bifurcation parameters M and N are appropriately tuned. The following equations must then be satisfied:

$$\beta_i(g_i, N, M) = 0\,, \quad \det\left(\frac{\partial\beta_i}{\partial g_j}\right)(g_i, N, M) = 0\,, \tag{4.62}$$

$$\mathrm{tr}\left[\bigwedge^3\left(\frac{\partial\beta_i}{\partial g_j}\right)\right] \equiv \det\left(\frac{\partial\beta_i}{\partial g_j}\right)\mathrm{tr}\left[\left(\frac{\partial\beta_i}{\partial g_j}\right)^{-1}\right] = 0\,. \tag{4.63}$$

Written in the form (4.62), we see that the conditions for a BT bifurcation are polynomial equations in g_i, M, and N, and so by Bézout's theorem there exist at most a finite number of points that satisfy these conditions. We refer to such points as Bogdanov-Takens (BT) points. For the QFT we are studying perturbatively, it can be verified that the beta functions exhibit several such points. Their existence can be checked to high numerical accuracy with the use of standard programs, e.g. PyDSTool [208]. Higher-loop

contributions will provide corrections to the precise locations of these points, but as long as we take ϵ to be sufficiently small, higher-order corrections will not alter the number or qualitative behaviour of BT points.

While two eigenvalues tend to zero as we approach a BT point, right at the BT point itself we do not have a pair of eigenvectors with zero eigenvalues for the reason that in this same limit, the two respective eigenvectors become linearly dependent. Rather, the stability matrix at a BT point has a Jordan block of size two with zero eigenvalue (see (4.67) in appendix 4.11). This means that the theory at the BT point possesses two operators $\mathcal{O}_{1,2}$ such that the generator D of dilatations acts in the following way

$$D\mathcal{O}_1 = d\mathcal{O}_1\,, \quad D\mathcal{O}_2 = d\mathcal{O}_2 + \mathcal{O}_1\,. \tag{4.64}$$

The possibility of indecomposable representations of the conformal group was extensively studied in [209, 210]. The upshot is that the BT theory constitutes a logarithmic CFT containing *generalized* marginal operators $\mathcal{O}_{1,2}$. In consequence, BT theories are non-unitary and we have

$$\langle \mathcal{O}_2(0)\mathcal{O}_2(x)\rangle = \frac{k_{\mathcal{O}}\log|x|}{|x|^{2d}}\,, \quad \langle \mathcal{O}_1(0)\mathcal{O}_2(x)\rangle = \frac{k_{\mathcal{O}}}{|x|^{2d}}\,.$$

The conditions (4.62) are not entirely sufficient to guarantee a BT bifurcation. One must also require smoothness, and a set of inequalities that are generically true. Violations of the inequalities typically require fine-tuning of additional parameters and signal bifurcations of codimension higher than two. In appendix 4.11 we give the precise statement of the Bogdanov-Takens bifurcation theorem, and we explicitly check that it applies to an example of a BT point in the QFT we are studying, situated at $M \approx 0.2945$ and $N \approx 4.036$. What this means is that we can transform the beta functions near the BT

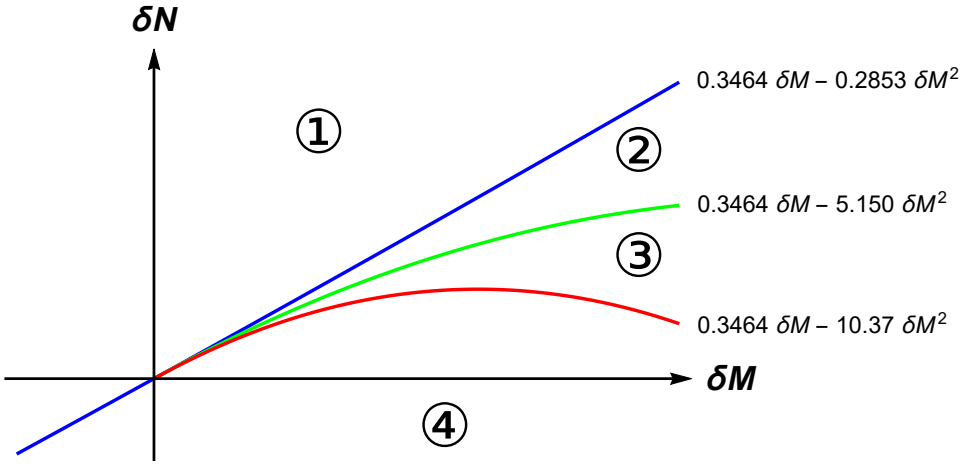

Figure 4.9: Bifurcation diagram around the Bogdanov-Takens bifurcation at $(M, N) = (M^*, N^*) = (0.2945, 4.036)$. $\delta M = M - M^*$, $\delta N = N - N^*$. The blue curve represents a saddle node bifurcation, the green curve represents a Hopf bifurcation, and the red curve represents a saddle homoclinic bifurcation. At the origin, these three codimension-one bifurcations coalesce.

point into a particularly simple form, known as Bogdanov normal form:

$$\begin{cases} \dot{\eta}_1 = \eta_2 \,, \\ \dot{\eta}_2 = \delta_1 + \delta_2 \eta_1 + \eta_1^2 + s\eta_1\eta_2 + \mathcal{O}\left(|\eta|^3\right) \,, \\ \dot{\eta}_i = \lambda_i \eta_i \quad \text{for } i > 2 \,, \end{cases} \tag{4.65}$$

where $s = -1$, and $\delta_{1,2}$ are functions of N and M that vanish right at the BT point.

By bringing the system into normal form, we can use the equations (4.65) to determine the behaviour of the system for small enough δ_1 and δ_2. In particular, we can constrain ourselves to studying the surface where only η_1 and η_2 are non-zero, noting that the dynamics in the transverse directions η_3 and η_4 are quite simple. Depending on the values of δ_1 and δ_2, the flow of $\eta_{1,2}$ falls into different topological types. The classification can be found in Kuznetsov's textbook [211] and amounts to the following. In the vicinity of the BT point at $\delta_1 = \delta_2 = 0$, there are four regimes with qualitatively different flows:

– Regime ①: The flow has no fixed point.

In the other three regimes, the flow has two fixed-points, which we will label left and right. The right point is always a saddle point.

– Region ②: The left point is unstable, and all flowlines starting near it terminate at

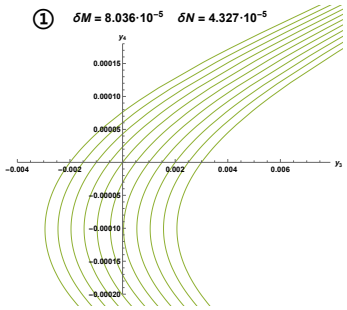

RG flow in region ①. In this regime, there are no fixed points near the origin, and all flow curves swerve downwards in the IR.

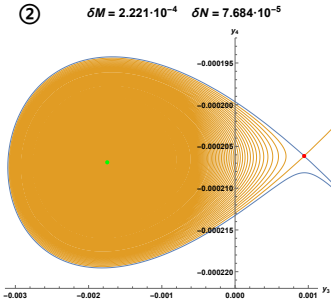

RG flow in region ②. The fixed point marked in red is a saddle point. The blue curves flow outwards from this point in the IR, while the orange curves flow inward. The fixed point marked in green is IR unstable.

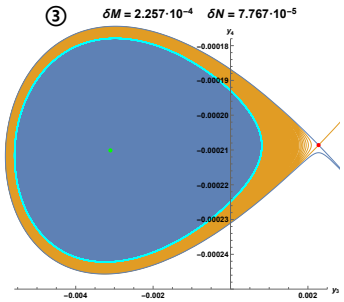

RG flow in region ③. In passing from region ② to ③, the fixed point marked in green has undergone a Hopf bifurcation and is now IR stable. An IR-repulsive limit cycle, marked in cyan, separates the two fixed points.

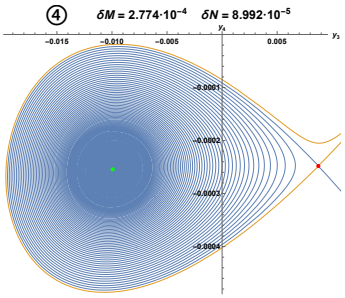

RG flow in region ④. In passing from region ③ to ④ the limit cycle collided with the red fixed point in a homoclinic bifurcation.

Figure 4.10: The topologically distinct types of RG flow in the vicinity of the Bogdanov-Takens bifurcation at $M = M^* = 0.2945$ and $N = N^* = 4.036$. The variables y_3 and y_4 are linear combinations of the four coupling constants g^i, with precise definitions given in appendix (4.11), and $\delta M = M - M^*$, $\delta N = N - N^*$.

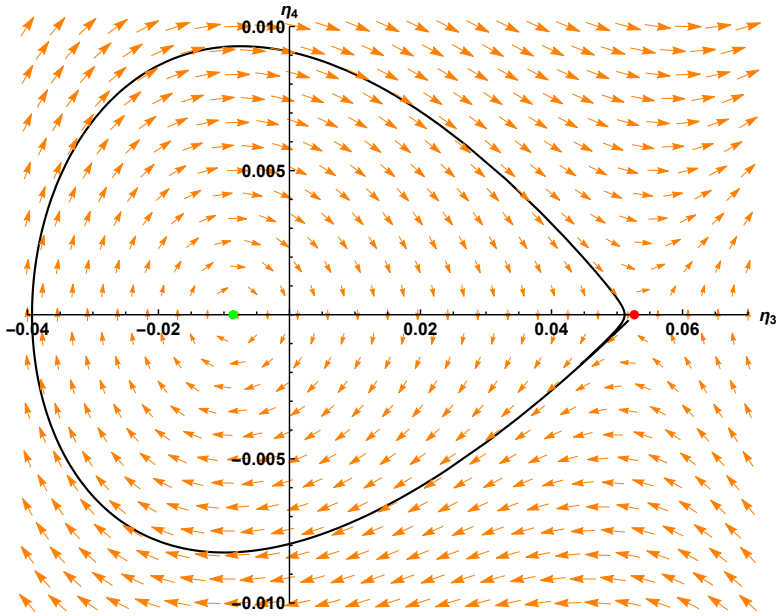

Figure 4.11: Flow diagram for a dynamical system containing a homoclinic orbit (marked in **black**), ie. a flowline that starts and ends at the same point. The system is described by equations (4.76) with parameters $\delta_1 = -0.000453178$ and $\delta_2 = -0.0440214$. The red and green dots indicate fixed points. The green dot is a "spooky" fixed point. The theory at the red dot is a homoclinic CFT.

the right fixed point.

– Region ③: The left point is now stable, and a repulsive limit cycle separates the two fixed points.

– Region ④: The left point is still stable, but the limit cycle has disappeared. Some flowlines starting near the right fixed point terminate at the left fixed point.

In the case of the BT point at $(M, N) \approx (0.2945, 4.036)$, the locations of these four adjoining regimes, as computed in appendix (4.65), is shown in figure 4.9. And the RG flow in each regimes is depicted in figure 4.10.

The four regimes are separated by different codimension-one bifurcations. Region ① is demarcated from regions ② and ④ by a saddle-node bifurcation happening at $\delta_1 = \frac{1}{4}\delta_2^2$. Regions ② and ③ are separated by an Andronov-Hopf bifurcation along the the half-curve $\delta_1 = 0$, $\delta_2 < 0$. And regions ③ and ④ are separated by a saddle homoclinic bifurcation along $\delta_1 = -\frac{6}{25}\delta_2^2 + \ldots$, $\delta_2 < 0$.

A saddle-node bifurcation corresponds to the collision and disappearance of two equi-

libria in dynamical systems. The phenomenon has been observed in a number of cases of RG flow, it happens for instance in in the critical $O(N)$ model [212], in prismatic models [3], and in QCD_4 [202, 213, 93, 214].

An Andronov-Hopf bifurcation represents a change of stability at a fixed point that has complex eigenvalues. The flow near the fixed point changes between spiraling inwards and spiraling outwards and gives birth to a limit cycle. In the context of RG, this bifurcation was recently studied in [5].

The most interesting and new phenomenon associated to the model of the present paper happens along the homoclinic bifurcation line. Here the flow exhibits what is known as a homoclinic orbit.

4.8 Homoclinic RG flow

A homoclinic orbit is a flowline that connects a stable and an unstable direction of a saddle point. Figure (4.11) depicts the kind of homoclinic orbit generated by a BT bifurcation, with the saddle point marked by a red dot. The homoclinic orbit is seen to envelop another fixed point marked in green. In a QFT context, the green point is "spooky": the couplings are real, but the eigenvalues of the stability matrix $\left(\frac{\partial \beta_i}{\partial g_j}\right)$ have non-zero imaginary parts. In contrast to such spooky points, and to complex CFTs [93, 177], the red saddle point is associated to real couplings and real eigenvalues of the stability matrix. These eigenvalues are small and have opposite signs: $\lambda_1, -\lambda_2 \langle 1$. The positive eigenvalue corresponds to a slightly relevant operator $\mathcal{O}_1$ with dimension $\Delta_1 = d + \lambda_1 > d$, and the negative eigenvalue to a slightly irrelevant operator $\mathcal{O}_2$ with dimension $\Delta_2 = d + \lambda_2 < d$. In this sense, the red saddle point corresponds to a real CFT.

Standard RG lore states that if we perturb a system in the direction of a relevant operator, then we expect for the system to either lose conformality altogether or to flow to a different CFT. In the terminology of dynamical systems, standard RG trajectories are heteroclinic orbits. The classical example is the Wilson-Fischer fixed point: by carefully perturbing a Gaussian theory in $4 - \epsilon$ dimension we flow to a weakly coupled interacting

CFT, which in three dimensions interpolates to the Ising model. Homoclinic bifurcations provide exotic counterexamples to this general picture: if we perturb the system in the direction of a relevant operator, we come back to the original fixed point, which tentatively we can term a *homoclinic CFT*. Such RG behaviour obviously violates the F-theorem so that homoclinic fixed points must be non-unitary, as is generally the case for CFTs with symmetry groups of non-integer rank [156].

If we tune the bifurcation parameters so as to approach the BT point along the saddle homoclinic bifurcation (the red curve in figure 4.9), then the homoclinic orbit shrinks to zero and vanishes. In this limit, the red homoclinic CFT and the green spooky fixed point merge and become a logarithmic CFT.

4.9 Zero-Hopf Bifurcations: The Road to Chaos

The Bogdanov-Takens bifurcation is not the only codimension-two bifurcation that can be observed to take place in the model (4.59). The theory also possesses two points in the space of g_i, M, and N where the stability matrix has a pair of purely imaginary eigenvalues and one zero eigenvalue. Such fixed points indicate what is known as a Zero-Hopf (ZH) or a Fold-Hopf bifurcation. This type of bifurcation was classified in [215] and can be divided into six sub-types. In the notation of [180], the model has a type I ZH bifurcation at $(M, N) \approx (0.8447, -1.807)$ and a type IIa ZH bifurcation at $(M, N) \approx (-3.816, 1.188)$. At a type I bifurcation point, a saddle-node bifurcation is incident to a pitchfork bifurcation, and there are no nearby cyclic orbits. At a type IIa point, a saddle-node bifurcation is again incident to a pitchfork bifurcation, but additionally a Hopf bifurcation is also incident to the point, except that the stability coefficient of the associated limit cycle (what was referred to as the Hopf constant in [5]) exactly vanishes in a quadratic approximation, so that cubic fluctuations or higher decide the fate of the cyclic flow near a type IIa point.

Generally, ZH bifurcation points are of particular interest because it is known that in their vicinity what is known as a Shilnikov homoclinic orbit may develop and render the system chaotic [211, 200]. Recently it was proven in [216] that the presence of

ZH bifurcations of type III guarantees the existence of a Shilnikov orbit and a nearby infinite set of saddle periodic orbits. This nontrivial invariant set can be embedded in an attracting domain, thus implying Shilnikov chaos.

The ZH points of the model in the present paper are not of type III, and we cannot claim that the system is chaotic. It may be worthwhile to investigate if there exist other models that meet the simple criteria for the assured appearance of chaos.

4.10 Future Outlook

The approach suggested and adopted in [141, 202, 5] of studying the beta functions and renormalization of QFTs from the general perspective of dynamical systems provides a method of understanding the full range of possible RG flows. A powerful tool to this end is offered by Bogdanov's and Taken's bifurcation theorem [158], which lists a simple set of conditions that guarantee the existence of a homoclinc RG orbit, and which can be checked already at first order in perturbation theory.

In this short letter we have presented a QFT that satisfies these conditions, namely a supersymmetric model with global symmetry group $O(N) \times O(M)$, where N and M play the role of the bifurcation parameters of the system. We determined a number of parameter values where a BT bifurcation takes place and investigated the nearby RG flow to uncover the presence of homoclinic orbits, where the perturbation of a fixed point by a relevant operator induces an RG flow that returns to its starting point along an irrelevant direction.

There are several bifurcation theorems that give simple criteria for other novel kinds of RG flows [180, 211, 182]. Some of these theorems allow for the determination of the onset of chaotic flow based on straightforward computations around fixed points [216]. It would be interesting to find out if QFTs give birth to chaos when N becomes fractional.

4.11 Transformation to Normal Form

At $M = M^* \approx 0.2945$ and $N = N^* \approx 4.036$, there exists an RG fixed point g^* such that stability matrix

$$M_i^j = \left.\frac{\partial \beta_i}{\partial g_j}\right|_{g^*} \tag{4.66}$$

has a zero eigenvalue of multiplicity two in addition to two non-zero eigenvalues: $\lambda_1 = 2$ and $\lambda_2 \approx -2.357$. This implies the existence of a matrix $V = \left(\vec{v}_1, \vec{v}_2, \vec{v}_3, \vec{v}_4\right)^\intercal$ such that

$$V^{-1}MV = \begin{pmatrix} \lambda_1 & 0 & 0 & 0 \\ 0 & \lambda_2 & 0 & 0 \\ 0 & 0 & 0 & \lambda_3 \\ 0 & 0 & 0 & 0 \end{pmatrix} \tag{4.67}$$

where $\vec{v}_i$ are (generalized) unit eigenvectors, and $\lambda_3 \approx 7.555$ is a generalized eigenvalue. That is,

$$M\vec{v}_{1,2} = \lambda_{1,2}\vec{v}_{1,2}, \quad M\vec{v}_3 = 0, \quad M\vec{v}_4 = \lambda_3\vec{v}_3\,.$$

By a change of variables from $\vec{g}$ to $\vec{h} = V^{-1}(\vec{g} - \vec{g}^*)$, we obtain differential equations where h_1, and h_2 do not mix linearly with h_3 and h_4:

$$\beta_{h_{1,2}} = \lambda_{1,2}h_{1,2} + \mathcal{O}(h^2)\,. \tag{4.68}$$

Consider now the case when $M = M^* + \delta M$ and $N = N^* + \delta M$, where δM and δN are each suppressed by a small parameter $\alpha\langle 1$. That is, $\delta M, \delta N \sim \alpha$. If we adopt the h variables, h_1 and h_2 will now mix linearly with each other and with h_3 and h_4, and their beta functions will contain constant terms. We can write

$$\frac{dh_1}{dt} = B_{0,1} + A_{1,1}h_1 + B_{1,2}h_2 + B_{1,3}h_3 + B_{1,4}h_4 + \mathcal{O}(h^2)$$

$$\frac{dh_2}{dt} = B_{0,0} + B_{2,1}h_1 + A_{2,2}h_2 + B_{2,3}h_3 + B_{2,4}h_4 + \mathcal{O}(h^2)\,,$$

for some coefficients $A_{i,j}$ and $B_{i,j}$, where the coefficients $B_{i,j}$ are all suppressed in α. Introducing new variables

$$y_1 = h_1 + C_{1,0} + C_{1,3}h_3 + C_{1,4}h_4\,, \tag{4.69}$$

$$y_2 = h_1 + C_{2,0} + C_{2,3}h_3 + C_{2,4}h_4\,, \tag{4.70}$$

we can choose the six coefficients $C_{i,j}$ such that $\dot{y}_{1,2}$ do not contain constant terms nor mix linearly with h_3 and h_4. This means that, studying only the RG flow near the origin so that cubic terms and higher can be disregarded, the surface $y_1 = y_2 = 0$ is an invariant manifold. On this surface, we can define variables $y_3 = h_3$ and $y_4 = \lambda_3 h_4$, whose RG flow to quadratic order in the dynamic variables is governed by the differential equations

$$\frac{dy_3}{dt} = a_{00} + a_{10}y_3 + a_{01}y_4 + \frac{1}{2}a_{20}y_3^2 + a_{11}y_3y_4 + \frac{1}{2}a_{02}y_4^2\,, \tag{4.71}$$

$$\frac{dy_4}{dt} = b_{00} + b_{10}y_3 + b_{01}y_4 + \frac{1}{2}b_{20}y_3^2 + b_{11}y_3y_4 + \frac{1}{2}b_{02}y_4^2\,. \tag{4.72}$$

For the specific BT point we are considering, omitting higher order terms in α, the values of the various coefficients are given by

$$\begin{gathered}
a_{00} = 12.75\,\delta N + 2.618\,\delta M, a_{10} = 46.93\,\delta N - 8.164\,\delta M \\
a_{01} = 1, \quad a_{20} = 0.6040 \\
a_{11} = -2.268, \quad a_{02} = -0.9708 \\
b_{00} = 19.49\,\delta N - 6.753\,\delta M - 638.9\,\delta N^2 \\
+99.89\,\delta M^2 - 71.61\,\delta N\,\delta M \\
b_{10} = -51.76\,\delta N + 17.38\,\delta M \\
b_{01} = -18.05\,\delta N - 0.4165\,\delta M \\
b_{20} = 2.775, \quad b_{11} = -0.7935, \quad b_{02} = -1.868\,.
\end{gathered} \tag{4.73}$$

We now restrict attention to the case when δN and δM are tuned such that $b_{00} \sim \alpha^2$, for the reason that this will turn out to be the regime where the existence of a homoclinic orbit can be reliably established. Working merely to leading order in α and to quadratic order in the dynamical variables, we perform a reparametrization from t to τ via

$$d\tau = -\frac{1}{2}\frac{b_{20}}{a_{20}+b_{11}}\Big(1-\frac{2a_{11}+b_{02}}{2}\,\frac{dy_3}{dt}\Big)^{-1}dt \tag{4.74}$$

and change to variables η_1 and η_2 given by

$$\begin{aligned}\eta_1 &= 2\frac{a_{20}+b_{11}}{b_{20}}\Big((a_{20}+b_{11})y_3+a_{01}+b_{01}-a_{00}a_{11}-a_{00}b_{02}\Big)\\ \eta_2 &= -4\frac{(a_{20}+b_{11})^3}{b_{20}^2}\times\\ &\times\Big(1-\frac{2a_{11}+b_{02}}{2}\Big(y_3+\frac{a_{10}b_{01}-a_{00}a_{11}-a_{00}b_{02}}{a_{20}+b_{11}}\Big)\Big)\frac{dy_3}{dt}\end{aligned} \tag{4.75}$$

where for $\frac{dy_3}{dt}$ one should substitute the RHS of (4.71). In these new variables, the differential equations of the dynamical system are brought into the normal form introduced by Bogdanov:

$$\begin{cases}\dot\eta_3 = \eta_4\,,\\ \dot\eta_4 = \delta_1+\delta_2\eta_3+\eta_3^2+\eta_3\eta_4\,,\end{cases} \tag{4.76}$$

where we have omitted terms of cubic order and higher in η, and the parameters δ_1 and δ_2 are given by

$$\begin{aligned}\delta_1 &= \frac{8(a_{20}+b_{11})^4}{b_{20}^3}\Bigg(b_{00}-a_{00}b_{01}+\frac{a_{00}^2b_{02}}{2}+\\ &+\frac{\big(a_{10}+b_{01}-a_{00}(a_{11}+b_{02})\big)(a_{00}b_{11}-b_{10})}{a_{20}+b_{11}}+\frac{\big(a_{10}+b_{01}-a_{00}(a_{11}+b_{02})\big)^2b_{20}}{2(a_{20}+b_{11})^2}\Bigg)\,,\\ \delta_2 &= \frac{4(a_{20}+b_{11})}{b_{20}^2}\Big((a_{20}+b_{11})(b_{10}-a_{00}b_{11})-\big(a_{10}+b_{01}-a_{00}(a_{11}+b_{02})\big)b_{20}\Big)\,.\end{aligned}$$

The transformations by which we arrived at the equations (4.76) can be applied more generally to dynamical systems where the stability matrix contains a Jordan block with

zero eigenvalues, as long as the following conditions are met:

$$\lambda_3 \neq 0\,, \quad b_{20} \neq 0\,, \quad a_{20} + b_{11} \neq 0\,. \tag{4.77}$$

This fact is known as a the Bogdanov-Takens bifurcation theorem [193, 194]. The precise formulation of the theorem is this:

Suppose we have a system of differential equations

$$\dot{\vec{x}} = \vec{f}(\vec{x}, \vec{\alpha}), \quad \vec{x} \in \mathbb{R}^n,\, \vec{\alpha} \in \mathbb{R}^2, \tag{4.78}$$

where $\vec{f}$ is smooth, and suppose further that $\vec{f}(0,0) = 0$ and that the stabililty matrix $\left(\frac{\partial \vec{f}}{\partial \vec{x}}\right)\Big|_{\vec{x}=\vec{\alpha}=0}$ has a Jordan cell of size two with zero eigenvalues: $\lambda_{1,2} = 0$ and other eigenvalues $\lambda_3, \ldots, \lambda_n$ with non-zero real parts. Assume that the map $(\vec{x}, \vec{\alpha}) \longmapsto \left(\vec{f}(\vec{x}, \vec{\alpha}), \mathrm{tr}\left(\frac{\partial f_i}{\partial x_j}\right), \det\left(\frac{\partial f_i}{\partial x_j}\right)\right)$ is smooth and that the non-degeneracy conditions (4.77) are satisfied. Then there exist a smooth invertible variable transformation, a direction-preserving time reparametrization, and a smooth invertible change of parameters that together reduce the system to the normal form (4.65), where $\delta_{1,2}$ are functions of $\vec{\alpha}$ and $s = \pm 1$.

Furthermore, there is a theorem stating that the suppressed terms of cubic order and higher in (4.65) do not change the local topology of the flow. But the topology of the flow of the normal form system, omitting cubic and higher terms, is well understood. In particular, it is known that depending on the values of δ_1 and δ_2, the flow near the origin can be divided into four distinct regions. As described in section 4.7, these four regions are separated by codimension-one bifurcations located on the curve $\delta_1 = \frac{1}{4}\delta_2^2$ and, for $\delta_2 < 0$, on the curves $\delta_1 = 0$ and $\delta_1 = -\frac{6}{25}\delta_2^2$. For the specific BT point at $M \approx 0.2945$ and $N \approx 4.036$, we can translate these equations into relations between δM and δN, whereby we arrive at the picture of figure 4.9.

4.12 Bifurcation Conditions

When working to two-loop level, the beta functions have the property that $\beta_i + \epsilon g_i$ is a homogeneous function of degree three. Hence, by Euler's theorem,

$$g_j \frac{\partial(\beta_i + \epsilon g_i)}{\partial g_j} = 3(\beta_i + \epsilon g_i)\,. \tag{4.79}$$

By evaluating this equation on an RG fixed point $\vec{g}^*$, one finds that

$$M^i_j\big|_{\vec{g}=\vec{g}^*}\, g^*_i = 2\epsilon g^*_j\,, \tag{4.80}$$

where $M^i_j = \frac{\partial \beta_j}{\partial g_i}$ is the stability matrix defined in (4.66). Hence, for any non-trivial fixed point, the stability matrix has an eigenvalue $\lambda_1 = 2\epsilon$ equal to two. This fact allows for simplifications in the conditions for bifurcations to occur.

Consider the determinant $\det(M - \lambda)$. Since it is a fourth order polynomial in λ, we can write

$$\det(M - \lambda) = \lambda^4 + A\lambda^3 + B\lambda^2 + C\lambda + D\,, \tag{4.81}$$

where A, B, C, and D are M- and N-dependent polynomials in the coupling constants. Specifically

$$A = -\mathrm{Tr}M\,, \quad B = M_{ij,ij}\,, \quad C = -M_{i,i}\,, \quad D = \det M\,,$$

where $M_{i,j}$ and $M_{ij,kl}$ are the first and second minors of the stability matrix. But when evaluated on a fixed point, we also have the following factorization in terms of eigenvalues

$$\det(M_* - \lambda) = (\lambda - 2)(\lambda - \lambda_2)(\lambda - \lambda_3)(\lambda - \lambda_4)\,.$$

By expanding out the factors on the RHS, we can relate A, B, and C to the eigenvalues.

A **saddle-node bifurcation** occurs when at a fixed point we have a zero-eigenvalue:

$\lambda_2 = 0$. In this case, one finds that

$$A = -2 - \lambda_3 - \lambda_4 \,, \quad B = 2(\lambda_3 + \lambda_4) + \lambda_3\lambda_4 \,,$$
$$C = -2\lambda_3\lambda_4 \,, \tag{4.82}$$

from which one can derive the equation

$$2B + C = -4(A + 2) \,. \tag{4.83}$$

Of course we also have the equation $D = 0$, but the condition (4.83) is easier to check numerically on account of the many terms in the determinant.

At a **Hopf bifurcation**, we have a conjugate pair of imaginary eigenvalues:

$$\lambda_3 = i\chi \,, \quad \lambda_4 = -i\chi \,, \tag{4.84}$$

where χ is a real number. Consequently we find that

$$A = -2 - \lambda_2 \,, \quad B - 2\lambda_2 + \chi^2 \,, \quad C = -(2 + \lambda_2)\chi^2 \,.$$

From these equations, we derive the condition

$$C = A(B + 4 + 2A) \,. \tag{4.85}$$

At a **Bogdanov-Takens bifurcation**, there are two zero eigenvalues: $\lambda_3 = \lambda_4 = 0$. From this, one obtains the conditions

$$B = -2(A + 2) \,, \qquad C = 0 \,. \tag{4.86}$$

We have a **Zero-Hopf bifurcation** when

$$\lambda_2 = 0 \,, \quad \lambda_3 = i\chi \,, \quad \lambda_4 = -i\chi \,, \tag{4.87}$$

with χ a real number. In this case

$$A = -2\,, \qquad C = -2B\,. \tag{4.88}$$

Appendices

A The beta functions up to four loops of $O(N)$ matrix models

In the main text we presented the large N beta functions for the matrix models we have studied. In this appendix we list the full beta functions for any N up to four-loops. Letting μ denote the renormalization scale, we take the beta function associated to a coupling g_i to be given by

$$\beta_{g_i} = \mu \frac{dg_i}{d\mu} = -2\epsilon g_i + \frac{1}{6!(8\pi)^2}\widetilde{\beta}^{(2)}_{g_i} + \frac{1}{(6!)^2(8\pi)^4}\widetilde{\beta}^{(4)}_{g_i} + \mathcal{O}(g^6)\,, \tag{A.1}$$

where we have separated out the two-loop contribution $\beta^{(2)}_{g_i}$ and the four-loop contribution $\beta^{(4)}_{g_i}$. The beta functions have been computed by use of the formulas for sextic theories in $d = 3 - \epsilon$ dimension listed in section 4.1.

A.1 Beta functions for the $O(N)^2$ matrix model

$$\begin{aligned}
\widetilde{\beta}^{(2)}_{g_1} =&\ 24(100 + 24N + 3N^2)g_1^2 + 384(9 + 4N)g_1g_2 + 3840g_1g_3 + 64(32 + N^2)g_2^2,\\
\widetilde{\beta}^{(2)}_{g_2} =&\ 144(8 + 3N)g_1^2 + 96(38 + 4N + N^2)g_1g_2 + 2304(1 + N)g_1g_3\\
&+128(8 + 7N)g_2^2 + 384(18 + N^2)g_2g_3,\\
\widetilde{\beta}^{(2)}_{g_3} =&\ 168g_1^2 + 96(3 + 2N)g_1g_2 + 1152g_1g_3 + 32(21 + 2N + N^2)g_2^2\\
&+768(1 + 2N)g_2g_3 + 192(22 + 3N^2)g_3^2
\end{aligned} \tag{A.2}$$

$$\widetilde{\beta}^{(4)}_{g_1} = -288\Big(47952 + 4780\pi^2 + N^4(17 + \pi^2) + N^3(372 + 25\pi^2) + 8N(3102 + 277\pi^2) + N^2(5248 + 412\pi^2)\Big)g_1^3 - 576\Big(64992 + 6860\pi^2 + 6N^3(104 + 7\pi^2) + 8N(4728 + 415\pi^2) + N^2(5928 + 465\pi^2)\Big)g_1^2g_2$$

$$-1152\Big(48N(274+27\pi^2)+N^2(2824+225\pi^2)+4(7640+891\pi^2)\Big)g_1^2g_3$$
$$-384\Big(3N^4(10+\pi^2)+18N^3(12+\pi^2)+48N(884+83\pi^2)+112(867+94\pi^2)+N^2(10836$$
$$+773\pi^2)\Big)g_1g_2^2-13824\Big(3984+448\pi^2+2N^3(20+\pi^2)+N^2(92+7\pi^2)+8N(292+31\pi^2)\Big)g_1g_2g_3$$
$$-4608\Big(5936-8N^4+720\pi^2+N^2(372+45\pi^2)\Big)g_1g_3^2-\frac{512}{3}\Big(N^3(960+46\pi^2)+64(900+97\pi^2)$$
$$+N^2(1704+137\pi^2)+16N(2124+203\pi^2)\Big)g_2^3-9216\Big(4N^4+384(9+\pi^2)+N^2(248+21\pi^2)\Big)g_2^2g_3, \tag{A.3}$$

$$\widetilde{\beta}_{g_2}^{(4)}=-432\Big(20400+2260\pi^2+2N^3(90+7\pi^2)+12N(940+91\pi^2)+N^2(1740+151\pi^2)\Big)g_1^3$$
$$-288\Big(3N^4(10+\pi^2)+6N^3(56+5\pi^2)+16(6408+683\pi^2)+N^2(11184+995\pi^2)+N(46896+4516\pi^2)\Big)$$
$$-1728\Big(N^3(248+22\pi^2)+N^2(1380+109\pi^2)+8N(1510+127\pi^2)+4(4132+401\pi^2)\Big)g_1^2g_3$$
$$-384\Big(2N^3(534+49\pi^2)+N^2(5148+443\pi^2)+8(8922+923\pi^2)+N(48384+4444\pi^2)\Big)g_1g_2^2$$
$$-4608\Big(2N^4(6+\pi^2)+6N^3(8+\pi^2)+6N(948+77\pi^2)+N^2(2748+197\pi^2)+2(8112+841\pi^2)\Big)g_1g_2g_3$$
$$-27648(1+N)\Big(N^2(62+3\pi^2)+2(532+51\pi^2)\Big)g_1g_3^2$$
$$-128\Big(95152+10024\pi^2+36N^3(6+\pi^2)+2N^4(36+7\pi^2)+24N(1264+113\pi^2)+N^2(14804$$
$$+1179\pi^2)\Big)g_2^3-768\Big(2N^4\pi^2+N^5\pi^2+134N^2(12+\pi^2)+16N^3(102+7\pi^2)+8(4308+433\pi^2)$$
$$+8N(4584+437\pi^2)\Big)g_2^2g_3-13824\Big(4816+512\pi^2+N^4(18+\pi^2)+N^2(644+57\pi^2)\Big)g_2g_3^2 \tag{A.4}$$

$$\widetilde{\beta}_{g_3}^{(4)}=-432\Big(2760+380\pi^2+N^2(210+23\pi^2)+4N(270+31\pi^2)\Big)g_1^3$$
$$-576\Big(7308+776\pi^2+N^3(78+8\pi^2)+N^2(483+45\pi^2)+6N(766+83\pi^2)\Big)g_1^2g_2$$
$$-576\Big(-48N^3-8N^4+6N(836+81\pi^2)+6(1984+189\pi^2)+N^2(1676+207\pi^2)\Big)g_1^2g_3$$
$$-768\Big(8772+894\pi^2+N^4(6+\pi^2)+N^3(36+5\pi^2)+10N(336+31\pi^2)+N^2(1269+140\pi^2)\Big)g_1g_2^2$$
$$-2304\Big(6096+550\pi^2+2N^3(84+17\pi^2)+N^2(432+59\pi^2)+N(6312+554\pi^2)\Big)g_1g_2g_3$$
$$-1152\Big(18N^3\pi^2+15N^4\pi^2+96N(35+3\pi^2)+8N^2(443+36\pi^2)+8(1876+177\pi^2)\Big)g_1g_3^2$$

$$-384\Big(41328+4192\pi^2+2N^4(54+19\pi^2)+N^3(216+38\pi^2)+8N(1536+125\pi^2)$$
$$+3N^2(3932+323\pi^2)\Big)g_2^2g_3-\frac{128}{3}\Big(49104+4784\pi^2+4N^4\pi^2+N^5\pi^2+12N^2(487+42\pi^2)$$
$$+N^3(2136+281\pi^2)+12N(4552+425\pi^2)\Big)g_2^3-3456(1+2N)\Big(N^4\pi^2+112(32+3\pi^2)$$
$$+4N^2(88+7\pi^2)\Big)g_2g_3^2-1152\Big(N^6\pi^2+N^4(424+34\pi^2)+32(826+85\pi^2)+N^2(6864+620\pi^2)\Big)g_3^3 \tag{A.5}$$

A.2 Beta functions for the anti-symmetric matrix model

$$\widetilde{\beta}_{g_1}^{(2)}=6(112-3N+3N^2)g_1^2+384(-1+2N)g_1g_2+3840g_1g_3+32(64-N+N^2)g_2^2 \tag{A.6}$$

$$\widetilde{\beta}_{g_2}^{(2)}=54(-1+2N)g_1^2+24(68-N+N^2)g_1g_2+576(-1+2N)g_1g_3+224(-1+2N)g_2^2$$
$$+192(36-N+N^2)g_2g_3 \tag{A.7}$$

$$\widetilde{\beta}_{g_3}^{(2)}=42g_1^2+(-24+48N)g_1g_2+576g_1g_3+8(40-N+N^2)g_2^2+384(-1+2N)g_2g_3$$
$$+96(44-3N+3N^2)g_3^2 \tag{A.8}$$

$$\widetilde{\beta}_{g_1}^{(4)}=-9\Big(-4N^3(17+\pi^2)+2N^4(17+\pi^2)+32(3209+293\pi^2)-N(10928+861\pi^2)+$$
$$N^2(10962+863\pi^2)\Big)g_1^3-72(-1+2N)\Big(-3N(104+7\pi^2)+3N^2(104+7\pi^2)$$
$$+4(4896+413\pi^2)\Big)g_1^2g_2-288\Big(-N(2824+225\pi^2)+N^2(2824+225\pi^2)+4(7804+945\pi^2)\Big)g_1^2g_3$$
$$-48\Big(198048+21616\pi^2-6N^3(10+\pi^2)+3N^4(10+\pi^2)$$
$$+2N^2(10479+746\pi^2)-N(20928+1489\pi^2)\Big)g_1g_2^2-3456(-1+2N)\Big(-N(20+\pi^2)+N^2(20+\pi^2)$$
$$+8(292+31\pi^2)\Big)g_1g_2g_3-2304\Big(8N^3-4N^4-3N(124+15\pi^2)+N^2(368+45\pi^2)$$
$$+32(371+45\pi^2)\Big)g_1g_3^2$$
$$-\frac{128}{3}(-1+2N)\Big(33984+3248\pi^2-N(480+23\pi^2)+N^2(480+23\pi^2)\Big)g_2^3$$
$$-4608\Big(-4N^3+2N^4+768(9+\pi^2)-N(248+21\pi^2)+N^2(250+21\pi^2)\Big)g_2^2g_3 \tag{A.9}$$

$$\widetilde{\beta}^{(4)}_{g_2} = -27(-1+2N)\Big(5760+557\pi^2 - N(90+7\pi^2) + N^2(90+7\pi^2)\Big)g_1^3 - 18\Big(-6N^3(10+\pi^2)$$
$$+3N^4(10+\pi^2) + 34N^2(579+52\pi^2) - N(19656+1765\pi^2) + 4(49956+5437\pi^2)\Big)g_1^2 g_2$$
$$-216(-1+2N)\Big(9536+830\pi^2 - N(124+11\pi^2) + N^2(124+11\pi^2)\Big)g_1^2 g_3$$
$$-48(-1+2N)\Big(39744+3739\pi^2$$
$$-N(534+49\pi^2) + N^2(534+49\pi^2)\Big)g_1 g_2^2 - 288\Big(-8N^3(6+\pi^2) + 4N^4(6+\pi^2) + 3N^2(3608+259\pi^2)$$
$$-N(10800+773\pi^2) + 4(25284+2719\pi^2)\Big)g_1 g_2 g_3 - 3456(-1+2N)\Big(-N(62+3\pi^2) + N^2(62+3\pi^2)$$
$$+4(532+51\pi^2)\Big)g1g3^2 - 32\Big(-2N^3(36+7\pi^2) + N^4(36+7\pi^2) - 4N(3656+291\pi^2) +$$
$$+N^2(14660+1171\pi^2)$$
$$+4(38180+4109\pi^2)\Big)g_2^3 - 48(-1+2N)\Big(-2N^3\pi^2 + N^4\pi^2 - 32N(102+7\pi^2) + 3N^2(1088+75\pi^2)$$
$$+32(4584+437\pi^2)\Big)g_2^2 g_3 - 3456\Big(-2N^3(18+\pi^2) + N^4(18+\pi^2) + 64(301+32\pi^2) - 2N(644+57\pi^2)$$
$$+N^2(1306+115\pi^2)\Big)g_2 g_3^2 \qquad \text{(A.10)}$$

$$\widetilde{\beta}^{(4)}_{g_3} = -27\Big(2760+422\pi^2 - N(210+23\pi^2) + N^2(210+23\pi^2)\Big)g_1^3 - 18(-1+2N)\Big(-2N(39+4\pi^2)$$
$$+N^2(78+8\pi^2) + 75(96+11\pi^2)\Big)g_1^2 g_2 - 72\Big(16724+8N^3 - 4N^4 + 1647\pi^2 + 3N^2(592+69\pi^2)$$
$$-N(1780+207\pi^2)\Big)g_1^2 g_3 - 12\Big(-8N^3(6+\pi^2) + 4N^4(6+\pi^2) + 256(402+43\pi^2) + 3N^2(3184+351\pi^2)$$
$$-N(9528+1049\pi^2)\Big)g_1 g_2^2 - 288(-1+2N)\Big(5952+518\pi^2 - N(84+17\pi^2) + N^2(84+17\pi^2)\Big)g_1 g_2 g_3$$
$$-144\Big(-30N^3\pi^2 + 15N^4\pi^2 + 224(253+24\pi^2) - N(7088+567\pi^2) + N^2(7088+582\pi^2)\Big)g_1 g_3^2$$
$$-\frac{4}{3}(-1+2N)\Big(-2N^3\pi^2 + N^4\pi^2 - 24N(178+23\pi^2) + N^2(4272+553\pi^2) + 8(24672+2359\pi^2)\Big)g_2^3$$
$$-96\Big(75984+7828\pi^2 - 2N^3(54+19\pi^2) + N^4(54+19\pi^2) + 3N^2(3914+327\pi^2)$$
$$-2N(5844+481\pi^2)\Big)g_2^2 g_3$$
$$-432(-1+2N)\Big(-2N^3\pi^2 + N^4\pi^2 + 448(32+3\pi^2) - 8N(88+7\pi^2) + N^2(704+57\pi^2)\Big)g_2 g_3^2$$
$$-144\Big(-3N^5\pi^2 + N^6\pi^2 + N^4(848+71\pi^2) + 256(826+85\pi^2) - N^3(1696+137\pi^2) -$$

$$16N(1716+155\pi^2)+4N^2(7076+637\pi^2)\Big)g_3^3 \tag{A.11}$$

A.3 Beta functions for the symmetric traceless matrix model

$$\begin{aligned}
\widetilde{\beta}^{(2)}_{g_1} =\ & 6\frac{2400-1200N+250N^2+51N^3+3N^4}{N^2}g_1^2+384\frac{2N^2+10N-35}{N}g_1g_2+3840g_1g_3\\
&+864\frac{-20+5N+N^2}{N}g_1g_4+32(62+N+N^2)g_2^2+4608g_2g_4+2592g_4^2\\
\widetilde{\beta}^{(2)}_{g_2} =\ & 18\frac{-150+35N+6N^2}{N}g_1^2+24\frac{480-120N+66N^2+9N^3+N^4}{N^2}g_1g_2\\
&+576\frac{-10+5N+2N^2}{N}g_1g_3+216\frac{80-20N+N^2}{N^2}g_1g_4+32\frac{-132+39N+14N^2}{N}g_2^2\\
&+192(34+N+N^2)g_2g_3+288\frac{-40+3N+N^2}{N}g_2g_4+3456g_3g_4+324\frac{-24+2N+N^2}{N}g_4^2\\
\widetilde{\beta}^{(2)}_{g_3} =\ & 42g_1^2+576g_1g_3+24\frac{-30+7N+2N^2}{N}g_1g_2-\frac{1080}{N}g_1g_4+384\frac{-6+3N+2N^2}{N}g_2g_3\\
&-288\frac{-24+3N+N^2}{N^2}g_2g_4+96(38+3N+3N^2)g_3^2\\
&+8\frac{288-36N+30N^2+5N^3+N^4}{N^2}g_2^2-\frac{3456}{N}g_3g_4-324\frac{-16+2N+N^2}{N^2}g_4^2\\
\widetilde{\beta}^{(2)}_{g_4} =\ & 24\frac{-200-75N^2+15N^3+3N^4}{N^3}g_1^2+192\frac{10-5N+N^2}{N^2}g_1g_2\\
&+12\frac{160-120N+34N^2+15N^3+3N^4}{N^2}g_1g_4-32\frac{62+N+N^2}{N}g_2^2+384\frac{-15+3N+N^2}{N}g_2g_4\\
&+3840g_3g_4+6\frac{-704+60N+28N^2+3N^3+N^4}{N}g_4^2
\end{aligned} \tag{A.12}$$

$$\begin{aligned}
\widetilde{\beta}^{(4)}_{g_1} =\ & -\frac{9}{N^4}\Big(2N^8(17+\pi^2)+4N^7(389+26\pi^2)+38400(1252+135\pi^2)-19200N(2159+225\pi^2)\\
&-60N^4(7338+455\pi^2)-1200N^3(4896+587\pi^2)+N^6(38822+3167\pi^2)+800N^2(30564+3215\pi^2)\\
&+N^5(279004+28019\pi^2)\Big)g_1^3-\frac{216}{N^3}\Big(2N^6(104+7\pi^2)+4320N(522+55\pi^2)+10N^3(-1416+131\pi^2)\\
&+N^5(4264+331\pi^2)-960(3344+375\pi^2)+5N^4(7096+681\pi^2)-40N^2(16616+1977\pi^2)\Big)g_1^2g_2\\
&-\frac{288}{N^2}\Big(1920(388+45\pi^2)+30N^2(1184+171\pi^2)+N^4(2824+225\pi^2)-120N(3628+405\pi^2)\\
&+N^3(29128+2817\pi^2)\Big)g_1^2g_3-\frac{54}{N^3}\Big(12N^6(95+7\pi^2)-20N^3(9940+471\pi^2)+3N^5(6608+561\pi^2)
\end{aligned}$$

$$-320N^2(9175+1104\pi^2)-1280(13166+1485\pi^2)+640N(17947+1890\pi^2)$$
$$+N^4(137468+13785\pi^2)\Big)g_1^2g_4$$
$$-\frac{48}{N^2}\Big(3N^6(10+\pi^2)+6N^5(82+7\pi^2)+9504(756+85\pi^2)-2160N(1581+172\pi^2)+2N^4(10971$$
$$+763\pi^2)+2N^2(37896+6847\pi^2)+N^3(177600+16271\pi^2)\Big)g_1g_2^2-\frac{3456}{N}\Big(2N^4(20+\pi^2)$$
$$+N^3(244+17\pi^2)-24(2372$$
$$+275\pi^2)+N^2(4108+447\pi^2)+2N(8588+975\pi^2)\Big)g_1g_2g_3-\frac{1728}{N^2}\Big(518304+58320\pi^2+$$
$$N^2(-3072+41\pi^2)+2N^4(555+49\pi^2)-48N(4834+525\pi^2)+N^3(10782+1037\pi^2)\Big)g_1g_2g_4$$
$$-2304\Big(-8N^3-4N^4+N^2(384+45\pi^2)+N(388+45\pi^2)+6(1852+225\pi^2)\Big)g_1g_3^2$$
$$-\frac{13824}{N}\Big(-47(388+45\pi^2)+N^2(1120+117\pi^2)+N(4844+540\pi^2)\Big)g_1g_3g_4$$
$$-\frac{108}{N^2}\Big(301N^5+41N^6+N^4(10882+1053\pi^2)-4N^2(26366+1755\pi^2)$$
$$+128(41992+4725\pi^2)+N^3(98224+9801\pi^2)-16N(140912+15255\pi^2)\Big)g_1g_4^2$$
$$-\frac{128}{3N}\Big(N^4(960+46\pi^2)+108N(2220+241\pi^2)+N^3(4848+343\pi^2)-324(3352+375\pi^2)$$
$$+7N^2(7584+749\pi^2)\Big)g_2^3-4608\Big(6424+4N^3+2N^4+726\pi^2+3N(80+7\pi^2)+N^2(242+21\pi^2)\Big)g_2^2g_3$$
$$-\frac{288}{N}\Big(N^4(120+7\pi^2)+N^3(660+43\pi^2)+6N^2(4426+437\pi^2)+24N(4957+534\pi^2)$$
$$-48(12638+1413\pi^2)\Big)g_2^2g_4-20736\Big(3368+378\pi^2+N(44+3\pi^2)+N^2(44+3\pi^2)\Big)g_2g_3g_4$$
$$-\frac{1296}{N}\Big(N^4(32+3\pi^2)+N^3(96+9\pi^2)-896(188+21\pi^2)+12N(2440+261\pi^2)$$
$$+N^2(7184+716\pi^2)\Big)g_2g_4^2-4478976(9+\pi^2)g_3g_4^2-\frac{1944}{N}\Big(36N^3+12N^4+96N(75+8\pi^2)-$$
$$192(242+27\pi^2)+N^2(2028+203\pi^2)\Big)g_4^3 \qquad \text{(A.14)}$$

$$\widetilde{\beta}^{(4)}_{g_2}=-\frac{27}{N^5}\Big(2N^8(90+7\pi^2)+24000N(20+9\pi^2)-96000(28+9\pi^2)-3200N^2(1443+170\pi^2)$$
$$-5N^5(8372+209\pi^2)+N^7(3750+323\pi^2)-100N^4(6542+785\pi^2)+400N^3(7120+797\pi^2)$$
$$+N^6(28350+3133\pi^2)\Big)g_1^3-\frac{18}{N^4}\Big(3N^8(10+\pi^2)-309600N(32+3\pi^2)+86400(212+23\pi^2)$$
$$+N^7(732+66\pi^2)-8N^4(13443+482\pi^2)+N^6(25770+2294\pi^2)-120N^3(29800+3209\pi^2)$$

$$+240N^2(46680+4993\pi^2)+N^5(200436+19313\pi^2)\Big)g_1^2g_2-\frac{216}{N^3}\Big(-7200(88+7\pi^2)$$

$$+N^6(248+22\pi^2)+600N(832+63\pi^2)$$

$$+N^5(3132+251\pi^2)+10N^3(2672+359\pi^2)-40N^2(6504+677\pi^2)+3N^4(8852+717\pi^2)\Big)g_1^2g_3$$

$$-\frac{162}{N^4}\Big(32000(92+9\pi^2)-16000N(104+9\pi^2)+N^6(1418+155\pi^2)$$

$$+320N^2(4644+521\pi^2)+N^5(12998$$

$$+1497\pi^2)-20N^3(19900+2381\pi^2)-N^4(42584+3431\pi^2)\Big)g_1^2g_4$$

$$-\frac{48}{N^3}\Big(2N^6(534+49\pi^2)+1620N(2044$$

$$+193\pi^2)-2160(3060+319\pi^2)+N^5(11898+1033\pi^2)-72N^2(14522+1613\pi^2)+3N^3(32656+4997\pi^2$$

$$+N^4(91914+8441\pi^2)\Big)g_1g_2^2-\frac{288}{N^2}\Big(4N^6(6+\pi^2)$$

$$+16N^5(15+2\pi^2)+720(1400+139\pi^2)+5N^4(2184+149\pi^2)$$

$$-180N(2568+229\pi^2)+N^3(52944+4095\pi^2)+N^2(47952+6716\pi^2)\Big)g_1g_2g_3$$

$$-\frac{216}{N^3}\Big(-36N^3(626+7\pi^2)$$

$$+2N^6(69+8\pi^2)+9N^5(194+19\pi^2)-11520(358+37\pi^2)+480N(4018+381\pi^2)$$

$$+N^4(15348+1549\pi^2)-8N^2(53892+6641\pi^2)\Big)g_1g_2g_4$$

$$-\frac{3456}{N}\Big((-10+5N+2N^2)(N(62+3\pi^2)+N^2(62+3\pi^2)+6(334+33\pi^2)\Big)g_1g_3^2$$

$$-\frac{2592}{N^2}\Big(N^4(492+35\pi^2)+160(988+99\pi^2)-2N^2(2248+179\pi^2)+N^3(3084+227\pi^2)$$

$$-20N(3176+291\pi^2)\Big)g_1g_3g_4-\frac{162}{N^3}\Big(36N^4(163+17\pi^2)+N^6(172+21\pi^2)$$

$$+7N^5(182+27\pi^2)+1600N(1028$$

$$+99\pi^2)-640(6016+621\pi^2)-24N^2(9098+1363\pi^2)-2N^3(17432+1635\pi^2)\Big)g_1g_4^2$$

$$-\frac{32}{N^2}\Big(N^6(36+7\pi^2)$$

$$+N^5(288+50\pi^2)+2N^4(7186+545\pi^2)+8N^3(8863+756\pi^2)$$

$$+216(11996+1265\pi^2)-54N(13992+1337\pi^2)$$

$$+N^2(30720+5671\pi^2)\Big)g_2^3-\frac{48}{N}\Big(13N^5\pi^2+2N^6\pi^2+8N^4(816+53\pi^2)-720(2872$$

$$+295\pi^2)+16N^2(15324+1499\pi^2)+N^3(22656+1637\pi^2)+36N(17072+1737\pi^2)\Big)g_2^2g_3$$

$$-\frac{288}{N^2}\Big(2N^4(771+59\pi^2)-144N(2041+200\pi^2)-4N^2(9261+824\pi^2)+N^3(9918+829\pi^2)+144(7988+$$

$$-3456\Big(2N^3(18+\pi^2)+N^4(18+\pi^2)+2N(608+55\pi^2)+N^2(1234+111\pi^2)+8(2095+228\pi^2)\Big)g_2g_3^2$$
$$-\frac{1728}{N}\Big(2N^4(24+\pi^2)+N^3(192+11\pi^2)$$
$$+6N(3168+281\pi^2)-48(3112+319\pi^2)+N^2(5952+481\pi^2)\Big)g_2g_3g_4$$
$$-\frac{324}{N^2}\Big(N^6(2+\pi^2)+2N^5(5+3\pi^2)$$
$$+N^4(1628+171\pi^2)-16N^2(3517+339\pi^2)+192(7024+735\pi^2)-32N(9160+933\pi^2)$$
$$+N^3(9376+974\pi^2)\Big)g_2g_4^2-20736\Big(N(62+3\pi^2)+N^2(62+3\pi^2)+6(334+33\pi^2)\Big)g_3^2g_4$$
$$-\frac{2592}{N}\Big(N^4(28+3\pi^2)+198N(32+3\pi^2)+N^3(84+9\pi^2)+N^2(2572+249\pi^2)-8(7960+813\pi^2)\Big)g_3g_4^2$$
$$-\frac{972}{N^2}\Big(20N^5+4N^6+N^4(146+21\pi^2)+4N^3(170+27\pi^2)-32N(1082+117\pi^2)+128(1526+159\pi^2)$$
$$-2N^2(4736+513\pi^2)\Big)g_4^3 \qquad \text{(A.15)}$$

$$\widetilde{\beta}^{(4)}_{g_3}=-\frac{9}{N^6}\Big(432000\pi^2+72000N^2(8+3\pi^2)+2400N^4(214+35\pi^2)-600N^5(312+41\pi^2)$$
$$+N^8(630+69\pi^2)$$
$$-2N^6(1200+137\pi^2)+N^7(7110+813\pi^2)\Big)g_1^3-\frac{18}{N^5}\Big(28800N(2+3\pi^2)+4N^8(39+4\pi^2)$$
$$-14400(112+27\pi^2)$$
$$-7200N^2(292+27\pi^2)+6N^7(361+34\pi^2)+240N^3(4272+427\pi^2)-20N^4(11754+869\pi^2)$$
$$+2N^6(8379+883\pi^2)+N^5(516+1189\pi^2)\Big)g_1^2g_2+\frac{72}{N^4}\Big(56N^7+4N^8+N^4(2220-519\pi^2)+1200N(-32$$
$$-1200(136+27\pi^2)$$
$$+240N^3(614+39\pi^2)-300N^2(896+75\pi^2)-N^6(1576+207\pi^2)-N^5(12524+1179\pi^2)\Big)g_1^2g_3$$
$$+\frac{162}{N^5}\Big(N^6(302+\pi^2)-4800N(2+3\pi^2)+19200(14+3\pi^2)+1600N^2(215+18\pi^2)-480N^3(321+31\pi^2)$$
$$+20N^4(587+74\pi^2)+N^5(5174+314\pi^2)\Big)g_1^2g_4$$
$$-\frac{12}{N^4}\Big(4N^8(6+\pi^2)+48N^7(7+\pi^2)-8640N(212+19\pi^2)$$
$$+12960(352+35\pi^2)+16N^4(-1119+188\pi^2)-192N^3(3093+241\pi^2)+3N^6(3440+367\pi^2)$$
$$+144N^2(16952+1693\pi^2)+N^5(55992+4967\pi^2)\Big)g_1g_2^2-\frac{288}{N^3}\Big(2880N(35+3\pi^2)+2N^6(84+17\pi^2)$$

$$-360(440+39\pi^2)+24N^3(770+69\pi^2)+N^5(1116+169\pi^2)-6N^2(10352+953\pi^2)$$
$$+N^4(10956+985\pi^2)\Big)g_1g_2g_3$$
$$-\frac{216}{N^4}\Big(3N^6(40+\pi^2)+9N^5(78+\pi^2)+3840(191+18\pi^2)-960N(317+27\pi^2)-24N^3(2503+192\pi^2)$$
$$+96N^2(3303+352\pi^2)-N^4(15564+995\pi^2)\Big)g_1g_2g_4-\frac{144}{N^2}\Big(66N^5\pi^2+15N^6\pi^2+600(112+9\pi^2)$$
$$+16N^4(443+33\pi^2)-60N(1120+87\pi^2)+6N^2(5216+567\pi^2)+N^3(20528+1377\pi^2)\Big)g_1g_3^2$$
$$+\frac{864}{N^3}\Big(84N^5+12N^6+N^4(148-27\pi^2)+N^3(1628+57\pi^2)+80(956+81\pi^2)-20N(2552+207\pi^2)$$
$$+2N^2(9808+1017\pi^2)\Big)g_1g_3g_4-\frac{162}{N^4}\Big(3N^5(-208+7\pi^2)+N^6(-94+9\pi^2)+1920(368+33\pi^2)$$
$$-480N(632+51\pi^2)-24N^3(1022+81\pi^2)-2N^4(5156+357\pi^2)+16N^2(14228+1707\pi^2)\Big)g_1g_4^2$$
$$-\frac{4}{3N^3}\Big(21N^7\pi^2+2N^8\pi^2+17280N(465+41\pi^2)+576N^3(433+80\pi^2)-432N^2(1464+205\pi^2)$$
$$+4N^6(2136+277\pi^2)-2592(9552+971\pi^2)+12N^4(28836+2929\pi^2)+N^5(59568+5281\pi^2)\Big)g_2^3$$
$$-\frac{96}{N^2}\Big(N^6(54+19\pi^2)+4N^5(81+19\pi^2)-108N(1264+103\pi^2)$$
$$+540(1112+109\pi^2)+15N^2(2064+281\pi^2)$$
$$+6N^3(5540+431\pi^2)+2N^4(5655+454\pi^2)\Big)g_2^2g_3$$
$$-\frac{72}{N^3}\Big(2N^6(24+\pi^2)+24N^2(492+\pi^2)+N^5(384+19\pi^2)$$
$$-N^4(2952+35\pi^2)-1728(1150+117\pi^2)-6N^3(4492+271\pi^2)+144N(3942+367\pi^2)\Big)g_2^2g_4$$
$$-\frac{432}{N}(-6+3N+2N^2)\Big(2N^3\pi^2+N^4\pi^2+N(704+52\pi^2)+N^2(704+53\pi^2)+4(3232+309\pi^2)\Big)g_2g_3^2$$
$$-\frac{1728}{N^2}\Big(27N^3(4+\pi^2)+4N^4(3+2\pi^2)-174N(104+9\pi^2)$$
$$+168(580+57\pi^2)-3N^2(1720+137\pi^2)\Big)g_2g_3g_4$$
$$-\frac{324}{N^3}\Big(4N^6+N^5(50+\pi^2)-N^4(1060+91\pi^2)+16N^2(1289+133\pi^2)-2N^3(3704+339\pi^2)$$
$$+16N(9704+975\pi^2)-64(9968+1017\pi^2)\Big)g_2g_4^2-144\Big(3N^5\pi^2+N^6\pi^2+N^4(848+65\pi^2)$$
$$+N^3(1696+125\pi^2)+4N(6016+555\pi^2)+24(6664+711\pi^2)+N^2(24912+2282\pi^2)\Big)g_3^3$$
$$-\frac{864}{N}\Big(-57056+752N-368N^2$$
$$-5472\pi^2+84N\pi^2+9N^3\pi^2+3N^4\pi^2\Big)g_3^2g_4+\frac{432}{N^2}\Big(20N^5+4N^6-N^4(52+9\pi^2)-2N^3(212+27\pi^2)$$
$$+10N^2(1580+153\pi^2)+4N(10064+963\pi^2)-16(17792+1755\pi^2)\Big)g_3g_4^2-\frac{486}{N^3}\Big(N^6(-8+\pi^2)$$

$$-10N^4(34+3\pi^2)$$

$$+N^5(-40+6\pi^2)-16N^3(94+13\pi^2)-512(400+41\pi^2)+64N(632+71\pi^2)+8N^2(1354+163\pi^2)\Big)g_4^3 \tag{A.16}$$

$$\widetilde{\beta}^{(4)}_{g_4} = -\frac{9}{N^5}\Big(-13824000+6912000N+N^8(360+22\pi^2)-2400N^4(448+43\pi^2)+9600N^3(395$$

$$+49\pi^2)-60N^5(1672+65\pi^2)-3200N^2(2352+275\pi^2)+N^7(6660+489\pi^2)+N^6(41220+4241\pi^2)\Big)g_1^3$$

$$-\frac{72}{N^4}\Big(172800(14+\pi^2)-14400N(68+3\pi^2)-2N^4(14844+131\pi^2)+N^6(1848+191\pi^2)$$

$$+480N^2(2120+243\pi^2)$$

$$+5N^5(3504+415\pi^2)-120N^3(3640+423\pi^2)\Big)g_1^2g_2-\frac{10368}{N^3}\Big(800N+20N^3(17+3\pi^2)$$

$$-200(28+3\pi^2)$$

$$+3N^4(32+5\pi^2)-5N^2(392+51\pi^2)\Big)g_1^2g_3-\frac{18}{N^4}\Big(670N^7+41N^8+38400(320+27\pi^2)$$

$$-9600N(467+27\pi^2)$$

$$-6N^4(32878+417\pi^2)+N^6(14413+801\pi^2)-120N^3(17800+1731\pi^2)+240N^2(22264+2481\pi^2)$$

$$+N^5(95816+8415\pi^2)\Big)g_1^2g_4-\frac{3456}{N^2}\Big(3N^3(-28+\pi^2)+N^4(-4+3\pi^2)+240(52+5\pi^2)$$

$$+2N^2(-148+9\pi^2)$$

$$-40N(152+15\pi^2)\Big)g_1g_2g_3-\frac{576}{N^2}\Big(960(94+9\pi^2)-240N(262+27\pi^2)+6N^2(728+153\pi^2)$$

$$+N^4(1160+153\pi^2)+N^3(6392+801\pi^2)\Big)g_1g_3g_4-\frac{48}{N^3}\Big(51840N(15+\pi^2)$$

$$-34560(57+5\pi^2)+N^6(48+7\pi^2)$$

$$+N^5(228+43\pi^2)+18N^4(346+101\pi^2)+4N^3(2526+1579\pi^2)-8N^2(54528+6997\pi^2)\Big)g_1g_2^2$$

$$-\frac{432}{N^3}\Big(7N^6(16+\pi^2)+10N^5(102+7\pi^2)-1920(296+27\pi^2)+480N(521+39\pi^2)+8N^3(437+221\pi^2)$$

$$+N^4(5556+727\pi^2)-4N^2(28812+3317\pi^2)\Big)g_1g_2g_4-\frac{108}{N^3}\Big(2514N^5+318N^6+88N^3(-241+18\pi^2)$$

$$-5120(289+27\pi^2)+7N^4(1084+99\pi^2)+320N(2350+189\pi^2)-16N^2(16366+1557\pi^2)\Big)g_1g_4^2+$$

$$+\frac{128}{3N^2}\Big(-63504(10+\pi^2)+N^4(528+\pi^2)+324N(532+53\pi^2)+N^3(3120+163\pi^2)+8N^2(4314$$

$$+337\pi^2)\Big)g_2^3$$

$$+\frac{4608}{N}\Big(6424+4N^3+2N^4+726\pi^2+3N(80+7\pi^2)+N^2(242+21\pi^2)\Big)g_2^2g_3$$
$$-\frac{144}{N^2}\Big(N^6(2+\pi^2)+N^5(12+7\pi^2)$$
$$+9408(88+9\pi^2)-6N^2(3476+93\pi^2)+N^4(2134+239\pi^2)-48N(4495+429\pi^2)$$
$$+N^3(12708+1351\pi^2)\Big)g_2^2g_4$$
$$-\frac{6912}{N}\Big(N^4(4+\pi^2)+4N^3(6+\pi^2)-72(184+21\pi^2)+3N^2(308+39\pi^2)+N(2488+306\pi^2)\Big)g_2g_3g_4$$
$$-\frac{2592}{N^2}\Big(68224+12N^5+2N^6+7104\pi^2-224N^2(15+\pi^2)+N^4(126+11\pi^2)+N^3(644+57\pi^2)$$
$$-16N(1043+93\pi^2)\Big)g_2g_4^2-2304\Big(-8N^3-4N^4+N^2(384+45\pi^2)+N(388+45\pi^2)+$$
$$+6(1852+225\pi^2)\Big)g_3^2g_4$$
$$-\frac{864}{N}\Big(27N^3(8+\pi^2)+9N^4(8+\pi^2)+4N^2(808+99\pi^2)-32(2584+297\pi^2)+N(8096+972\pi^2)\Big)g_3g_4^2$$
$$-\frac{108}{N^2}\Big(13N^5+5N^6+N^4(1198+45\pi^2)+4N^3(1723+63\pi^2)-8N^2(6253+414\pi^2)-$$
$$32N(5692+459\pi^2)+128(6388+675\pi^2)\Big)g_4^3 \qquad \text{(A.17)}$$

B The F-function and metric for the symmetric traceless model

Working up to the two-loop order, we find that the F-function which enters the gradient flow expression (4.42) is given by $F=F^{(1)}+F^{(2)}$, where

$$F^{(1)}=-\frac{\epsilon}{576N^3}$$
$$\times\Big[\Big(2N^2\Big(48g_2\Big(4g_3N^5+(10g_3+3g_4)N^4+3(6g_3+5g_4)N^3+6(4g_3-7g_4)N^2$$
$$-72(g_3+2g_4)N+288g_4\Big)+4g_2^2\Big(N^6+6N^5+45N^4+124N^3-168N^2-720N+1296\Big)$$
$$+3\Big(\Big(16g_3^2+3g_4^2\Big)N^6+\Big(32g_3^2+15g_4^2\Big)N^5+24\Big(6g_3^2+g_4^2\Big)N^4+4\Big(32g_3^2+48g_4g_3+15g_4^2\Big)N^3$$
$$+96\Big(2g_3^2+4g_4g_3-5g_4^2\Big)N^2-192g_4(8g_3+7g_4)N+3072g_4^2\Big)\Big)$$
$$+12g_1N\Big(9g_4N^6+(80g_3+63g_4)N^5+(272g_3-42g_4)N^4-120(2g_3+7g_4)N^3$$
$$-240(4g_3-g_4)N^2+4g_2\Big(2N^6+15N^5+11N^4-140N^3+720N-720\Big)+960(g_3+4g_4)N-3840g_4\Big)$$
$$+3g_1^2\Big(N^8+14N^7+83N^6+46N^5-960N^4+4800N^2-9600N+9600\Big)\Big)\Big] \qquad \text{(B.1)}$$

and $F^{(2)}$ may be written in terms of the 3-point functions in the free theory in $d = 3$ [163, 164]:

$$F^{(2)} \sim C_{ijk} g^i g^j g^k \ , \qquad \langle O_i(x) O_j(y) O_k(z) \rangle = \frac{C_{ijk}}{|x-y|^3 |x-z|^3 |y-z|^3} \ . \tag{B.2}$$

Explicitly, we find

$$\begin{aligned}
F^{(2)} &= \frac{3}{13271040 N^5 \pi^2} \\
&\times \Big[\big(3N^{12} + 93N^{11} + 1717N^{10} + 13103N^9 + 15072N^8 - 227572N^7 - 326400N^6 \\
&+2596800N^5 - 758400N^4 - 12288000N^3 + 29952000N^2 - 40704000N + 29184000 \big) g_1^3 \\
&+ \frac{16}{3} N g_2 \big(27 \big(6N^{10} + 109N^9 + 878N^8 + 1885N^7 - 10882N^6 - 28000N^5 + 122880N^4 + 28800N^3 \\
&-672000N^2 + 1411200N - 1094400 \big) g_1^2 + 9N \big(N^{10} + 15N^9 + 405N^8 + 3493N^7 + 8634N^6 \\
&-30684N^5 - 102504N^4 + 351168N^3 + 408960N^2 - 2194560N + 1969920 \big) g_2 g_1 \\
&+8N^2 \big(26N^8 + 219N^7 + 1446N^6 + 5399N^5 - 714N^4 - 57456N^3 + 30240N^2 + 343440N - 443232 \big) g_2^2 \big) \\
&+192 N^2 g_3 \big(2 \big(\big(N^8 + 7N^7 + 181N^6 + 757N^5 + 1990N^4 + 3832N^3 - 7296N^2 - 27504N + 49248 \big) g_2^2 \\
&+12N \big(6N^6 + 21N^5 + 118N^4 + 253N^3 + 270N^2 + 348N - 1368 \big) g_3 g_2 + 4N^2 \big(3N^6 + 9N^5 \\
&+71N^4 + 127N^3 + 402N^2 + 340N + 456 \big) g_3^2 \big) N^2 + 12 g_1 \big(\big(2N^8 + 17N^7 + 174N^6 + 773N^5 \\
&+162N^4 - 6176N^3 + 240N^2 + 28080N - 27360 \big) g_2 + 2N \big(15N^6 + 66N^5 + 196N^4 + 421N^3 \\
&-570N^2 - 2100N + 2280 \big) g_3 \big) N + 3 \big(29N^8 + 310N^7 + 997N^6 - 1612N^5 - 10020N^4 \\
&+15600N^3 + 38400N^2 - 112800N + 91200 \big) g_1^2 \big) - 18N \big(-N^2 - 2N + 8 \big) g_4 \big(\big(N^8 + 6N^7 + 47N^6 \\
&+198N^5 + 1428N^4 + 7416N^3 - 32512N^2 - 121344N + 311296 \big) g_4^2 N^2 + 32 \big(\big(N^6 + 7N^5 + 113N^4 \\
&+629N^3 - 1470N^2 - 7920N + 16416 \big) g_2^2 + 24N \big(N^4 + 4N^3 + 41N^2 + 114N - 456 \big) g_3 g_2 \\
&+48N^2 \big(3N^2 + 3N + 38 \big) g_3^2 \big) N^2 + 96 \big(\big(N^6 + 6N^5 + 46N^4 + 225N^3 - 728N^2 - 3192N + 7296 \big) g_2 \\
&+2N \big(5N^4 + 15N^3 + 86N^2 + 228N - 1216 \big) g_3 \big) g_4 N^2 + 192 g_1 \big(\big(7N^6 + 65N^5 + 52N^4 - 964N^3 - 650N^2 \\
&+7680N - 9120 \big) g_2 + +2N \big(27N^4 + 141N^3 - 190N^2 - 1140N + 1520 \big) g_3 \big) N + 3 \big(3N^8 + 24N^7 \\
&+325N^6 + 2364N^5 - 100N^4 - 41712N^3 - 10240N^2 + 318720N - 389120 \big) g_1 g_4 N + 3 \big(21N^8 + 294N^7 \\
&+1599N^6 + 30N^5 - 27920N^4 + 209600N^2 - 499200N + 486400 \big) g_1^2 \Big]
\end{aligned} \tag{B.3}$$

The metric G_{ij} is given by

$$
\begin{aligned}
G_{11} &= \frac{1}{192N^3}\left(N^8+14N^7+83N^6+46N^5-960N^4+4800N^2-9600N+9600\right),\\
G_{12} = G_{21} &= \frac{1}{24N^2}\left(2N^6+15N^5+11N^4-140N^3+720N-720\right),\\
G_{13} = G_{23} &= \frac{1}{6N}\left(5N^4+17N^3-15N^2-60N+60\right),\\
G_{14} = G_{41} &= \frac{1}{32N^2}(N-2)(N+4)\left(3N^4+15N^3-20N^2-120N+160\right),\\
G_{22} &= \frac{1}{72N}\left(N^6+6N^5+45N^4+124N^3-168N^2-720N+1296\right),\\
G_{23} = G_{32} &= \frac{1}{6}\left(2N^4+5N^3+9N^2+12N-36\right),\\
G_{24} = G_{42} &= \frac{1}{4N}(N-2)(N+4)\left(N^2+3N-12\right),\\
G_{33} = \frac{1}{6}N^3\left(N^4+2N^3+9N^2+8N+12\right), &\quad G_{34} = G_{43} = (N-2)N^3(N+4),\\
G_{44} &= \frac{1}{32N}(N-2)^2(N+4)^2\left(N^2+N+16\right). \qquad \text{(B.4)}
\end{aligned}
$$

At this order it is independent of the couplings g^i and is proportional to the matrix of two-point functions (4.43) in the free theory in $d = 3$.

C Beta Functions of $O(M) \times O(N)$ Supersymmetric Model

The beta functions of the four coupling constants admit of loop expansions

$$\beta_i = -\epsilon g_i + \beta_i^{(2)} + \mathcal{O}(g^5)\,, \qquad \text{(C.1)}$$

where $\beta_i^{(2)}$ denotes the two-loop contributions, which are cubic in the couplings. By explicit computation, we find that these are given by

$$
\begin{aligned}
\beta_1^{(2)} = \frac{1}{8\pi^2N^2}\Big(&32g_1^2g_4N(-40-8M+8N+7MN+8N^2)+16g_1^2g_3N(-80-24M+30N+\\
&+4MN+7N^2+4MN^2)+16g_1g_3^2N^2(32+2M+N+MN+N^2+MN^2)+64g_1g_2g_4N(-32-
\end{aligned}
$$

$$-4M+16N+2MN+5N^2+2MN^2)+4g_2^2g_3N(-256-64M+72N+10MN+19N^2+2MN^2)+$$
$$+64g_1g_4^2N^2(22-2M+MN+MN^2)+16g_1g_2g_3N(-144-40M+42N+17MN+$$
$$+21N^2+5MN^2)+128g_1g_3g_4N^2(3+5M+N+N^2)+g_2^3(896+128M-352N-48MN-$$
$$-12N^2-12MN^2+7N^3+2MN^3)+96g_2^2g_4(-8+N)N+4g_1^2g_2(928+224M-392N-$$
$$-100MN-2N^2+11MN^2+23N^3+7MN^3+4N^4)+768g_2g_3g_4N^2$$
$$+4g_1^3(352+96M-152N-44MN+10N^3+3MN^3+MN^4)+16g_2g_3^2N^2(16+7M+N+N^2)$$
$$+2g_1g_2^2(1600+320M-656N-136MN+32N^2+10MN^2+50N^3+10MN^3+5N^4+2MN^4)\Big),$$

$$\beta_2^{(2)}=\frac{1}{8\pi^2N^2}\Big(64g_1g_2g_4N(-80-16M+16N+5MN+7N^2)+16g_2g_3^2N^2(48+9M+2N+$$
$$+MN+2N^2+MN^2)+16g_1^2g_3N(-128-32M+32N+12MN+14N^2+3MN^2)+$$
$$+128g_2g_3g_4N^2(9+5M+N+N^2)+16g_1g_2g_3N(-272-72M+82N+15MN+24N^2+6MN^2)+$$
$$+192g_1^2g_4N(-12-2M+4N+N^2)+16g_2^2g_4N(-176-40M+58N+14MN+17N^2+11MN^2)+$$
$$+32g_1g_3^2N^2(16+7M+N+N^2)+4g_2^2g_3N(-576-160M+176N+54MN+74N^2+17MN^2)+$$
$$+64g_2g_4^2N^2(22-2M+MN+MN^2)+8g_1^3(288+64M-112N-24MN-6N^2+3MN^2+$$
$$+5N^3+2MN^3+N^4)+1536g_1g_3g_4N^2+2g_1g_2^2(3968+1024M-1600N-416MN-$$
$$-56N^2-22MN^2+85N^3+17MN^3+11N^4)+4g_1^2g_2(1856+448M-736N-176MN-$$
$$-22N^2-5MN^2+43N^3+8MN^3+3N^4+2MN^4)+$$
$$+g_2^3(2816+768M-1152N-320MN+12N^2-12MN^2+69N^3+30MN^3+7N^4+5MN^4)\Big),$$

$$\beta_3^{(2)}=\frac{1}{8\pi^2N^3}\Big(32g_3^2g_4N^3(18+14M+7N+7N^2)+96g_1^2g_4N(8+2N^2+MN^2)+$$
$$+384g_1g_2g_4N(4+N^2)+24g_3^3N^3(16+2M+2N+MN+2N^2+MN^2)+64g_2g_3g_4N^2(-20-$$
$$-4M+10N+2MN+5N^2+2MN^2)+16g_1g_3^2N^2(-52-14M+26N+7MN+14N^2+7MN^2)+$$
$$+128g_1g_3g_4N^2(-10-2M+5N+MN+5N^2)+8g_2g_3^2N^2(-104-28M+52N+14MN+38N^2+$$
$$+7MN^2)+64g_3g_4^2N^3(22-2M+MN+MN^2)+16g_1g_2g_3N(208+56M-48N-12MN+$$
$$+12N^2+3MN^2+8N^3+MN^3+2N^4)+96g_2^2g4N(8+N^2)+8g_1^2g_3N(208+56M-48N-$$

$$-12MN+12N^2+6MN^2+4N^3+3MN^3+MN^4)+8g_1^3(-96-16M+24N+4MN-20N^2-$$
$$-10MN^2+6N^3+2MN^3+N^4+MN^4)+4g_2^2g_3N(416+112M-96N-24MN+18N^2+$$
$$+6MN^2+12N^3+4MN^3+2N^4+MN^4)+g_2^3(-768-128M+192N+32MN-96N^2+32N^3+$$
$$+4MN^3+7N^4+2MN^4)+2g_1g_2^2(-1152-192M+288N+48MN-176N^2-40MN^2+$$
$$+70N^3+10MN^3+21N^4+2MN^4)+4g_1^2g_2(-576-96M+144N+24MN-104N^2-40MN^2+$$
$$+34N^3+13MN^3+11N^4+3MN^4)\Big),$$

$$\beta_4^{(2)}=\frac{1}{8\pi^2N^3}\Big(8g_1^2g_3N(80+16M-12N+4N^2+2MN^2+3N^3+N^4)$$
$$+224g_1g_4^2N^2(-4-2M+2N+MN+2N^2)+16g_1g_3^2N^2(-16-2M+8N+MN+7N^2)$$
$$+96g_4^3N^3(8-2M+MN+MN^2)+64g_2g_3g_4N^2(-14-4M+7N+2MN+6N^2+MN^2)$$
$$+224g_2g_4^2N^2(-4-2M+2N+MN+N^2+MN^2)+32g_3^2g_4N^3(22+N+MN+N^2+MN^2)$$
$$+64g_1g_3g_4N^2(-14-4M+7N+2MN+2N^2+2MN^2)$$
$$+8g_2g_3^2N^2(-32-4M+16N+2MN+9N^2+2MN^2)+24g_3^3N^3(4+2M+N+N^2)$$
$$+16g_1g_2g_3N(80+16M-12N+7N^2+2MN^2+N^3)+224g_3g_4^2N^3(2M+N+N^2)$$
$$+4g_2^2g_3N(160+32M-24N+17N^2+7MN^2+4N^3+N^4)$$
$$+32g_1g_2g_4N(96+36M-24N-12MN+2N^2-2MN^2+4N^3+MN^3+N^4)$$
$$+4g_1^3(-160-48M+40N+12MN+4N^2+2MN^2+4N^3+MN^3+2N^4)$$
$$+2g_1g_2^2(-960-288M+240N+72MN-88N^2-20MN^2+39N^3+7MN^3+13N^4)$$
$$+16g_1^2g_4N(96+36M-24N-12MN-4N^2-2MN^2+2N^3+3MN^3+MN^4)$$
$$+8g_1^2g_2(-240-72M+60N+18MN-8N^2-MN^2+6N^3+2MN^3+N^4+MN^4)$$
$$+8g_2^2g_4N(192+72M-48N-24MN+10N^2+2MN^2+6N^3+4MN^3+N^4+MN^4)$$
$$+g_2^3(-640-192M+160N+48MN-96N^2-24MN^2+36N^3+12MN^3+10N^4+5MN^4)\Big).$$

It can be checked that there exists a function F of the couplings such that the beta-

functions can be cast in the form

$$\beta_i = G_{ij}\frac{\partial F}{\partial g_j} \tag{C.2}$$

where the metric has the components

$$\begin{aligned}
G_{11} =& \frac{MN^4+3MN^3+2N^3-2MN^2-4N^2-12MN-24N+24M+48}{2N^2}\,,\\
G_{12} =& \frac{N^4+MN^3+4N^3-2MN^2-4N^2-12MN-24N+24M+48}{2N^2}\,,\\
G_{13} =& 2\,\frac{MN^2+N^2+MN+2N-2M-4}{N}\,, \quad G_{14} = 2\,\frac{2N^2+MN+2N-2M-4}{N}\,,\\
G_{22} =& \frac{MN^4+N^4+4MN^3+6N^3-4MN^2-8N^2-24MN-48N+48M+96}{4N^2}\,,\\
G_{23} =& \frac{MN^2+3N^2+2MN+4N-4M-8}{N}\,, \quad G_{24} = 2\frac{MN^2+N^2+MN+2N-2M-4}{N}\,,\\
G_{33} =& \frac{MN^3+N^3+MN^2+N^2+4N}{N}\,, \quad G_{34} = 2(N^2+N+2M)\,,\\
G_{44} =& 2(4-2M+MN+MN^2)\,.
\end{aligned}$$

Taking the determinant of this metric, one arrives at (4.61).

References

[1] I. R. Klebanov, P. N. Pallegar, and F. K. Popov, *Majorana fermion quantum mechanics for higher rank tensors*, *Physical Review D* **100** (oct, 2019) 086003.

[2] G. Gaitan, I. R. Klebanov, K. Pakrouski, P. N. Pallegar, and F. K. Popov, *Hagedorn Temperature in Large N Majorana Quantum Mechanics*, *Phys. Rev. D* **101** (2020), no. 12 126002, [arXiv:2002.02066].

[3] S. Giombi, I. R. Klebanov, F. Popov, S. Prakash, and G. Tarnopolsky, *Prismatic Large N Models for Bosonic Tensors*, *Phys. Rev. D* **98** (2018), no. 10 105005, [arXiv:1808.04344].

[4] F. K. Popov, *Supersymmetric tensor model at large N and small ϵ*, *Phys. Rev. D* **101** (2020), no. 2 026020, [arXiv:1907.02440].

[5] C. B. Jepsen, I. R. Klebanov, and F. K. Popov, *RG limit cycles and unconventional fixed points in perturbative QFT*, *Phys. Rev. D* **103** (2021), no. 4 046015, [arXiv:2010.15133].

[6] C. B. Jepsen and F. K. Popov, *Homoclinic RG flows, or when relevant operators become irrelevant*, arXiv:2105.01625.

[7] S. Brothers, *One billion years before the end of the world*. Strelbytskyy Multimedia Publishing, 2021.

[8] A. Doxiadis, *Uncle Petros and Goldbach's Conjecture: A Novel of Mathematical Obsession*. Bloomsbury Publishing USA, 2001.

[9] C. Marchal, *The three-body problem*, .

[10] D. J. Gross, T. Piran, and S. Weinberg, *Two Dimensional Quantum Gravity And Random Surfaces-8th Jerusalem Winter School For Theoretical Physics*, vol. 8. World Scientific, 1991.

[11] T. H. Berlin and M. Kac, *The Spherical Model of a Ferromagnet*, *Physical Review* **86** (June, 1952) 821–835.

[12] H. E. Stanley, *Spherical model as the limit of infinite spin dimensionality*, *Phys. Rev.* **176** (1968) 718–722.

[13] M. Moshe and J. Zinn-Justin, *Quantum field theory in the large N limit: A Review*, *Phys. Rept.* **385** (2003) 69–228, [hep-th/0306133].

[14] I. R. Klebanov, F. Popov, and G. Tarnopolsky, *TASI Lectures on Large N Tensor Models*, *PoS* **TASI2017** (2018) 004, [arXiv:1808.09434].

[15] J. Maldacena, *Tasi 2019 lectures on large n*, .

[16] G. 't Hooft, *A Planar Diagram Theory for Strong Interactions*, *Nucl. Phys.* **B72** (1974) 461.

[17] E. Brezin, C. Itzykson, G. Parisi, and J. B. Zuber, *Planar Diagrams*, *Commun. Math. Phys.* **59** (1978) 35.

[18] L. D. Faddeev and V. N. Popov, *Feynman diagrams for the yang-mills field*, *Physics Letters B* **25** (1967), no. 1 29–30.

[19] I. R. Klebanov and G. Tarnopolsky, *Uncolored random tensors, melon diagrams, and the Sachdev-Ye-Kitaev models*, *Phys. Rev. D* **95** (2017), no. 4 046004, [arXiv:1611.08915].

[20] R. Gurau, *Colored Group Field Theory*, *Commun. Math. Phys.* **304** (2011) 69–93, [arXiv:0907.2582].

[21] R. Gurau, *Invitation to Random Tensors*, *SIGMA* **12** (2016) 094, [arXiv:1609.06439].

[22] S. Carrozza and A. Tanasa, *$O(N)$ Random Tensor Models*, *Lett. Math. Phys.* **106** (2016), no. 11 1531–1559, [arXiv:1512.06718].

[23] E. Witten, *An SYK-Like Model Without Disorder*, *J. Phys. A* **52** (2019), no. 47 474002, [arXiv:1610.09758].

[24] J. Maldacena and D. Stanford, *Remarks on the sachdev-ye-kitaev model*, *Physical Review D* **94** (nov, 2016) 106002.

[25] A. Kitaev, *A simple model of quantum holography*, . http://online.kitp.ucsb.edu/online/entangled15/kitaev/,http://online.kitp.ucsb.edu/online/entangled15/kitaev2/. Talks at KITP, April 7, 2015 and May 27, 2015.

[26] S. Giombi, I. R. Klebanov, and G. Tarnopolsky, *Bosonic tensor models at large N and small ϵ*, *Phys. Rev. D* **96** (2017), no. 10 106014, [arXiv:1707.03866].

[27] I. R. Klebanov and G. Tarnopolsky, *On Large N Limit of Symmetric Traceless Tensor Models*, *JHEP* **10** (2017) 037, [arXiv:1706.00839].

[28] F. Ferrari, V. Rivasseau, and G. Valette, *A New Large N Expansion for General Matrix-Tensor Models*, arXiv:1709.07366.

[29] S. S. Gubser, C. Jepsen, Z. Ji, and B. Trundy, *Higher melonic theories*, arXiv:1806.04800.

[30] A. Z. Patashinskii and V. L. Pokrovskii, *Second Order Phase Transitions in a Bose Fluid*, *JETP* **19** (1964) 677.

[31] E. Fradkin, S. A. Kivelson, and J. M. Tranquada, *Colloquium: Theory of intertwined orders in high temperature superconductors*, *Rev. Mod. Phys.* May 457–482.

[32] P. A. Lee, N. Nagaosa, and X.-G. Wen, *Doping a Mott insulator: Physics of high-temperature superconductivity*, *Rev. Mod. Phys.* Jan 17–85.

[33] A. Georges, G. Kotliar, W. Krauth, and M. J. Rozenberg, *Dynamical mean-field theory of strongly correlated fermion systems and the limit of infinite dimensions*, *Rev. Mod. Phys.* Jan 13–125.

[34] J. Hubbard and B. H. Flowers, *Electron correlations in narrow energy bands*, *Proceedings of the Royal Society of London. Series A. Mathematical and Physical Sciences* no. 1365 238–257, [https://royalsocietypublishing.org/doi/pdf/10.1098/rspa.1963.0204].

[35] *The Hubbard model at half a century*, *Nature Physics* no. 9 523–523.

[36] J. Spatek and A. Oleś, *Ferromagnetism in narrow s-band with inclusion of intersite correlations*, *Physica B+C* 375–377.

[37] S. Sachdev and J. Ye, *Gapless spin fluid ground state in a random, quantum Heisenberg magnet*, *Phys. Rev. Lett.* **70** (1993) 3339, [cond-mat/9212030].

[38] S. Sachdev, *Bekenstein-Hawking Entropy and Strange Metals*, *Phys. Rev.* **X5** (2015), no. 4 041025, [arXiv:1506.05111].

[39] J. Polchinski and V. Rosenhaus, *The spectrum in the sachdev-ye-kitaev model*, *Journal of High Energy Physics* **2016** (apr, 2016) 1–25.

[40] A. Kitaev and S. J. Suh, *The soft mode in the Sachdev-Ye-Kitaev model and its gravity dual*, *JHEP* **05** (2018) 183, [arXiv:1711.08467].

[41] O. Bohigas and J. Flores, *Two-body random hamiltonian and level density*, *Phys. Lett.* **34B** (1971) 261–263.

[42] J. B. French and S. S. M. Wong, *Validity of random matrix theories for many-particle systems*, *Phys. Lett.* **33B** (1970) 449–452.

[43] G. Sarosi, *AdS_2 holography and the SYK model*, *PoS* **Modave2017** (2018) 001, [arXiv:1711.08482].

[44] V. Rosenhaus, *An introduction to the SYK model*, *Journal of Physics A: Mathematical and Theoretical* **52** (jul, 2019) 323001.

[45] Y. Gu, A. Kitaev, S. Sachdev, and G. Tarnopolsky, *Notes on the complex Sachdev-Ye-Kitaev model*, arXiv:1910.14099.

[46] J. Maldacena and X.-L. Qi, *Eternal traversable wormhole*, arXiv:1804.00491.

[47] A. M. García-García, T. Nosaka, D. Rosa, and J. J. M. Verbaarschot, *Quantum chaos transition in a two-site Sachdev-Ye-Kitaev model dual to an eternal traversable wormhole*, *Phys. Rev.* **D100** (2019), no. 2 026002, [arXiv:1901.06031].

[48] J. Kim, I. R. Klebanov, G. Tarnopolsky, and W. Zhao, *Symmetry Breaking in Coupled SYK or Tensor Models*, *Phys. Rev.* **X9** (2019), no. 2 021043, [arXiv:1902.02287].

[49] Y. Gu, X.-L. Qi, and D. Stanford, *Local criticality, diffusion and chaos in generalized Sachdev-Ye-Kitaev models*, *JHEP* **05** (2017) 125, [arXiv:1609.07832].

[50] A. A. Patel and S. Sachdev, *Critical strange metal from fluctuating gauge fields in a solvable random model*, *Phys. Rev.* **B98** (2018), no. 12 125134, [arXiv:1807.04754].

[51] R. Gurau, *Notes on Tensor Models and Tensor Field Theories*, arXiv:1907.03531.

[52] R. Gurau and V. Rivasseau, *The 1/N expansion of colored tensor models in arbitrary dimension*, *Europhys. Lett.* **95** (2011), no. 5 50004, [arXiv:1101.4182].

[53] R. Gurau, *The complete 1/N expansion of colored tensor models in arbitrary dimension*, *Annales Henri Poincare* **13** (2012) 399–423, [arXiv:1102.5759].

[54] V. Bonzom, R. Gurau, A. Riello, and V. Rivasseau, *Critical behavior of colored tensor models in the large N limit*, *Nucl. Phys. B* **853** (2011) 174–195, [arXiv:1105.3122].

[55] A. Tanasa, *Multi-orientable Group Field Theory*, *J. Phys.* **A45** (2012) 165401, [arXiv:1109.0694].

[56] V. Bonzom, R. Gurau, and V. Rivasseau, *Random tensor models in the large N limit: Uncoloring the colored tensor models*, *Phys. Rev.* **D85** (2012) 084037, [arXiv:1202.3637].

[57] A. Tanasa, *The Multi-Orientable Random Tensor Model, a Review*, *SIGMA* **12** (2016) 056, [arXiv:1512.02087].

[58] J. Yoon, *SYK Models and SYK-like Tensor Models with Global Symmetry*, *JHEP* **10** (2017) 183, [arXiv:1707.01740].

[59] S. Prakash and R. Sinha, *Melonic Dominance in Subchromatic Sextic Tensor Models*, *Phys. Rev. D* **101** (2020), no. 12 126001, [arXiv:1908.07178].

[60] X.-C. Wu, C.-M. Jian, and C. Xu, *Lattice models for non-Fermi liquids with tunable transport scalings*, *Phys. Rev. B* **100** (Aug, 2019) 075101.

[61] K. Bulycheva, I. R. Klebanov, A. Milekhin, and G. Tarnopolsky, *Spectra of Operators in Large N Tensor Models*, *Phys. Rev.* **D97** (2018), no. 2 026016, [arXiv:1707.09347].

[62] I. R. Klebanov, A. Milekhin, F. Popov, and G. Tarnopolsky, *Spectra of eigenstates in fermionic tensor quantum mechanics*, *Phys. Rev. D* **97** (2018), no. 10 106023, [arXiv:1802.10263].

[63] F. Ferrari, *The Large D Limit of Planar Diagrams*, arXiv:1701.01171.

[64] D. Anninos and G. A. Silva, *Solvable Quantum Grassmann Matrices*, *J. Stat. Mech.* **1704** (2017), no. 4 043102, [arXiv:1612.03795].

[65] A. Csordás, É. Szöke, and P. Szépfalusy, *Cluster states of fermions in the single l-shell model*, *The European Physical Journal D* no. 1 113–124.

[66] R. Hagedorn, *Statistical thermodynamics of strong interactions at high-energies*, *Nuovo Cim. Suppl.* **3** (1965) 147–186.

[67] J. J. Atick and E. Witten, *The Hagedorn Transition and the Number of Degrees of Freedom of String Theory*, *Nucl. Phys.* **B310** (1988) 291–334.

[68] J. S. Cotler, G. Gur-Ari, M. Hanada, J. Polchinski, P. Saad, S. H. Shenker, D. Stanford, A. Streicher, and M. Tezuka, *Black Holes and Random Matrices*, *JHEP* **05** (2017) 118, [arXiv:1611.04650].

[69] K. Pakrouski, I. R. Klebanov, F. Popov, and G. Tarnopolsky, *Spectrum of Majorana Quantum Mechanics with $O(4)^3$ Symmetry*, arXiv:1808.07455.

[70] P. Cvitanović, *Group theory: birdtracks, Lie's, and exceptional groups*. Princeton University Press, 2008.

[71] W. Fulton and J. Harris, *Representation theory: a first course*. Springer Science & Business Media.

[72] I. G. Macdonald, *Symmetric functions and Hall polynomials*. Oxford university press.

[73] D. Littlewood, *Invariant theory under orthogonal groups*, *Proceedings of the London Mathematical Society* **2** (1948), no. 1 349–379.

[74] K. Koike and I. Terada, *Young-diagrammatic methods for the representation theory of the classical groups of type Bn, Cn, Dn*, *Journal of Algebra* no. 2 466–511.

[75] D. P. Zhelobenko, *The classical groups. Spectral analysis of their finite-dimensional representations*, *Russian Mathematical Surveys* no. 1 1.

[76] A. Jevicki, K. Suzuki, and J. Yoon, *Bi-local holography in the SYK model*, *Journal of High Energy Physics* **2016** (jul, 2016).

[77] D. J. Gross and V. Rosenhaus, *A Generalization of Sachdev-Ye-Kitaev*, *JHEP* **02** (2017) 093, [arXiv:1610.01569].

[78] V. Rosenhaus, *An introduction to the SYK model*, *J. Phys. A* **52** (2019) 323001, [arXiv:1807.03334].

[79] J. Murugan, D. Stanford, and E. Witten, *More on Supersymmetric and 2d Analogs of the SYK Model*, *JHEP* **08** (2017) 146, [arXiv:1706.05362].

[80] A. Dymarsky, I. Klebanov, and R. Roiban, *Perturbative search for fixed lines in large N gauge theories*, *JHEP* **08** (2005) 011, [hep-th/0505099].

[81] E. Pomoni and L. Rastelli, *Large N Field Theory and AdS Tachyons*, *JHEP* **04** (2009) 020, [arXiv:0805.2261].

[82] D. Grabner, N. Gromov, V. Kazakov, and G. Korchemsky, *Strongly γ-Deformed $\mathcal{N} = 4$ Supersymmetric Yang-Mills Theory as an Integrable Conformal Field Theory*, *Phys. Rev. Lett.* **120** (2018), no. 11 111601, [arXiv:1711.04786].

[83] S. Prakash and R. Sinha, *A Complex Fermionic Tensor Model in d Dimensions*, *JHEP* **02** (2018) 086, [arXiv:1710.09357].

[84] P. Breitenlohner and D. Z. Freedman, *Stability in Gauged Extended Supergravity*, *Annals Phys.* **144** (1982) 249.

[85] I. R. Klebanov and E. Witten, *AdS / CFT correspondence and symmetry breaking*, *Nucl. Phys.* **B556** (1999) 89–114, [hep-th/9905104].

[86] J. Liu, E. Perlmutter, V. Rosenhaus, and D. Simmons-Duffin, *d-dimensional SYK, AdS Loops, and $6j$ Symbols*, arXiv:1808.00612.

[87] K. Bulycheva, *$\mathcal{N} = 2$ SYK model in the superspace formalism*, *JHEP* **04** (2018) 036, [arXiv:1801.09006].

[88] C.-M. Chang, S. Colin-Ellerin, and M. Rangamani, *On Melonic Supertensor Models*, *JHEP* **10** (2018) 157, [arXiv:1806.09903].

[89] H. Osborn and A. C. Petkou, *Implications of conformal invariance in field theories for general dimensions*, *Annals Phys.* **231** (1994) 311–362, [hep-th/9307010].

[90] S. Giombi, S. Prakash, and X. Yin, *A Note on CFT Correlators in Three Dimensions*, *JHEP* **07** (2013) 105, [arXiv:1104.4317].

[91] D. B. Kaplan, J.-W. Lee, D. T. Son, and M. A. Stephanov, *Conformality Lost*, *Phys. Rev. D* **80** (2009) 125005, [arXiv:0905.4752].

[92] S. Giombi, I. R. Klebanov, and G. Tarnopolsky, *Conformal QED_d, F-Theorem and the ϵ Expansion*, *J. Phys. A* **49** (2016), no. 13 135403, [arXiv:1508.06354].

[93] V. Gorbenko, S. Rychkov, and B. Zan, *Walking, Weak first-order transitions, and Complex CFTs*, *JHEP* **10** (2018) 108, [arXiv:1807.11512].

[94] G. Parisi, *How to measure the dimension of the parton field*, *Nucl. Phys.* **B59** (1973) 641–646.

[95] C. G. Callan, Jr. and D. J. Gross, *Bjorken scaling in quantum field theory*, *Phys. Rev.* **D8** (1973) 4383–4394.

[96] A. L. Fitzpatrick, J. Kaplan, D. Poland, and D. Simmons-Duffin, *The Analytic Bootstrap and AdS Superhorizon Locality*, *JHEP* **12** (2013) 004, [arXiv:1212.3616].

[97] Z. Komargodski and A. Zhiboedov, *Convexity and Liberation at Large Spin*, *JHEP* **11** (2013) 140, [arXiv:1212.4103].

[98] J. Gracey, I. Jack, and C. Poole, *The a-function in six dimensions*, *JHEP* **01** (2016) 174, [arXiv:1507.02174].

[99] H. Osborn and A. Stergiou, *Seeking fixed points in multiple coupling scalar theories in the ϵ expansion*, *JHEP* **05** (2018) 051, [arXiv:1707.06165].

[100] R. D. Pisarski, *Fixed point structure of ϕ^6 in three-dimensions at large N*, *Phys. Rev. Lett.* **48** (1982) 574–576.

[101] J. Hager, *Six-loop renormalization group functions of O(n)-symmetric phi**6-theory and epsilon-expansions of tricritical exponents up to epsilon**3*, *J. Phys. A* **35** (2002) 2703–2711.

[102] R. Gurau, *The complete $1/N$ expansion of a SYK–like tensor model*, *Nucl. Phys.* **B916** (2017) 386–401, [arXiv:1611.04032].

[103] L. Fei, S. Giombi, and I. R. Klebanov, *Critical $O(N)$ models in $6-\epsilon$ dimensions*, *Phys. Rev. D* **90** (2014), no. 2 025018, [arXiv:1404.1094].

[104] L. Fei, S. Giombi, I. R. Klebanov, and G. Tarnopolsky, *Three loop analysis of the critical O(N) models in 6-ε dimensions*, *Phys. Rev. D* **91** (2015), no. 4 045011, [arXiv:1411.1099].

[105] T. Azeyanagi, F. Ferrari, and F. I. Schaposnik Massolo, *Phase Diagram of Planar Matrix Quantum Mechanics, Tensor, and Sachdev-Ye-Kitaev Models*, *Phys. Rev. Lett.* **120** (2018), no. 6 061602, [arXiv:1707.03431].

[106] T. Azeyanagi, F. Ferrari, P. Gregori, L. Leduc, and G. Valette, *More on the New Large D Limit of Matrix Models*, *Annals Phys.* **393** (2017) 308–326, [arXiv:1710.07263].

[107] S. Choudhury, A. Dey, I. Halder, L. Janagal, S. Minwalla, and R. Poojary, *Notes on melonic $O(N)^{q-1}$ tensor models*, *JHEP* **06** (2018) 094, [arXiv:1707.09352].

[108] A. Almheiri and J. Polchinski, *Models of AdS_2 backreaction and holography*, *JHEP* **11** (2015) 014, [arXiv:1402.6334].

[109] J. Maldacena, D. Stanford, and Z. Yang, *Conformal symmetry and its breaking in two dimensional Nearly Anti-de-Sitter space*, *PTEP* **2016** (2016), no. 12 12C104, [arXiv:1606.01857].

[110] J. Engelsoy, T. G. Mertens, and H. Verlinde, *An investigation of AdS_2 backreaction and holography*, *JHEP* **07** (2016) 139, [arXiv:1606.03438].

[111] K. Jensen, *Chaos in AdS_2 Holography*, *Phys. Rev. Lett.* **117** (2016), no. 11 111601, [arXiv:1605.06098].

[112] L. Lionni and J. Thurigen, *Multi-critical behaviour of 4-dimensional tensor models up to order 6*, arXiv:1707.08931.

[113] I. R. Klebanov, F. Popov, and G. Tarnopolsky, *work in progress*, .

[114] N. Delporte and V. Rivasseau, *The Tensor Track V: Holographic Tensors*, arXiv:1804.11101.

[115] J. M. Maldacena, *The Large N limit of superconformal field theories and supergravity*, *Int. J. Theor. Phys.* **38** (1999) 1113–1133, [hep-th/9711200]. [Adv. Theor. Math. Phys.2,231(1998)].

[116] S. S. Gubser, I. R. Klebanov, and A. M. Polyakov, *Gauge theory correlators from noncritical string theory*, *Phys. Lett.* **B428** (1998) 105–114, [hep-th/9802109].

[117] E. Witten, *Anti-de Sitter space and holography*, *Adv. Theor. Math. Phys.* **2** (1998) 253–291, [hep-th/9802150].

[118] P. Gao, D. L. Jafferis, and A. Wall, *Traversable Wormholes via a Double Trace Deformation*, *JHEP* **12** (2017) 151, [arXiv:1608.05687].

[119] J. Maldacena, D. Stanford, and Z. Yang, *Diving into traversable wormholes*, *Fortsch. Phys.* **65** (2017), no. 5 1700034, [arXiv:1704.05333].

[120] S. Choudhury, A. Dey, I. Halder, L. Janagal, S. Minwalla, and R. Poojary, *Notes on Melonic $SO(N)^{q-1}$ Tensor Models*, .

[121] A. Mironov and A. Morozov, *Correlators in tensor models from character calculus*, arXiv:1706.03667.

[122] D. Benedetti, S. Carrozza, R. Gurau, and M. Kolanowski, *The $1/N$ expansion of the symmetric traceless and the antisymmetric tensor models in rank three*, *Commun. Math. Phys.* **371** (2019), no. 1 55–97, [arXiv:1712.00249].

[123] D. Benedetti and R. Gurau, *2PI effective action for the SYK model and tensor field theories*, *JHEP* **05** (2018) 156, [arXiv:1802.05500].

[124] H. Itoyama, A. Mironov, and A. Morozov, *Ward identities and combinatorics of rainbow tensor models*, *JHEP* **06** (2017) 115, [arXiv:1704.08648].

[125] H. Itoyama, A. Mironov, and A. Morozov, *Cut and join operator ring in tensor models*, *Nucl. Phys.* **B932** (2018) 52–118, [arXiv:1710.10027].

[126] I. R. Klebanov and A. A. Tseytlin, *A Nonsupersymmetric large N CFT from type 0 string theory*, *JHEP* **03** (1999) 015, [hep-th/9901101].

[127] W. Fu, D. Gaiotto, J. Maldacena, and S. Sachdev, *Supersymmetric Sachdev-Ye-Kitaev models*, *Phys. Rev.* **D95** (2017), no. 2 026009, [arXiv:1610.08917]. [Addendum: Phys. Rev.D95,no.6,069904(2017)].

[128] C. Peng, M. Spradlin, and A. Volovich, *A Supersymmetric SYK-like Tensor Model*, *JHEP* **05** (2017) 062, [arXiv:1612.03851].

[129] C. Peng, M. Spradlin, and A. Volovich, *Correlators in the $\mathcal{N} = 2$ Supersymmetric SYK Model*, *JHEP* **10** (2017) 202, [arXiv:1706.06078].

[130] C.-M. Chang, S. Colin-Ellerin, and M. Rangamani, *Supersymmetric Landau-Ginzburg Tensor Models*, arXiv:1906.02163.

[131] S. J. Gates Jr, M. T. Grisaru, M. Rocek, and W. Siegel, *Superspace, or one thousand and one lessons in supersymmetry*, *arXiv preprint hep-th/0108200* (2001).

[132] I. R. Klebanov, P. N. Pallegar, and F. K. Popov, *Majorana Fermion Quantum Mechanics for Higher Rank Tensors*, arXiv:1905.06264.

[133] S. Carrozza, *Large N limit of irreducible tensor models: $O(N)$ rank-3 tensors with mixed permutation symmetry*, *JHEP* **06** (2018) 039, [arXiv:1803.02496].

[134] D. Benedetti, R. Gurau, and S. Harribey, *Line of fixed points in a bosonic tensor model*, *JHEP* **06** (2019) 053, [arXiv:1903.03578].

[135] L. Avdeev, G. Grigoryev, and D. Kazakov, *Renormalizations in abelian chern-simons field theories with matter*, *Nuclear Physics B* **382** (1992), no. 3 561–580.

[136] I. Jack, D. Jones, and C. Poole, *Gradient flows in three dimensions*, *JHEP* **09** (2015) 061, [arXiv:1505.05400].

[137] J. Gracey, I. Jack, C. Poole, and Y. Schröder, *a-function for n= 2 supersymmetric gauge theories in three dimensions*, *Physical Review D* **95** (2017), no. 2 025005.

[138] C. Krishnan and K. V. P. Kumar, *Towards a Finite-N Hologram*, *JHEP* **10** (2017) 099, [arXiv:1706.05364].

[139] C. Krishnan and K. V. Pavan Kumar, *Exact Solution of a Strongly Coupled Gauge Theory in 0+1 Dimensions*, arXiv:1802.02502.

[140] K. Wilson and J. B. Kogut, *The Renormalization group and the epsilon expansion*, *Phys. Rept.* **12** (1974) 75–199.

[141] S. Gukov, *RG Flows and Bifurcations*, *Nucl. Phys. B* **919** (2017) 583–638, [arXiv:1608.06638].

[142] S. D. Glazek and K. G. Wilson, *Limit cycles in quantum theories*, *Phys. Rev. Lett.* **89** (2002) 230401, [hep-th/0203088]. [Erratum: Phys.Rev.Lett. 92, 139901 (2004)].

[143] E. Braaten and D. Phillips, *Renormalization-group limit cycle for the $\frac{1}{r^2}$-potential*, *Physical Review A* **70** (Nov, 2004).

[144] A. Gorsky and F. Popov, *Atomic collapse in graphene and cyclic renormalization group flow*, *Phys. Rev. D* **89** (2014), no. 6 061702, [arXiv:1312.7399].

[145] S. M. Dawid, R. Gonsior, J. Kwapisz, K. Serafin, M. Tobolski, and S. Glazek, *Renormalization group procedure for potential $-g/r^2$*, *Phys. Lett. B* **777** (2018) 260–264, [arXiv:1704.08206].

[146] V. Efimov, *Energy levels arising from resonant two-body forces in a three-body system*, *Physics Letters B* **33** (1970), no. 8 563–564.

[147] K. M. Bulycheva and A. S. Gorsky, *Limit cycles in renormalization group dynamics*, *Phys. Usp.* **57** (2014) 171–182, [arXiv:1402.2431].

[148] J.-F. Fortin, B. Grinstein, and A. Stergiou, *Limit Cycles in Four Dimensions*, *JHEP* **12** (2012) 112, [arXiv:1206.2921].

[149] J.-F. Fortin, B. Grinstein, and A. Stergiou, *Limit Cycles and Conformal Invariance*, *JHEP* **01** (2013) 184, [arXiv:1208.3674].

[150] M. A. Luty, J. Polchinski, and R. Rattazzi, *The a-theorem and the Asymptotics of 4D Quantum Field Theory*, *JHEP* **01** (2013) 152, [arXiv:1204.5221].

[151] J. L. Cardy, *Is There a c Theorem in Four-Dimensions?*, *Phys. Lett. B* **215** (1988) 749–752.

[152] I. Jack and H. Osborn, *Analogs for the c Theorem for Four-dimensional Renormalizable Field Theories*, *Nucl. Phys. B* **343** (1990) 647–688.

[153] Z. Komargodski and A. Schwimmer, *On Renormalization Group Flows in Four Dimensions*, *JHEP* **12** (2011) 099, [arXiv:1107.3987].

[154] A. Morozov and A. J. Niemi, *Can renormalization group flow end in a big mess?*, *Nucl. Phys. B* **666** (2003) 311–336, [hep-th/0304178].

[155] T. L. Curtright, X. Jin, and C. K. Zachos, *RG flows, cycles, and c-theorem folklore*, *Phys. Rev. Lett.* **108** (2012) 131601, [arXiv:1111.2649].

[156] D. J. Binder and S. Rychkov, *Deligne Categories in Lattice Models and Quantum Field Theory, or Making Sense of $O(N)$ Symmetry with Non-integer N*, *JHEP* **04** (2020) 117, [arXiv:1911.07895].

[157] M. Hogervorst, S. Rychkov, and B. C. van Rees, *Unitarity violation at the Wilson-Fisher fixed point in 4-ϵ dimensions*, *Phys. Rev. D* **93** (2016), no. 12 125025, [arXiv:1512.00013].

[158] E. Hopf, *Bifurcation of a periodic solution from a stationary solution of a system of differential equations*, *Berlin Mathematische Physics Klasse, Sachsischen Akademic der Wissenschaften Leipzig* **94** (1942) 3–32.

[159] R. C. Myers and A. Sinha, *Seeing a c-theorem with holography*, *Phys. Rev. D* **82** (2010) 046006, [arXiv:1006.1263].

[160] D. L. Jafferis, I. R. Klebanov, S. S. Pufu, and B. R. Safdi, *Towards the F-Theorem: N=2 Field Theories on the Three-Sphere*, *JHEP* **06** (2011) 102, [arXiv:1103.1181].

[161] I. R. Klebanov, S. S. Pufu, and B. R. Safdi, *F-Theorem without Supersymmetry*, *JHEP* **10** (2011) 038, [arXiv:1105.4598].

[162] H. Casini and M. Huerta, *On the RG running of the entanglement entropy of a circle*, *Phys. Rev. D* **85** (2012) 125016, [arXiv:1202.5650].

[163] S. Giombi and I. R. Klebanov, *Interpolating between a and F*, *JHEP* **03** (2015) 117, [arXiv:1409.1937].

[164] L. Fei, S. Giombi, I. R. Klebanov, and G. Tarnopolsky, *Generalized F-Theorem and the ϵ Expansion*, *JHEP* **12** (2015) 155, [arXiv:1507.01960].

[165] I. Jack and C. Poole, *a-function in three dimensions: Beyond the leading order*, *Phys. Rev. D* **95** (2017), no. 2 025010, [arXiv:1607.00236].

[166] T. Eguchi and H. Kawai, *Reduction of Dynamical Degrees of Freedom in the Large N Gauge Theory*, *Phys. Rev. Lett.* **48** (1982) 1063.

[167] S. Kachru and E. Silverstein, *4-D conformal theories and strings on orbifolds*, *Phys. Rev. Lett.* **80** (1998) 4855–4858, [hep-th/9802183].

[168] A. E. Lawrence, N. Nekrasov, and C. Vafa, *On conformal field theories in four-dimensions*, *Nucl. Phys. B* **533** (1998) 199–209, [hep-th/9803015].

[169] M. Bershadsky, Z. Kakushadze, and C. Vafa, *String expansion as large N expansion of gauge theories*, *Nucl. Phys. B* **523** (1998) 59–72, [hep-th/9803076].

[170] M. Bershadsky and A. Johansen, *Large N limit of orbifold field theories*, *Nucl. Phys. B* **536** (1998) 141–148, [hep-th/9803249].

[171] A. Armoni, M. Shifman, and G. Veneziano, *Exact results in non-supersymmetric large N orientifold field theories*, *Nucl. Phys. B* **667** (2003) 170–182, [hep-th/0302163].

[172] P. Kovtun, M. Unsal, and L. G. Yaffe, *Necessary and sufficient conditions for non-perturbative equivalences of large N(c) orbifold gauge theories*, *JHEP* **07** (2005) 008, [hep-th/0411177].

[173] M. Unsal and L. G. Yaffe, *(In)validity of large N orientifold equivalence*, *Phys. Rev. D* **74** (2006) 105019, [hep-th/0608180].

[174] M. R. Douglas and G. W. Moore, *D-branes, quivers, and ALE instantons*, hep-th/9603167.

[175] A. A. Tseytlin and K. Zarembo, *Effective potential in nonsupersymmetric SU(N) x SU(N) gauge theory and interactions of type 0 D3-branes*, *Phys. Lett. B* **457** (1999) 77–86, [hep-th/9902095].

[176] A. Dymarsky, I. Klebanov, and R. Roiban, *Perturbative gauge theory and closed string tachyons*, *JHEP* **11** (2005) 038, [hep-th/0509132].

[177] V. Gorbenko, S. Rychkov, and B. Zan, *Walking, Weak first-order transitions, and Complex CFTs II. Two-dimensional Potts model at $Q > 4$*, *SciPost Phys.* **5** (2018), no. 5 050, [arXiv:1808.04380].

[178] P. Hartman, *A lemma in the theory of structural stability of differential equations*, *Proceedings of the American Mathematical Society* **11** (1960), no. 4 610–620.

[179] D. M. Grobman, *Homeomorphism of systems of differential equations*, *Doklady Akademii Nauk SSSR* **128** (1959), no. 5 880–881.

[180] J. Guckenheimer and P. Holmes, *Nonlinear oscillations, dynamical systems, and bifurcations of vector fields*, vol. 42. Springer Science & Business Media, 2013.

[181] S.-N. Chow and J. Mallet-Paret, *Integral averaging and bifurcation*, *Journal of differential equations* **26** (1977), no. 1 112–159.

[182] V. I. Arnold, *Geometrical methods in the theory of ordinary differential equations*, vol. 250. Springer Science & Business Media, 2012.

[183] M. J. Feigenbaum, *Quantitative universality for a class of nonlinear transformations*, *Journal of statistical physics* **19** (1978), no. 1 25–52.

[184] A. B. Zamolodchikov, *Irreversibility of the flux of the renormalization group in a 2d field theory*, *JETP lett* **43** (1986), no. 12 730–732.

[185] A. Morozov and A. J. Niemi, *Can renormalization group flow end in a big mess?*, *Nuclear Physics B* **666** (2003), no. 3 311–336.

[186] D. Bernard and A. LeClair, *Strong weak coupling duality in anisotropic current interactions*, *Phys. Lett. B* **512** (2001) 78–84, [hep-th/0103096].

[187] A. LeClair, J. M. Roman, and G. Sierra, *Log periodic behavior of finite size effects in field theories with RG limit cycles*, *Nucl. Phys. B* **700** (2004) 407–435, [hep-th/0312141].

[188] A. Leclair, J. M. Roman, and G. Sierra, *Russian doll renormalization group, Kosterlitz-Thouless flows, and the cyclic sine-Gordon model*, *Nucl. Phys. B* **675** (2003) 584–606, [hep-th/0301042].

[189] S. D. Glazek and K. G. Wilson, *Renormalization of overlapping transverse divergences in a model light front Hamiltonian*, *Phys. Rev. D* **47** (1993) 4657–4669.

[190] A. LeClair, J. M. Roman, and G. Sierra, *Russian doll renormalization group and superconductivity*, *Phys. Rev. B* **69** (2004) 020505, [cond-mat/0211338].

[191] E. Braaten and D. Phillips, *The Renormalization group limit cycle for the 1/r**2 potential*, *Phys. Rev. A* **70** (2004) 052111, [hep-th/0403168].

[192] P.-G. De Gennes and P.-G. Gennes, *Scaling concepts in polymer physics*. Cornell university press, 1979.

[193] R. Bogdanov, *Bifurcations of a limit cycle for a family of vector fields on the plane.*, *Selecta Math. Soviet* **1** (1981) 373–388.

[194] F. Takens, *Forced oscillations and bifurcations*, *Applications of Global Analysis I, Comm* **3** (2001) 1–62.

[195] P. Cvitanovic, *Universality in chaos*. Routledge, 2017.

[196] D. Ruelle and F. Takens, *On the nature of turbulence*, *Les rencontres physiciens-mathématiciens de Strasbourg-RCP25* **12** (1971) 1–44.

[197] V. E. Zakharov, V. S. L'vov, and G. Falkovich, *Kolmogorov spectra of turbulence I: Wave turbulence*. Springer Science & Business Media, 2012.

[198] E. N. Lorenz, *Deterministic nonperiodic flow*, *Journal of atmospheric sciences* **20** (1963), no. 2 130–141.

[199] D. J. Gross and V. Rosenhaus, *Chaotic scattering of highly excited strings*, arXiv:2103.15301.

[200] L. P. Shilnikov, *A case of the existence of a denumerable set of periodic motions*, in *Doklady Akademii Nauk*, vol. 160, pp. 558–561, Russian Academy of Sciences, 1965.

[201] T. Oliynyk, V. Suneeta, and E. Woolgar, *A Gradient flow for worldsheet nonlinear sigma models*, *Nucl. Phys. B* **739** (2006) 441–458, [hep-th/0510239].

[202] F. Kuipers, U. Gürsoy, and Y. Kuznetsov, *Bifurcations in the RG-flow of QCD*, *JHEP* **07** (2019) 075, [arXiv:1812.05179].

[203] J. C. Collins, *Renormalization: An Introduction to Renormalization, The Renormalization Group, and the Operator Product Expansion*, vol. 26 of *Cambridge Monographs on Mathematical Physics*. Cambridge University Press, Cambridge, 1986.

[204] M. Bos, *An Example of Dimensional Regularization With Antisymmetric Tensors*, *Annals Phys.* **181** (1988) 177.

[205] M. J. Dugan and B. Grinstein, *On the vanishing of evanescent operators*, *Phys. Lett. B* **256** (1991) 239–244.

[206] J. A. Gracey, *Four loop MS-bar mass anomalous dimension in the Gross-Neveu model*, *Nucl. Phys. B* **802** (2008) 330–350, [arXiv:0804.1241].

[207] M. Hogervorst, S. Rychkov, and B. C. van Rees, *Truncated conformal space approach in d dimensions: A cheap alternative to lattice field theory?*, *Phys. Rev. D* **91** (2015) 025005, [arXiv:1409.1581].

[208] "Pydstool homepage." https://pydstool.github.io/PyDSTool/ProjectOverview.html.

[209] V. Gurarie, *Logarithmic operators in conformal field theory*, *Nucl. Phys. B* **410** (1993) 535–549, [hep-th/9303160].

[210] M. Hogervorst, M. Paulos, and A. Vichi, *The ABC (in any D) of Logarithmic CFT*, *JHEP* **10** (2017) 201, [arXiv:1605.03959].

[211] Y. A. Kuznetsov, *Elements of applied bifurcation theory*, vol. 112. Springer Science & Business Media, 2013.

[212] L. Fei, S. Giombi, I. R. Klebanov, and G. Tarnopolsky, *Three loop analysis of the critical o (n) models in 6- ε dimensions*, *Physical Review D* **91** (2015), no. 4 045011.

[213] D. B. Kaplan, J.-W. Lee, D. T. Son, and M. A. Stephanov, *Conformality lost*, *Physical Review D* **80** (2009), no. 12 125005.

[214] H. Gies and J. Jaeckel, *Chiral phase structure of QCD with many flavors*, *Eur. Phys. J. C* **46** (2006) 433–438, [hep-ph/0507171].

[215] F. Takens, *Singularities of vector fields*, *Publications Mathématiques de l'Institut des Hautes Études Scientifiques* **43** (1974), no. 1 47–100.

[216] I. Baldomá, S. Ibánez, and T. Seara, *Hopf-zero singularities truly unfold chaos*, *Communications in Nonlinear Science and Numerical Simulation* **84** (2020) 105162.